INTRINSIC FEATURES OF NONLINEAR WAVES IN DUSTY PLASMAS

A thesis submitted in partial fulfillment of the requirements for the degree of

**DOCTOR OF PHILOSOPHY
IN
MATHEMATICS**

By

MD. ABDUS SALAM

Student ID: 1913021501, Session: 2018-2019

**Department of Mathematics Faculty of Science, University of Rajshahi
Rajshahi-6205, Bangladesh.**

March 2024

প্রফেসর ড. মো. সাহেদ জামান
ডীন
বিজ্ঞান অনুষদ
রাজশাহী বিশ্ববিদ্যালয়
রাজশাহী-৬২০৫, বাংলাদেশ
ফোন : ০২৫৮৮৮৬৪১১৫ (অফিস)
ইমেল : zmshahed@ru.ac.bd
ফ্যাক্স : 02588866673

Prof. Dr. Md. Shahed Zaman
Dean
Faculty of Science
University of Rajshahi
Rajshahi-6205, Bangladesh
Phone : 02588864115 (Off)
E-mail : zmshahed@ru.ac.bd
fax : 02588866673

স্মারক নং (Ref. No) :

তারিখ (Date) : 31 JUL 2023

Recommendation

This is to certify that **Md. Abdus Salam**, Ph.D. Fellow, Session: 2018-2019, Roll No.: 1913021501, Registration No.: 1913021501, Department of Mathematics, University of Rajshahi, Bangladesh. His Ph.D. thesis entitled "**INTRINSIC FEATURES OF NONLINEAR WAVES IN DUSTY PLASMAS**" has been checked for Plagiarism and it is found overall **25%** similarity, including 14**%** on self-citation (Ref. 1, 2, 3). Therefore, the actual similarity is 11%, which is within the limit approved by the University of Rajshahi. The thesis is eligible for submission.

I wish him every success in life.

31.7.23

(Professor Dr. Md. Shahed Zaman)
Dean
Faculty of Science
University of Rajshahi-6205
Bangladesh.

Certificate

This is to certify that the thesis entitled **"INTRINSIC FEATURES OF NONLINEAR WAVES IN DUSTY PLASMAS"** by Md. Abdus Salam, in partial fulfillment of the requirements for the degree of Doctor of Philosophy (Ph.D.) in Mathematics in the Department of Mathematics, University of Rajshahi, Rajshahi-6205, Bangladesh, has been completed under our supervision. We acknowledge that this research work is authentic, and has not been submitted elsewhere for any degree.

We wish him success in his research work and future life as well.

25.3.2024

(Signature of the supervisor)

Date:

Professor Dr. M. Zulfikar Ali
Department of Mathematics
University of Rajshahi
Rajshahi-6205, Bangladesh.

25.03.24

(Signature of the co-supervisor)

Date:

Professor Dr. Md. Ali Akbar
Department of Applied Mathematics
University of Rajshahi
Rajshahi-6205, Bangladesh.

Declaration

I, Md. Abdus Salam, hereby state that the Ph.D. thesis entitled **"INTRINSIC FEATURES OF NONLINEAR WAVES IN DUSTY PLASMAS"** is my original work, and it has not been submitted elsewhere before for receiving any degree or diploma in the country or abroad. I declare that this thesis has been written by myself, and to the best of my knowledge, I have not taken any unethical help in this regard.

Md. Abdus Salam
Ph.D. Candidate
Department of Mathematics
University of Rajshahi
Rajshahi-6205, Bangladesh.

Date: 25.03.2024

Dedication

To the departed souls

of

my parents and father-in-law

Acknowledgment

At first, I remember Almighty Allah, the most merciful and gracious, who has enabled me to embark on my doctoral journey. I would like to express my deepest regard to my supervisor, Professor Dr. M. Zulfikar Ali, Department of Mathematics, University of Rajshahi, Rajshahi-6205, Bangladesh, and my co-supervisor, Professor Dr. Md. Ali Akbar, Department of Applied Mathematics, University of Rajshahi, Rajshahi-6205, Bangladesh, for their valuable guidance to pursue the research work. I have been immensely delighted to work under their supervision. I thank the chairman and all teachers of the Department of Mathematics, University of Rajshahi, Rajshahi-6205, Bangladesh, and my colleagues working in the Department of Mathematics, Mawlana Bhashani Science and Technology University, Tangail-1902, Bangladesh, for their kind help in every step.

I am grateful to Professor Dr. Md. Masum Haider, Department of Physics, Mawlana Bhashani Science and Technology University, Tangail-1902, Bangladesh, from whom I received fruitful advice and help to understand physics. I am thankful to Md. Tahamid Ar Rabbi, Senior Lecturer, Department of English, East West University, Dhaka-1212, Bangladesh, for his linguistic help in developing my writing.

Special thanks are due to my beloved wife, Tamanna Ferdous, caring mother-in-law, Mst. Zannatul Ferdous, affectionate brother, Md. Habibur Rahman, adorable son, Abrar Fahad Ohi, cute daughter, Nure Zannat Ariba, and other family members for their love, affection, and continuous mental support during the period of the thesis work.

Last but not least, I acknowledge the “study leave” granted by my working institution Mawlana Bhashani Science and Technology University, Tangail-1902, Bangladesh. I also acknowledge the “UGC Ph.D. Fellowship 2020-2021” provided by the University Grants Commission (UGC), Bangladesh, for this Ph.D. work.

Abstract

Dusty plasmas are electrically conducting ionized gases (macroscopically quasi-neutral) that comprise positively and negatively charged dust particles in addition to ions and electrons. Dusty plasmas exist in the Earth's magnetosphere, cometary tails, planetary rings, asteroid rings, rotating stars, and many other astronomical environments. In dusty plasmas, various types of nonlinear waves, such as solitary waves, shock waves, etc., may be propagated. The presence of dust particles makes the plasma system more complex. Besides, the characteristics of nonlinear waves can be substantially affected by different forces and plasma parameters.

We theoretically investigate the characteristics of dust-ion-acoustic solitary and shock waves, where the plasma species follow different particle distributions. The higher-order nonlinear and dispersive (or dissipative) effects on the waves are examined. We also investigate various kinds of effects, such as magnetic, adiabatic, parametric, etc., while it is illustrated that how they change the wave characteristics. An inhomogeneous KdV-type or modified KdV-type equation is obtained for demonstrating the solitary waves, whereas an inhomogeneous modified Burgers-type equation is obtained for the shock waves. The reductive perturbation method is extensively used for incorporating the higher-order effects into the KdV, modified KdV, and modified Burgers equations. The re-normalization technique, the Abel's theorem, and the method of variation of parameters are used for adding higher-order nonlinear and dispersive (or dissipative) effects into the solutions.

We deal with the theoretical investigation of the combined effect of the magnetic field and plasma rotation on the nonlinear features of obliquely propagated dust-ion-acoustic solitary waves in a magnetized dusty plasma. From the investigation, it is found that the overall impact of the magnetic field, oblique rotation, electron temperature, and dust concentration

has a crucial role in changing the amplitude, width, and phase speed of the dust-ion-acoustic solitary waves. The results are expected to be helpful in describing the rotating flows of magnetized plasma that are believed to exist in the rotating stars, the pulsar magnetosphere, and other rotating astronomical objects.

We also explore the dynamic behaviors of multi-solitons as well as multi-shocks that propagate in a magnetized dusty plasma. The simplified Hirota method and the Cole-Hopf transformation are applied to construct the multi-soliton or multi-shock solutions. We observe that the magnetic field has a decreasing effect on the multi-soliton amplitudes and widths, whereas the dust concentration has an increasing effect on the amplitudes and widths of both types of waves.

The obtained results might be helpful to describe the solitary and shock waves propagated in the Earth's mesosphere, Jupiter's magnetosphere, cometary tails, etc., in which dust particles are commonly seen.

List of Contents

Certificate	ii
Declaration	iii
Dedication	iv
Acknowledgement	v
Abstract	vi
List of Contents	viii
List of Figures	xii
Notations and Abbreviations	xix
List of Publications	xx

Chapter One: Introduction **1-16**

1.1	Historical background of plasma	1
1.2	Definition of plasma	1
1.3	Characteristics of dusty plasma	3
1.4	Magnetized plasma	7
1.5	Classification of plasmas	9
1.6	Acoustic waves in dusty plasma	10
1.7	Nonlinear waves in plasma	12
1.8	Governing equations	13
1.9	Stretched coordinates	14
1.10	The reductive perturbation technique	15
1.11	Different particle distributions	15

Chapter Two: Literature review and thesis outline **17-23**

2.1 Introduction 17

2.2 Literature review 18

2.3 Objectives of the thesis 21

2.4 Outline of the thesis 22

Chapter Three: Effects of magnetic field, obliquity, and higher-order nonlinear and dispersive terms on DIA subsonic solitary waves **24-46**

3.1 Introduction 24

3.2 Plasma model 26

3.3 Derivation of the KdV-type equation 27

3.4 Dressed solution 33

3.5 Results and discussion 36

3.6 Summary 46

Chapter Four: Higher-order nonlinear, dispersive, and parametric effects on DIA solitary waves **47-68**

4.1 Introduction 47

4.2 Plasma model 49

4.3 Derivation of the mKdV-type equation 50

4.4 Dressed solution 54

4.5 Results and discussion 56

4.6 Summary 67

Chapter Five: **Higher-order nonlinear and parametric effects on DIA shock waves** **69-82**

5.1 Introduction 69

5.2 Plasma model 71

5.3 Derivation of the wave equations 72

5.3.1 The modified Burgers equation 73

5.3.2 The modified Burgers-type inhomogeneous equation 74

5.4 Dressed solution 74

5.5 Results and discussion 76

5.5.2 Lower-order effect 76

5.5.3 Higher-order effect 79

5.6 Summary 82

Chapter Six: **Dynamic behaviors of DIA solitary waves in magneto-rotating dusty plasmas** **83-99**

6.1 Introduction 83

6.2 Plasma model 84

6.3 Derivation of the mKdV equation and its solution 86

6.4 Results and discussion 89

6.4.1 Effects on the amplitude 91

6.4.2 Effects on the width 94

6.4.3 Effects on the phase speed 97

6.5 Summary 98

Chapter Seven: Dynamic behaviors of multi-solitons and multi-shocks in magnetized dusty plasmas **100-124**

7.1 Introduction 100

7.2 Plasma model 101

7.3 Derivation of the wave equations 102

7.3.1 The KdV equation 102

7.3.2 The Burgers equation 104

7.4 Outline of the solution technique 105

7.4.1 Solution technique for the KdV equation 106

7.4.2 Solution technique for the Burgers equation 106

7.5 Multi-soliton and multi-shock solutions 107

7.6 Results and discussion 110

7.6.1 Parametric effects on the multi-solitons 110

7.6.2 Parametric effects on the multi-shocks 120

7.6.3 Parametric effects on the phase speed 123

7.7 Summary 124

Chapter Eight: Conclusion and future studies **125-127**

8.1 Conclusion 125

8.2 Future studies 126

References **127-146**

Appendix **147-151**

List of Figures

Figure 1.1	Different states of matter	2
Figure 1.2	Examples of plasmas	3
Figure 1.3	Debye shielding	4
Figure 1.4	Circular motion of a charged particle	8
Figure 1.5	Maxwell-Boltzmann distribution	15
Figure 1.6	Vortex-like distribution of particles	16
Figure 3.1	The ratio $\left\|\psi^{(2)}\right\|/\left\|\psi^{(1)}\right\|$ vs. ξ, when $\mu_d = 0.3, \omega_{ci} = 0.4$, $\Delta M = 0.01$, $\theta = 80^0, \tau = 1$.	36
Figure 3.2	3D plots of ψ, $\psi^{(1)}$, and $\psi^{(2)}$, when $\mu_d = 0.3, \omega_{ci} = 0.4$, $\Delta M = 0.01, \theta = 80^0$.	37
Figure 3.3	2D plots of ψ, $\psi^{(1)}$, and $\psi^{(2)}$ at $\tau = 1$, when $\mu_d = 0.3$, $\omega_{ci} = 0.4, \Delta M = 0.01, \theta = 80^0$.	37
Figure 3.4	Time evolutions of $\psi^{(1)}$ and ψ at $\tau = 0.0$, 50, 100.	38
Figure 3.5	3D plots of $\psi^{(1)}$ and ψ for $\omega_{ci} = 0.2$, $\omega_{ci} = 0.3$, $\omega_{ci} = 0.4$	39
Figure 3.6	2D plots of $\psi^{(1)}$ and ψ for $\omega_{ci} = 0.2$, $\omega_{ci} = 0.3$, $\omega_{ci} = 0.4$ at $\tau = 1$.	39
Figure 3.7	Shows different amplitudes for $\psi^{(1)}$ and ψ in the interval $\omega_{ci}\ \epsilon$ [0.2, 0.4], when $\mu_d = 0.3, \Delta M = 0.01, \theta = 80^0$.	40
Figure 3.8	Shows the same width for $\psi^{(1)}$ and ψ in the interval $\omega_{ci}\ \epsilon$[0.2, 0.4], when $\mu_d = 0.3, \Delta M = 0.01, \theta = 80^0$.	40
Figure 3.9	3D plots of $\psi^{(1)}$ and ψ for $\theta = 70^0, \theta = 75^0, \theta = 80^0$.	41
Figure 3.10	2D plots of $\psi^{(1)}$ and ψ for $\theta = 70^0, \theta = 75^0, \theta = 80^0, \tau = 1$.	41
Figure 3.11	Amplitudes of $\psi^{(1)}$ and ψ in the interval $\theta\ \epsilon\ [0^0, 87^0]$.	42
Figure 3.12	Shows the same width for $\psi^{(1)}$ and ψ in the interval $\theta\ \epsilon\ [0^0, 87^0]$, while the parameters are: $\mu_d = 0.3, \Delta M = 0.01, \omega_{ci} = 0.4$.	42

Figure 3.13 3D plots of $\psi^{(1)}$ and ψ for $\mu_d = 0.1$, $\mu_d = 0.3$, $\mu_d = 0.5$. 43

Figure 3.14 2D plots of $\psi^{(1)}$ and ψ for $\mu_d = 0.1$, $\mu_d = 0.3$, $\mu_d = 0.5$, $\tau = 1$. 43

Figure 3.15 Amplitudes of $\psi^{(1)}$ and ψ in the interval $\mu_d \epsilon [0, 0.6]$. 44

Figure 3.16 Shows the same width for $\psi^{(1)}$ and ψ in the interval $\mu_d \epsilon [0, 0.6]$, while the parameters are: $\omega_{ci} = 0.4$, $\Delta M = 0.01$,$\theta = 80^0$, $\tau = 1$. 44

Figure 3.17 Phase speed vs. μ_d in the interval $[0, 0.6]$, when $\theta = 80^0$. 45

Figure 3.18 Phase speed vs. θ in the interval $[0^0, 90^0]$, when $\mu_d = 0.3$. 45

Figure 4.1 $\frac{|\psi^{(2)}|}{|\psi^{(1)}|}$ vs. ξ in the presence of positively ($j = 1$) and negatively ($j = -1$) charged dust particles, when $\beta_n = -0.9$, $\alpha = 10$, $\sigma_i = 0.2$, $\mu_d = 0.4$, $\mu_n = 0.7$, $\gamma = 1.67$, $\omega_{ci} = 0.9$, $\Delta M = 0.01$, $\theta = 15^0$, $\tau = 1$. 57

Figure 4.2 Wave structures of ψ, $\psi^{(1)}$, and $\psi^{(2)}$ in the presence of positively charged dust particles ($j = 1$), when $\beta_n = -0.9$, $\alpha = 10$, $\sigma_i = 0.2$, $\mu_d = 0.4$, $\mu_n = 0.7$, $\gamma = 1.67$, $\omega_{ci} = 0.9$, $\Delta M = 0.01$, $\theta = 15^0$. 58

Figure 4.3 Wave structures of ψ, $\psi^{(1)}$, and $\psi^{(2)}$ in the presence of negatively charged dust particles ($j = -1$), when $\beta_n = -0.9$, $\alpha = 10$, $\sigma_i = 0.2$, $\mu_d = 0.4$, $\mu_n = 0.7$, $\gamma = 1.67$, $\omega_{ci} = 0.9$, $\Delta M = 0.01$, $\theta = 15^0$. 58

Figure 4.4 Change in wave structures of $\psi = \psi^{(1)} + \psi^{(2)}$(solid curves) and $\psi^{(1)}$ (dashed curves) for $\omega_{ci} = 0.7$ (red), $\omega_{ci} = 0.8$ (green), and $\omega_{ci} = 0.9$ (blue), when $j = 1$, $\beta_n = -0.9$, $\alpha = 10$, $\sigma_i = 0.2$, $\mu_d = 0.4$, $\mu_n = 0.7$, $\gamma = 1.67$, $\Delta M = 0.01$, $\theta = 15^0$. 59

Figure 4.5 Change in wave structures of $\psi = \psi^{(1)} + \psi^{(2)}$ (solid curves) and $\psi^{(1)}$ (dashed curves) for $\omega_{ci} = 0.7$ (red), $\omega_{ci} = 0.8$ (green), and $\omega_{ci} = 0.9$ (blue), when $j = -1$, $\beta_n = -0.9$, $\alpha = 10$, $\sigma_i = 0.2$, $\mu_d = 0.4$, $\mu_n = 0.7$, $\gamma = 1.67$, $\Delta M = 0.01$, $\theta = 15^0$. 60

Figure 4.6 Amplitude (ψ_{A12}) vs. gyro-frequency (ω_{ci}). 60

Figure 4.7 Width (W) vs. gyro-frequency (ω_{ci}). 61

Figure 4.8	Variation in wave structures of ψ (solid curves) and $\psi^{(1)}$ (dashed curves) for $\gamma = 1.75$ (red), $\gamma = 2.25$ (green), and $\gamma = 2.75$ (blue), when $j = 1$ and $\beta_n = -0.9$, $\alpha = 10$, $\sigma_i = 0.2$, $\mu_d = 0.4$, $\mu_n = 0.7$, $\omega_{ci} = 0.9$, $\Delta M = 0.01$, $\theta = 15^0$.	61
Figure 4.9	Variation in wave structures of ψ (solid curves) and $\psi^{(1)}$ (dashed curves) for $\gamma = 1.75$ (red), $\gamma = 2.25$ (green), and $\gamma = 2.75$ (blue), when $j = -1$ and $\beta_n = -0.9$, $\alpha = 10$, $\sigma_i = 0.2$, $\mu_d = 0.4$, $\mu_n = 0.7$, $\omega_{ci} = 0.9$, $\Delta M = 0.01$, $\theta = 15^0$.	62
Figure 4.10	Variation in wave structures of ψ (solid curves) and $\psi^{(1)}$ (dashed curves) for $\sigma_i = 0.2$ (red), $\sigma_i = 0.3$ (green), and $\sigma_i = 0.4$ (blue), when $j = 1$ and $\beta_n = -0.9$, $\alpha = 10$, $\gamma = 1.67$, $\mu_d = 0.4$, $\mu_n = 0.7$, $\omega_{ci} = 0.9$, $\Delta M = 0.01$, $\theta = 15^0$.	62
Figure 4.11	Variation in wave structures of ψ (solid curves) and $\psi^{(1)}$ (dashed curves) for $\sigma_i = 0.2$ (red), $\sigma_i = 0.3$ (green), and $\sigma_i = 0.4$ (blue), when $j = -1$ and $\beta_n = -0.9$, $\alpha = 10$, $\gamma = 1.67$, $\mu_d = 0.4$, $\mu_n = 0.7$, $\omega_{ci} = 0.9$, $\Delta M = 0.01$, $\theta = 15^0$.	63
Figure 4.12	Variation of ψ (solid curves) and $\psi^{(1)}$ (dashed curves) for $\mu_d = 0.2,\ 0.5,\ 0.8$, when $j = 1$ and $\beta_n = -0.9$, $\alpha = 10$, $\gamma = 1.67$, $\sigma_i = 0.2$, $\mu_n = 0.7$, $\omega_{ci} = 0.9$, $\Delta M = 0.01$, $\theta = 15^0$.	64
Figure 4.13	Variation of ψ (solid curves) and $\psi^{(1)}$ (dashed curves) for $\mu_d = 0.2,\ 0.5,\ 0.8$, when $j = -1$ and $\beta_n = -0.9$, $\alpha = 10$, $\gamma = 1.67$, $\sigma_i = 0.2$, $\mu_n = 0.7$, $\omega_{ci} = 0.9$, $\Delta M = 0.01$, $\theta = 15^0$.	64
Figure 4.14	V_0 vs. σ_i, when $\alpha = 10$, $\mu_d = 0.3$, $\mu_n = 0.2$, $\omega_{ci} = 0.9$, $\theta = 15^0$.	65
Figure 4.15	V_0 vs. μ_n, when $\alpha = 10$, $\mu_d = 0.3$, $\sigma_i = 0.2$, $\omega_{ci} = 0.9$, $\theta = 15^0$.	65
Figure 4.16	V_0 vs. α , when $\mu_d = 0.3$, $\mu_n = 0.2$, $\sigma_i = 0.3$, $\omega_{ci} = 0.9$, $\theta = 15^0$.	66
Figure 4.17	V_0 vs. θ, when $\alpha = 0.3$, $\mu_d = 0.3$, $\mu_n = 0.2$, $\sigma_i = 0.2$, $\omega_{ci} = 0.9$.	66
Figure 4.18	V_0 vs. μ_d, when $\alpha = 10$, $\sigma_i = 0.2$, $\mu_n = 0.3$, $\omega_{ci} = 0.9$, $\theta = 15^0$.	67
Figure 5.1	Waves profile variations for different angles (θ), when $\mu_d = 0.34$, $\beta_e = -0.9$, $\gamma = 5/3$, $\sigma_i = 0.02$, $U_0 = 0.1$, $\eta = 0.8$, $\tau = 1$.	77

Figure 5.2	Wave-amplitude vs. β_e and μ_d, when $\gamma = 5/3$, $\sigma_i = 0.02$, $U_0 = 0.1, \eta = 0.8, \theta = 15^0$.	77
Figure 5.3	Variation in width with η and U_0.	78
Figure 5.4	Effects of μ_d and σ_i on the phase speed, when $\theta = 15^0$, $\gamma = 5/3$.	79
Figure 5.5	Structures of $\psi^{(1)}, \psi^{(2)}$ and ψ, when $\beta_e = -0.9, \sigma_i = 0.02$, $\mu_d = 0.34, \gamma = 5/3, \omega_{ci} = 0.8, U_0 = 0.1, \theta = 15^0, \eta = 0.8, \tau = 1$.	80
Figure 5.6	Structures of $\psi^{(1)}$ and ψ for $\beta_e = -0.3$ (green), $\beta_e = -0.5$ (blue), $\beta_e = -0.7$ (red), when $\sigma_i = 0.02, \mu_d = 0.34, \gamma = 5/3$, $\omega_{ci} = 0.8, U_0 = 0.1, \theta = 15^0, \eta = 0.8, \tau = 1$.	80
Figure 5.7	Variation in shock structures of ψ and $\psi^{(1)}$ for $\mu_d = 0.1$(green), $\mu_d = 0.3$(blue), $\mu_d = 0.5$(red), when $\beta_e = -0.9$, $\sigma_i = 0.02$, $\gamma = 5/3, \omega_{ci} = 0.8, U_0 = 0.1, \theta = 15^0, \eta = 0.8, \tau = 1$.	81
Figure 5.8	Variation in shock profiles of $\psi = \psi^{(1)} + \psi^{(2)}$(solid lines) and $\psi^{(1)}$ (black solid line) for $\omega_{ci} = 0.2$ (green), $\omega_{ci} = 0.4$ (blue) and $\omega_{ci} = 0.6$ (red), when $\beta_e = -0.9$, $\sigma_i = 0.02$, $\mu_d = 0.34$, $\gamma = 5/3, U_0 = 0.1, \theta = 15^0, \eta = 0.8$.	82
Figure 6.1	Solitary wave structures at different wave speeds for positively charged dust particles (i.e., $j = 1$) while the dashed curves are plotted in the absence of Coriolis force ($\Omega_0 = 0$) at $U_0 = 0.05$ (red), $U_0 = 0.10$ (green), $U_0 = 0.15$ (gold), and the solid curves are plotted in the presence of Coriolis force ($\Omega_0 = 0.03$) at $U_0 = 0.05$ (blue), $U_0 = 0.1$ (black), $U_0 = 0.15$ (cyan). The other parameters are: $\alpha = 2$, $\mu_d = 0.42$, $\mu_e = 0.5$, $\beta_n = -0.3$, $\gamma = 5/3, \sigma_i = 0.3, l_x = 0.87, l_y = 0.5, \theta = 30^0$.	90
Figure 6.2	Solitary wave structures at different wave speeds for negatively charged dust particles (i.e., $j = -1$), whereas the dashed curves are plotted in the absence of Coriolis force ($\Omega_0 = 0$) at $U_0 = 0.05$ (red), $U_0 = 0.10$ (green), $U_0 = 0.15$ (gold), and the solid curves are plotted in the presence of Coriolis force ($\Omega_0 = 0.03$) at $U_0 = 0.05$ (blue), $U_0 = 0.1$ (black), $U_0 = 0.15$ (cyan). The other parameters are: $\alpha = 2$, $\mu_d = 0.42$, $\mu_e = 0.5$, $\beta_n = -0.3$, $\gamma = 5/3, \sigma_i = 0.3, l_x = 0.87, l_y = 0.5, \theta = 30^0$.	90

Figure 6.3	Wave-amplitude against ω_{ci} and Ω_0, when $j = 1$ and $\alpha = 2$, $\mu_d = 0.42$, $\mu_e = 0.5$, $\beta_n = -0.3$, $U_0 = 0.1$, $\gamma = 5/3$, $\sigma_i = 0.3$, $l_x = 0.87$, $l_y = 0.5$, $\theta = 30^0$.	91
Figure 6.4	Wave-amplitude against ω_{ci} and Ω_0, when $j = -1$ and $\alpha = 2$, $\mu_d = 0.42$, $\mu_e = 0.5$, $\beta_n = -0.3$, $U_0 = 0.1$, $\gamma = 5/3$, $\sigma_i = 0.3$, $l_x = 0.87$, $l_y = 0.5$, $\theta = 30^0$.	92
Figure 6.5	Variation of amplitude with μ_e and μ_d for positively charged dust particles, when $\alpha = 2$, $\beta_n = -0.3$, $U_0 = 0.1$, $\gamma = 5/3$, $\sigma_i = 0.3$, $l_x = 0.87$, $\omega_{ci} = 0.3$, $\Omega_0 = 0.03$, $l_y = 0.5$, $\theta = 30^0$.	93
Figure 6.6	Variation of amplitude with μ_e and μ_d for negatively charged dust particles, when $\alpha = 2$, $\beta_n = -0.3$, $U_0 = 0.1$, $\gamma = 5/3$, $\sigma_i = 0.3$, $l_x = 0.87$, $\omega_{ci} = 0.3$, $\Omega_0 = 0.03$, $l_y = 0.5$, $\theta = 30^0$.	93
Figure 6.7	Variation of the amplitude with θ and σ_i for positive and negatively charged dust particles (upper and lower surfaces, respectively), when $\alpha = 2$, $\mu_d = 0.42$, $\mu_e = 0.5$, $\beta_n = -0.3$, $U_0 = 0.1$, $\gamma = 5/3$, $l_x = 0.87$, $\omega_{ci} = 0.3$, $\Omega_0 = 0.03$, $l_y = 0.5$.	94
Figure 6.8	Width against ω_{ci} and Ω_0, when $j = 1$ and $\alpha = 2$, $\mu_d = 0.42$, $\mu_e = 0.5$, $\beta_n = -0.3$, $U_0 = 0.1$, $\gamma = 5/3$, $\sigma_i = 0.3$, $l_x = 0.87$, $l_y = 0.5$, $\theta = 30^0$.	95
Figure 6.9	Width against ω_{ci} and Ω_0, when $j = -1$ and $\alpha = 2$, $\mu_d = 0.42$, $\mu_e = 0.5$, $\beta_n = -0.3$, $U_0 = 0.1$, $\gamma = 5/3$, $\sigma_i = 0.3$, $l_x = 0.87$, $l_y = 0.5$, $\theta = 30^0$.	95
Figure 6.10	Solitary wave-width against μ_e and μ_d , when $j = 1$ and $\alpha = 2$, $\beta_n = -0.3$, $U_0 = 0.1$, $\gamma = 5/3$, $\sigma_i = 0.3$, $l_x = 0.87$, $\omega_{ci} = 0.3$, $\Omega_0 = 0.03$, $l_y = 0.5$, $\theta = 30^0$.	96
Figure 6.11	Solitary wave-width against μ_e and μ_d, when $j = -1$ and $\alpha = 2$, $\beta_n = -0.3$, $U_0 = 0.1$, $\gamma = 5/3$, $\sigma_i = 0.3$, $l_x = 0.87$, $\omega_{ci} = 0.3$, $\Omega_0 = 0.03$, $l_y = 0.5$, $\theta = 30^0$.	96
Figure 6.12	Variation of the width with θ and σ_i for $j = 1$ and $j = -1$ (lower and upper surfaces respectively) when $\alpha = 2$, $\mu_d = 0.42$, $\mu_e = 0.5$, $\beta_n = -0.3$, $U_0 = 0.1$, $\gamma = 5/3$, $l_x = 0.87$, $\omega_{ci} = 0.3$, $\Omega_0 = 0.03$, $l_y = 0.5$.	97

Figure 6.13	Effects of ω_{ci} and Ω_0 on phase speed for $j = 1$, when $\alpha = 2$, $\mu_d = 0.42$, $\mu_e = 0.5$, $\beta_n = -0.3$, $U_0 = 0.1$, $\gamma = 5/3$, $\sigma_i = 0.3$, $l_x = 0.87$, $l_y = 0.5$, $\theta = 30^0$.	97
Figure 6.14	Effects of ω_{ci} and Ω_0 on phase speed for $j = -1$, when $\alpha = 2$, $\mu_d = 0.42$, $\mu_e = 0.5$, $\beta_n = -0.3$, $U_0 = 0.1$, $\gamma = 5/3$, $\sigma_i = 0.3$, $l_x = 0.87$, $l_y = 0.5$, $\theta = 30^0$.	98
Figure 7.1	Single-soliton of (7.28) when $\alpha = 1.1$, $\omega_{ci} = 0.6$, $\theta = 15^0$, $\mu_d = 0.5$, $\mu_p = 0.4$, $U_1 = 0.4$ in the interval $\xi \in [-10, 10]$ and $\tau \in [0, 10]$.	111
Figure 7.2	Single-soliton at $\tau = 0, 5, 10$ in the interval $\xi \in [-10, 10]$ while the parameters are: $\alpha = 1.1$, $\omega_{ci} = 0.6$, $\theta = 15^0$, $\mu_d = 0.5$, $\mu_p = 0.4$, $U_1 = 0.4$.	111
Figure 7.3	Two-soliton profile of (7.31) when $\alpha = 1.1$, $\omega_{ci} = 0.6$, $\theta = 15^0$, $\mu_d = 0.5$, $\mu_p = 0.4$, $U_1 = 0.4$, $U_2 = 0.6$ in the interval $\xi \in [-8, 12]$, $\tau \in [0, 2]$.	112
Figure 7.4	Two-soliton at $\tau = 0, 5, 10$ in the interval $\xi \in [-8, 12]$, when $\alpha = 1.1$, $\omega_{ci} = 0.6$, $\theta = 15^0$, $\mu_d = 0.5$, $\mu_p = 0.4$, $U_1 = 0.4$, $U_2 = 0.6$.	112
Figure 7.5	Three-soliton profile of (7.35), when $\alpha = 1.1$, $\omega_{ci} = 0.6$, $\theta = 15^0$, $\mu_d = 0.5$, $\mu_p = 0.4$, $U_1 = 0.4$, $U_2 = 0.6$, $U_3 = 0.8$ and $\xi \in [-5, 15]$ and $\tau \in [0, 2]$.	113
Figure 7.6	Three-solitons at $\tau = 0, 5, 10$ in the interval $\xi \in [-5, 20]$, when $\alpha = 1.1$, $\omega_{ci} = 0.6$, $\theta = 45^0$, $\mu_d = 0.5$, $\mu_p = 0.4$, $U_1 = 0.4$, $U_2 = 0.6$, $U_3 = 0.8$.	113
Figure 7.7	Single-soliton profiles for $\omega_{ci} = 0.2, 0.4, 0.6$, when $\alpha = 1.1$, $\omega_{ci} = 0.6$, $\theta = 15^0$, $\mu_d = 0.5$, $\mu_p = 0.4$, $U_1 = 0.4$, $\tau = 1$.	114
Figure 7.8	Two-soliton profiles for $\omega_{ci} = 0.2, 0.4, 0.6$, when $\alpha = 1.1$, $\omega_{ci} = 0.6$, $\theta = 1$, $\mu_d = 0.5$, $\mu_p = 0.4$, $U_1 = 0.4$, $U_2 = 0.6, 0.8$, $\tau = 1$.	115
Figure 7.9	Three-soliton profiles for $\omega_{ci} = 0.2, 0.4, 0.6$, when $\alpha = 1.1$, $\omega_{ci} = 0.6$, $\theta = 15^0$, $\mu_d = 0.5$, $\mu_p = 0.4$, $U_1 = 0.4$, $U_2 = 0.6$, $U_3 = 0.8$, $\tau = 1$.	115
Figure 7.10	Single-soliton profiles for $\mu_d = 0.3, 0.5, 0.7$, when $\alpha = 1.1$, $\mu_p = 0.4$, $\theta = 15^0$, $U_1 = 0.4$, $\omega_{ci} = 0.6$, $\tau = 1$.	116

Figure 7.11	Two-soliton profiles for $\mu_d = 0.3,\ 0.5,\ 0.7$, when $\alpha = 1.1$, $\mu_p = 0.4$, $\theta = 15^0$, $\omega_{ci} = 0.6$, $U_1 = 0.4$, $U_2 = 0.6$, $\tau = 1$.	116
Figure 7.12	Three-soliton profiles for $\mu_d = 0.3, 0.5, 0.7$, when $\alpha = 1.1$, $\mu_p = 0.4$, $\theta = 15^0$, $\omega_{ci} = 0.6$, $U_1 = 0.4$, $U_2 = 0.6$, $U_3 = 0.8$, $\tau = 1$.	117
Figure 7.13	Single-soliton profiles for different angle (θ), when $\alpha = 1.1$, $\mu_p = 0.4$, $\mu_d = 0.5$, $U_1 = 0.4$, $\omega_{ci} = 0.6$, $\tau = 1$.	117
Figure 7.14	Two-soliton profiles for different angle (θ), when $\alpha = 1.1$, $\omega_{ci} = 0.6$, $\mu_d = 0.5$, $\mu_p = 0.4$, $U_1 = 0.4$, $U_2 = 0.6$, $\tau = 1$.	118
Figure 7.15	Three-soliton profiles for different angle (θ), when $\alpha = 1.1$, $\omega_{ci} = 0.6$, $\mu_d = 0.5$, $\mu_p = 0.4$, $U_1 = 0.4$, $U_2 = 0.6$, $U_3 = 0.8$, $\tau = 1$.	118
Figure 7.16	Single-soliton profiles for $\mu_p = 0.2, 0.4, 0.6$, when $\alpha = 1.1$, $\mu_d = 0.5$, $\theta = 15^0$, $\omega_{ci} = 0.6$, $U_1 = 0.4$, $\tau = 1$.	119
Figure 7.17	Two-soliton profiles for $\mu_p = 0.2, 0.4, 0.6$, when $\alpha = 1.1$, $\mu_d = 0.5$, $\theta = 15^0$, $\omega_{ci} = 0.6$, $U_1 = 0.4$, $U_2 = 0.6$, $\tau = 1$.	119
Figure 7.18	Three-soliton profiles for $\mu_p = 0.2, 0.4, 0.6$, when $\alpha = 1.1$, $\mu_d = 0.5$, $\theta = 15^0$, $\omega_{ci} = 0.6$, $U_1 = 0.4$, $U_2 = 0.6$, $U_3 = 0.8$, $\tau = 1$.	120
Figure 7.19	Single-front profile when the parameters are: $\alpha = 1.1$, $\mu_d = 0.5$, $\theta = 15^0$, $\eta = 0.5$, $U_1 = 0.4$.	120
Figure 7.20	Two-front profile when the parameters are: $\alpha = 1.1$, $\mu_d = 0.5$, $\theta = 15^0$, $\eta = 0.5$, $U_1 = 0.4$, $U_2 = 0.6$.	121
Figure 7.21	Three-front profile when the parameters are: $\alpha = 1.1$, $\mu_d = 0.5$, $\theta = 15^0$, $\eta = 0.5$, $U_1 = 0.4$, $U_2 = 0.4$, $U_3 = 0.6$.	121
Figure 7.22	Single-front profiles for $\mu_d = 0.3,\ 0.5,\ 0.7$, when $\alpha = 1.1$, $\mu_p = 0.4$, $\theta = 15^0$, $\eta = 0.5$, $U_1 = 0.4$, $\tau = 1$.	122
Figure 7.23	Two-front profiles for $\mu_d = 0.3,\ 0.5,\ 0.7$, when $\alpha = 1.1$, $\mu_p = 0.4$, $\theta = 15^0$, $\eta = 0.5$, $U_1 = 0.4$, $U_2 = 0.6$, $\tau = 1$.	122
Figure 7.24	Three-front profiles for $\mu_d = 0.3, 0.5, 0.7$, when $\alpha = 1.1$, $\mu_p = 0.4$, $\theta = 15^0$, $\eta = 0.5$, $U_1 = 0.4$, $U_2 = 0.6$, $U_3 = 0.8$, $\tau = 1$.	123
Figure 7.25	Phase speed vs. μ_d and α, when $\mu_p = 0.4$, $\theta = 15^0$.	123

Notations and Abbreviations

- IA = Ion-acoustic.
- DIA = Dust-ion-acoustic.
- DA = Dust-acoustic.
- PCD = Positively charged dust.
- KdV = Korteweg-de Vries.
- mKdV = Modified Korteweg-de Vries.
- CHT = Cole-Holf transformation
- V_0 = Phase speed of the waves.
- u_i = Velocity of the ions.
- m_i = Mass of the positive ions.
- T_s = Temperature of the species s.
- λ_D = Debye length.
- n_{s0} = Equilibrium number density of species s.
- β_s = Fraction of trapping species s.
- K_B = Boltzmann constant.
- ψ = Normalized electrostatic wave potential.
- ω_{ci} = Positive ion gyro-frequency.
- Z_d = Number of electrons residing on the surface of stationary dust.
- p_i = Positive ion fluid pressure.
- γ = Adiabatic index.
- ϵ = Strength of the nonlinearity.
- θ = Angle between the directions of the wave propagation and the magnetic field.
- η = Kinematic viscosity.
- Ω_0 = Rotational frequency.
- B_0 = Magnitude of the magnetic field.
- e = Magnitude of an electron charge.

List of Publications

1. Akbar, M. A., **Salam, M. A**., and Ali, M. Z. (2023). Investigating the parametric impacts on dust-ion-acoustic solitary waves in magnetized rotating plasmas. *Results in Physics*, 51, 106682.

2. **Salam, M. A**., Akbar, M. A., Ali, M. Z., and Mustafa Inc. (2022). The higher-order nonlinearity and parametric effects on dust-ion-acoustic shock waves. *Physica Scripta*, 97(12), 125605.

3. **Salam, M. A**., Akbar, M. A., and Ali, M. Z. (2022). Higher-order nonlinear and dispersive effects on dust-ion-acoustic solitary waves in magnetized dusty plasmas. *Results in Physics*, 32, 105114.

4. **Salam, M. A**., Akbar, M. A., Ali, M. Z., and Haider, M. M. (2021). The magnetorotating and parametric effects on the dust-ion-acoustic solitary waves in a dusty plasma with trapped negative ions. *Results in Physics*, 26, 104376.

5. **Salam, M. A**., Akbar, M. A., and Ali, M. Z. (2024). The effects of magnetic field, obliquity, and positively charged dust on dust-ion-acoustic subsonic solitary waves. *Indian Journal of Physics*, 98(4): 1509–1518.

Chapter One

Introduction

1.1 Historical background of plasma

The scientific term ‘plasma’ was first used by Czech physiologist Johannes Evangelist Purkinje (1787–1869) in the mid-19th century. He introduced the term plasma (which comes from the Greek word ‘πλασμα’ that means jelly or moldable substance) to describe the straw-colored and clear liquid portion of blood remaining after the elimination of numerous corpuscles (red and white cells, as well as other cellular components) from blood.

In 1927, the Nobel laureate American chemist Irving Langmuir and his colleague Lewi Tonks used this term for the first time to demonstrate the interior of a blazing ionized gas induced by an electric discharge in a tube. Their observation of electrons, ions, and impurities in an electrified fluid reminded them of blood plasma which contains red and white blood cells, and germs. Together with Tonks, Langmuir analyzed the chemistry and physics of tungsten-filament bulbs to significantly increase the filament's longevity. As a result of his work, he developed the concept of plasma sheath which refers to the boundary interface between plasma and electrodes, and discovered Langmuir waves that refer to periodic variations of the electron density in plasmas. It was the genesis of plasma physics (Richard, 2008).

1.2 Definition of plasma

In physics, plasma represents an electrically conducting ionized gas (macroscopically quasi-neutral) with a nearly equal number of positively and negatively charged particles (basically, electrons and ions). Neutral particles can also be present there depending on the temperature and density. In contrast to the solid, liquid, and gaseous forms, it is sometimes known as the fourth state of matter. Different states of matter are shown in Figure 1.1.

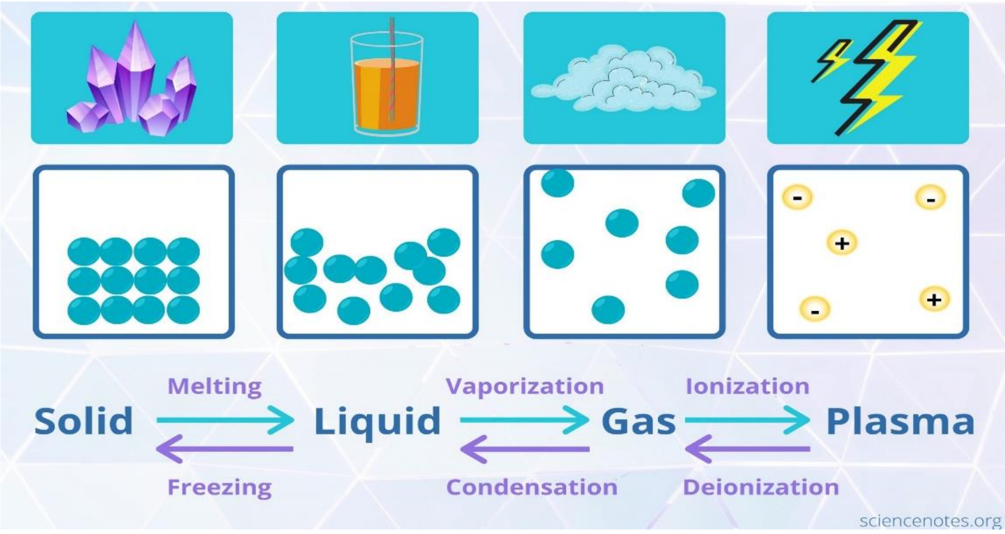

Figure 1.1: Different states of matter (Courtesy: https://sciencenotes.org/states-of-matter/)

Along with the gravitational force, which affects all of the matters, the electromagnetic forces act on a plasma, and this is the exceptionality of the plasma from other states. As electromagnetic forces act over a large distance, plasma behaves collectively, much like a fluid.

A plasma that contains charged dust particles (10^{-6} m to 10^{-9} m sized) in addition to ions and electrons is known as dusty plasma. About 99% of the matter in the space where charged dust particles are omnipresent components is in the form of plasma. The dust particles are not neutral. In response to their surrounding plasma environments, they become negatively or positively charged. A dusty plasma is also known as a complex plasma because it is subject to additional complexity due to the existence of charged dust elements (Shukla and Mamun, 2002).

Figure 1.2 exhibits some examples of plasmas, the majority of which are dusty plasmas.

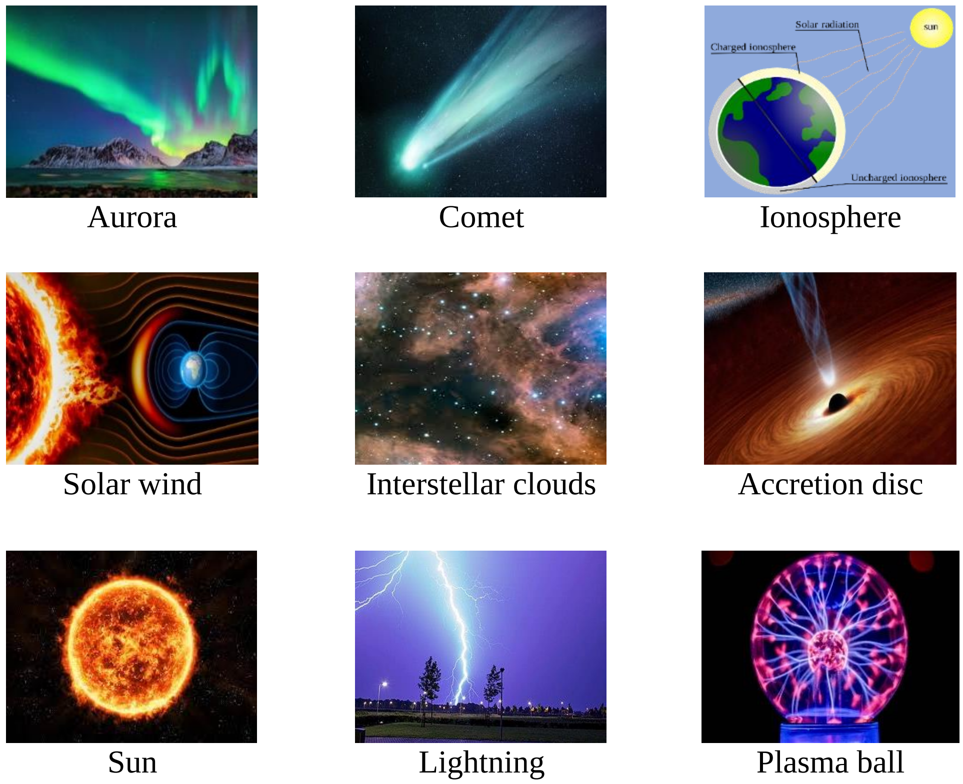

Figure 1.2: Examples of plasmas (Collected from the Internet)

1.3 Characteristics of dusty plasma

Simply speaking, plasma is electrically neutral, i.e., plasma's overall charge is zero. The charged particles contained in plasma are unbound but not free. Charges produce magnetic fields and electrical currents while traveling, and they are influenced by the fields. The main characteristics of dusty plasma are discussed below.

Similar to an electron-ion plasma, a dusty plasma is macroscopically neutral when there is no outside disturbance. This indicates that, in equilibrium without the presence of any external influences, the resultant electric charge is zero. As a result, for a dusty plasma, the charge neutrality condition at the equilibrium state is expressed as follows (Shukla and Mamun, 2002; Bittencourt, 2004):

$$q_i n_{i0} = e n_{e0} - q_d n_{d0}, \tag{1.1}$$

where n_{s0} is the number density of the species s at equilibrium state ($s = e, i, d$ refers to electrons, ions, and dust grains, respectively), $q_i = Z_i e$ is the ion charge (the ion charge state $Z_i = 1$ is used), and $q_d = Z_d e$ $(-Z_d e)$ is the charge of dust particles when the grains are positively (negatively) charged. A dust grain typically accumulates one thousand to several hundred thousand elementary charges, and $Z_d n_{d0}$ could be comparable to n_{i0}, even for $n_{d0} \ll n_{i0}$. However, in many plasma environments, the majority of background electrons may adhere to the surface of the dust grains at the time of the charging operations that may lead to a large reduction in the electron number density in the surrounding dusty plasma. So, for negatively charged dust grains, equation (1.1) becomes

$$n_{i0} \approx Z_d n_{d0}. \quad (1.2)$$

To measure the existence of plasma, Debye length is an important physical parameter. It refers to the distance over which the impact of an individual charged particle’s electric field is experienced by the other charged particles. Arrangements of charged particles shield electrostatic fields within the range of the Debye length, and this shielding is a consequence of the collective effect of the particles. Plasma exists only when the system's physical dimensions exceed the Debye length. Debye was the first to determine the shielding distance for an electrolyte. The Debye length (λ_D) is given by

$$\lambda_D = \sqrt{\frac{K_B T_e}{4\pi e^2 n_e}}. \quad (1.3)$$

The following is an explanation of Debye shielding for dusty plasma.

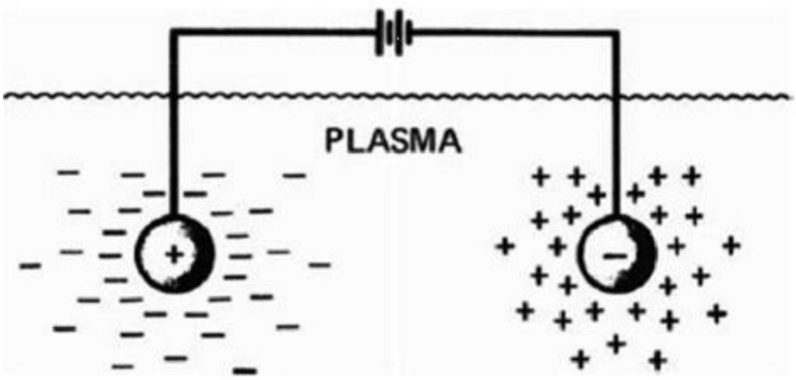

Figure 1.3: Debye shielding (Courtesy: Chen, 2015).

Consider a plasma that contains electrons, ions, and charged dust species. In the plasma, a charged ball is placed to apply an electric field. If the charged ball is positive (negative), a cloud of electrons (ions) and negatively charged dust particles (positively charged dust particles) will cover it (Figure 1.3). Further, suppose that the plasma particle recombination does not take place on the ball's surface. For a cold plasma (where charged particles are not agitated), the number of charges in the cloud and that in the ball are equal. As a result, the electric field would not exist in the plasma frame outside of the cloud, and this provides a perfect shielding. However, for finite temperatures, particles at the cloud's boundary may have sufficient thermal energy to release from the cloud. The cloud's boundary then appears at the radius where the potential energy is about equal to the particles' thermal energy. It means an imperfect shielding.

Now, the thickness of such charged cloud (sheath) will be estimated. It is considered that the potential $\varphi_s(r)$ at the center $(r = 0)$ of the cloud is φ_{s0}. Additionally, suppose that m_d/m_i is so high for which dust elements' inertia stops them from moving. A huge amount of dust particles just provides a consistent background of negative charges. Assume that electrons and ions have the following number densities.

$$n_e = n_{e0}\, e^{\left(\frac{e\varphi_s}{\kappa_B T_e}\right)}, \tag{1.4}$$

and

$$n_i = n_{i0}\, e^{\left(-\frac{e\varphi_s}{\kappa_B T_i}\right)}. \tag{1.5}$$

For the considered dusty plasma scenario, the Poisson equation can be expressed as:

$$\nabla^2\varphi_s = 4\pi(en_e - en_i - q_d n_d), \tag{1.6}$$

where n_d indicates the dust particles' number density. Using the assumption $q_d n_d = q_d n_{d0} = en_{e0} - en_{i0}$ and (1.4) - (1.5) in equation (1.6), and assuming $e\varphi_s/\kappa_B T_e \ll 1$ and $e\varphi_s/\kappa_B T_i \ll 1$, we get (Shukla and Mamun, 2002)

$$\nabla^2 \varphi_s = \left(\frac{1}{\lambda_{De}^2} + \frac{1}{\lambda_{Di}^2}\right) \varphi_s, \tag{1.7}$$

where $\lambda_{De} = \left(\frac{\kappa_B T_e}{4\pi n_{e0} e^2}\right)^{1/2}$ and $\lambda_{Di} = \left(\frac{\kappa_B T_i}{4\pi n_{i0} e^2}\right)^{1/2}$ represent the electron and ion Debye radii, respectively. Assuming $\varphi_s = \varphi_{s0}\, e^{(-r/\lambda_D)}$, we find from equation (1.7), the dusty plasma Debye radius is

$$\lambda_D = \frac{\lambda_{De}\, \lambda_{Di}}{\sqrt{\lambda_{De}^2 + \lambda_{Di}^2}}, \tag{1.8}$$

which gives the shielding distance. For a dusty plasma with negatively charged dust particles, we have $n_{eo} \ll n_{i0}$ and $T_e \geq T_i$, i.e., $\lambda_{De} \gg \lambda_{Di}$. Accordingly, we have $\lambda_D \simeq \lambda_{Di}$. In contrast, if the dust grains become positively charged, and the majority of the ions are connected to dust surface, i.e., when $T_e n_{i0} \ll\ T_i n_{e0}$, we have $\lambda_{De} \ll \lambda_{Di}$; that is $\lambda_D \simeq \lambda_{De}$.

The collective effect is another fundamental characteristic that distinguishes the behavior of plasma from that of common fluids and solids. The interaction among the particles has a substantial effect on the plasma properties. A plasma's long-range electromagnetic forces cause each charged particle to interact simultaneously with a large number of other charged particles, producing significant collective effects that lead to the wealth of physical phenomena that occur in it. A plasma exhibits collective behavior when it reacts to outside forces as a single entity. Of course, every particle experiences the force and adjusts its momentum as a result. However, if all of the particles react similarly, we can treat the reaction as a whole rather than take into account every single particle. A plasma oscillation is the most basic collective response. Plasmas can frequently be thought of as being electrically neutral because of the high mobility of electrons, which makes them ideal electrical conductors. One example of the collective behavior of plasma is the creation of a Debye shielding close to the plasma container's wall or the plasma particles encircling a test particle.

An instantaneous disturbance of plasma's equilibrium causes an internal electric field that tends to bring back the charge neutrality. The electric field develops a collective motion of particles, and it is characterized by the plasma frequency ω_p (which is the natural frequency of oscillations). For an unmagnetized dusty plasma that comprises dust particles with electrons and ions, the plasma frequency is given by the relation (Shukla and Mamun, 2002)

$$\omega_p^2 = \sum_s \frac{4\pi n_{s0} q_s^2}{m_s} = \sum_s \omega_{ps}^2 \, , \tag{1.9}$$

where $\omega_{ps} = (4\pi n_{s0} q_s^2 / m_s)^{1/2}$ gives the plasma frequency related to the elements s. The plasma frequency can be described as follows:

When plasma particles move from their equilibrium state, a space charge field is created in such a way as to draw the particles back to their original state and restore the plasma neutrality. However, they will overshoot due to their inertia, and again be drawn back to their starting places by the opposing polarity's space charge field. Once more, their inertia will lead them to overshoot, and thus, oscillate repeatedly around their equilibrium locations. Naturally, the oscillation frequency will vary depending on the particles' mass and charge, and will not be the same for all particles. For instance, electron plasma frequency (where electrons oscillate around ions) $\omega_{pe} = (4\pi n_{e0} e^2 / m_e)^{1/2}$, ion plasma frequency (where ions oscillate around dust grains) $\omega_{pi} = (4\pi n_{i0} e^2 / m_i)^{1/2}$, and dust plasma frequency (where dust particles oscillate around their equilibrium positions) $\omega_{pd} = (4\pi n_{d0} \, Z_d^2 e^2 / m_d)^{1/2}$.

1.4 Magnetized plasma

The plasma where the strong magnetic field dramatically influences the motion of charged particles is called magnetized plasma. A typical quantitative criterion of a particle is that it usually performs at least one rotation around the magnetic-field line prior to collision with other particles, i.e., $\upsilon_{ce}/\upsilon_{coll} > 1$, where υ_{ce} is the gyro-frequency of electrons and υ_{coll} is the collision rate of electrons. It frequently happens that the ions are not magnetized, whereas the electrons are. Particularly, magnetized plasma is anisotropic, which means that the plasma has different characteristics in the magnetic field's parallel and perpendicular directions. It is to be noted that if a magnetized plasma moves with velocity $\vec{v}$, then there exists an electric field $\vec{E} = -\vec{v} \times \vec{B}$ on which the Debye shielding has no effect.

Now, we will discuss the gyro-radius and gyro-frequency of the circular motion of a charged particle in a magnetic field. Suppose a charged particle is moving with velocity $\vec{v}$ under the action of a magnetic field $\vec{B}$ (Figure 1.4). In a uniform magnetic field, the gyro-radius (also known as the Larmor radius or cyclotron radius) measures the radius of the circular motion of a charged particle. In SI units, the gyro-radius is defined as

$$r_c = \frac{mv_\perp}{|q|\, B}, \tag{1.10}$$

where m is the particle mass, $v_\perp$ is the velocity component perpendicular to the magnetic field, q is the particle electric charge, and B is the magnetic field strength.

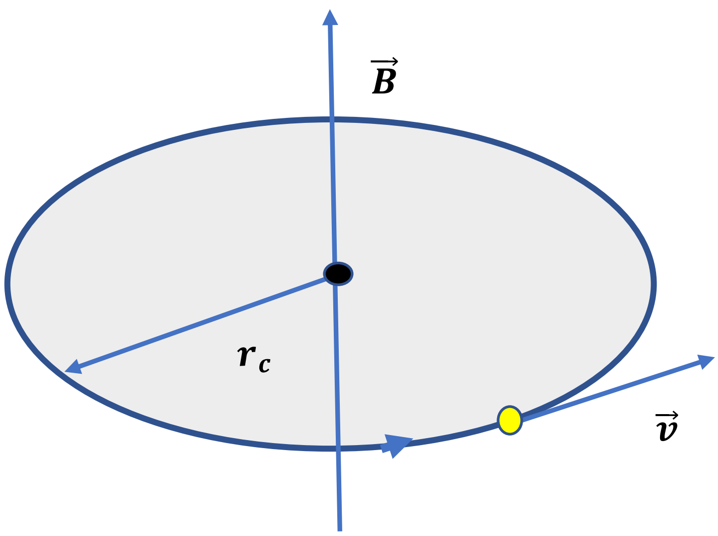

Figure 1.4: Circular motion of a charged particle (Courtesy: Wiesemann, 2014)

The angular frequency of a charged particle's circular motion is known as the gyro-frequency or cyclotron frequency, which can be represented as

$$\omega_c = \frac{|q|\, B}{m} \text{ radians /second.} \tag{1.11}$$

The gyro-frequency is dependent on the particle's mass, charge, and magnetic flux density but independent of the particle's velocity.

We know that an electron carries a negative charge (q) of 1.602 x 10^{-19} coulomb and electron mass (m) has a value of about 9.109 x 10^{-31} kg. Thus, the electron gyro-frequency is

$$\omega_c \text{ (electron)} = 1.76 \times 10^{11}\, B \text{ (rad/s).} \tag{1.12}$$

In the same way, for a proton, m = 1.673 x 10^{-27} kg. Then the proton gyro-frequency is

$$\omega_c \text{ (proton)} = 9.58 \times 10^{7}\, B \text{ (rad/s).} \tag{1.13}$$

In CGS-units, the gyro-radius $r_c = \frac{mcv_{\perp}}{|q|\, B}$ and the corresponding gyro-frequency $\omega_c = \frac{|q|\, B}{mc}$.

1.5 Classification of plasmas

Plasmas can be categorized in numerous ways based on their characteristics, including temperature, collision, degree of ionization, etc. (Banu et al., 2012).

Depending on the thermodynamic equilibrium property, plasmas can be divided into two types: nonthermal and thermal. In nonthermal plasmas or cold plasmas, the temperature of an electron is substantially higher than that of a heavy species (ions and neutrals). So, they are not in thermodynamic equilibrium. Maxwell-Boltzmann velocity distributions of electrons differ significantly from those of ions because electrons are thermalized only. In cold plasmas, ion thermal motion can be overlooked. The Earth's ionosphere is an example of a cold plasma (about 1000K). The mercury vapor gas in a fluorescent lamp is a common nonthermal plasma, where electron gas reaches 20000 K, and the remaining gases, ions, and neutral atoms remain barely above room temperature. As a result, the bulb can be touched while it is functioning. On the other hand, when the plasmas get close to local thermodynamic equilibrium, they are regarded as thermal. The term thermal plasma can also refer to hot plasma. Atmospheric arcs, sparks, and flames can produce such plasmas.

Again, the plasmas may be collisional or collisionless. If the collision mean-free-path is considerably smaller compared to the system length, the plasma system is considered collisional. The opposite scenario of collisional plasma, where the mean-free-path is bigger compared to the system length, leads to a collisionless system. In a collisionless plasma, the collisions between particles have no substantial consequence in the system.

The degree of ionization in fully ionized plasmas approaches 1 (i.e., 100%). Stellar interiors (the Sun's core) and fusion plasmas are examples of fully ionized plasmas. Many astrophysical environments contain partially ionized plasmas, such as the solar atmosphere, molecular clouds, interstellar medium, planet ionospheres, accretion disks, and cometary tails. The degree of ionization can change from very low to nearly full.

1.6 Acoustic waves in dusty plasma

Acoustic waves are longitudinal waves (which have the same vibration direction as the propagation direction) produced by the oscillations of pressure traveling through a solid, liquid, gas, or plasma. Acoustic waves travel at the same speed as sound.

Plasma physics describes the ion-acoustic wave as a longitudinal oscillation of ions and electrons. Ion-acoustic waves, however, can interact with ions' electromagnetic fields as well as collide because they move through positively charged ions. Acoustic waves and ion-acoustic waves are often used interchangeably in plasmas. Magnetized and unmagnetized plasmas both can produce ion-acoustic waves. In uniform, unmagnetized, collision-free dusty plasmas, there are two different kinds of acoustic modes, called dust-acoustic (DA) and dust-ion-acoustic (DIA).

Rao et al. (1990) made the theoretical prediction of DA waves based on the plasma constituents, such as electrons, ions, and negatively charged dust particles. The phase velocity of the DA waves is much lower than the thermal speeds of the electrons and ions. As a result, ions as well as inertia-less electrons set up equilibrium in the DA wave potential. The restoring force in the DA waves is caused by the pressures of the inertia-less electrons and ions, whereas the mass of dust supplies the inertia to maintain the waves. The dust plasma frequency is markedly higher than that of the DA waves. In many lab investigations, the DA waves were notably visible (Barkan et al., 1995; Pieper and Goree, 1996). Since the observed frequencies are in the range of 10–20 Hz, we can see them with the naked eye.

The DIA waves were anticipated by Shukla and Silin (1992). The DIA wave phase velocity is significantly lower (higher) than the electron thermal speed (ion and dust thermal speeds). In the long wavelength, the phase velocity is given by

$$\frac{\omega}{k} = \left(\frac{n_{i0}}{n_{e0}}\right)^{1/2} c_s, \tag{1.14}$$

where the ion-acoustic speed $c_s = \left(\frac{k_B T_e}{m}\right)^{1/2}$. Equation (1.14) shows that the phase velocity $\left(V_p = \frac{\omega}{k}\right)$ of the DIA waves is larger than c_s because $n_{i0} > n_{e0}$ for negatively charged dust grains. The increasing phase velocity is caused by the depletion of electron density in the background plasma, resulting in a larger electron Debye radius. Because of this, the electric field seems to be stronger, and the field enhances the phase velocity. Laboratory investigations have also shown that DIA waves exist. (Barkan et al., 1996; Nakamura et al., 1999). Typical frequencies of the DIA waves for laboratory plasma parameters are tens of kHz.

1.7 Nonlinear waves in plasma

A number of factors can lead to the development of nonlinear waves in nature or our everyday lives. Nonlinear Lorentz forces, particle trapping, ponderomotive forces, etc., are the sources of nonlinearities. Waves can be locally confined due to plasma nonlinearities, and this leads to a variety of coherent structures (such as solitary waves, shock waves, and vortices) that are interesting theoretically and experimentally. We will discuss solitary waves and shock waves here because these are our research interests.

Solitons, or solitary waves, are self-reinforcing wave packets that propagate at a constant velocity while maintaining their shapes. Waveforms can become permanent or localized as a result of dispersion and nonlinearity. Here, there is one global peak within the envelope of the wave, and the envelope decays away from it rapidly. Solitons are such nonlinear solitary waves with the additional property of retaining their own structure, even when they interact with other solitons. Due to certain nonlinear phenomena that counteract dispersive effects, solitons typically travel across long distances without dissipating. For instance, two propagating solitons that move in different directions can properly cross each other without breaking.

In accordance with Drazin and Johnson (1989), solitons possess three properties: (i) they possess a permanent form; (ii) they persist within a region; and (iii) they can interact with other solitons and remain unchanged, except for phase shifts.

The soliton phenomenon was first described by John Scott Russell (1808–1882) in 1834 while he was observing a solitary wave in the Union Canal in Scotland. Solitons originate from a broad class of weakly nonlinear dispersive PDEs, such as Korteweg-de Vries (KdV) and KdV-type equations that describe such physical systems.

A shock wave, often known as a shock, is a kind of disturbance that propagates throughout a medium faster than local sound speed. The cancellation of nonlinear and dissipative effects results in shock waves. Similar to a normal wave, a shock wave carries energy, and can travel through a plasma medium. An abrupt change in the temperature, pressure, and density of the medium may be the cause of creating a shock wave. The Burgers or Burgers-type equations are generally used to describe shock waves.

1.8 Governing equations

DIA waves are generally described by the KdV equation, Burgers equation, KdV, or Burgers-type equations, and these equations are deduced from some governing equations by the reductive perturbation technique. For a magnetized plasma system that consists of adiabatic ions, Maxwellian electrons, and positively charged dust particles, the dynamic of the DIA wave is designated generally by the continuity, momentum, energy, and Poisson equations. The equations are discussed below:

The continuity equation describes how a fluid conserves mass by maintaining a constant rate of mass leaving and entering a fluid system. For the considered plasma system, the continuity equation is of the form

$$\frac{\partial n_i}{\partial t} + \nabla \cdot (n_i \vec{u}_i) = 0, \tag{1.15}$$

and describes the conservation of charge. Here, n_i indicates the ion number density.

Newton's second law of motion for a plasma fluid element is reduced to the following momentum equation:

$$\frac{\partial \vec{u}_i}{\partial t} + (\vec{u}_i \cdot \nabla)\vec{u}_i = -\frac{1}{m_i\, n_i}\nabla p_i - \frac{e}{m_i}\nabla\psi + \omega_{ci}\,(\vec{u}_i \times \hat{x}), \tag{1.16}$$

where m_i is the ion mass, p_i is the pressure, $\omega_{ci} = \frac{e\, B_0}{m\, c}$ is the ion gyro-frequency, and $\vec{B} = B_0\hat{x}$. The pressure gradient force $-\nabla p_i$ pushes plasma from high-pressure area to low-pressure area. The last two terms of the right side of the equation (1.16) are electric and magnetic forces, respectively, and are known as the Lorentz force together.

Equation (1.16) illustrates the theory of conservation of momentum. All external forces acting on a micro-unit in a flow field result in the same rate of change in its total momentum.

Again, the following is the form of the energy equation.

$$\frac{\partial p_i}{\partial t} + (\vec{u}_i \cdot \nabla)p_i + \gamma p_i \, \nabla \cdot \vec{u}_i = 0. \tag{1.17}$$

The equation represents the conservation of energy. According to this equation, a moving fluid's entry rate of energy depends on how much work it does in its surroundings and how much energy it accumulates inside the fluid.

And, the mathematical form of the Poisson equation is

$$\nabla^2 \psi = 4\pi e(n_e - n_i - Z_d n_{d0}), \tag{1.18}$$

where ψ is the potential energy per unit charge, and the right side of (1.18) gives the source of the field. The equation amounts to finding the electric potential for a charge distribution.

1.9 Stretched coordinates

Stretched coordinates enable one to perceive more clearly what occurs at various time or distance scales. For instance, even though a boundary layer is typically thin, a lot of events occur there. Coordinate stretching cannot be accomplished with a single method. It is an "art" that needs more practice. In 1965, Gardner and Morikawa (1965) proposed the use of space- and time-stretching coordinates, and transformed the quantum hydrodynamics equations into a solvable evolution equation. The stretched coordinates reduce the magneto-hydrodynamic equation to a solvable equation, and its asymptotic solution describes a weakly nonlinear wave. Physically, it demonstrates that localized excitations can be produced when weak nonlinearity, dispersion, and dissipation effects are balanced over a long period and long distances.

1.10 The reductive perturbation technique

Taniuti and Wei (1968) established the reductive perturbation technique for the evolution of nonlinear small amplitude waves. This method is very suitable for developing a simplified model that describe nonlinear wave propagation and interaction. The scheme allows state variables that are extended around equilibrium states through a smallness parameter ($\varepsilon \ll 1$), which corresponds to a weak perturbation effect. The method can produce a variety of nonlinear equations, including KdV, modified Korteweg-de Vries (mKdV), KdV-Burgers, and Burgers equations, which can admit various types of coherent excitations.

1.11 Different particle distributions

Particle distribution functions are frequently used in plasma physics for describing wave-particle interactions. Additionally, distribution functions are employed in nuclear physics, plasma physics, fluid mechanics as well as statistical mechanics.

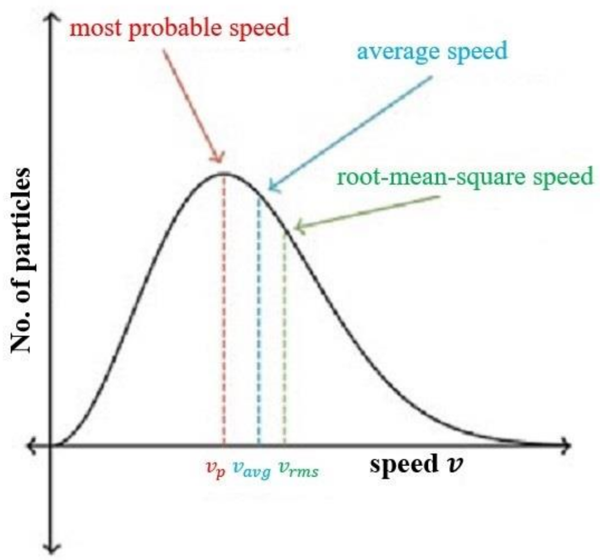

Figure 1.5: Maxwell-Boltzmann distribution (Courtesy: www.khanacademy.org)

The Maxwell-Boltzmann distribution shows how the speeds of particles are distributed. A velocity distribution is a slightly asymmetrical curve that results from plotting the proportion of particles whose velocities fall within a set of constrained ranges. The most probable velocity would fall within the range of the peak of this curve. This velocity distribution curve is known as the Maxwell-Boltzmann distribution. The Maxwell-Boltzmann distribution is often represented by the graph depicted in Figure 1.5.

In fluid dynamics, vortices are regions in fluids where the flow revolves around a straight or curved axis line. For example, tornados and whirlpools are vortices. Figure 1.6 shows a vortex-like distribution of some particles.

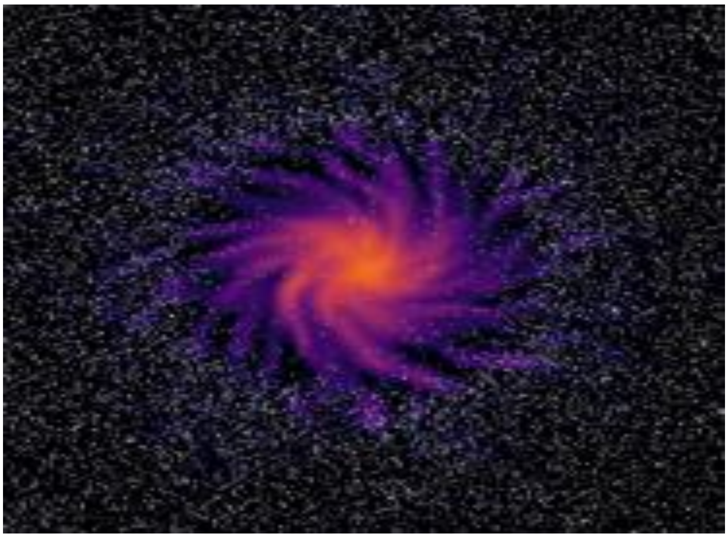

Figure 1.6: Vortex-like distribution of particles
(Courtesy*:* Shuai and Kasbaoui, 2022).

Chapter Two

Literature review and thesis outline

2.1 Introduction

Dusty plasmas, which contain charged dust particles in addition to ions and electrons, are frequently observed in space. Plasma systems get more complex when dust particles are present. For instance, they can make a modification to the existing low-frequency waves as well as introduce new kinds of dusty waves (Shukla and Mamun, 2002). In recent decades, a number of physicists have shown considerable interest in investigating solitary and shock waves that are produced by the dominating effects of dispersive and dissipative terms, respectively.

Different types of forces (such as the Lorentz force, the Coriolis force, etc.) and plasma parameters affect the salient nature of the waves. Nowadays, plasma researchers are much interested in investigating these effects on the wave characteristics. Numerous theoretical and experimental works on the DIA solitary and shock waves have been conducted in magnetized plasma systems (sometimes, the systems are considered rotating) while the particles are distributed in different manners.

Besides, the consideration of higher-order nonlinear and dispersive (or dissipative) effects is significant in order to reduce the discrepancy between theoretical predictions and practical results. On the other hand, the inspections of the dynamic behaviors and overtaking collisions of multi-solitons and multi-shocks in plasmas are recent hot topics.

The main purpose of addressing this chapter is to discuss the literature review of relevant works, the research objectives, and the thesis framework.

2.2 Literature review

Dust particles (negatively or positively charged) are omnipresent species of the dusty plasmas, and the particles introduce new kinds of low-frequency dust-related waves, such as DA waves, DIA waves, DA solitary or shock waves, and DIA solitary or shock waves (Shukla and Mamun, 2002). Tonks and Langmuir (1929) were the first to predict the occurrence of ion-acoustic (IA) waves in a plasma, and it was verified experimentally by Revans (1933). The propagating nature of IA waves were studied by several researchers both theoretically and experimentally (Ullah et al., 2020-a; Singh et al., 2021). Shukla and Silin (1992) predicted the DIA waves, and then Barkan et al. (1996) and Nakamura et al. (1999) observed their existence experimentally. Nonlinearity leads to various types of waves (namely, solitary waves, shock waves, vortices, etc.). Numerous theoretical studies on DIA solitary and shock waves were conducted by numerous plasma researchers while the dust particles were taken as positively or negatively charged (Mamun and Shukla, 2009-a; Alinejad, 2010; Yasmin et al., 2013; Kaur and Saini, 2018; Islam et al., 2019; Boro et al., 2021; Kamran et al., 2021; Khan et al., 2022). Solitary waves occur when the dispersive and nonlinear terms balance each other, whereas shock waves take place due to the cancellation of the dissipative and nonlinear terms.

Researchers are currently working to improve their research findings, and they seek to incorporate a variety of effects, such as the magnetic effect, adiabatic effect, etc., into the plasma model because these effects have a key role in the change of nonlinear wave natures (Haider et al., 2020; Sultana, 2021; Salam et al., 2021). Atteya et al. (2018) inspected the effect of the super-thermality of electrons as well as the impacts of ion temperature and number density on the DIA solitary waves. Pakzad and Javidan (2022) studied the characteristics of DIA solitary waves under the impact of a non-uniform magnetic field. Anowar and Mamun (2008) examined the characteristics of DIA solitary waves in hot adiabatic magnetized dusty plasma containing negatively charged static dust particles. Recently, many researchers (Nobaha and Pakzad, 2019; Rahman and Haider, 2019; Islam et al., 2019; Haider et al., 2020; Abdelsalam, 2021; Younsi et al., 2022; Ghasemloo, 2022; Halder et al., 2022) have investigated DIA solitary or shock waves theoretically in magnetized and adiabatic plasma systems.

The KdV or mKdV equation is often used to describe the dynamics of solitary waves, whereas the Burgers or modified Burgers equation is used to describe shock wave properties. These equations contain lower-order nonlinear and dispersive (or dissipative) terms. But, with the help of the above equations, theoretical predictions on the nature of the waves vary with experimental observations (Ikezi, 1973; Watanable, 1978). As a consequence, a number of plasma researchers examined the higher-order nonlinear and dispersive or dissipative effects on the solitary as well as shock waves in order to get better results (Kodama and Taniuti, 1978; Lai, 1979; Esfandyari et al., 2008; Mehdipoor and Esfandyari, 2012; Hossen et al., 2014; El-Labany et al., 2014; Kaur et al., 2021; Abdelwahed, 2015; Ferdousi et al., 2015; El-Monier and Atteya, 2019; Ahmed et al., 2020; Mahmood et al., 2021; Fayad et al., 2021; Paul et al., 2021). The reductive perturbation technique is used to add the higher-order effects, and this type of inclusion yields the higher-order KdV-type or mKdV-type inhomogeneous equation (for solitary waves) and the Burgers-type or modified Burgers-type inhomogeneous equation (for shock waves). The re-normalization technique of Kodama and Taniuti (1978) is used for finding higher-order solutions or dressed solutions. Lai (1979) studied the higher-order impact on IA waves propagated in a plasma containing warm ions and hot electrons. Paul et al. (2021) examined the higher-order nonlinear and dispersive effects on IA solitary waves in a degenerate plasma. El-Labany et al. (2014), Hossen et al. (2014), and El-Monier et al. (2019) investigated the salient nature of DIA shock in degenerate dense and quantum plasmas. Moreover, Abdelwahed (2015) and Kaur et al. (2021) examined the higher-order nonlinear and dissipative effects on shocks in the auroral zone and white dwarfs, respectively.

Like the Lorentz force, the Coriolis force also changes the nature of DIA waves. Chandrasekhar (1953), for the first time, described the vital role of the Coriolis force in cosmic phenomena. The finding of Chandrasekhar was supported by Lehnert (1954) who found that the Coriolis force impacts the sun's magneto-hydrodynamic waves. Researchers have recently become interested in the study of magneto-rotating flows as well as their numerous applications. In space plasmas, such as gas cloud formation, pulsar radiations, fusion devices, etc., the magneto-rotating effect can be observed. A theoretical investigation on a strongly magnetized and rotating plasma containing fluid ions, charged dust species, superthermal electrons, and positrons was studied by Saini et al. (2016). A four-component magneto-rotating dusty plasma with opposite-polarity dust was investigated using the concepts of one-fluid and two-fluid models by Farooq and Ahmad (2017). Kaur and Saini (2018) inspected DIA shocks in a magneto-rotating plasma containing non-extensive electrons and positrons, and negatively charged dust particles. Moreover, Singh et al. (2019) studied solitary waves in a magneto-rotating plasma with Kappa-Cairns distributed electrons, whereas Mehdipoor and Asri (2021) studied the same types of waves in a degenerate relativistic magneto-rotating quantum plasma.

In various plasma phenomena (chemical reactions, volcanic eruptions, information technology, etc.), multi-solitons and multi-shocks were observed experimentally (Chan et. al., 1981; Reed et al., 2003; Harvey et al., 2010; Medici and Waite, 2016; Boruah et al., 2016; Tang et al., 2021). Only the completely integrable partial differential equations give multi-soliton or multi-shock solutions, and a variety of physical systems are described by the solutions (Wazwaz, 2010). In the area of integrable systems and soliton (or shock) theory, the research importance of exact solutions and the integrability of non-linear partial differential equations (NLPDEs) has grown in recent years (Biazar and Ghazvini, 2009; Zhang et al., 2018; Wang and Wang, 2018; Ma et al., 2018; Wang et al., 2019; Ren et al., 2019; Gharib et al., 2021; Alimirzaluo et al., 2021). Among the existing methods for multi-soliton or multi-shock solutions (Hirota, 2004; Griffiths, 2012; Kumar and Mohan, 2021; Kumar and Mohan, 2022; Alsayyed et al., 2016; Chen et al., 2019; Ullah et al., 2020-b; Ismael et al., 2020), the Hirota bilinear method is the most used, but it requires a bilinear transformation that may be challenging for some equations. To remove this complexity, Hereman and Zhuang (1991) introduced a simplified form of the Hirota bilinear method, namely the simplified Hirota bilinear method which was used by numerous researchers to examine several higher-order nonlinear equations (Wazwaz, 2016; Wazwaz, 2021-a; Wazwaz, 2021-b).

2.3 Objectives of the thesis

This section explores the research objectives that we find from the gaps in the previous works, and it plays a key role in conducting the present research work.

We have examined the combined effect of the magnetic field, obliquity, and higher-order terms on the characteristics of the DIA subsonic solitary waves propagated in an electron-ion-PCD plasma. To the best of our knowledge, no such investigation on the three-dimensional electron-ion-PCD plasma system has been done yet.

Again, taking magnetic and adiabaticity effects into account, we have contemplated a new three-dimensional plasma system containing adiabatic positive ions (which are mobile), trapped light ions (negatively charged), arbitrarily charged dust particles, and isothermal electrons. For this plasma model, the higher-order nonlinear and dispersive effects have been inspected for the first time.

Moreover, we have investigated the higher-order nonlinear effect on the shock waves by deriving the modified Burgers-type inhomogeneous equation while the magnetized dusty plasma contains trapped electrons along with positive ions and negatively charged dust particles. As far as we know, the plasma system under consideration has not yet undergone the same research.

We have considered the Coriolis force into a magnetized plasma system that contains adiabatic positive mobile ions, negative trapped ions, Maxwellian electrons, and arbitrarily charged dust particles. This type of consideration has made the system magneto-rotating. For the first time, the overall impact of an external magnetic field, oblique rotation, electrons, and dust concentration on such plasma has been examined.

Using multiple regular soliton and shock solutions, the nature of multi-solitons and multi-shocks in a magnetized dusty plasma (wherein species are positive ions, Maxwellian electrons and positrons, and stationary negatively charged dust particles) has been investigated. To the best of our knowledge, we use the simplified Hirota method for the first time for such a plasma model.

2.4 Outline of the thesis

The dissertation entitled "**Intrinsic features of nonlinear waves in dusty plasmas**" has been divided into eight chapters. The first two chapters are devoted to an introductory discussion, a literature review, and an outline of the thesis work. We have discoursed the main research work in chapter three to chapter seven, while the results and discussion, and summary of the results have been included at the end of the corresponding chapter. The research topics discussed in different chapters are given below:

In chapter one, the historical background of plasma, definitions of important terms, and some topics relevant to this work have been discussed. **In chapter two,** the brief literature review, objectives of the thesis, and chapter-wise work plan have been included.

In chapter three, we have investigated the higher-order nonlinear and dispersive effects on the structures of the DIA subsonic solitary waves propagated in an electron-ion-PCD plasma. Besides, the magnetic, obliquity, and different parametric effects have been examined. **In chapter four**, we have examined how the fundamental characteristics of DIA solitary waves in a magnetized adiabatic dusty plasma are affected by higher-order nonlinear and dispersive phenomena. **In chapter five**, the higher-order nonlinear effect on DIA shock waves has been inspected. The parametric effects on the shock nature have also been investigated.

In chapter six, we have investigated the combined impact of magnetic field and plasma rotation on the nonlinear structures of DIA solitary waves in a magneto-rotating dusty plasma. **In chapter seven,** we have examined the dynamic behavior of multi-solitons and multi-shocks in a magnetized dusty plasma. Moreover, the effects of the magnetic field, electron and positron concentrations on the multi-solitons and multi-shocks have been examined.

In the last chapter, we have come to the conclusion of the whole thesis with a brief discussion. Besides, some proposals have been proposed for conducting future research, and we expect that these will develop the present work.

Chapter Three

Effects of magnetic field, obliquity, and higher-order nonlinear and dispersive terms on DIA subsonic solitary waves

3.1 Introduction

The DIA solitary waves are low-frequency waves in which the mass density of the ions provides the inertia and the thermal pressure of the electrons provides the restoring force. Here, the dust particles acquire electrical charges by collecting the electrons and ions from plasmas, and maintain the plasma neutrality. The presence of positively charged dust (PCD) particles makes the plasma systems more complex and alters the behavior of the plasmas significantly (Mamun, 2021; Mamun and Mannan, 2021). The various types of wave phenomena, namely solitary waves (solitons), shocks, double layers, etc., may be propagated in dusty plasmas. Solitary waves are produced when dispersion and nonlinearity balance each other. The characteristics of DIA solitary waves were elaborately investigated both in unmagnetized and magnetized plasma systems by several plasma researchers (Haider and Nahar, 2017; Atteya et al., 2018; Rahman and Haider, 2019; Khalid et al., 2021; Abdikian and Eghbali, 2022; Pakzad and Javidan, 2022; Halder et al., 2022). They discussed the effects of plasma parameters on the wave structures in various dusty plasma systems where electrons are super-thermal, Kaniadakis distributed, non-extensive, or trapped.

To describe the features of DIA solitary waves, Maxwellian distributed electrons were considered in different dusty plasma systems (Kourakis and Shukla, 2003; Ma et al., 2013). There are numerous environments in space, such as Earth's mesosphere, cometary tails, Jupiter's magnetosphere, etc., where PCD species have been identified (Horányi et al., 1993; Horányi, 1996; Tsintikidis et al., 1996; Mendis et al., 2004). The three main ways that make the dust species positively charged are: (a) photo-emission of electrons from the dust surface caused by a photon flux (Rosenberg et al., 1996), (b) thermionic emission of electrons from the dust grain surface by intense radiative heating (Rosenberg and Mendis, 1995), and (c) secondary emission of electrons from the dust surface by the influence of highly energetic plasma particles (Chow et al., 1993). Besides, positively charged dust particle contributions to the form of IA subsonic solitary waves (in which wave velocities are smaller than sound velocity) in a one-dimensional unmagnetized plasma system containing PCD species have been discussed very recently by Mamun (2021).

The IA solitary waves are typically described by the KdV or mKdV equation. The equations, which contain lower-order nonlinear and dispersion terms, explain solitary waves of smaller amplitudes. However, the soliton descriptions for any of the IA waves vary with the results of the experimental studies (Ikezi, 1973; Watanable, 1978). As a result, some researchers investigated higher-order nonlinear effects on solitary waves in various plasmas in order to decrease the discrepancy between theoretical predictions and practical results (Kodama and Taniuti, 1978; Lai, 1979; Esfandyari et al., 2008; Mehdipoor and Esfandyari, 2012; Ferdousi et al., 2015; Ahmed et al., 2020; Mahmood et al., 2021; Fayad et al., 2021; Paul et al., 2021). They added higher-order terms by expanding the usage of the reductive perturbation method. Higher-order KdV-type or mKdV-type inhomogeneous differential equations are found in this context. The solutions to these examined equations (referred to as the dressed solutions) are found by the re-normalization technique of Kodama and Taniuti (1978).

This chapter focuses on examining the influence of the magnetic field, obliquity, and stationary PCD species on the characteristics of the DIA subsonic solitary waves of small amplitudes. Moreover, the higher-order effect (nonlinear and dispersive terms) on the subsonic waves propagated in the considered three-dimensional plasma system is examined. To the best of our knowledge, no such investigation on the considered electron-ion-PCD plasma system has been done by the KdV-type equation.

3.2 Plasma model

We contemplate a three-dimensional magnetized plasma system that comprises positive ions (mobile), electrons (Maxwellian distributed), and dust particles (stationary and positively charged). Thus, in such an electron-ion-PCD plasma system (where $\vec{B} = B_0\hat{z}$), the nonlinear evolution of the DIA solitary waves is guided by the following equations:

$$\frac{\partial n_i}{\partial t} + \nabla \cdot (n_i \vec{u}_i) = 0, \tag{3.1}$$

$$\frac{\partial \vec{u}_i}{\partial t} + (\vec{u}_i \cdot \nabla)\vec{u}_i = -\frac{e}{m_i}\nabla\psi + \omega_{ci}\,(\vec{u}_i \times \hat{z}), \tag{3.2}$$

$$\nabla^2\psi = 4\pi e(n_e - n_i - Z_d n_{d0}), \tag{3.3}$$

where n_s denotes the number density of plasma species s (here $s = i$ and e refer to positive ions and electrons, respectively), u_i is the positive ion fluid speed, $\omega_{ci} = \frac{eB_0}{m_i c}$ is the positive ion gyro-frequency, m_i is the mass of positive ions, ψ is the wave potential, and Z_d is the electron number inhabiting on the uppermost layer of stationary dust grains.

It is assumed that electrons obey the Maxwellian distribution of the form (Kourakis and Shukla, 2003; Ma et al., 2013)

$$n_e = n_{e0}\, e^{\frac{e\psi}{K_B T_e}}. \tag{3.4}$$

The following notational modifications can be used to convert equations (3.1) - (3.4) to a normalized form.

$$\tilde{n}_s \equiv \frac{n_s}{n_{s0}}\ (s = i, e),\ \ \tilde{t} \equiv \frac{t}{\omega_{pi}^{-1}\left(=\sqrt{\frac{m_i}{4\pi e^2 n_{i0}}}\right)},\ \ \tilde{r} \equiv \frac{r}{\lambda_D\left(=\sqrt{\frac{K_B T_e}{4\pi e^2 n_{i0}}}=\frac{C_{si}}{\omega_{pi}}\right)},$$

$$\tilde{u}_i \equiv \frac{u_i}{C_{si}\left(=\sqrt{\frac{K_B T_e}{m_i}}\right)},\quad \tilde{\psi} \equiv \frac{\psi}{\frac{K_B T_e}{e}},\quad \widetilde{\omega}_{ci} \equiv \frac{\omega_{ci}}{\omega_{pi}\left(=\sqrt{\frac{4\pi e^2 n_{i0}}{m_i}}\right)}. \tag{3.5}$$

The normalized form of (3.1) - (3.3) is as follows:

$$\frac{\partial \tilde{n}_i}{\partial \tilde{t}} + \widetilde{\nabla}\cdot(\tilde{n}_i\,\tilde{u}_i) = 0, \tag{3.6}$$

$$\frac{\partial \tilde{u}_i}{\partial \tilde{t}} + \left(\tilde{u}_i\cdot\widetilde{\nabla}\right)\tilde{u}_i = -\widetilde{\nabla}\widetilde{\psi} + \widetilde{\omega}_{ci}\,(\tilde{u}_i \times \hat{z}), \tag{3.7}$$

$$\widetilde{\nabla}^2\widetilde{\psi} = \tilde{n}_e\mu_e - \tilde{n}_i - \mu_d, \tag{3.8}$$

where $\mu_e = \frac{n_{e0}}{n_{i0}}$ and $\mu_d = \frac{Z_d n_{d0}}{n_{i0}}$.

Similarly, the normalized form of the distribution of electron number density is (where $\tilde{\psi} \ll 1$)

$$\tilde{n}_e = e^{\widetilde{\psi}}. \tag{3.9}$$

The variables denoted by tildes in equations (3.6) - (3.9) are all dimensionless, and thus, the equations also are in dimensionless form. The tildes are omitted below for simplicity, while all the quantities are considered dimensionless. The charge neutrality condition is $n_{e0} = n_{i0} + Z_d n_{d0}$, and hence $\mu_e = 1 + \mu_d$.

3.3 Derivation of the KdV-type equation

The formulation of the KdV-type equation is a crucial task of this section since the various effects cause the plasma system to be complex. The stretched coordinates are chosen as follows (Esfandyari et al., 2008, Mamun, 2021):

$$\xi = \epsilon^{1/2}\,(l_x x + l_y y + l_z z - V_0 t)\ \text{ and }\ \tau = \epsilon^{3/2} t, \tag{3.10}$$

where ϵ is the dimensionless parameter ($0 < \epsilon < 1$) that indicates the strength of the nonlinearity of the system; l_x, l_y, l_z are the direction cosines of the wave vector $\vec{k}$, i.e.,

$l_x^2 + l_y^2 + l_z^2 = 1$ and $l_z = \frac{\vec{k}\cdot\hat{z}}{k} = cos\theta$, where θ is the angle between the directions of the wave propagation and the external magnetic field, and V_0 is the phase speed of the wave.

The extended form of the perturbed quantities n_i, u_{ix}, u_{iy}, u_{iz}, and ψ in terms of ϵ is (Ferdousi et al., 2015; Atteya et al., 2018):

$$n_i = 1 + \epsilon\, n_i^{(1)} + \epsilon^2\, n_i^{(2)} + \epsilon^3\, n_i^{(3)} + \cdots, \tag{3.11}$$

$$u_{ix} = \epsilon^{3/2}\, u_{ix}^{(1)} + \epsilon^2\, u_{ix}^{(2)} + \epsilon^{5/2}\, u_{ix}^{(3)} + \cdots, \tag{3.12}$$

$$u_{iy} = \epsilon^{3/2}\, u_{iy}^{(1)} + \epsilon^2\, u_{iy}^{(2)} + \epsilon^{5/2}\, u_{iy}^{(3)} + \cdots, \tag{3.13}$$

$$u_{iz} = \epsilon\, u_{iz}^{(1)} + \epsilon^2\, u_{iz}^{(2)} + \epsilon^3\, u_{iz}^{(3)} + \cdots, \tag{3.14}$$

$$\psi = \epsilon\, \psi^{(1)} + \epsilon^2 \psi^{(2)} + \epsilon^3 \psi^{(3)} + \cdots. \tag{3.15}$$

As the magnetic field induces anisotropy, u_{ix} and u_{iy} appear at higher-order in ϵ than u_{iz}, which implies that the positive-ion gyro motion is measured as a higher-order effect.

Now, we put (3.9) - (3.15) into (3.6) - (3.8), and collect the terms in analogous powers of ϵ. Equating the coefficients of $\epsilon^{3/2}$ from the continuity and momentum equations, and the coefficient of ϵ from the Poisson equation, we obtain

$$l_z \frac{\partial u_{iz}^{(1)}}{\partial \xi} - V_0 \frac{\partial n_i^{(1)}}{\partial \xi} = 0, \tag{3.16}$$

$$-\omega_{ci}\, u_{iy}^{(1)} + l_x \frac{\partial \psi^{(1)}}{\partial \xi} = 0, \tag{3.17}$$

$$\omega_{ci}\, u_{ix}^{(1)} + l_y \frac{\partial \psi^{(1)}}{\partial \xi} = 0, \tag{3.18}$$

$$-V_0\, \frac{\partial u_{iz}^{(1)}}{\partial \xi} + l_z \frac{\partial \psi^{(1)}}{\partial \xi} = 0, \tag{3.19}$$

$$n_i^{(1)} - \mu_e \psi^{(1)} = 0. \tag{3.20}$$

Hence, the first-order expressions are obtained from (3.16) - (3.20) as

$$u_{ix}^{(1)} = -\frac{l_y}{\omega_{ci}} \frac{\partial \psi^{(1)}}{\partial \xi},\; u_{iy}^{(1)} = \frac{l_x}{\omega_{ci}} \frac{\partial \psi^{(1)}}{\partial \xi},\; u_{iz}^{(1)} = \frac{l_z}{V_0} \psi^{(1)},\; n_i^{(1)} = \mu_e \psi^{(1)}. \tag{3.21}$$

And the phase speed is determined as

$$V_0 = \frac{l_z}{\sqrt{1+\mu_d}}\,. \tag{3.22}$$

Equating the coefficients of ϵ^2 from the x and y-components of the momentum equation, and the Poisson equation, we get

$$\omega_{ci} u_{ix}^{(2)} - V_0 \frac{\partial\, u_{iy}^{(1)}}{\partial \xi} = 0, \tag{3.23}$$

$$-\omega_{ci} u_{iy}^{(2)} - V_0 \frac{\partial\, u_{ix}^{(1)}}{\partial \xi} = 0, \tag{3.24}$$

$$\frac{\partial^2 \psi^{(1)}}{\partial \xi^2} - \mu_e \psi^{(2)} - \frac{\mu_e}{2}\left[\psi^{(1)}\right]^2 + n_i^{(2)} = 0. \tag{3.25}$$

Equations (3.23) - (3.25) yield $u_{ix}^{(2)}$, $u_{iy}^{(2)}$, and $n_i^{(2)}$, respectively, as

$$u_{ix}^{(2)} = \frac{l_x V_0}{\omega_{ci}^2} \frac{\partial^2 \psi^{(1)}}{\partial \xi^2}, \tag{3.26}$$

$$u_{iy}^{(2)} = \frac{l_y V_0}{\omega_{ci}^2} \frac{\partial^2 \psi^{(1)}}{\partial \xi^2}, \tag{3.27}$$

and

$$n_i^{(2)} = \mu_e \psi^{(2)} - \frac{\partial^2 \psi^{(1)}}{\partial \xi^2} + \frac{\mu_e}{2}\left[\psi^{(1)}\right]^2. \tag{3.28}$$

Similarly, the following equations are obtained by equating the coefficients of $\epsilon^{5/2}$ from the continuity equation and the z-component of the momentum equation.

$$\frac{\partial n_i^{(1)}}{\partial \tau} - V_0 \frac{\partial\, n_i^{(2)}}{\partial \xi} + l_x \frac{\partial u_{ix}^{(2)}}{\partial \xi} + l_y \frac{\partial u_{iy}^{(2)}}{\partial \xi} + l_z \frac{\partial u_{iz}^{(2)}}{\partial \xi} + l_z \frac{\partial}{\partial \xi}\left(n_i^{(1)} u_{iz}^{(1)}\right) = 0, \tag{3.29}$$

$$\frac{\partial u_{iz}^{(1)}}{\partial \tau} - V_0 \frac{\partial u_{iz}^{(2)}}{\partial \xi} + l_z \frac{\partial \psi^{(2)}}{\partial \xi} + l_z u_{iz}^{(1)} \frac{\partial u_{iz}^{(1)}}{\partial \xi} = 0. \tag{3.30}$$

The equation (3.30) gives

$$\frac{\partial u_{iz}^{(2)}}{\partial \xi} = \frac{l_z}{V_0} \frac{\partial \psi^{(2)}}{\partial \xi} + \frac{l_z}{V_0^2} \frac{\partial \psi^{(1)}}{\partial \tau} + \frac{l_z^3}{V_0^3} \psi^{(1)} \frac{\partial \psi^{(1)}}{\partial \xi}. \tag{3.31}$$

Now, putting the second-order terms $u_{ix}^{(2)}$, $u_{iy}^{(2)}$, $n_i^{(2)}$, and $\frac{\partial u_{iz}^{(2)}}{\partial \xi}$ in (3.29), we obtain

$$\mu_e \frac{\partial \psi^{(1)}}{\partial \tau} - V_0 \left(\mu_e \frac{\partial \psi^{(2)}}{\partial \xi} - \frac{\partial^3 \psi^{(1)}}{\partial \xi^3} + \mu_e \psi^{(1)} \frac{\partial \psi^{(1)}}{\partial \xi}\right) + \frac{l_x^2 V_0}{\omega_{ci}^2} \frac{\partial^3 \psi^{(1)}}{\partial \xi^3} + \frac{l_y^2 V_0}{\omega_{ci}^2} \frac{\partial^3 \psi^{(1)}}{\partial \xi^3} +$$

$$l_z\left(\frac{l_z}{V_0}\frac{\partial\psi^{(2)}}{\partial\xi}+\frac{l_z}{V_0^2}\frac{\partial\psi^{(1)}}{\partial\tau}+\frac{l_z^3}{V_0^3}\psi^{(1)}\frac{\partial\psi^{(1)}}{\partial\xi}\right)+\frac{2\mu_e l_z^2}{V_0}\psi^{(1)}\frac{\partial\psi^{(1)}}{\partial\xi}=0.$$

$$\Rightarrow\ 2\mu_e\frac{\partial\psi^{(1)}}{\partial\tau}+\left(\frac{l_z^4}{V_0^3}-\mu_e V_0+\frac{2l_z^2\mu_e}{V_0}\right)\psi^{(1)}\frac{\partial\psi^{(1)}}{\partial\xi}+V_0\left(1+\frac{l_x^2+l_y^2}{\omega_{ci}^2}\right)\frac{\partial^3\psi^{(1)}}{\partial\xi^3}=0.$$

$$\Rightarrow\ \frac{\partial\psi^{(1)}}{\partial\tau}+\frac{3l_z}{2\mu_e^{1/2}}\left(\mu_e-\frac{1}{3}\right)\psi^{(1)}\frac{\partial\psi^{(1)}}{\partial\xi}+\frac{l_z}{2\mu_e^{3/2}}\left(1+\frac{1-l_z^2}{\omega_{ci}^2}\right)\frac{\partial^3\psi^{(1)}}{\partial\xi^3}=0.$$

$$\Rightarrow\ \frac{\partial\psi^{(1)}}{\partial\tau}+\frac{3l_z}{2(1+\mu_d)^{1/2}}\left(\mu_d+\frac{2}{3}\right)\psi^{(1)}\frac{\partial\psi^{(1)}}{\partial\xi}+\frac{l_z}{2(1+\mu_d)^{3/2}}\left(1+\frac{1-l_z^2}{\omega_{ci}^2}\right)\frac{\partial^3\psi^{(1)}}{\partial\xi^3}=0.$$

$$\Rightarrow\ \frac{\partial\psi^{(1)}}{\partial\tau}+\delta_1\psi^{(1)}\frac{\partial\psi^{(1)}}{\partial\xi}+\delta_2\frac{\partial^3\psi^{(1)}}{\partial\xi^3}=0, \tag{3.32}$$

where $\delta_1=\frac{3l_z}{2(1+\mu_d)^{1/2}}\left(\mu_d+\frac{2}{3}\right)$ and $\delta_2=\frac{l_z}{2(1+\mu_d)^{3/2}}\left(1+\frac{1-l_z^2}{\omega_{ci}^2}\right)$. (3.33)

Equation (3.32) is the KdV equation, while δ_1 and δ_2 are the nonlinear and dispersive coefficients, respectively. Here, the middle and last terms of the equation specify the lower-order nonlinearity and dispersion effects, and provide solitary waves balancing each other.

We will now include the higher-order effect to the KdV equation. Equating the coefficients of $\epsilon^{5/2}$ from the x and y-components of the momentum equation, we get

$$l_y\frac{\partial\psi^{(2)}}{\partial\xi}+\omega_{ci}u_{ix}^{(3)}-V_0\frac{\partial u_{iy}^{(2)}}{\partial\xi}=0, \tag{3.34}$$

$$l_x\frac{\partial\psi^{(2)}}{\partial\xi}-\omega_{ci}u_{iy}^{(3)}-V_0\frac{\partial u_{ix}^{(2)}}{\partial\xi}=0. \tag{3.35}$$

Equating the coefficients of ϵ^3 from the x and y-components of the momentum equation, and the Poisson equation, the following set of equations is obtained.

$$\omega_{ci}u_{ix}^{(4)}-V_0\frac{\partial u_{iy}^{(3)}}{\partial\xi}+\frac{\partial u_{iy}^{(1)}}{\partial\tau}+l_z\,u_{iz}^{(1)}\frac{\partial u_{iy}^{(1)}}{\partial\xi}=0, \tag{3.36}$$

$$-\omega_{ci}u_{iy}^{(4)}-V_0\frac{\partial u_{ix}^{(3)}}{\partial\xi}+\frac{\partial u_{ix}^{(1)}}{\partial\tau}+l_z\,u_{iz}^{(1)}\frac{\partial u_{ix}^{(1)}}{\partial\xi}=0, \tag{3.37}$$

$$n_i^{(3)}-\frac{\mu_e}{6}\left[\psi^{(1)}\right]^3-\mu_e\psi^{(3)}+\frac{\partial^2\psi^{(2)}}{\partial\xi^2}-\mu_e\psi^{(1)}\psi^{(2)}=0. \tag{3.38}$$

Again, equating the coefficients of $\epsilon^{7/2}$ from the continuity equation and the z-component of the momentum equation, we found

$$l_y \frac{\partial u_{iy}^{(4)}}{\partial \xi} + l_z n_i^{(1)} \frac{\partial u_{iz}^{(2)}}{\partial \xi} + l_z \frac{\partial u_{iz}^{(3)}}{\partial \xi} + l_z n_i^{(2)} \frac{\partial u_{iz}^{(1)}}{\partial \xi} + l_x u_{ix}^{(2)} \frac{\partial n_i^{(1)}}{\partial \xi} + l_x \frac{\partial u_{ix}^{(4)}}{\partial \xi} + \frac{\partial n_i^{(2)}}{\partial \tau} + l_y u_{iy}^{(2)} \frac{\partial n_i^{(1)}}{\partial \xi}$$

$$+ l_x n_i^{(1)} \frac{\partial u_{ix}^{(2)}}{\partial \xi} + l_y n_i^{(1)} \frac{\partial u_{iy}^{(2)}}{\partial \xi} + l_z u_{iz}^{(2)} \frac{\partial n_i^{(1)}}{\partial \xi} - V_0 \frac{\partial n_i^{(3)}}{\partial \xi} + l_z u_{iz}^{(1)} \frac{\partial n_i^{(2)}}{\partial \xi} = 0, \tag{3.39}$$

$$l_z \frac{\partial \psi^{(3)}}{\partial \xi} + \frac{\partial u_{iz}^{(2)}}{\partial \tau} + l_z u_{iz}^{(2)} \frac{\partial u_{iz}^{(1)}}{\partial \xi} - V_0 \frac{\partial u_{iz}^{(3)}}{\partial \xi} + l_y u_{iy}^{(2)} \frac{\partial u_{iz}^{(1)}}{\partial \xi} + l_z u_{iz}^{(1)} \frac{\partial u_{iz}^{(2)}}{\partial \xi} + l_x u_{ix}^{(2)} \frac{\partial u_{iz}^{(1)}}{\partial \xi} = 0. \tag{3.40}$$

Differentiation of (3.28) w. r. to τ, gives

$$\frac{\partial n_i^{(2)}}{\partial \tau} = \mu_e \frac{\partial \psi^{(2)}}{\partial \tau} + 3\delta_1 \frac{\partial \psi^{(1)}}{\partial \xi} \frac{\partial^2 \psi^{(1)}}{\partial \xi^2} + \delta_1 \psi^{(1)} \frac{\partial^3 \psi^{(1)}}{\partial \xi^3} + \delta_2 \frac{\partial^5 \psi^{(1)}}{\partial \xi^5} - \mu_e \delta_1 \left[\psi^{(1)}\right]^2 \frac{\partial \psi^{(1)}}{\partial \xi} -$$

$$\mu_e \delta_2 \psi^{(1)} \frac{\partial^3 \psi^{(1)}}{\partial \xi^3}. \tag{3.41}$$

Equation (3.31) implies [using (3.32)]

$$\frac{\partial u_{iz}^{(2)}}{\partial \xi} = \frac{l_z}{V_0} \frac{\partial \psi^{(2)}}{\partial \xi} + \left(\frac{l_z^3}{V_0^3} - \frac{l_z\, \delta_1}{V_0^2}\right) \psi^{(1)} \frac{\partial \psi^{(1)}}{\partial \xi} - \frac{l_z\, \delta_2}{V_0^2} \frac{\partial^3 \psi^{(1)}}{\partial \xi^3}. \tag{3.42}$$

$$\Rightarrow\; u_{iz}^{(2)} = \frac{l_z}{V_0} \psi^{(2)} + \frac{1}{2}\left(\frac{l_z^3}{V_0^3} - \frac{l_z \delta_1}{V_0^2}\right) \left[\psi^{(1)}\right]^2 - \frac{l_z \delta_2}{V_0^2} \frac{\partial^2 \psi^{(1)}}{\partial \xi^2}. \tag{3.43}$$

$$\Rightarrow\; \frac{\partial u_{iz}^{(2)}}{\partial \tau} = \frac{l_z}{V_0} \frac{\partial \psi^{(2)}}{\partial \tau} - \delta_1 \left(\frac{l_z^3}{V_0^3} - \frac{l_z\, \delta_1}{V_0^2}\right) \left[\psi^{(1)}\right]^2 \frac{\partial \psi^{(1)}}{\partial \xi} - \delta_2 \left(\frac{l_z^3}{V_0^3} - \frac{2 l_z\, \delta_1}{V_0^2}\right) \psi^{(1)} \frac{\partial^3 \psi^{(1)}}{\partial \xi^3} +$$

$$\frac{3\delta_1 \delta_2 l_z}{V_0^2} \frac{\partial \psi^{(1)}}{\partial \xi} \frac{\partial^2 \psi^{(1)}}{\partial \xi^2} + \frac{l_z\, \delta_2^2}{V_0^2} \frac{\partial^5 \psi^{(1)}}{\partial \xi^5} \text{(After simplification)}. \tag{3.44}$$

We get the following third-order perturbed quantities from (3.34), (3.35), and (3.38).

$$u_{ix}^{(3)} = \frac{l_y V_0^2}{\omega_{ci}^3} \frac{\partial^3 \psi^{(1)}}{\partial \xi^3} - \frac{l_y}{\omega_{ci}} \frac{\partial \psi^{(2)}}{\partial \xi}, \quad u_{iy}^{(3)} = \frac{l_x}{\omega_{ci}} \frac{\partial \psi^{(2)}}{\partial \xi} - \frac{l_x V_0^2}{\omega_{ci}^3} \frac{\partial^3 \psi^{(1)}}{\partial \xi^3}, \tag{3.45}$$

and $\quad n_i^{(3)} = \mu_e \psi^{(3)} + \frac{1}{6} \mu_e \left[\psi^{(1)}\right]^3 - \frac{\partial^2 \psi^{(2)}}{\partial \xi^2} + \mu_e\, \psi^{(1)}\, \psi^{(2)}.$

Differentiating $n_i^{(3)}$ w.r.to ξ, we get

$$\Rightarrow \frac{\partial n_i^{(3)}}{\partial \xi} = \mu_e \frac{\partial \psi^{(3)}}{\partial \xi} + \frac{1}{2}\mu_e \left[\psi^{(1)}\right]^2 \frac{\partial \psi^{(1)}}{\partial \xi} - \frac{\partial^3 \psi^{(2)}}{\partial \xi^3} + \mu_e \frac{\partial}{\partial \xi}\left(\psi^{(1)}\,\psi^{(2)}\right). \tag{3.46}$$

Similarly, the fourth-order perturbed quantities and their derivatives w.r.to ξ are

$$u_{ix}^{(4)} = \frac{l_x V_0}{\omega_{ci}^2}\frac{\partial^2 \psi^{(2)}}{\partial \xi^2} + l_x\left(\frac{\delta_2}{\omega_{ci}^2} - \frac{V_0^3}{\omega_{ci}^4}\right)\frac{\partial^4 \psi^{(1)}}{\partial \xi^4} + \frac{l_x \delta_1}{\omega_{ci}^2}\left(\frac{\partial \psi^{(1)}}{\partial \xi}\right)^2 + l_x\left(\frac{\delta_1}{\omega_{ci}^2} - \frac{l_z^2}{\omega_{ci}^2 V_0}\right)\psi^{(1)}\frac{\partial^2 \psi^{(1)}}{\partial \xi^2}.$$

$$\Rightarrow \frac{\partial u_{ix}^{(4)}}{\partial \xi} = \frac{l_x V_0}{\omega_{ci}^2}\frac{\partial^3 \psi^{(2)}}{\partial \xi^3} + l_x\left(\frac{\delta_2}{\omega_{ci}^2} - \frac{V_0^3}{\omega_{ci}^4}\right)\frac{\partial^5 \psi^{(1)}}{\partial \xi^5} + l_x\left(\frac{3\delta_1}{\omega_{ci}^2} - \frac{l_z^2}{\omega_{ci}^2 V_0}\right)\frac{\partial \psi^{(1)}}{\partial \xi}\frac{\partial^2 \psi^{(1)}}{\partial \xi^2} +$$
$$l_x\left(\frac{\delta_1}{\omega_{ci}^2} - \frac{l_z^2}{\omega_{ci}^2 V_0}\right)\psi^{(1)}\frac{\partial^3 \psi^{(1)}}{\partial \xi^2}. \tag{3.47}$$

$$u_{iy}^{(4)} = \frac{l_y V_0}{\omega_{ci}^2}\frac{\partial^2 \psi^{(2)}}{\partial \xi^2} + l_y\left(\frac{\delta_2}{\omega_{ci}^2} - \frac{V_0^3}{\omega_{ci}^4}\right)\frac{\partial^4 \psi^{(1)}}{\partial \xi^4} + \frac{l_y \delta_1}{\omega_{ci}^2}\left(\frac{\partial \psi^{(1)}}{\partial \xi}\right)^2 + l_y\left(\frac{\delta_1}{\omega_{ci}^2} - \frac{l_z^2}{\omega_{ci}^2 V_0}\right)\psi^{(1)}\frac{\partial^2 \psi^{(1)}}{\partial \xi^2}.$$

$$\Rightarrow \frac{\partial u_{iy}^{(4)}}{\partial \xi} = \frac{l_y V_0}{\omega_{ci}^2}\frac{\partial^3 \psi^{(2)}}{\partial \xi^3} + l_y\left(\frac{\delta_2}{\omega_{ci}^2} - \frac{V_0^3}{\omega_{ci}^4}\right)\frac{\partial^5 \psi^{(1)}}{\partial \xi^5} + l_y\left(\frac{3\delta_1}{\omega_{ci}^2} - \frac{l_z^2}{\omega_{ci}^2 V_0}\right)\frac{\partial \psi^{(1)}}{\partial \xi}\frac{\partial^2 \psi^{(1)}}{\partial \xi^2} +$$
$$l_y\left(\frac{\delta_1}{\omega_{ci}^2} - \frac{l_z^2}{\omega_{ci}^2 V_0}\right)\psi^{(1)}\frac{\partial^3 \psi^{(1)}}{\partial \xi^2}\,. \tag{3.48}$$

Dividing (3.39) and (3.40) by l_z and V_0, respectively, and then adding the two results, we obtain the following KdV-type inhomogeneous equation.

$$\frac{\partial \psi^{(2)}}{\partial \tau} + \delta_1 \frac{\partial}{\partial \xi}\left(\psi^{(1)}\psi^{(2)}\right) + \delta_2 \frac{\partial^3 \psi^{(2)}}{\partial \xi^3} = S\left(\psi^{(1)}\right), \tag{3.49}$$

where the source term $S\left(\psi^{(1)}\right)$ is given by

$$S\left(\psi^{(1)}\right) = \delta_3 \left[\psi^{(1)}\right]^2 \frac{\partial \psi^{(1)}}{\partial \xi} + \delta_4 \frac{\partial \psi^{(1)}}{\partial \xi}\frac{\partial^2 \psi^{(1)}}{\partial \xi^2} + \delta_5\, \psi^{(1)}\frac{\partial^3 \psi^{(1)}}{\partial \xi^3} + \delta_6 \frac{\partial^5 \psi^{(1)}}{\partial \xi^5}. \tag{3.50}$$

The coefficients $\delta_i (i = 3, 4, 5, 6)$ occurring in (3.50) are given in section A.1 of the Appendix. Here, (3.32) is the nonlinear KdV equation in $\psi^{(1)}$, and (3.49) is the KdV-type inhomogeneous equation in $\psi^{(2)}$ with source term $S\left(\psi^{(1)}\right)$. The source term may contain secular (resonant) terms having the same frequency as that of the natural frequency of the system, for which the second-order potential becomes infinite. Removing the secular behavior, we can find the desired solution up to the second-order perturbed potential.

3.4 Dressed solution

The aim of this section is to find the dressed solution to the equation (3.49) while the re-normalization method of Kodama and Taniuti (1978) is used to exclude secular behavior. Following the method, (3.32) and (3.49) are modified, respectively, as

$$\frac{\partial\psi^{(1)}}{\partial\tau}+\delta_1\psi^{(1)}\frac{\partial\psi^{(1)}}{\partial\xi}+\delta_2\frac{\partial^3\psi^{(1)}}{\partial\xi^3}+\delta\lambda\frac{\partial\psi^{(1)}}{\partial\xi}=0, \tag{3.51}$$

and $$\frac{\partial\psi^{(2)}}{\partial\tau}+\delta_1\frac{\partial}{\partial\xi}\left(\psi^{(1)}\psi^{(2)}\right)+\delta_2\frac{\partial^3\psi^{(2)}}{\partial\xi^3}+\delta\lambda\frac{\partial\psi^{(2)}}{\partial\xi}=S(\psi^{(1)})+\delta\lambda\frac{\partial\psi^{(1)}}{\partial\xi}, \tag{3.52}$$

where $\psi^{(1)}$ and $\psi^{(2)}$ refer to the re-normalization variables.

Now, consider $\eta=\xi-(\lambda+\delta\lambda)\tau$. Here, λ is related to $M=\frac{V}{C_S}$ (Lai, 1979; Esfandyari et al., 2008; Gill et al., 2010) by $\lambda+\delta\lambda=M-1=\Delta M$, where $C_S=K\left(\frac{T_e}{m_e}\right)^{1/2}$, M is the Mach number and V is the soliton's velocity. Under this transformation, (3.51) and (3.52) become, respectively

$$\delta_2\frac{d^3\psi^{(1)}}{d\eta^3}+\delta_1\psi^{(1)}\frac{d\psi^{(1)}}{d\eta}-\lambda\frac{d\psi^{(1)}}{d\eta}=0, \tag{3.53}$$

and $$\delta_2\frac{d^3\psi^{(2)}}{d\eta^3}+\delta_1\frac{d}{d\eta}\left(\psi^{(1)}\psi^{(2)}\right)-\lambda\frac{d\psi^{(2)}}{d\eta}=S(\psi^{(1)})+\delta\lambda\frac{d\psi^{(1)}}{d\eta}. \tag{3.54}$$

It is quite possible to integrate (3.53) and (3.54) subject to the boundary conditions

$$\psi^{(1)}=\psi^{(2)}=\frac{d\psi^{(1)}}{d\eta}=\frac{d\psi^{(2)}}{d\eta}=\frac{d^2\psi^{(1)}}{d\eta^2}=\frac{d^2\psi^{(2)}}{d\eta^2}=0,\ \text{as } |\eta|\to\infty. \tag{3.55}$$

Thus, we obtain

$$\frac{d^2\psi^{(1)}}{d\eta^2}+\frac{1}{\delta_2}\left(\frac{\delta_1}{2}\psi^{(1)}-\lambda\right)\psi^{(1)}=0, \tag{3.56}$$

and $$\frac{d^2\psi^{(2)}}{d\eta^2}+\frac{1}{\delta_2}\left(\delta_1\psi^{(1)}-\lambda\right)\psi^{(2)}=\frac{1}{\delta_2}\int_{-\infty}^{\eta}\left[S(\psi^{(1)})+\delta\lambda\frac{d\psi^{(1)}}{d\eta}\right]d\eta. \tag{3.57}$$

The one-soliton solution of (3.56) is given by (please, see Appendix A.2)

$$\psi^{(1)}=\psi_{A1}\,\text{sech}^2\left(\frac{\eta}{W}\right), \tag{3.58}$$

where the amplitude (ψ_{A1}) and width (W) are, respectively, given by

$$\psi_{A1} = \frac{3\,\lambda}{\delta_1} \text{ and } W = \sqrt{\frac{4\,\delta_2}{\lambda}}. \tag{3.59}$$

Thus, the term $\frac{1}{\delta_2}\int_{-\infty}^{\eta}\left[S(\psi^{(1)}) + \delta\lambda\frac{d\psi^{(1)}}{d\eta}\right] d\eta$ becomes

$$M_1 \operatorname{sech}^4\left(\frac{\eta}{W}\right) + M_2 \operatorname{sech}^6\left(\frac{\eta}{W}\right) + \frac{\psi_{A1}}{\delta_2}\left[\delta\lambda + \frac{16\,\delta_6}{W^4}\right]\operatorname{sech}^2\left(\frac{\eta}{W}\right), \tag{3.60}$$

where $M_1 = \frac{\psi_{A1}}{\delta_2 W^4}(2\delta_4\psi_{A1}W^2 + 2\delta_5\,\psi_{A1}W^2 - 120\delta_6)$,

$$M_2 = \frac{\psi_{A1}}{\delta_2 W^4}\left(\frac{1}{3}\delta_3\,\psi_{A1}^2 W^4 - 2\delta_4\,\psi_{A1}W^2 - 4\,\delta_5\,\psi_{A1}W^2 + 120\delta_6\right).$$

In order to cancel the secular term from $S(\psi^{(1)})$, we put $\delta\lambda = -\frac{16\,\delta_6}{W^4} = -\frac{\lambda^2\delta_6}{\delta_2^2}$ (Lai, 1979; Mehdipoor and Esfandyari, 2012; Kodama and Taniuti, 1978; Ahmed et al., 2020; Mahmood et al., 2021; Fayad et al., 2021; Paul et al., 2021). Hence, we define another new variable $z = \tanh\left(\frac{\eta}{W}\right)$ to reduce (3.57) in the following form:

$$\frac{d}{dz}\left[(1-z^2)\frac{d\psi^{(2)}}{dz}\right] + \left(12 - \frac{4}{1-z^2}\right)\psi^{(2)} = M(1-z^2) + N(1-z^2)^2 = T(z), \text{say} \tag{3.61}$$

where $M = M_1 W^2$ and $N = M_2 W^2$.

Comparing the homogeneous equation $\frac{d}{dz}\left[(1-z^2)\frac{d\psi^{(2)}}{dz}\right] + \left(12 - \frac{4}{1-z^2}\right)\psi^{(2)} = 0$ with the associated Legendre differential equation $\frac{d}{dz}\left[(1-z^2)\frac{dy}{dz}\right] + \left[n(n+1) - \frac{m^2}{1-z^2}\right]y = 0$, we get $m = 2$ and $n = 3$.

The homogenous equation has two independent solutions in terms of associated Legendre polynomials $P_3^2(z)$ and $Q_3^2(z)$ (Esfandyari et al., 2008; Gill et al., 2010), and these two polynomials can be determined by the following generalized formulae (Haggard, 1988):

$$P_n^m(z) = (-1)^m(1-z^2)^{m/2}\frac{d^m}{dz^m}(P_n) \text{ and } Q_n^m(z) = (-1)^m(1-z^2)^{m/2}\frac{d^m}{dz^m}(Q_n),$$

where $P_n = \frac{1}{2^n\,n!}\frac{d^n}{dz^n}(z^2-1)^n$ and $Q_n = \frac{1}{2}P_n\ln\left(\frac{1+z}{1-z}\right) - \sum_{i=1}^{n}\frac{P_{i-1}(z)\cdot P_{n-i}(z)}{i}, -1 < z < 1.$

Thus, $P_3^2(z)$ and $Q_3^2(z)$ are obtained as follows:

$$P_3^2(z) = 15z(1-z^2) \text{ and } Q_3^2(z) = \frac{15}{2} z(1-z^2)\ln\left(\frac{1+z}{1-z}\right) - 15(1-z^2) + 5 + \frac{2}{(1-z^2)}.$$

The complementary function (C. F.) $\psi_c^{(2)} = c_1 P_3^2(z) + c_2 Q_3^2(z)$ vanishes because the first term is a secular one, which can be eliminated by renormalizing the amplitude, (Lai, 1979), and also $c_2 = 0$ as a result of vanishing boundary conditions for $\psi^{(2)}$.

The particular integral (P. I.) of (3.61) is obtained by the method of variation of parameters as

$$\psi_p^{(2)} = q_1(z)P_3^2(z) + q_2(z)Q_3^2(z) = \frac{1}{24}(4M+3N)(1-z^2) + \frac{N}{8}z^2(1-z^2), \quad (3.62)$$

where $q_1 = -\int \frac{Q_3^2(z)\,T(z)}{(1-z^2)\,W(P_3^2,Q_3^2)}dz$, $q_2 = \int \frac{P_3^2(z)\,T(z)}{(1-z^2)\,W(P_3^2,Q_3^2)}dz$ and $W(P_3^2, Q_3^2) = \frac{120}{1-z^2}$.

Thus, the dressed solution $\psi(=\psi^{(1)} + \psi^{(2)})$ up to the second-order of ΔM is given by (Esfandyari et. al., 2008; Gill et al., 2010)

$$\psi = \frac{3\,\Delta M}{\delta_1}\,\mathrm{sech}^2\left(\frac{\eta}{W}\right) + \frac{4M+3N}{24}\,\mathrm{sech}^2\left(\frac{\eta}{W}\right) + \frac{N}{8}\mathrm{sech}^2\left(\frac{\eta}{W}\right)\tanh^2\left(\frac{\eta}{W}\right), \quad (3.63)$$

where the modified amplitude (ψ_{A12}) and width (W) are defined as

$$\psi_{A12} = \frac{3\,\Delta M}{\delta_1} + \frac{1}{24}(4M+3N) \text{ and } W = \sqrt{\frac{4\,\delta_2}{\lambda}} = 2\sqrt{\frac{\delta_2}{\Delta M}}\left(1 - \frac{\delta_6}{2\delta_2^2}\Delta M\right). \quad (3.64)$$

Here, the second-order potential $\psi^{(2)}$, i.e., the sum of the last two terms of (3.63), gives the higher-order effect on the DIA solitary wave solution. Moreover, ψ_{A1} and ψ_{A12} represent the amplitudes of the waves before and after the inclusion of the contribution of the higher-order effect, respectively. The dressed solution reveals that the magnetic field (ω_{ci}), obliquity (θ), and dust concentrations (μ_d) affect the wave nature significantly (since from (3.60), (3.63), and Appendix A.1, it is clear that M and N are the functions of these parameters).

3.5 Results and discussion

In this segment, the effects of magnetic field, obliquity, dust concentration as well as the influence of higher-order terms (nonlinear and dispersion) have been examined.

In order to investigate the aforementioned parametric impacts, the corresponding parametric values $n_{i0} = 5 \times 10^8\ cm^{-3}$, $T_i = 0.05\ eV$, $T_e = 2 - 3\ eV, n_{d0} = 10^4 - 10^5\ cm^{-3}, Z_d = 10^3 - 3 \times 10^3$ are taken from the investigation of Rosenberg et al. (2008), and $\omega_{ci} = 0.2 - 0.4$ rad/s is taken from theoretical work of Rahman and Haider (2019). As per the reductive perturbation method, the prerequisite condition for adding the higher-order effect is $\frac{|\psi^{(2)}|}{|\psi^{(1)}|} \leq 1$. Here, Figure 3.1 confirms that the condition holds for the considered plasma system.

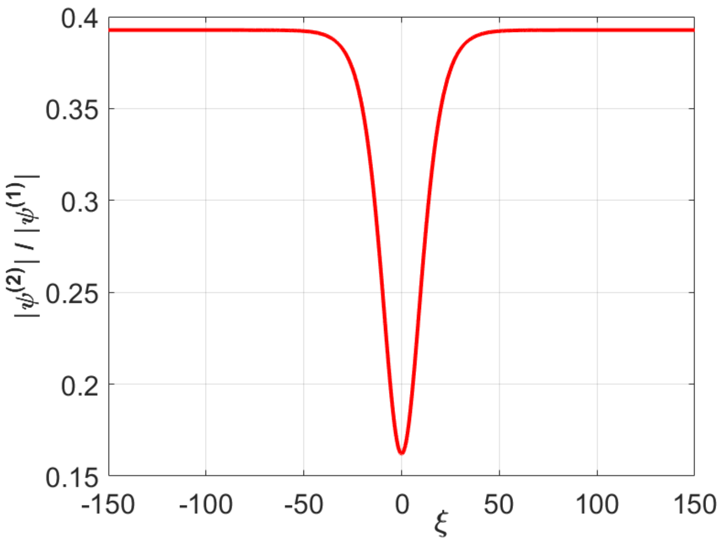

Figure 3.1: The ratio $|\psi^{(2)}|/|\psi^{(1)}|$ vs. ξ, when $\mu_d = 0.3, \omega_{ci} = 0.4, \Delta M = 0.01, \theta = 80^0, \tau = 1$.

The consequence of higher-order terms (i.e., second-order potential $\psi^{(2)}$) in dressed solution (ψ) is depicted in Figures 3.2 and 3.3 that display the wave profiles in 3D and 2D, respectively. Moreover, Figure 3.4 shows the time evolution of the solitary waves at time $\tau = 0, 50, 100$ forwarding in the positive direction of ξ. The dressed solution yields compressive solitary waves only. The figures illustrate that (where $\mu_d = 0.3$, $\omega_{ci} = 0.4$, $\Delta M = 0.01$, $\theta = 80^0$ are taken particularly) the addition of higher-order nonlinearity and dispersive terms causes a rise in the amplitudes, but has no contribution in the change of the widths. Thus, $\psi^{(1)}$ and $\psi = \psi^{(1)} + \psi^{(2)}$ provide different amplitudes and the same widths.

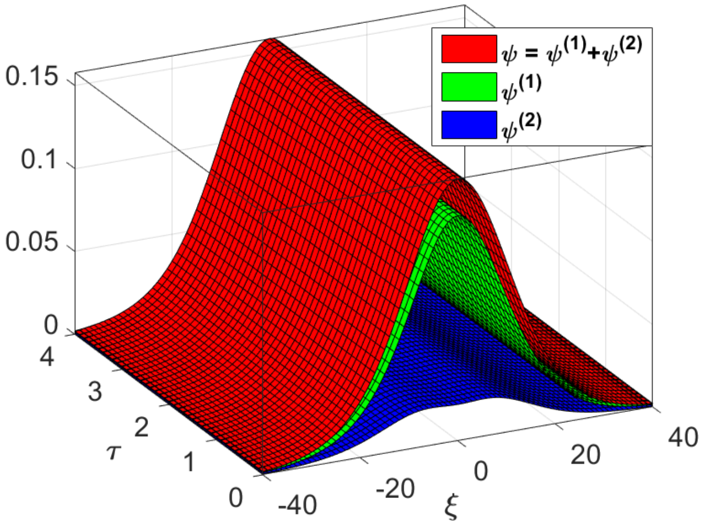

Figure 3.2: 3D plots of $\psi^{(1)}$, $\psi^{(2)}$, and ψ, when $\mu_d = 0.3$, $\omega_{ci} = 0.4$, $\Delta M = 0.01$, $\theta = 80^0$.

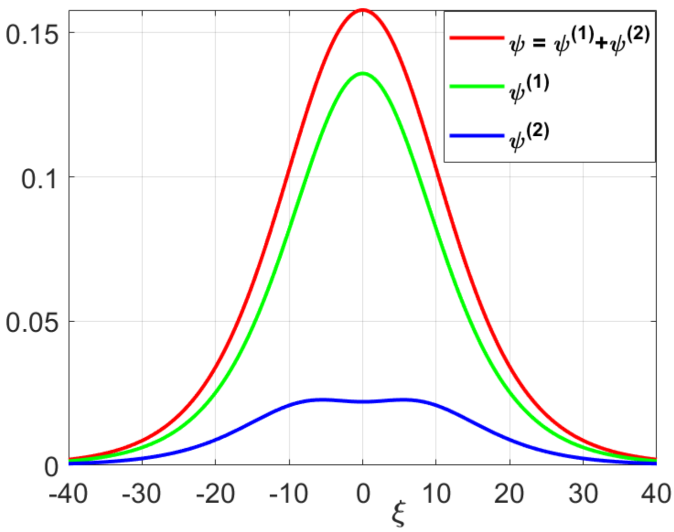

Figure 3.3: 2D plots of ψ, $\psi^{(1)}$, and $\psi^{(2)}$ at $\tau = 1$, when $\mu_d = 0.3$, $\omega_{ci} = 0.4$, $\Delta M = 0.01$, $\theta = 80^0$.

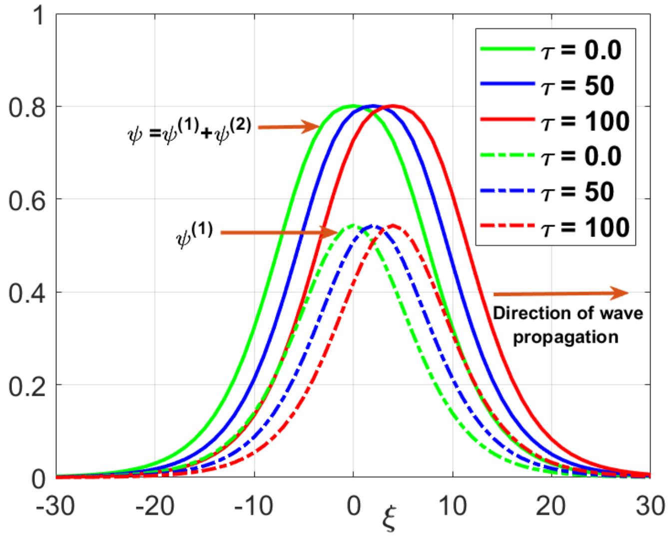

Figure 3.4: Time evolutions of $\psi^{(1)}$ and ψ at τ = 0.0, 50, 100.

As δ_i(i = 3, 4, 5, 6) are functions of gyro-frequency (ω_{ci}) and different parameters, we perceive from the dressed solution (3.63) that the magnetic field has a substantial impact on the amplitude and width. Figures 3.5 -3.8 show the variations in wave structures (amplitude and width) for different ion gyro-frequencies. The 3D and 2D plots of the wave profiles are drawn, respectively in Figures 3.5 and 3.6 against $\omega_{ci} = 0.2$, $\omega_{ci} = 0.3$, and $\omega_{ci} = 0.4$ (where $\mu_d = 0.3$, $\Delta M = 0.01$, $\theta = 80^0$). From Figures 3.7 and 3.8, it is seen that the magnetic field decreases the amplitudes (when $\psi^{(2)}$ is taken into consideration) and widths. Besides, the slightly decreasing effect on the amplitude ψ_{A12} is observed only owing to the inclusion of higher-order terms. On the other hand, if we do not consider the higher-order effect, it is seen that the amplitude will not be affected by the magnetic field, i.e., ψ_{A1} is independent of the magnetic field.

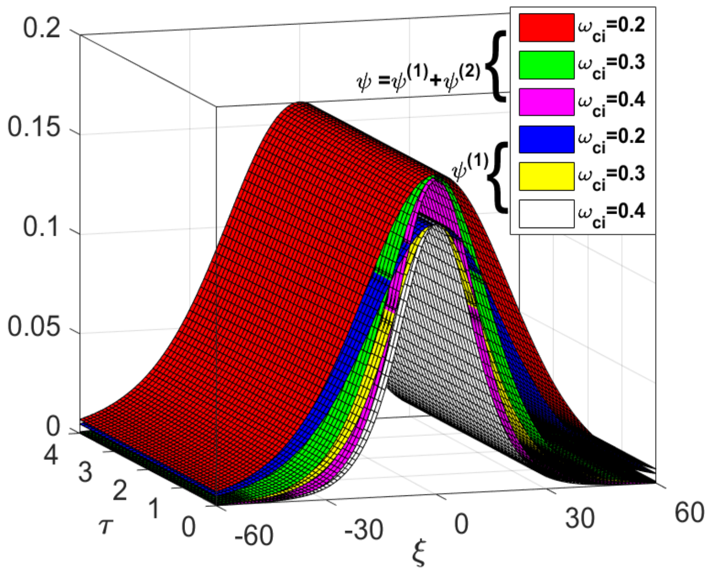

Figure 3.5: 3D plots of $\psi^{(1)}$and ψ for $\omega_{ci} = 0.2$, $\omega_{ci} = 0.3$, $\omega_{ci} = 0.4$.

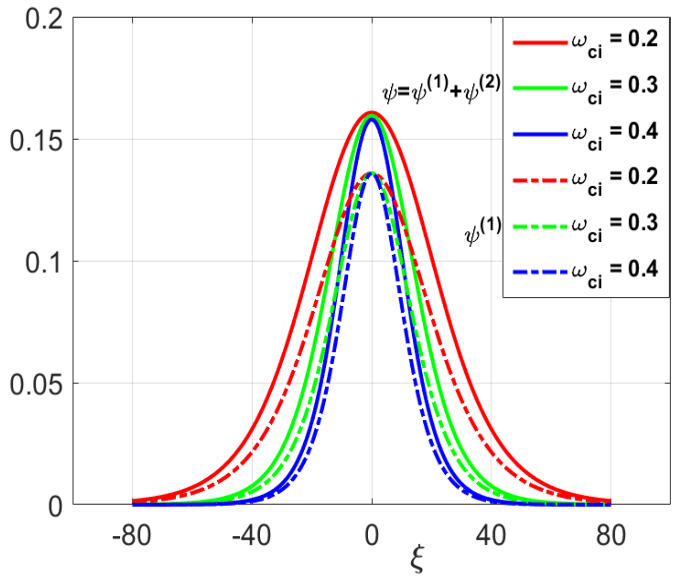

Figure 3.6: 2D plots of $\psi^{(1)}$ and ψ for $\omega_{ci} = 0.2$, $\omega_{ci} = 0.3$, $\omega_{ci} = 0.4$ at $\tau = 1$.

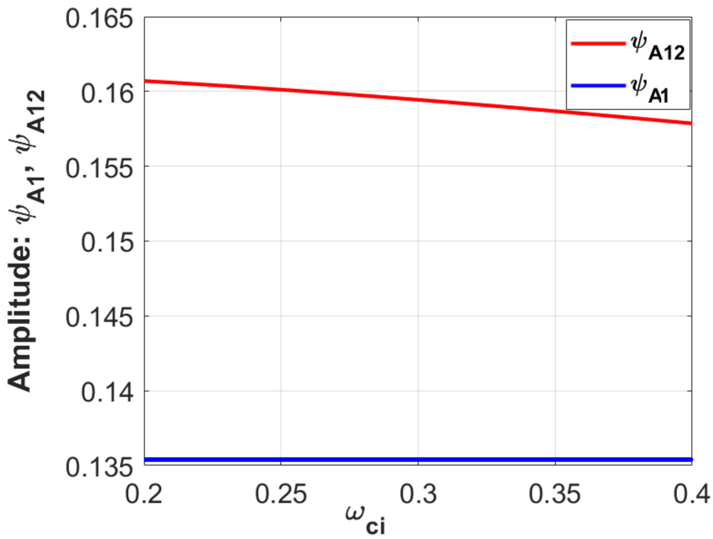

Figure 3.7: Shows different amplitudes for $\psi^{(1)}$ and ψ in the interval $\omega_{ci} \epsilon$ [0.2, 0.4], when $\mu_d = 0.3$, $\Delta M = 0.01$, $\theta = 80^0$.

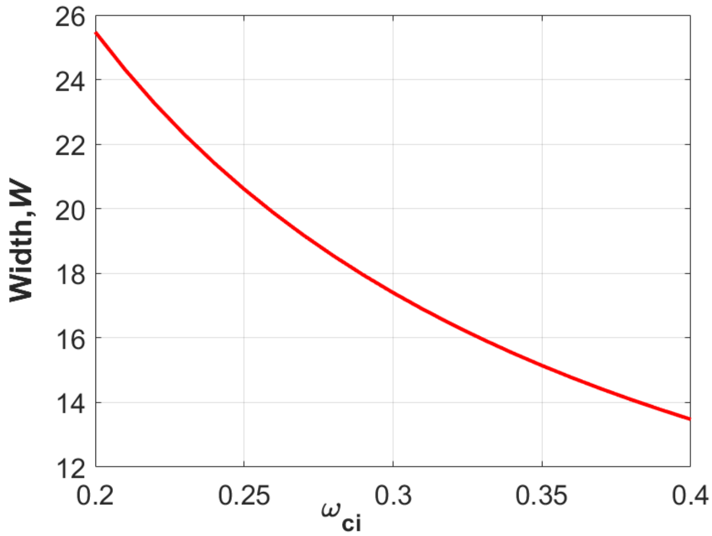

Figure 3.8: Shows the same width for $\psi^{(1)}$ and ψ in the interval $\omega_{ci} \epsilon$ [0.2, 0.4], when $\mu_d = 0.3$, $\Delta M = 0.01$, $\theta = 80^0$.

Figures 3.9 -3.12 show the changes in the solitary wave profiles, i.e., changes in amplitude and width for different angles θ (where $\mu_d = 0.3$, $\Delta M = 0.01$, $\omega_{ci} = 0.4$). Figure 3.11 shows that the amplitude grows gradually when θ is less than about 75^0, and it grows rapidly in the range (75^0, 90^0), and ultimately becomes infinite for $\theta = 90^0$ which is invalid for this plasma system. On the other hand, as shown in Figure 3.12, the width increases (decreases) when $\theta < (>) 53^0$. If $\theta = 0^0$ (i.e., when the direction of wave propagation is parallel to the direction of the magnetic field), equation (3.63) shows that the amplitude and width will not be affected by the magnetic field.

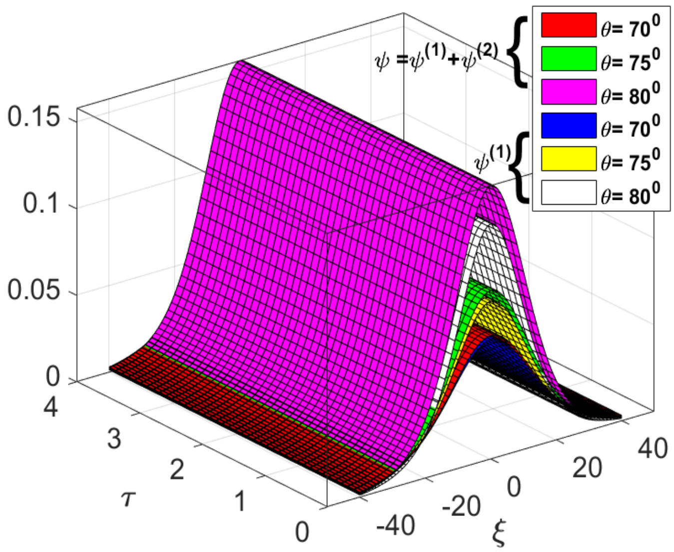

Figure 3.9: 3D plots of $\psi^{(1)}$and ψ for $\theta = 70^0$, $\theta = 75^0$, $\theta = 80^0$.

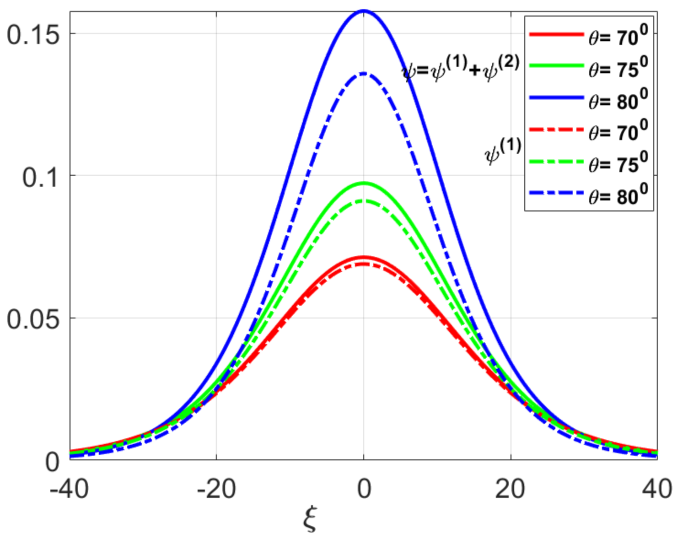

Figure 3.10: 2D plots of $\psi^{(1)}$and ψ for $\theta = 70^0$, $\theta = 75^0$, $\theta = 80^0$, $\tau = 1$.

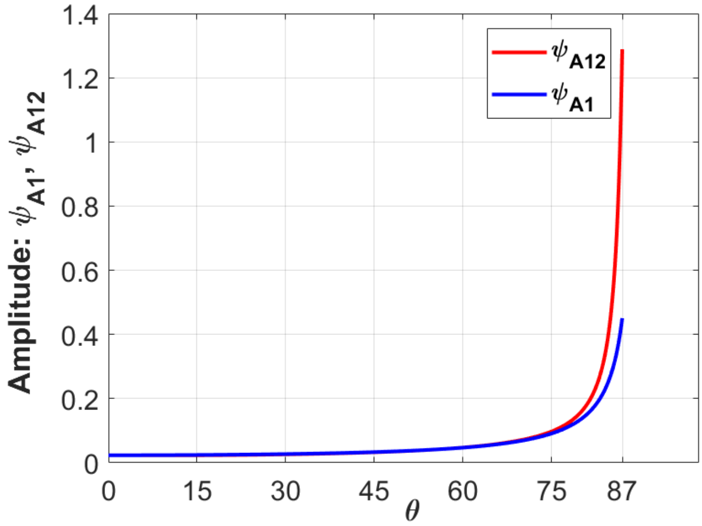

Figure 3.11: Amplitudes of $\psi^{(1)}$ and ψ in the interval $\theta \in [0^0, 87^0]$.

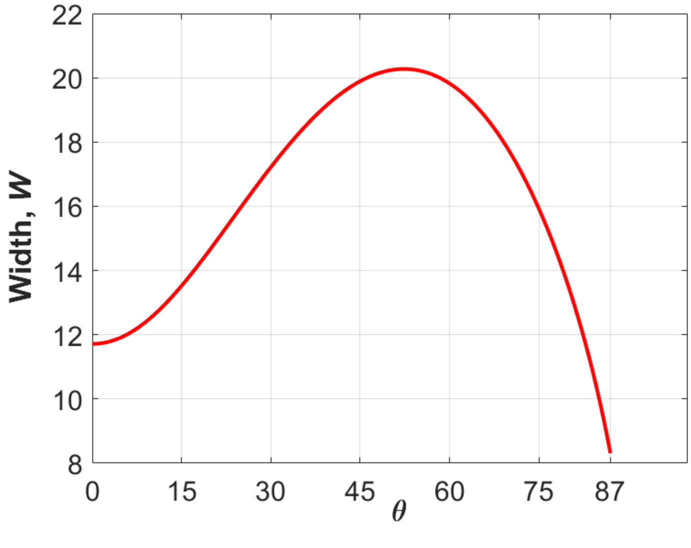

Figure 3.12: Shows the same width for $\psi^{(1)}$ and ψ in the interval $\theta \in [0^0, 87^0]$, while the parameters are: $\mu_d = 0.3$, $\Delta M = 0.01$, $\omega_{ci} = 0.4$.

Figures 3.13 and 3.14 depict the fluctuations of the amplitudes and widths with the growing μ_d, when $\omega_{ci} = 0.4$, $\Delta M = 0.01$, $\theta = 80^0$. The figures show that, in the presence of positive dust particles, the higher-order terms (nonlinear and dispersive) have an increasing effect on the amplitudes but no effect on the widths. However, the changes in amplitudes and widths are visualized in Figures 3.15 and 3.16, respectively. It is found from these figures that the increasing number of positive dust particles causes the wave amplitudes and widths to decrease.

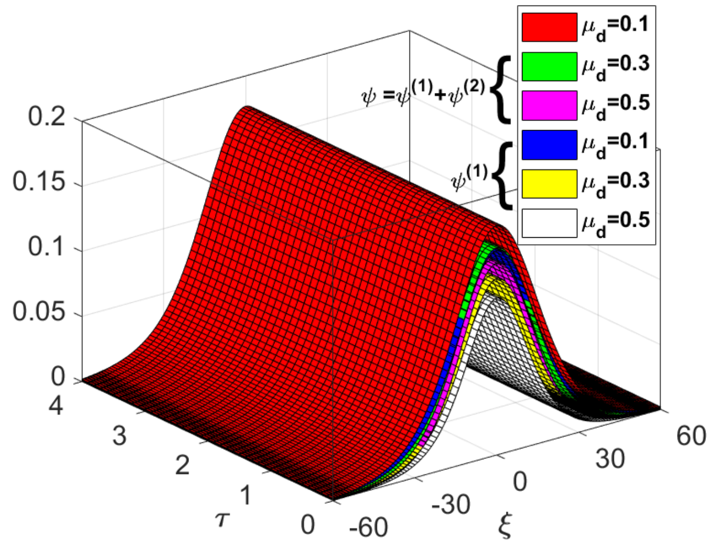

Figure 3.13: 3D plots of $\psi^{(1)}$ and ψ for $\mu_d = 0.1$, $\mu_d = 0.3$, $\mu_d = 0.5$.

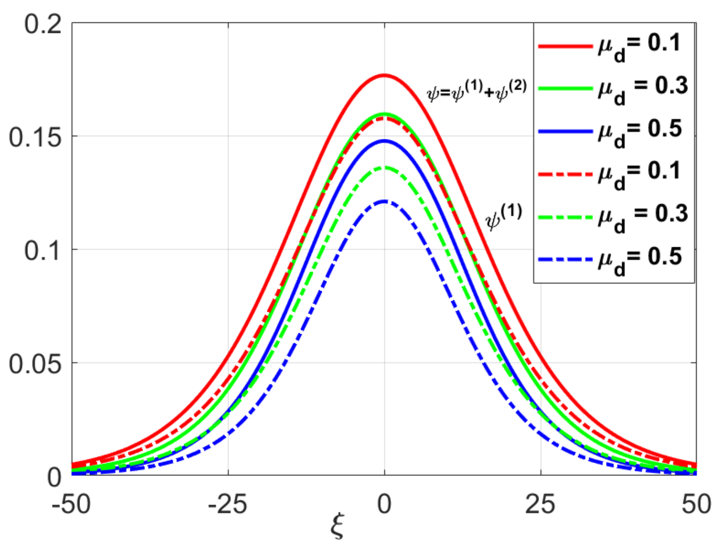

Figure 3.14: 2D plots of $\psi^{(1)}$ and ψ for $\mu_d = 0.1$, $\mu_d = 0.3$, $\mu_d = 0.5$, $\tau = 1$.

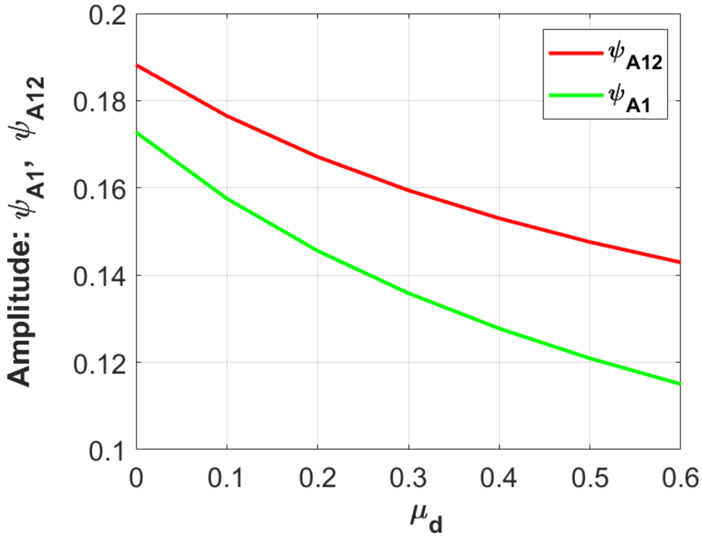

Figure 3.15: Amplitudes of $\psi^{(1)}$ and ψ in the interval $\mu_d \ \epsilon \ [0, 0.6]$.

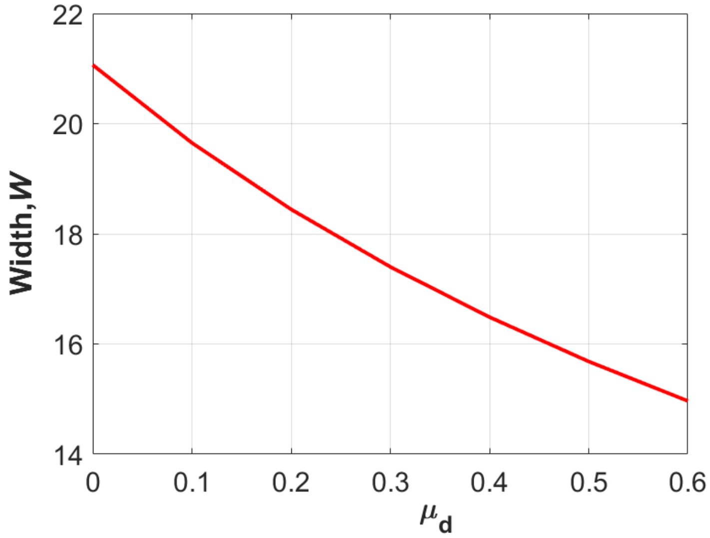

Figure 3.16: Shows the same width for $\psi^{(1)}$and ψ in the interval $\mu_d \ \epsilon \ [0, 0.6]$, while the parameters are: $\omega_{ci} = 0.4$, $\Delta M = 0.01$, $\theta = 80^0$, $\tau = 1$.

From the equation (3.22), it is seen that the dust concentration μ_d and the angle θ have a significant impact on the phase speed of the DIA subsonic solitary waves. As shown in Figures 3.17 and 3.18, both μ_d and θ decrease the phase speed considerably. Since l_z lies between 0 and 1, and $0 < \mu_d < \infty$ is valid for the electron-ion-PCD plasmas, the stationary PCD particles cause the IA subsonic solitary waves (Mamun, 2021). Besides, the phase speed is unaffected by the magnetic field. Here, the production of DIA subsonic solitary waves with positive potential in electron-ion-PCD plasmas is caused by the presence of immobile PCD particles. This is because when the number density and charge of stationary PCD species increase, the phase speed of the IA waves decreases. In addition, the higher-order nonlinear and dispersive effects, as well as the magnetic field, have no impact on the phase speed.

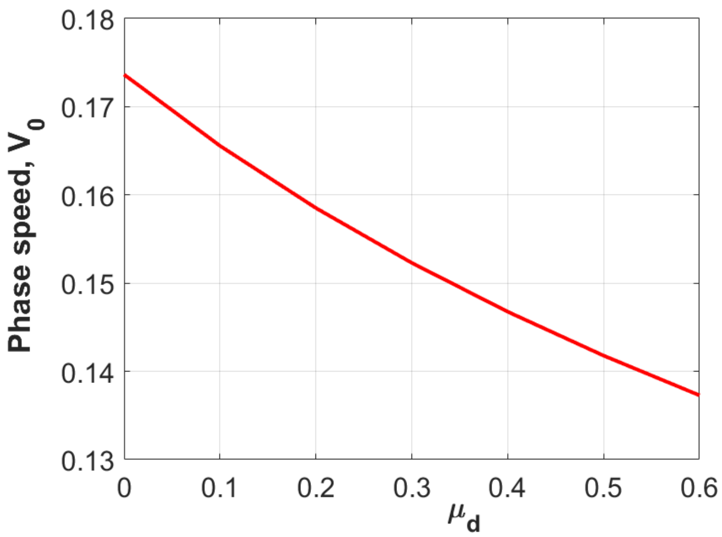

Figure 3.17: Phase speed vs. μ_d in the interval $[0, 0.6]$, when $\theta = 80^0$.

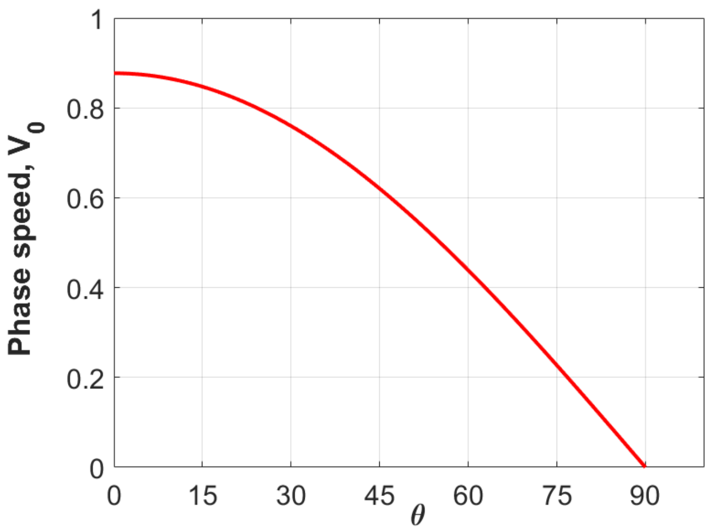

Figure 3.18: Phase speed vs. θ in the interval $[0^0, 90^0]$, when $\mu_d = 0.3$.

3.6 Summary

We explore the combined impact of magnetic field, obliquity, dust concentrations, etc., on the amplitude and width of DIA solitary waves, and we reveal that the wave features are significantly influenced by the parameters. Besides, the impact of higher-order terms has been incorporated for getting a better result. The key findings are given below:

i. *Magnetic effect*: Amplitude and width are decreased by the magnetic field.

ii. *Effect of the obliqueness* (θ): The amplitude increases as the value of θ increases, and approaches to ∞ when $\theta \to 90^0$ which suggests that the angle should be less than 90^0. Besides, the growing values of θ in the range (0^0, 90^0) have a reducing impact on the phase speed. If $\theta = 0^0$, the magnetic field does not affect the amplitude and width.

iii. *Effect of the dust concentration*: The IA subsonic solitary waves are formed as a result of the existence of the static PCD species, while the dust particle concentration (μ_d) has a reducing impact on the phase speed and width.

iv. *Higher-order effect*: Higher-order nonlinear and dispersive terms have a growing impact on the amplitude, whereas they do not affect the width.

Chapter Four

Higher-order nonlinear, dispersive, and parametric effects on DIA solitary waves

4.1 Introduction

As previously mentioned, along with ions and electrons, dust particles are also ever-present in dusty plasmas. The properties of waves are significantly influenced by negative ions that obey the Maxwellian or vortex-like distribution. To demonstrate the characteristics of DIA solitary waves, several physicists predicted the Maxwellian distribution of negative ions (Franklin and Snell, 2000; Bogdanov and Kudryavtsev, 2001). Many astrophysical objects contain heavier and lighter substances, such as Hydrogen, Helium, Carbon, Oxygen, Iron, Rubidium, etc., and they follow different particle distributions in plasmas (Chandrasekhar, 1931; Kosester and Chanmugam, 1990; Chamel et al., 2008). Sometimes, the energy of negative light ions may not be sufficient to overcome their potential. Consequently, the ions become vortex-like, and depart from the isothermal distribution to follow a nonthermal distribution (Schamel, 1972; Schamel, 1975; Mamun, 1998). Rahman and Haider (2016) theoretically investigated the characteristics of DIA solitary waves in a one-dimensional plasma system which comprises trapped negative ions in addition to three other elements, namely positive ions, Maxwellian distributed electrons, and stationary dust particles. Rahman and Haider (2019), in their other work, explored the dynamics of DIA solitary waves as well as the stabilization in a magnetized dusty plasma considering the same type of components. Recently, the investigation of adiabaticity in plasma systems has also received a lot of attention, and several researchers have noticed the adiabatic influence on wave propagations. Mamun et al. (2009) explicitly examined the fundamental characteristics of DIA and DA solitary waves with regard to the combined impact of the adiabaticities of electrons and ions, and negatively charged static or mobile dust particles. Anowar and Mamun (2008) examined the nature of DIA waves of small amplitude as well as their multi-dimensional instability by investigating the effects of ion and electron adiabaticities and ion-dust collisions. Besides, Haider et al. (2020) studied the impacts of Chandrasekhar limits in adiabatic plasmas, where the parameters are valid for white dwarfs and other compact objects.

In chapters two and three, it has been stated that the behaviors of solitary wave propagations can be described by using the KdV or mKdV equation, but the theoretical explanations do not completely match the results of the experimental works. Both in the literature review and chapter three, a number of references to previous works have been included that address the higher-order nonlinear and dispersive effects. In their investigations, the researchers worked to achieve better results by adding the higher-order effects. Moreover, Gill et al. (2010) investigated the slow and fast modes of IA solitary waves in a multi-species plasma that includes trapped electrons, and El-Tibany and Moslem (2005) examined electron-acoustic solitary waves with cold and trapped electrons in which both plasma systems are considered unmagnetized.

In this chapter, we consider a three-dimensional magnetized and adiabatic plasma system containing negative trapped ions in addition to positive ions, Maxwellian electrons, and dust particles, while the DIA solitary waves propagate obliquely. We emphasize the investigation of the higher-order nonlinear and dispersion effects, and various parametric impacts on the waves. To examine the higher-order effects, an inhomogeneous mKdV-type equation is derived here.

4.2 Plasma model

We contemplate a propagation of DIA solitary waves in a magnetized, collision-free, four-component plasma made up of adiabatic positive ions (which are mobile), trapped light ions (negative), arbitrarily charged dust particles, and isothermal electrons to examine the higher-order effects on the salient features of the waves. Let us assume that the magnetic field is directed along the x-axis, i.e., $\vec{B} = B_0\hat{x}$. Hence, the equations listed below govern the nonlinear dynamics of the waves.

$$\frac{\partial n_i}{\partial t} + \nabla \cdot (n_i\vec{u}_i) = 0, \tag{4.1}$$

$$\frac{\partial \vec{u}_i}{\partial t} + (\vec{u}_i \cdot \nabla)\vec{u}_i = -\frac{e}{m_i}\nabla\psi + \omega_{ci}\,(\vec{u}_i \times \hat{x}) - \frac{1}{m_i\, n_i}\nabla p_i, \tag{4.2}$$

$$\frac{\partial p_i}{\partial t} + (\vec{u}_i \cdot \nabla)p_i + \gamma p_i\,(\nabla \cdot \vec{u}_i) = 0, \tag{4.3}$$

$$\nabla^2\psi = 4\pi e(n_e + n_n - n_i - jZ_d n_{d0}). \tag{4.4}$$

Here, p_i is the positive ion fluid pressure, γ is the adiabatic index, and the existence of positively (negatively) charged dust particles is indicated by $j = +1(-1)$. The other variables used in (4.1) - (4.4) have been defined in section 3.2.

The vortex-like distribution of negative ions and Maxwell's distribution of electrons are assumed, respectively, to follow (Rahman and Haider, 2016; Sultana et al., 2019-a)

$$n_n = n_{n0}\left[1 + \left(\frac{e\psi}{K_BT_n}\right) - \frac{4}{3}\frac{(1-\beta_n)}{\sqrt{\pi}}\left(\frac{e\psi}{K_BT_n}\right)^{\frac{3}{2}} + \frac{1}{2}\left(\frac{e\psi}{K_BT_n}\right)^2 + \cdots\right], \tag{4.5}$$

and $$n_e = n_{e0}\, e^{\left(\frac{e\psi}{K_BT_e}\right)}. \tag{4.6}$$

The following notational modifications can be used to transform equations (4.1) - (4.6) into normalized form.

$$\tilde{n}_s \equiv \frac{n_s}{n_{s0}},\ (s = i, n, e),\ \ \tilde{t} \equiv \frac{t}{\omega_{pi}^{-1}\left(=\sqrt{\frac{m_i}{4\pi e^2 n_{i0}}}\right)},\ \tilde{r} \equiv \frac{r}{\lambda_D\left(=\sqrt{\frac{K_BT_e}{4\pi e^2 n_{i0}}}=\frac{C_{si}}{\omega_{pi}}\right)},\ \ \tilde{u}_i \equiv \frac{u_i}{C_{si}\left(=\sqrt{\frac{K_BT_e}{m_i}}\right)},$$

$$\tilde{\psi} \equiv \frac{\psi}{\frac{K_B T_e}{e}}, \quad \tilde{\omega}_{ci} \equiv \frac{\omega_{ci}}{\omega_{pi}\left(=\sqrt{\frac{4\pi e^2 n_{i0}}{m_i}}\right)}, \quad \tilde{p}_i \equiv \frac{p_i}{p_{i0}(=n_{i0}K_B T_i)}.$$

The normalized form of (4.1) - (4.4) is as follows:

$$\frac{\partial \tilde{n}_i}{\partial \tilde{t}} + \tilde{\nabla} \cdot (\tilde{n}_i\, \tilde{u}_i) = 0, \tag{4.7}$$

$$\frac{\partial \tilde{u}_i}{\partial \tilde{t}} + \left(\tilde{u}_i \cdot \tilde{\nabla}\right)\tilde{u}_i = -\tilde{\nabla}\tilde{\psi} + \tilde{\omega}_{ci}\,(\tilde{u}_i \times \hat{x}) - \frac{\sigma_i}{\tilde{n}_i}\tilde{\nabla}\tilde{p}_i, \tag{4.8}$$

$$\frac{\partial \tilde{p}_i}{\partial \tilde{t}} + \left(\tilde{u}_i \cdot \tilde{\nabla}\right)\tilde{p}_i + \gamma\, \tilde{p}_i\, (\tilde{\nabla} \cdot \tilde{u}_i) = 0, \tag{4.9}$$

$$\tilde{\nabla}^2\tilde{\psi} = \tilde{n}_e\mu_e + \tilde{n}_n\mu_n - \tilde{n}_i - j\mu_d, \tag{4.10}$$

where $\sigma_i = \frac{T_i}{T_e}$, $\mu_e = \frac{n_{e0}}{n_{i0}}$, $\mu_n = \frac{n_{n0}}{n_{i0}}$, and $\mu_d = \frac{Z_d n_{d0}}{n_{i0}}$.

Similarly, the respective normalized form of the distributions of negative ion and electron number densities is (where $\tilde{\psi} \ll 1$)

$$\tilde{n}_n = 1 + \alpha\tilde{\psi} - \frac{4}{3}\frac{(1-\beta_n)}{\sqrt{\pi}}\alpha^{\frac{3}{2}}\,\tilde{\psi}^{\frac{3}{2}} + \frac{1}{2}\alpha^2\tilde{\psi}^2, \tag{4.11}$$

and

$$\tilde{n}_e = e^{\tilde{\psi}}. \tag{4.12}$$

Here, $\alpha = \frac{T_e}{T_n}$ (where T_n is the negative ion's temperature), and β_n specifies the fraction of trapped negative ions. We are interested in $\beta_n < 0$, that relates to vortex-like distribution. The equilibrium condition is stated as $n_{e0} + n_{n0} = n_{i0} + j\, Z_d n_{d0}$, and this implies that $\mu_e = 1 - \mu_n + j\mu_d$.

The variables symbolized by tildes in equations (4.7) -(4.12) are all dimensionless, and they make the equations dimensionless. From now on, the tildes will be removed for simplicity.

4.3 Derivation of the mKdV-type equation

This segment aims to derive the mKdV-type equation for describing different effects (such as the magnetic, adiabatic, etc.). We use the Schamel's approach (Sultana et al., 2019-b;

Sultana, 2021) to characterize the DIA solitary waves efficiently, where the stretched coordinates are assumed as

$$\xi = \epsilon^{1/4}\,(l_x x + l_y y + l_z z - V_0 t) \text{ and } \tau = \epsilon^{3/4} t. \tag{4.13}$$

Here, $l_x^2 + l_y^2 + l_z^2 = 1$ and $l_x = \frac{\vec{k}\cdot\hat{x}}{k} = cos\theta$, where θ is the angle between $\hat{k}$ and $\vec{B}$.

The expanded form of the perturbed quantities n_i, p_i, u_{ix}, u_{iy}, u_{iz}, and ψ in terms of ϵ is:

$$n_i = 1 + \epsilon\, n_i^{(1)} + \epsilon^{3/2}\, n_i^{(2)} + \cdots, \tag{4.14}$$

$$p_i = 1 + \epsilon\, p_i^{(1)} + \epsilon^{3/2}\, p_i^{(2)} + \cdots, \tag{4.15}$$

$$u_{ix} = \epsilon\, u_{ix}^{(1)} + \epsilon^{3/2}\, u_{ix}^{(2)} + \cdots, \tag{4.16}$$

$$u_{iy} = \epsilon^{5/4}\, u_{iy}^{(1)} + \epsilon^{3/2}\, u_{iy}^{(2)} + \cdots, \tag{4.17}$$

$$u_{iz} = \epsilon^{5/4}\, u_{iz}^{(1)} + \epsilon^{3/2}\, u_{iz}^{(2)} + \cdots, \tag{4.18}$$

$$\psi = \epsilon\, \psi^{(1)} + \epsilon^{3/2}\psi^{(2)} + \cdots. \tag{4.19}$$

Now, we use (4.11) - (4.13) and substitute (4.14) - (4.19) into (4.7) - (4.10), and finally accumulate the terms in similar powers of ϵ. The 1st-order equations are found by collecting the coefficients of $\epsilon^{5/4}$ from (4.7) - (4.9) and the coefficient of ϵ from (4.10) as

$$l_x \frac{\partial u_{ix}^{(1)}}{\partial \xi} - V_0 \frac{\partial n_i^{(1)}}{\partial \xi}, \tag{4.20}$$

$$\sigma_i l_{\mathrm{x}} \frac{\partial p_i^{(1)}}{\partial \xi} - V_0 \frac{\partial u_{ix}^{(1)}}{\partial \xi} + l_x \frac{\partial \psi^{(1)}}{\partial \xi} = 0, \tag{4.21}$$

$$\sigma_i l_{\mathrm{y}} \frac{\partial p_i^{(1)}}{\partial \xi} - \omega_{ci} u_{iz}^{(1)} + l_y \frac{\partial \psi^{(1)}}{\partial \xi} = 0, \tag{4.22}$$

$$\sigma_i l_{\mathrm{z}} \frac{\partial p_i^{(1)}}{\partial \xi} + \omega_{ci} u_{iy}^{(1)} + l_z \frac{\partial \psi^{(1)}}{\partial \xi} = 0, \tag{4.23}$$

$$-V_0 \frac{\partial p_i^{(1)}}{\partial \xi} + \gamma l_x \frac{\partial u_{ix}^{(1)}}{\partial \xi} = 0, \tag{4.24}$$

$$n_i^{(1)} - (\mu_n \alpha + \mu_e)\psi^{(1)} = 0. \tag{4.25}$$

Thus, the 1st -order expressions are given by

$$u_{ix}^{(1)} = \frac{V_0 G_1}{l_x}\psi^{(1)}, \quad u_{iy}^{(1)} = -\frac{l_z}{\omega_{ci}}(1+\gamma\sigma_i G_1)\frac{\partial\psi^{(1)}}{\partial\xi}, \quad u_{iz}^{(1)} = \frac{l_y}{\omega_{ci}}(1+\gamma\sigma_i G_1)\frac{\partial\psi^{(1)}}{\partial\xi},$$

$$p_i^{(1)} = \gamma G_1\psi^{(1)}, \quad n_i^{(1)} = G_1\psi^{(1)}. \tag{4.26}$$

And the phase speed is determined as

$$V_0 = l_x\sqrt{\frac{(1+\gamma\sigma_i G_1)}{G_1}}\text{, where } G_1 = \mu_n\alpha + \mu_e. \tag{4.27}$$

Equating the coefficients of $\epsilon^{3/2}$ from the y and z-components of (4.8), and (4.10), we get

$$-\omega_{ci}u_{iz}^{(2)} - V_0\frac{\partial\, u_{iy}^{(1)}}{\partial\xi} = 0, \tag{4.28}$$

$$\omega_{ci}u_{iy}^{(2)} - V_0\frac{\partial\, u_{iz}^{(1)}}{\partial\xi} = 0, \tag{4.29}$$

$$G_1\psi^{(2)} - \frac{4}{3\sqrt{\pi}}\mu_n\alpha^{\frac{3}{2}}(1-\beta_n)[\psi^{(1)}]^{\frac{3}{2}} - n_i^{(2)} - \frac{\partial^2\psi^{(1)}}{\partial\xi^2} = 0. \tag{4.30}$$

Similarly, equating the coefficients of $\epsilon^{\frac{7}{4}}$ from (4.7), the x-component of (4.8), and (4.9), the resulting set of equations is obtained as

$$\frac{\partial n_i^{(1)}}{\partial\tau} - V_0\frac{\partial\, n_i^{(2)}}{\partial\xi} + l_x\frac{\partial u_{ix}^{(2)}}{\partial\xi} + l_y\frac{\partial u_{iy}^{(2)}}{\partial\xi} + l_z\frac{\partial u_{iz}^{(2)}}{\partial\xi} = 0, \tag{4.31}$$

$$\frac{\partial u_{ix}^{(1)}}{\partial\tau} - V_0\frac{\partial u_{ix}^{(2)}}{\partial\xi} + l_x\frac{\partial\psi^{(2)}}{\partial\xi} + \sigma_i l_x\frac{\partial p_i^{(2)}}{\partial\xi} = 0, \tag{4.32}$$

$$\frac{\partial p_i^{(1)}}{\partial\tau} + \gamma l_x\frac{\partial u_{ix}^{(2)}}{\partial\xi} + \gamma l_y\frac{\partial u_{iy}^{(2)}}{\partial\xi} + \gamma l_z\frac{\partial u_{iz}^{(2)}}{\partial\xi} - V_0\frac{\partial p_i^{(2)}}{\partial\xi} = 0. \tag{4.33}$$

The 2nd-order terms are completely removed from (4.28) - (4.33) to obtain the mKdV equation of the form

$$\frac{\partial\psi^{(1)}}{\partial\tau} + \delta_1\sqrt{\psi^{(1)}}\frac{\partial\psi^{(1)}}{\partial\xi} + \delta_2\frac{\partial^3\psi^{(1)}}{\partial\xi^3} = 0, \tag{4.34}$$

where $\delta_1 = \frac{V_0\,\mu_n\alpha^{3/2}\,(1-\beta_n)}{\sqrt{\pi}\,G_1(1+\gamma\sigma_i G_1)}$ and $\delta_2 = \frac{V_0}{2G_1(1+\gamma\sigma_i G_1)}\left[1 + \frac{(1-l_x^2)\,(1+\gamma\sigma_i G_1)^2}{\omega_{ci}^2}\right]$. (4.35)

Now, the higher-order effects will be incorporated into the mKdV equation. To the next order in ϵ, the 2nd-order perturbed quantities are obtained in terms of $\psi^{(1)}$ and $\psi^{(2)}$ as follows:

$$u_{ix}^{(2)} = \frac{V_0 G_1}{l_x}\psi^{(2)} - \frac{2G_1\delta_1}{3l_x}(1+2\gamma\sigma_i G_1)\left[\psi^{(1)}\right]^{\frac{3}{2}} - \frac{1}{l_x}\left(G_1\delta_2 + \frac{V_0\gamma\sigma_i G_1}{1+\gamma\sigma_i G_1}\right)\frac{\partial^2\psi^{(1)}}{\partial\xi^2},$$

$$u_{iy}^{(2)} = \frac{l_y V_0}{\omega_{ci}^2}(1+\gamma\sigma_i G_1)\frac{\partial^2\psi^{(1)}}{\partial\xi^2},\ u_{iz}^{(2)} = \frac{l_z V_0}{\omega_{ci}^2}(1+\gamma\sigma_i G_1)\frac{\partial^2\psi^{(1)}}{\partial\xi^2}, \quad (4.36)$$

$$n_i^{(2)} = G_1\psi^{(2)} - \frac{4}{3}\frac{G_1\delta_1}{V_0}(1+\gamma\sigma_i G_1)\left[\psi^{(1)}\right]^{\frac{3}{2}} - \frac{\partial^2\psi^{(1)}}{\partial\xi^2},\ p_i^{(2)} = \gamma n_i^{(2)}.$$

Similarly, the following 3rd-order perturbed quantities and a system of equations (omitted in the text) are obtained in terms of $u_{ix}^{(3)}$, $p_i^{(3)}$, $\psi^{(3)}$, $u_{iy}^{(4)}$, and $u_{iz}^{(4)}$.

$$u_{iy}^{(3)} = -\frac{l_z(1+\gamma\sigma_i G_1)}{\omega_{ci}}\frac{\partial\psi^{(2)}}{\partial\xi} + \frac{2\gamma\sigma_i G_1 l_z\delta_1}{V_0\omega_{ci}}(1+\gamma\sigma_i G_1)\sqrt{\psi^{(1)}}\frac{\partial\psi^{(1)}}{\partial\xi}$$
$$+\frac{l_z}{\omega_{ci}}\left[\frac{V_0^2}{\omega_{ci}^2}(1+\gamma\sigma_i G_1)+\gamma\sigma_i\right]\frac{\partial^3\psi^{(1)}}{\partial\xi^3}, \quad (4.37)$$

$$u_{iz}^{(3)} = \frac{l_y(1+\gamma\sigma_i G_1)}{\omega_{ci}}\frac{\partial\psi^{(2)}}{\partial\xi} - \frac{2\gamma\sigma_i G_1 l_y\delta_1}{V_0\omega_{ci}}(1+\gamma\sigma_i G_1)\sqrt{\psi^{(1)}}\frac{\partial\psi^{(1)}}{\partial\xi}$$
$$-\frac{l_y}{\omega_{ci}}\left[\frac{V_0^2}{\omega_{ci}^2}(1+\gamma\sigma_i G_1)+\gamma\sigma_i\right]\frac{\partial^3\psi^{(1)}}{\partial\xi^3}, \quad (4.38)$$

$$n_i^{(3)} = G_1\psi^{(3)} + \frac{1}{2}(\mu_n\alpha^2+\mu_e)\left[\psi^{(1)}\right]^2 - \frac{\partial^2\psi^{(2)}}{\partial\xi^2} - \frac{2\mu_n\alpha^{\frac{3}{2}}(1-\beta_n)}{\sqrt{\pi}}\sqrt{\psi^{(1)}}\,\psi^{(2)}. \quad (4.39)$$

Finally, the obtained mKdV-type inhomogeneous equation takes the following form

$$\frac{\partial\psi^{(2)}}{\partial\tau} + \delta_1\frac{\partial}{\partial\xi}\left(\sqrt{\psi^{(1)}}\psi^{(2)}\right) + \delta_2\frac{\partial^3\psi^{(2)}}{\partial\xi^3} = S\left(\psi^{(1)}\right), \quad (4.40)$$

where the source term $S\left(\psi^{(1)}\right)$ is given by

$$S\left(\psi^{(1)}\right) = M_1\,\psi^{(1)}\frac{\partial\psi^{(1)}}{\partial\xi} + M_2\frac{\left(\frac{\partial\psi^{(1)}}{\partial\xi}\right)^3}{\left[\psi^{(1)}\right]^{\frac{3}{2}}} + M_3\sqrt{\psi^{(1)}}\frac{\partial^3\psi^{(1)}}{\partial\xi^3} + M_4\frac{1}{\sqrt{\psi^{(1)}}}\frac{\partial\psi^{(1)}}{\partial\xi}\frac{\partial^2\psi^{(1)}}{\partial\xi^2}$$
$$+M_5\,\frac{\partial^5\psi^{(1)}}{\partial\xi^5}. \quad (4.41)$$

The coefficients $M_i (i = 1, 2, 3, 4, 5)$ occurred in (4.41) are specified in Appendix A.3. In this case, (4.34) is a nonlinear mKdV equation in $\psi^{(1)}$, whereas (4.40) is a linear inhomogeneous equation in $\psi^{(2)}$ with the term $S(\psi^{(1)})$ which may include secular or resonant terms. We can construct the required solution up to the second-order perturbed potential by eliminating secular behavior.

4.4 Dressed solution

The purpose of this segment is to acquire the dressed solution of (4.40) while the re-normalization method of Kodama and Taniuti (1978) will be used for removing secular behavior from the solution. In accordance with the method, (4.34) and (4.40) are modified, respectively, as

$$\frac{\partial\psi^{(1)}}{\partial\tau} + \delta_1\sqrt{\psi^{(1)}}\frac{\partial\psi^{(1)}}{\partial\xi} + \delta_2\frac{\partial^3\psi^{(1)}}{\partial\xi^3} + \delta\lambda\frac{\partial\psi^{(1)}}{\partial\xi} = 0, \tag{4.42}$$

and $$\frac{\partial\psi^{(2)}}{\partial\tau} + \delta_1\,\frac{\partial}{\partial\xi}\left(\psi^{(2)}\sqrt{\psi^{(1)}}\right) + \delta_2\frac{\partial^3\psi^{(2)}}{\partial\xi^3} + \delta\lambda\frac{\partial\psi^{(2)}}{\partial\xi} = S(\psi^{(1)}) + \delta\lambda\frac{\partial\psi^{(1)}}{\partial\xi}. \tag{4.43}$$

Let us now introduce a new variable $\eta = \xi - (\lambda + \delta\lambda)\tau$. Here, λ is connected to the Mach number $M = \frac{V}{C_S}$ (Esfandyari et al., 2008; Gill et al., 2010) by $\lambda + \delta\lambda = M - 1 = \Delta M$, where $C_S = K\left(\frac{T_e}{m_e}\right)^{1/2}$. Thus, (4.42) and (4.43) are transformed, respectively, as

$$\delta_2\frac{d^3\psi^{(1)}}{d\eta^3} + \delta_1\sqrt{\psi^{(1)}}\frac{d\psi^{(1)}}{d\eta} - \lambda\frac{d\psi^{(1)}}{d\eta} = 0, \tag{4.44}$$

and $$\delta_2\frac{d^3\psi^{(2)}}{d\eta^3} + \delta_1\,\frac{d}{d\eta}\left(\psi^{(2)}\sqrt{\psi^{(1)}}\right) - \lambda\frac{d\psi^{(2)}}{d\eta} = S(\psi^{(1)}) + \delta\lambda\frac{d\psi^{(1)}}{d\eta}. \tag{4.45}$$

We can integrate the ordinary differential equations (4.44) and (4.45) under the boundary conditions

$$\psi^{(1)} = \psi^{(2)} = \frac{d\psi^{(1)}}{d\eta} = \frac{d\psi^{(2)}}{d\eta} = \frac{d^2\psi^{(1)}}{d\eta^2} = \frac{d^2\psi^{(2)}}{d\eta^2} = 0, \text{ as } |\eta| \to \infty. \tag{4.46}$$

Thus, we obtain

$$\frac{d^2\psi^{(1)}}{d\eta^2}+\frac{1}{\delta_2}\left(\frac{2\delta_1}{3}\left[\psi^{(1)}\right]^{\frac{1}{2}}-\lambda\right)\psi^{(1)}=0, \tag{4.47}$$

and $$\frac{d^2\psi^{(2)}}{d\eta^2}+\frac{1}{\delta_2}\left(\delta_1\left[\psi^{(1)}\right]^{\frac{1}{2}}-\lambda\right)\psi^{(2)}=\frac{1}{\delta_2}\int_{-\infty}^{\eta}\left[S(\psi^{(1)})+\delta\lambda\frac{d\psi^{(1)}}{d\eta}\right]\,d\eta. \tag{4.48}$$

The following one-soliton solution of (4.47) is given by Salam et al. (2021).

$$\psi^{(1)}=\psi_{A1}\operatorname{sech}^4\left(\frac{\eta}{W}\right), \tag{4.49}$$

where the amplitude (ψ_{A1}) and width (W) are, respectively, given by

$$\psi_{A1}=\left(\frac{15\,\lambda}{8\,\delta_1}\right)^2 \text{ and } W=\sqrt{\frac{16\delta_2}{\lambda}}. \tag{4.50}$$

Again, the right-hand side of (4.48) becomes

$$\frac{1}{\delta_2}\int_{-\infty}^{\eta}\left[S(\psi^{(1)})+\delta\lambda\frac{d\psi^{(1)}}{d\eta}\right]\,d\eta=T\operatorname{sech}^8\left(\frac{\eta}{W}\right)+\frac{\psi_{A1}}{\delta_2}\left[\delta\lambda+\frac{256M_5}{W^4}\right]\operatorname{sech}^4\left(\frac{\eta}{W}\right),$$

where $T=\frac{\psi_{A1}}{2\delta_2W^4}\left[M_1\psi_{A1}W^4-(16M_2+30M_3+20M_4)\sqrt{\psi_{A1}}W^2+1680\,M_5\right]$. (4.51)

The secular term is canceled out from $S(\psi^{(1)})$ by setting $\delta\lambda=-\frac{256M_5}{W^4}=-\frac{\lambda^2M_5}{\delta_2^2}$ (Mahmood et al., 2021; Fayad et al., 2021; Paul et al., 2021). Hence, $z=\tanh\left(\frac{\eta}{W}\right)$ reduces (4.48) to

$$(1-z^2)\frac{d^2\psi^{(2)}}{dz^2}-2z\frac{d\psi^{(2)}}{dz}+\left(30-\frac{16}{1-z^2}\right)\psi^{(2)}=T(1-z^2)^3=F(z). \tag{4.52}$$

The homogenous part of (4.52), i.e., $(1-z^2)\frac{d^2\psi^{(2)}}{dz^2}-2z\frac{d\psi^{(2)}}{dz}+\left(30-\frac{16}{1-z^2}\right)\psi^{(2)}=0$ has two independent solutions in terms of associated Legendre polynomials $P_5^4(z)$ and $Q_5^4(z)$ (Gill et al., 2010; El-Labani et al., 2014), where the generalized formulae (given in section 3.4) of $P_n^m(z)$ and $Q_n^m(z)$ are used to determine the polynomials by setting $m=4$ and $n=5$. Thus, we obtain

$$P_5^4(z)=945z(1-z^2)^2,$$

and

$$Q_5^4(z) = \frac{945}{2} z(1-z^2)^2 \ln\left(\frac{1+z}{1-z}\right) - 945(1-z^2)^2 + 315(1-z^2) + 126 + \frac{72(1-z^2)+48}{(1-z^2)^2}.$$

The C. F. $\psi_c^{(2)} = c_1 P_5^4(z) + c_2 Q_5^4(z)$ becomes vanished as $P_5^4(z)$ is the secular one (Lai, 1979) and also $c_2 = 0$ due to the boundary conditions (4.46).

The P. I. of (4.52) can be found by means of the variation of parameter method as

$$\psi_p^{(2)} = q_1(z) P_5^4(z) + q_2(z) Q_5^4(z) = \frac{T}{6}(1-z^2)^2 \left[1 - \frac{1}{2}(1-z^2)\right], \tag{4.53}$$

where $q_1 = -\int \frac{Q_5^4(z)\, F(z)}{(1-z^2)\, W(P_5^4, Q_5^4)} dz$, $q_2 = \int \frac{P_5^4(z)\, F(z)}{(1-z^2)\, W(P_5^4, Q_5^4)} dz$, and $W(P_5^4, Q_5^4) = \frac{328860}{1-z^2}$.

Hence, the dressed solution up to the 2nd -order of ΔM is provided by (Gill et al., 2010; El-Labani et al., 2014)

$$\psi = \psi^{(1)} + \psi^{(2)} = \left(\frac{15\,\Delta M}{8\,\delta_1}\right)^2 \operatorname{sech}^4\left(\frac{\eta}{W}\right) + \frac{T}{6}\left[1 - \frac{1}{2}\operatorname{sech}^2\left(\frac{\eta}{W}\right)\right] \operatorname{sech}^4\left(\frac{\eta}{W}\right), \tag{4.54}$$

where $\lambda = \Delta M\left(1 + \frac{M_5}{\delta_2^2}\Delta M\right)$. As we can see from (4.54), the second term of the right side indicates the higher-order effect on the solution, and the modified amplitude and width are $\psi_{A12} = \left(\frac{15\,\Delta M}{8\,\delta_1}\right)^2 + \frac{T}{12}$ and $W = \sqrt{\frac{16\delta_2}{\lambda}} = 4\sqrt{\frac{\delta_2}{\Delta M}}\left(1 - \frac{M_5}{2\delta_2^2}\Delta M\right)$, respectively. It is observed that the amplitude changes due to the addition of higher-order terms, but the width remains unchanged.

4.5 Results and discussion

In this part, we have looked into the characteristics of DIA waves with respect to higher-order terms and compared the findings of higher-order terms with those of lower-order terms. To observe the influence of higher-order effects, a numerical analysis of the solution has been carried out. The solution depends on various parameters, such as negative ion concentration (μ_n), electron concentration (μ_e), trapping parameter ($\beta_n < 0$), temperature ratio $\sigma_i = \frac{T_i}{T_e}$, etc., and it gives compressive solitary waves. The values of different parameters have been selected from the neutrality condition, plasma assumptions, and previous works (Anower and Mamun, 2008; Rahman and Haider, 2019). Again, in accordance with the rule of reductive perturbation theory, the higher-order terms (i.e., $\psi^{(2)}$) must satisfy the criterion $\frac{|\psi^{(2)}|}{|\psi^{(1)}|} \leq 1$. With the parametric values taken into consideration, the resulting solution (4.54) satisfies the requirement for both types of charged dust particles (Figure 4.1).

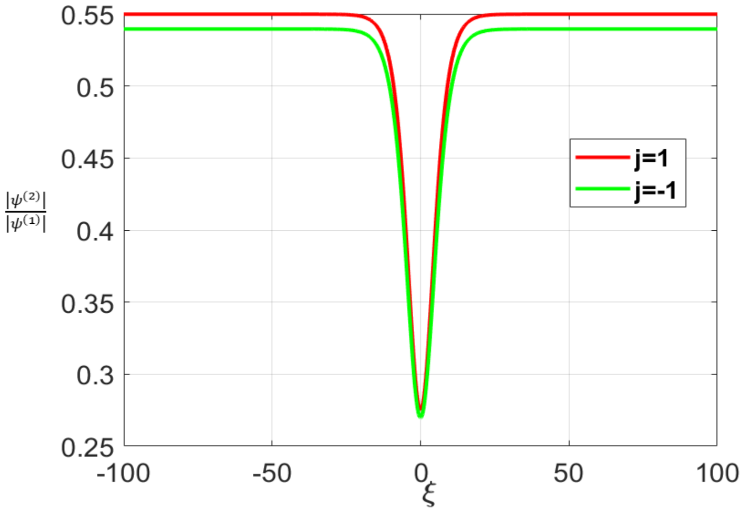

Figure 4.1: $\frac{|\psi^{(2)}|}{|\psi^{(1)}|}$ vs. ξ in the presence of positively ($j = 1$) and negatively ($j = -1$) charged dust particles, when $\beta_n = -0.9, \alpha = 10, \sigma_i = 0.2, \mu_d = 0.4, \mu_n = 0.7, \gamma = 1.67, \omega_{ci} = 0.9, \Delta M = 0.01, \theta = 15^0, \tau = 1$.

We plot lower-order potential $\psi^{(1)}$, higher-order correction $\psi^{(2)}$, and dressed solution ψ in Figures 4.2 and 4.3 to illustrate graphically the influence of higher-order terms in the cases of positively and negatively charged dust particles, respectively. Both figures show that (when $\beta_n = -0.9, \alpha = 10, \sigma_i = 0.2, \mu_d = 0.4, \mu_n = 0.7, \gamma = 1.67, \omega_{ci} = 0.9, \Delta M = 0.01, \theta = 15^0$ are chosen for effective explanation) the plasma model under consideration only allows positive potentials. Besides, the total wave amplitude increases when the higher-order nonlinearity is present, and the earlier findings support it (Esfandyari et al., 2008; Gill et al., 2010). It is important to note that PCD particles produce waves with higher amplitudes than negatively charged dust particles do.

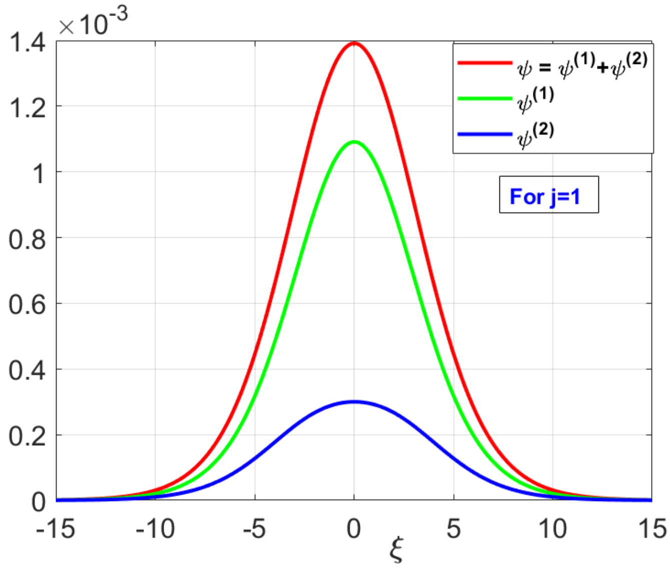

Figure 4.2: Wave structures of ψ, $\psi^{(1)}$, and $\psi^{(2)}$ in presence of positively charged dust particles ($j = 1$), when $\beta_n = -0.9$, $\alpha = 10$, $\sigma_i = 0.2$, $\mu_d = 0.4$, $\mu_n = 0.7$, $\gamma = 1.67$, $\omega_{ci} = 0.9$, $\Delta M = 0.01$, $\theta = 15^0$.

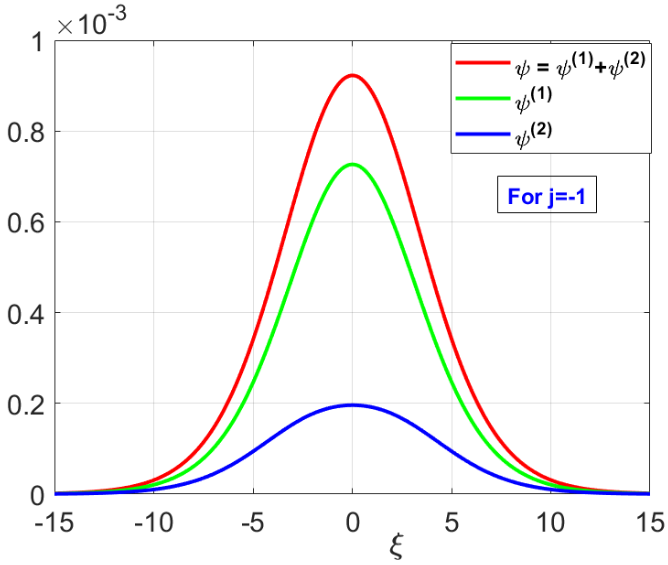

Figure 4.3: Wave structures of ψ, $\psi^{(1)}$, and $\psi^{(2)}$ in presence of negatively charged dust particles ($j = -1$), when $\beta_n = -0.9$, $\alpha = 10$, $\sigma_i = 0.2$, $\mu_d = 0.4$, $\mu_n = 0.7$, $\gamma = 1.67$, $\omega_{ci} = 0.9$, $\Delta M = 0.01$, $\theta = 15^0$.

It is clear from (4.54) that the external magnetic field, ion and electron concentrations, adiabaticity effect, etc., have a considerable impact on the wave characteristics. The modifications of the solitary wave profiles for various ω_{ci} in the presence of positively and negatively charged dust particles are shown in Figures 4.4 and 4.5, respectively. The wave structures are displayed here against $\omega_{ci} = 0.7$, $\omega_{ci} = 0.8$, and $\omega_{ci} = 0.9$ (when $\beta_n = -0.9,\ \alpha = 10,\ \sigma_i = 0.2,\ \mu_d = 0.4,\ \mu_n = 0.7,\ \gamma = 1.67,\ \Delta M = 0.01,\ \theta = 15^0$). Moreover, as shown in Figures 4.6 and 4.7, the magnetic field exhibits a decreasing effect on the wave's amplitudes and widths in the presence of higher-order nonlinear and dispersive effects. We also observe here an issue, which is that the magnetic field does not influence the amplitude when the lower-order nonlinear effect ($\psi^{(1)}$) is taken into consideration only, whereas it is seen that the magnetic field has a diminishing effect on the amplitude when the higher-order effect is considered. Moreover, amplitude and width are found to be higher for higher-order terms compared to lower-order terms.

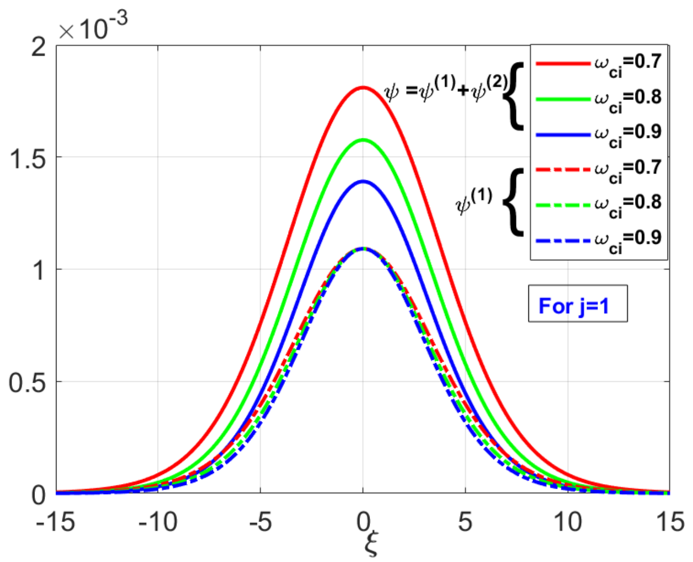

Figure 4.4: Change in wave structures of $\psi = \psi^{(1)} + \psi^{(2)}$ (solid curves) and $\psi^{(1)}$ (dashed curves) for $\omega_{ci} = 0.7$ (red), $\omega_{ci} = 0.8$ (green), and $\omega_{ci} = 0.9$ (blue), when $j = 1$, $\beta_n = -0.9$, $\alpha = 10$, $\sigma_i = 0.2$, $\mu_d = 0.4$, $\mu_n = 0.7$, $\gamma = 1.67$, $\Delta M = 0.01$, $\theta = 15^0$.

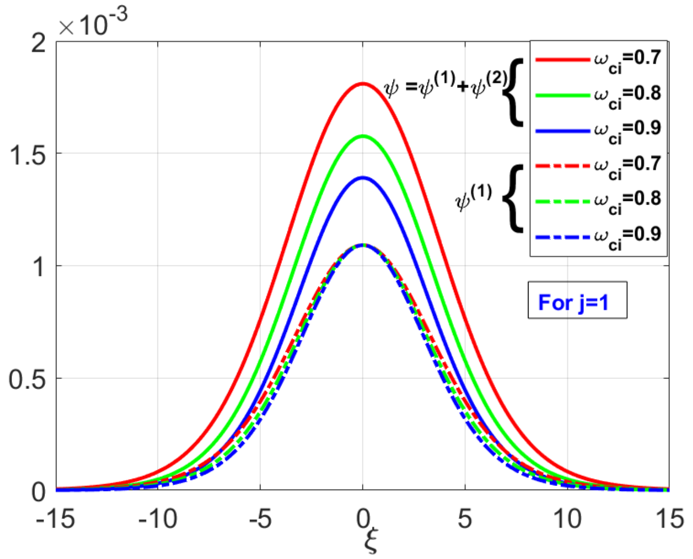

Figure 4.5: Change in wave structures of $\psi = \psi^{(1)} + \psi^{(2)}$ (solid curves) and $\psi^{(1)}$ (dashed curves) for $\omega_{ci} = 0.7$ (red), $\omega_{ci} = 0.8$ (green), and $\omega_{ci} = 0.9$ (blue), when $j = -1$, $\beta_n = -0.9$, $\alpha = 10$, $\sigma_i = 0.2$, $\mu_d = 0.4$, $\mu_n = 0.7$, $\gamma = 1.67$, $\Delta M = 0.01$, $\theta = 15^0$.

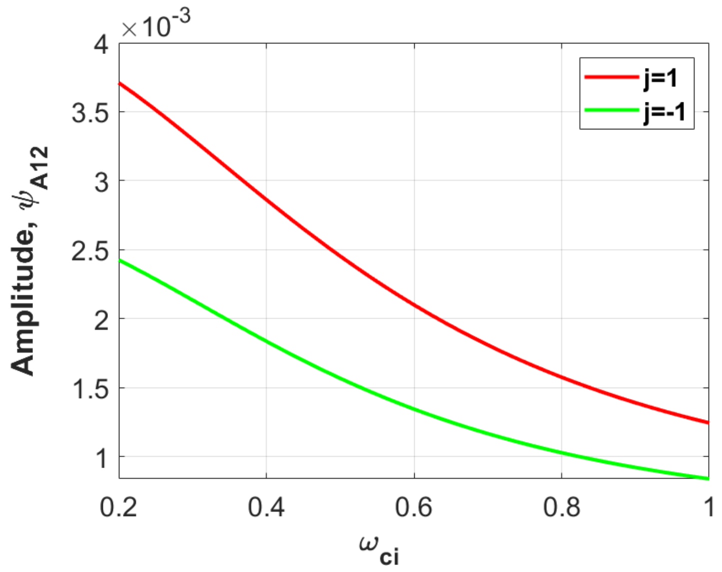

Figure 4.6: Amplitude (ψ_{A12}) vs. gyro-frequency (ω_{ci}).

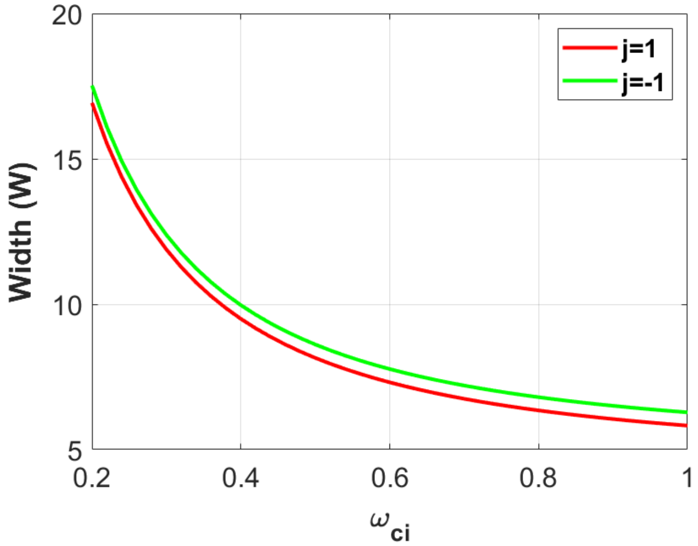

Figure 4.7: Width (W) vs. gyro-frequency (ω_{ci}).

The adiabaticity effect on the DIA solitary wave structures, where $\beta_n = -0.9$, $\alpha = 10$, $\sigma_i = 0.2$, $\mu_d = 0.4$, $\mu_n = 0.7$, $\omega_{ci} = 0.4$, $\Delta M = 0.01$, $\theta = 15^0$, is investigated in Figures 4.8 and 4.9. The figures show that, in the presence of dust particles that are positively or negatively charged, the amplitude and width increase as the value of γ rises, i.e., it boosts the energy of the waves. Like the effect of γ, the ratio of temperatures σ_i also has a growing effect on the wave's structures (Figures 4.10 and 4.11).

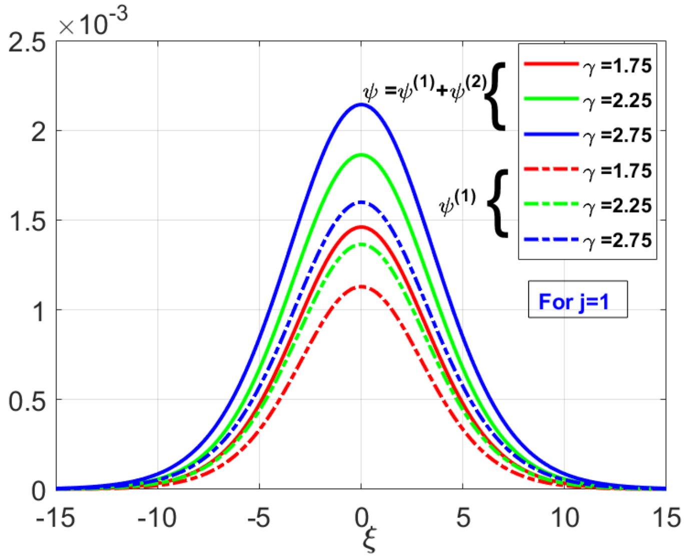

Figure 4.8: Variation in wave structures of ψ (solid curves) and $\psi^{(1)}$ (dashed curves) for $\gamma = 1.75$ (red), $\gamma = 2.25$ (green), and $\gamma = 2.75$ (blue), when $j = 1$ and $\beta_n = -0.9$, $\alpha = 10$, $\sigma_i = 0.2$, $\mu_d = 0.4$, $\mu_n = 0.7$, $\omega_{ci} = 0.9$, $\Delta M = 0.01$, $\theta = 15^0$.

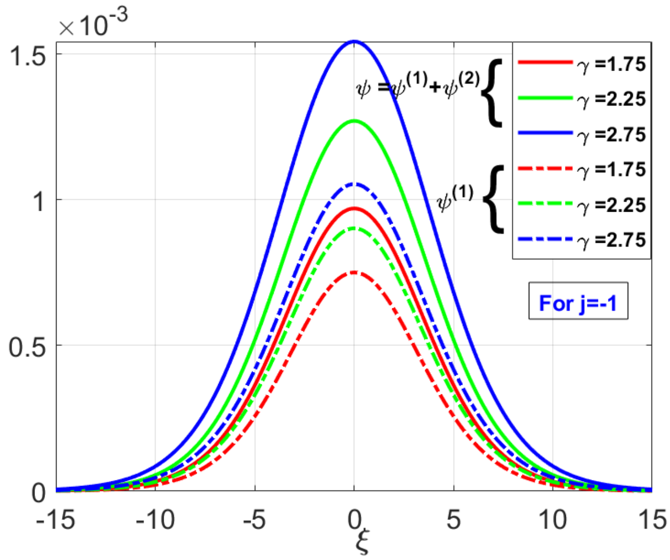

Figure 4.9: Variation in wave structures of ψ (solid curves) and $\psi^{(1)}$ (dashed curves) for $\gamma = 1.75$ (red), $\gamma = 2.25$ (green), and $\gamma = 2.75$ (blue), when $j = -1$ and $\beta_n = -0.9$, $\alpha = 10$, $\sigma_i = 0.2$, $\mu_d = 0.4$, $\mu_n = 0.7$, $\omega_{ci} = 0.9$, $\Delta M = 0.01$, $\theta = 15^0$.

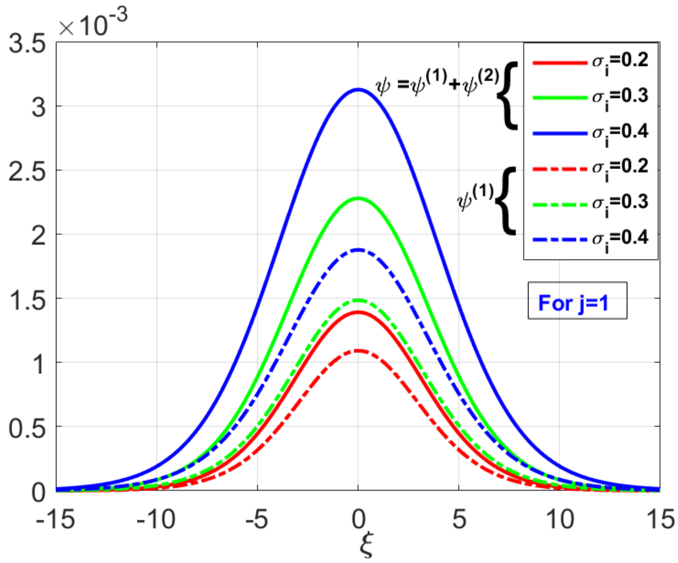

Figure 4.10: Variation in wave structures of ψ (solid curves) and $\psi^{(1)}$ (dashed curves) for $\sigma_i = 0.2$ (red), $\sigma_i = 0.3$ (green), and $\sigma_i = 0.4$ (blue), when $j = 1$ and $\beta_n = -0.9$, $\alpha = 10$, $\gamma = 1.67$, $\mu_d = 0.4$, $\mu_n = 0.7$, $\omega_{ci} = 0.9$, $\Delta M = 0.01$, $\theta = 15^0$.

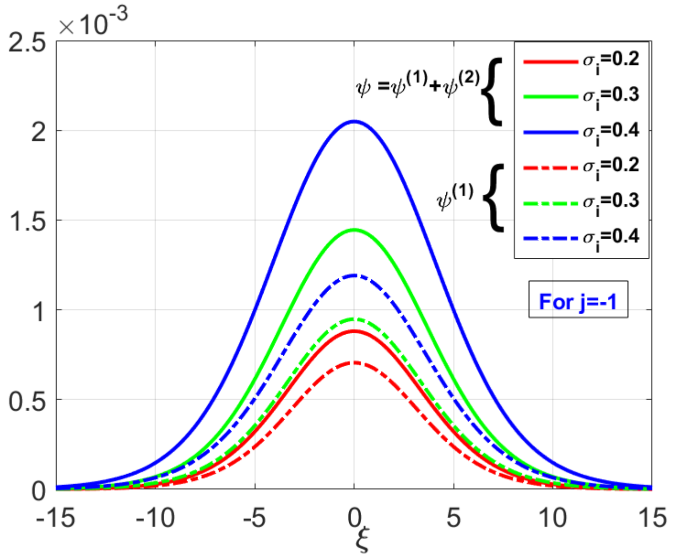

Figure 4.11: Variation in wave structures of ψ (solid curves) and $\psi^{(1)}$ (dashed curves) for $\sigma_i = 0.2$ (red), $\sigma_i = 0.3$ (green), and $\sigma_i = 0.4$ (blue), when $j = -1$ and $\beta_n = -0.9$, $\alpha = 10$, $\gamma = 1.67$, $\mu_d = 0.4$, $\mu_n = 0.7$, $\omega_{ci} = 0.9$, $\Delta M = 0.01$, $\theta = 15^0$.

The changes of the solitary wave profiles for various μ_d are shown in Figures 4.12 and 4.13 in the presence of positively and negatively charged dust particles, respectively. These figures exhibit the wave structures against the dust concentrations $\mu_d = 0.2$, $\mu_d = 0.5$, and $\mu_d = 0.8$ (where $\beta_n = -0.9$, $\alpha = 10$, $\sigma_i = 0.2$, $\mu_n = 0.7$, $\gamma = 1.67$, $\omega_{ci} = 0.9$, $\Delta M = 0.01$, $\theta = 15^0$). From Figures 4.12 and 4.13, it is observed that the positively (negatively) charged dust concentration has an increasing (decreasing) effect on the amplitudes of the DIA solitary waves in the presence of higher-order nonlinear and dispersive effects.

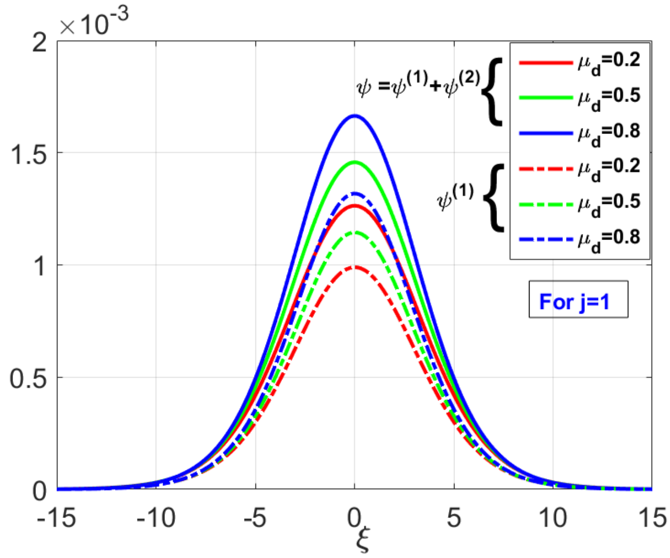

Figure 4.12: Variation of ψ (solid curves) and $\psi^{(1)}$ (dashed curves) for $\mu_d = 0.2$, 0.5, 0.8, when $j = 1$ and $\beta_n = -0.9$, $\alpha = 10$, $\gamma = 1.67$, $\sigma_i = 0.2$, $\mu_n = 0.7$, $\omega_{ci} = 0.9$, $\Delta M = 0.01$, $\theta = 15^0$.

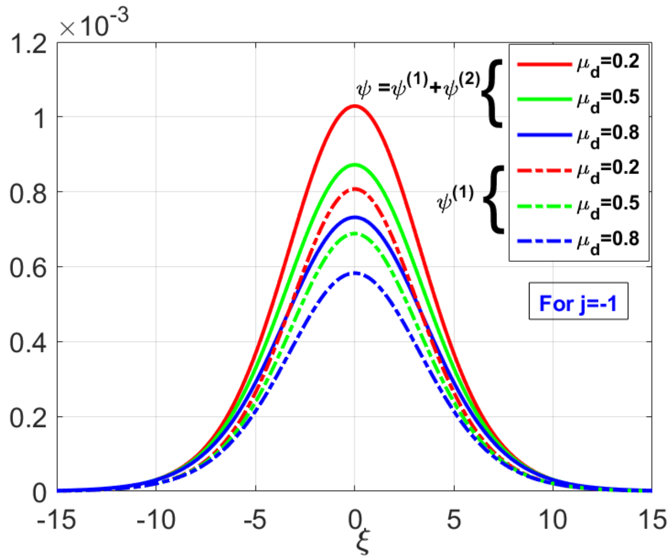

Figure 4.13: Variation of ψ (solid curves) and $\psi^{(1)}$ (dashed curves) for $\mu_d = 0.2$, 0.5, 0.8, when $j = -1$ and $\beta_n = -0.9$, $\alpha = 10$, $\gamma = 1.67$, $\sigma_i = 0.2$, $\mu_n = 0.7$, $\omega_{ci} = 0.9$, $\Delta M = 0.01$, $\theta = 15^0$.

Effects of σ_i, α, θ, μ_n, etc., on the phase speed are drawn in Figures 4.14 - 4.18 while σ_i has an increasing effect and α, θ, and μ_n have a decreasing effect on the phase speed. Besides, μ_d has decreasing (increasing) effect on the phase speed for $j = 1(-1)$.

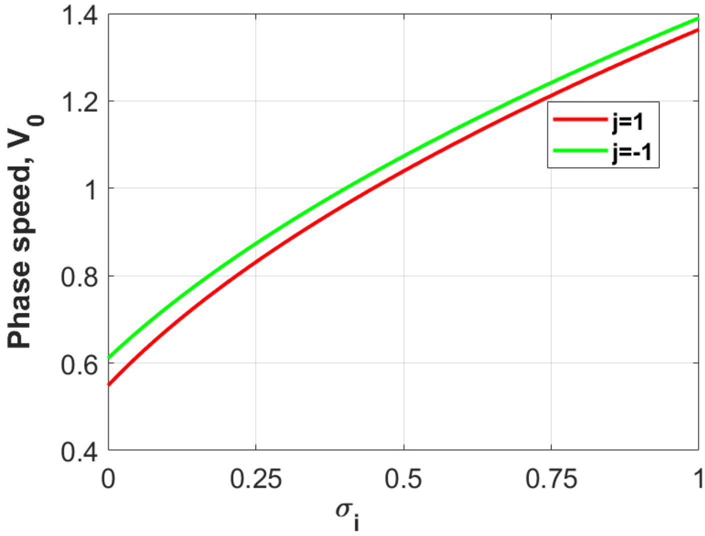

Figure 4.14: V_0 vs. σ_i, when $\alpha = 10$, $\mu_d = 0.3$, $\mu_n = 0.2$, $\omega_{ci} = 0.9$, $\theta = 15^0$.

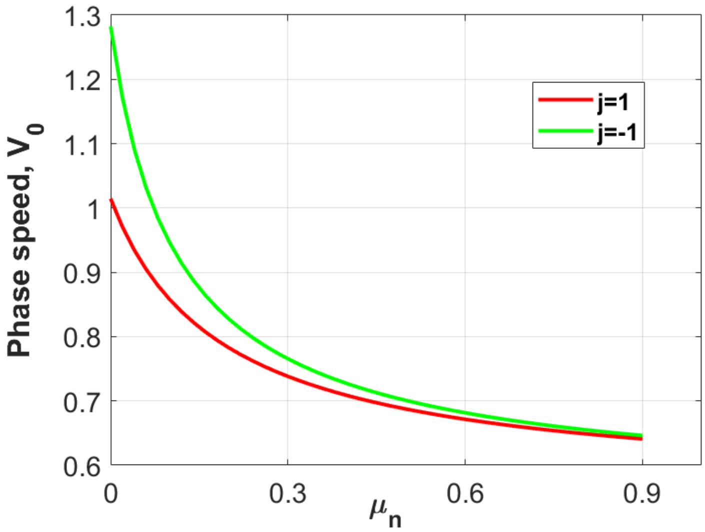

Figure 4.15: V_0 vs. μ_n, when $\alpha = 10$, $\mu_d = 0.3$, $\sigma_i = 0.2$, $\omega_{ci} = 0.9$, $\theta = 15^0$.

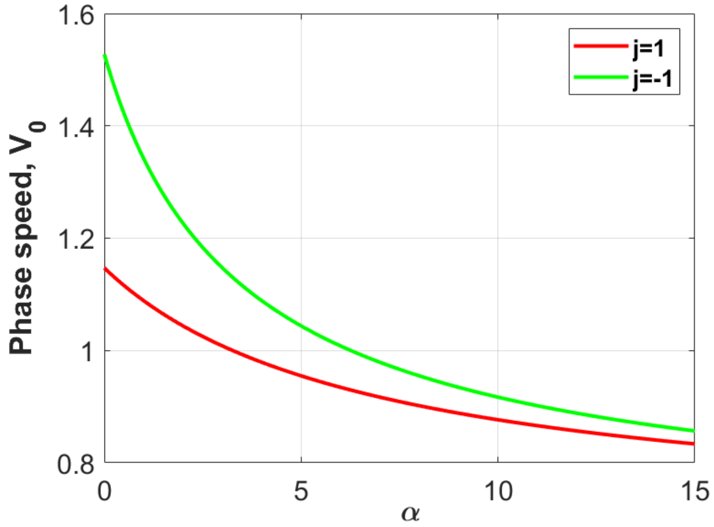

Figure 4.16: V_0 vs. α, when $\mu_d = 0.3$, $\mu_n = 0.2$, $\sigma_i = 0.3$, $\omega_{ci} = 0.9$, $\theta = 15^0$.

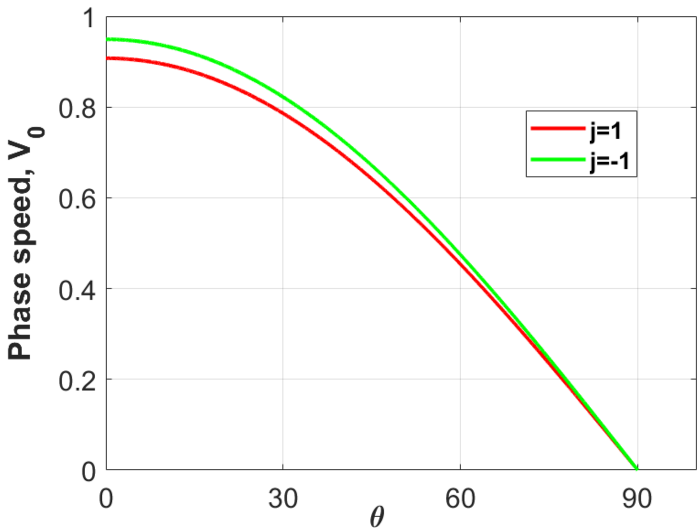

Figure 4.17: V_0 vs. θ, when $\alpha = 0.3$, $\mu_d = 0.3$, $\mu_n = 0.2$, $\sigma_i = 0.2$, $\omega_{ci} = 0.9$.

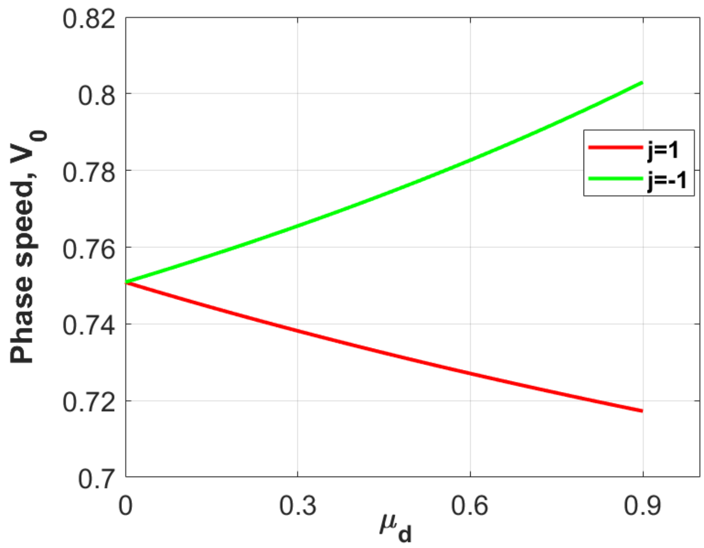

Figure 4.18: V_0 vs. μ_d, when $\alpha = 10$, $\sigma_i = 0.2$, $\mu_n = 0.3$, $\omega_{ci} = 0.9$, $\theta = 15^0$.

4.6 Summary

We have looked into how the characteristics of the DIA solitary waves in dusty plasma are affected by the higher-order nonlinear and dispersive terms. The result clearly shows that the parameters and higher-order terms have a significant impact on the wave properties. Plasma researchers also have observed similar results in past theoretical investigations (El-Taibany et al., 2005; Ahmed et al., 2020), where they included one or more of the following effects. These are the main findings (in the presence of positively or negatively charged dust particles):

i. *Higher-order effect*: The amplitude is increasingly influenced by the higher-order nonlinear and dispersive terms.

ii. *Magnetic effect:* The DIA solitary waves propagate with reduced amplitude and narrower width when the magnetic influence is in play. The magnetic field does not affect the wave amplitude when there are lower-order effects present, but it does so when there are higher-order effects.

iii. *Adiabatic effect*: In the presence of higher-order terms, adiabaticity affects the amplitude and width of the solitary wave increasingly.

iv. *Effect of the obliqueness* (θ): When θ increases, the solitary wave's phase speed decreases. Besides the amplitude becomes infinite at the limit $\theta \to 90^0$ which indicates that the angle should be small.

v. *Dust effect:* Positively (negatively) charged dust particles has an increasing (decreasing) effect on the amplitudes. Besides, dust has decreasing (increasing) effect on the phase speed in the presence of positively(negatively) charged dust particles.

Chapter Five

Higher-order nonlinear and parametric effects on DIA shock waves

5.1 Introduction

The dissipative and nonlinear terms combine to form the shock waves. In a plasma system, dissipation can happen in a variety of ways, including particle-particle interfaces, multi-ion streaming, viscosity, etc. It was proved by several laboratory studies (Nakamura, 2002; Fortov et al., 2005; Sarma and Nakamura, 2009) that DIA shock waves exist in many physical phenomena. Moreover, the DIA shock waves in the solar F Corona region were studied by Boro et al. (2020). In a plasma containing both stationary and charge fluctuation dust particles, Kamran et al. (2021) studied the DIA shocks and found that the shock amplitude reduces as the ion-electron temperature ratio rises. In order to better understand the shock waves in the context of a dusty plasma with two-temperature electrons, Bansal et al. (2021) examined cylindrical and spherical DIA shock waves. Besides, numerous researchers discussed the DIA shock and solitary wave natures in various circumstances (Samanta et al., 2013; Kanti et al., 2017; Ghasemloo, 2022; Khan et al., 2022; El-Helbawy, 2022).

In the majority of space plasmas, the generation of a phase space vortex causes electrons to become trapped while electrons follow the nonthermal distribution (vortex-like) rather than the Maxwellian distribution. Under certain conditions, electrons become trapped because they lack enough energy to overcome their potential. The confined particles drastically change the nonlinearity of the system. Many research findings (Ergun et al., 1998; Goldman et al., 2003; Cattell et al., 2003; Schippers et al., 2008; Zaghbeer, 2022) confirmed the trapping of electron particles, and to describe the DIA shock and solitary waves' nature, trapped electrons were considered components in various plasma frameworks. (Khater, 2022; Abdikian and Eghbali, 2022).

In general, the Burgers, modified Burgers, and KdV-Burgers equations incorporate nonlinear and dissipation effects of lower-order, and the equations are used to characterize the dynamics of DIA shock waves. Although the dispersion term is included in the KdV-Burgers equation, the dissipative term dominates it and controls the shock's nature. Researchers employed the reductive perturbation method (Selim et al., 2022-a; Selim et al., 2022-b; El-Monier and Attteya, 2022) to include the higher-order nonlinear and dissipative terms, that yield an inhomogeneous differential equation. Numerous researchers (El-Labany et al., 2014; Hossen et al., 2014; Abdelwahed, 2015; El-Monier and Atteya, 2019; Kaur et al., 2021) investigated the effect of higher-order terms on shock wave behaviors in the last decade. In order to better understand the DIA shock structures in dense plasmas, El-Labany et al. (2014), El-Monier and Atteya (2019), and Hossen et al. (2014) studied them theoretically. Moreover, Abdelwahed (2015) examined higher-order corrections to broadband electrostatic shock noise in the auroral zone, and Kaur et al. (2021) explored light and heavy nuclei acoustic dressed shocks for white dwarfs.

The focus of this chapter is on the investigation of the consequences of different parameters and higher-order nonlinear terms on the shock wave structures. We graphically compare the lower- and higher-order effects. A modified Burgers-type inhomogeneous equation is derived for this investigation. As far as we know, no analytical study has been done yet to examine the impact of higher-order nonlinearity using the inhomogeneous equation. The equation is derived using the reductive perturbation approach, and the higher-order effects are added to the dressed solution using the Abel's theorem and the method of variation of parameters.

5.2 Plasma model

Considering a magnetized plasma with positive ions, electrons (trapped), and dust particles (stationary and negatively charged), we investigate the higher-order impact and parametric effects on the DIA shock waves. Hence, for the magnetized adiabatic plasma (where $\vec{B} = B_0\hat{x}$), the equations presented below govern the nonlinear evolution of the shock waves.

$$\frac{\partial n_i}{\partial t} + \nabla \cdot (n_i \vec{u}_i) = 0, \tag{5.1}$$

$$\frac{\partial \vec{u}_i}{\partial t} + (\vec{u}_i \cdot \nabla)\vec{u}_i = -\frac{e}{m_i}\nabla\psi + \omega_{ci}\,(\vec{u}_i \times \hat{x}) - \frac{1}{m_i\, n_i}\nabla p_i + \eta\nabla^2\vec{u}_i, \tag{5.2}$$

$$\frac{\partial p_i}{\partial t} + (\vec{u}_i \cdot \nabla)p_i + \gamma p_i(\nabla \cdot \vec{u}_i) = 0, \tag{5.3}$$

$$\nabla^2\psi = 4\pi e(n_e - n_i + Z_d n_{d0}), \tag{5.4}$$

where n_i and n_e represent the ion number density and electron number density, respectively, $\gamma = \frac{N+2}{N}$ (N indicates the number of degrees of freedom while $N = 1$ for the one-dimensional case and $N = 3$ for the three-dimensional case), and η is the kinematic viscosity.

The vortex-like distribution of trapped electrons is assumed to follow (Sultana, 2021; Zaghbeer, 2022; Khater, 2022; Abdikian and Eghbali, 2022)

$$n_e = n_{e0}\left[1 + \left(\frac{e\psi}{K_B T_e}\right) - \frac{4}{3}\frac{(1-\beta_e)}{\sqrt{\pi}}\left(\frac{e\psi}{K_B T_e}\right)^{\frac{3}{2}} + \frac{1}{2}\left(\frac{e\psi}{K_B T_e}\right)^2 + \cdots\right]. \tag{5.5}$$

We can write equations (5.1) - (5.5) in normalized form using the following notations.

$$\tilde{n}_s \equiv \frac{n_s}{n_{s0}}\,(s = i, e),\quad \tilde{t} \equiv \frac{t}{\omega_{pi}^{-1}\left(=\sqrt{\frac{m_i}{4\pi e^2 n_{i0}}}\right)},\quad \tilde{r} \equiv \frac{r}{\lambda_D\left(=\sqrt{\frac{K_B T_e}{4\pi e^2 n_{i0}}}=\frac{C_{si}}{\omega_{pi}}\right)},\quad \tilde{u}_i \equiv \frac{u_i}{C_{si}\left(=\sqrt{\frac{K_B T_e}{m_i}}\right)},$$

$$\tilde{\psi} \equiv \frac{\psi}{\frac{K_B T_e}{e}},\quad \tilde{\omega}_{ci} \equiv \frac{\omega_{ci}}{\omega_{pi}\left(=\sqrt{\frac{4\pi e^2 n_{i0}}{m_i}}\right)},\quad \tilde{p}_i \equiv \frac{p_i}{p_{i0}(=n_{i0}K_B T_i)},\quad \tilde{\eta} \equiv \frac{\eta}{\omega_{pi}\lambda_D^2}. \tag{5.6}$$

The normalized form of (5.1) - (5.4) is as follows:

$$\frac{\partial \tilde{n}_i}{\partial \tilde{t}} + \tilde{\nabla} \cdot (\tilde{n}_i\,\tilde{u}_i) = 0, \tag{5.7}$$

$$\frac{\partial \tilde{u}_i}{\partial \tilde{t}} + (\tilde{u}_i \cdot \tilde{\nabla})\tilde{u}_i = -\tilde{\nabla}\tilde{\psi} + \tilde{\omega}_{ci}\,(\tilde{u}_i \times \hat{x}) - \frac{\sigma_i}{\tilde{n}_i}\tilde{\nabla}\tilde{p}_i + \tilde{\eta}\tilde{\nabla}^2\tilde{u}_i, \tag{5.8}$$

$$\frac{\partial \tilde{p}_i}{\partial \tilde{t}} + (\tilde{u}_i \cdot \tilde{\nabla})\tilde{p}_i + \gamma\tilde{p}_i(\tilde{\nabla} \cdot \tilde{u}_i) = 0, \tag{5.9}$$

$$\tilde{\nabla}^2\tilde{\psi} = \tilde{n}_e\mu_e - \tilde{n}_i + \mu_d, \tag{5.10}$$

where $\sigma_i = \frac{T_i}{T_e}$, $\mu_e = \frac{n_{e0}}{n_{i0}}$, and $\mu_d = \frac{Z_d n_{d0}}{n_{i0}}$.

Similarly, equation (5.5) is reduced to the normalized form (where $\tilde{\psi} \ll 1$)

$$\tilde{n}_e = 1 + \tilde{\psi} - \frac{4}{3}\frac{(1-\beta_e)}{\sqrt{\pi}}\,\tilde{\psi}^{\frac{3}{2}} + \frac{1}{2}\tilde{\psi}^2. \tag{5.11}$$

Here, β_e specifies the fraction of trapped electrons. We are interested in $\beta_e < 0$, that relates to the vortex-like distribution. The equilibrium condition takes the form $n_{e0} = n_{i0} - Z_d n_{d0}$, hence $\mu_e = 1 - \mu_d$.

5.3 Derivation of the wave equations

The dissipative effect may dominate the dispersive effect in nonlinear plasma waves, and this causes shock structures rather than solitary structures. In order to get the nonlinear wave equations (viz. the modified Burgers and modified Burgers-type inhomogeneous equations that generate the shock waves), we consider the stretched coordinates (Sumi et al., 2019)

$$\xi = \epsilon^{1/2}\,(l_x x + l_y y + l_z z - V_0 t) \text{ and } \tau = \epsilon\, t, \tag{5.12}$$

where $0 < \epsilon < 1$, $l_x^2 + l_y^2 + l_z^2 = 1$, and $l_x = \frac{\vec{k}\cdot\hat{x}}{k} = cos\theta$.

Substituting (5.11) - (5.12) and (4.14) - (4.19) into (5.7) - (5.10), and accumulating the terms in similar powers of ϵ, the following 1st-order quantities are obtained from the lowest-order terms of ϵ as

$$u_{ix}^{(1)} = \frac{V_0\mu_e}{l_x}\psi^{(1)},\;\; p_i^{(1)} = \gamma\mu_e\psi^{(1)},\;\; n_i^{(1)} = \mu_e\psi^{(1)}. \tag{5.13}$$

And the phase speed is determined as

$$V_0 = l_x\sqrt{\frac{1+\gamma\sigma_i\,\mu_e}{\mu_e}}\text{, where } \mu_e = 1-\mu_d. \tag{5.14}$$

5.3.1 The modified Burgers equation

Equating the coefficients of $\epsilon^{3/2}$ from the y and z-components of (5.8), and (5.10), we get

$$\sigma_i l_y \frac{\partial p_i^{(1)}}{\partial \xi} - \omega_{ci} u_{iz}^{(2)} + l_y \frac{\partial \psi^{(1)}}{\partial \xi} = 0, \tag{5.15}$$

$$\sigma_i l_z \frac{\partial p_i^{(1)}}{\partial \xi} + \omega_{ci} u_{iy}^{(2)} + l_z \frac{\partial \psi^{(1)}}{\partial \xi} = 0, \tag{5.16}$$

$$\mu_e \psi^{(2)} - \frac{4}{3\sqrt{\pi}}\mu_e\left(1-\beta_e\right)\left[\psi^{(1)}\right]^{\frac{3}{2}} - n_i^{(2)} = 0. \tag{5.17}$$

Likewise, collecting the coefficients of ϵ^2 from (5.7), the x-component of (5.8), and (5.9), the following equations are obtained.

$$\frac{\partial n_i^{(1)}}{\partial \tau} - V_0 \frac{\partial\, n_i^{(2)}}{\partial \xi} + l_x \frac{\partial u_{ix}^{(2)}}{\partial \xi} + l_y \frac{\partial u_{iy}^{(2)}}{\partial \xi} + l_z \frac{\partial u_{iz}^{(2)}}{\partial \xi} = 0, \tag{5.18}$$

$$\frac{\partial u_{ix}^{(1)}}{\partial \tau} - V_0 \frac{\partial u_{ix}^{(2)}}{\partial \xi} + l_x \frac{\partial \psi^{(2)}}{\partial \xi} + \sigma_i l_x \frac{\partial p_i^{(2)}}{\partial \xi} - \eta \frac{\partial^2 u_{ix}^{(1)}}{\partial \xi^2} = 0, \tag{5.19}$$

$$\frac{\partial p_i^{(1)}}{\partial \tau} + \gamma l_x \frac{\partial u_{ix}^{(2)}}{\partial \xi} + \gamma l_y \frac{\partial u_{iy}^{(2)}}{\partial \xi} + \gamma l_z \frac{\partial u_{iz}^{(2)}}{\partial \xi} - V_0 \frac{\partial p_i^{(2)}}{\partial \xi} = 0. \tag{5.20}$$

The 2nd-order quantities are eliminated from (5.15)- (5.20) and we obtain the following equation

$$\frac{\partial \psi^{(1)}}{\partial \tau} + A\sqrt{\psi^{(1)}}\frac{\partial \psi^{(1)}}{\partial \xi} = B\frac{\partial^2 \psi^{(1)}}{\partial \xi^2}, \tag{5.21}$$

where $A = \frac{V_0\,(1-\beta_e)}{\sqrt{\pi}\,(1+\gamma\sigma_i\mu_e)}$ and $B = \frac{\eta}{2}$. (5.22)

Equation (5.21) is referred to as the modified Burgers equation, where the right-hand side term of the equation gives the dissipative effect, i.e., it characterizes the shock nature.

5.3.2 The modified Burgers-type inhomogeneous equation

The modified Burgers-type equation will be derived in this section to incorporate the effect of higher-order nonlinearity. To the next order in ϵ, the following 2nd-order quantities are obtained in terms of $\psi^{(1)}$ and $\psi^{(2)}$.

$$u_{ix}^{(2)} = \frac{(1+\gamma\sigma_i\mu_e)l_x}{V_0}\psi^{(2)} - \frac{2}{3}\frac{A\mu_e}{l_x}(1+2\gamma\sigma_i\mu_e)\left[\psi^{(1)}\right]^{\frac{3}{2}} - \frac{\eta\mu_e}{2l_x}\frac{\partial\psi^{(1)}}{\partial\xi},$$

$$u_{iy}^{(2)} = -\frac{l_z(1+\gamma\sigma_i\mu_e)}{\omega_{ci}}\frac{\partial\psi^{(1)}}{\partial\xi}, \;\; u_{iz}^{(2)} = \frac{l_y(1+\gamma\sigma_i\mu_e)}{\omega_{ci}}\frac{\partial\psi^{(1)}}{\partial\xi}, \tag{5.23}$$

$$n_i^{(2)} = \mu_e\psi^{(2)} - \frac{4}{3}\frac{\mu_e\,(1-\beta_e)}{\sqrt{\pi}}\left[\psi^{(1)}\right]^{\frac{3}{2}}, \;\; p_i^{(2)} = \gamma n_i^{(2)}.$$

The 3rd -order perturbed quantity $n_i^{(3)}$ is obtained as

$$n_i^{(3)} = \mu_e\psi^{(3)} + \frac{1}{2}\mu_e\left[\psi^{(1)}\right]^2 - \frac{\partial^2\psi^{(1)}}{\partial\xi^2} - \frac{2\mu_e(1-\beta_e)}{\sqrt{\pi}}\sqrt{\psi^{(1)}}\,\psi^{(2)}. \tag{5.24}$$

Moreover, a set of equations, given in (A.14) - (A.23) of Appendix A.4, is obtained in terms of $u_{ix}^{(3)}$, $p_i^{(3)}$, $\psi^{(3)}$, $u_{iy}^{(4)}$, $u_{iz}^{(4)}$, and their derivatives.

Finally, the modified Burgers-type linear inhomogeneous equation in $\psi^{(2)}$ is derived as

$$\frac{\partial\psi^{(2)}}{\partial\tau} + A\,\frac{\partial}{\partial\xi}\left(\sqrt{\psi^{(1)}}\psi^{(2)}\right) - B\,\frac{\partial^2\psi^{(2)}}{\partial\xi^2} = S\left(\psi^{(1)}\right), \tag{5.25}$$

where $S\left(\psi^{(1)}\right)$ is defined by

$$S\left(\psi^{(1)}\right) = M_1\,\psi^{(1)}\frac{\partial\psi^{(1)}}{\partial\xi} + M_2\frac{\left(\frac{\partial\psi^{(1)}}{\partial\xi}\right)^2}{\sqrt{\psi^{(1)}}} + M_3\sqrt{\psi^{(1)}}\frac{\partial^2\psi^{(1)}}{\partial\xi^2} + M_4\frac{\partial^3\psi^{(1)}}{\partial\xi^3}. \tag{5.26}$$

The derivation of the equation (5.25) and $M_i(i = 1, 2, 3, 4)$ in (5.26) are provided in Appendices A.4 and A.5, respectively.

5.4 Dressed solution

Introduce $Z = \lambda(\xi - U_0\tau)$ that provides the solution of (5.21) as

$$\psi^{(1)} = \psi_m[1-\tanh Z]^2 = \psi_m\left[1-\tanh\left(\frac{\xi-U_0\tau}{W}\right)\right]^2, \tag{5.27}$$

where the amplitude (ψ_m) and width (W) are respectively, given by

$$\psi_m = \left(\frac{3U_0}{4\,A}\right)^2 \quad \text{and} \quad W = \lambda^{-1} = \frac{4B}{U_0}. \tag{5.28}$$

Again, the transformation $Z = \lambda(\xi - U_0\tau)$ modifies (5.25) to

$$\frac{d^2\psi^{(2)}}{dZ^2} + \frac{d}{dZ}\left[(1 + 3\tanh Z)\psi^{(2)}\right] = F(Z), \tag{5.29}$$

where $F(Z) = N_1[\tanh Z - 1]\ \operatorname{sech}^2 Z + \operatorname{sech}^4 Z\,[N_2 + N_3 \tanh Z]$,

$N_1 = \frac{81}{8}\frac{U_0^3 M_1}{A^4} + \frac{27}{8}\frac{U_0^3 M_3}{A^3 B} + \frac{9}{8}\frac{U_0^3 M_4}{A^2 B^2}$, $N_2 = \frac{243}{32}\frac{U_0^3 M_1}{A^4} + \frac{27}{16}\frac{U_0^3 M_2}{A^3 B} + \frac{135}{32}\frac{U_0^3 M_3}{A^3 B} + \frac{27}{16}\frac{U_0^3 M_4}{A^2 B^2}$,

$N_3 = -\frac{81}{32}\frac{U_0^3 M_1}{A^4} - \frac{27}{16}\frac{U_0^3 M_2}{A^3 B} - \frac{81}{32}\frac{U_0^3 M_3}{A^3 B} - \frac{27}{8}\frac{U_0^3 M_4}{A^2 B^2}$.

The homogeneous equation $\frac{d^2\psi^{(2)}}{dZ^2} + \frac{d}{dZ}\left[(1 + 3\tanh Z)\psi^{(2)}\right] = 0$ has two independent solutions. One of them is $\psi_{1c}^{(2)} = e^{-Z}\ \operatorname{sech}^3 Z$, and another solution can be obtained by the Abel's theorem (El-Labany et al., 2014) as $\psi_{2c}^{(2)} = [2\cosh^3 Z \sinh Z + 3\cosh Z \sinh Z + 3Z + 2\cosh^4 Z]\, e^{-Z}\ \operatorname{sech}^3 Z$. Here, the C. F. $\psi_c^{(2)} = c_1\psi_{1c}^{(2)} + c_2\psi_{2c}^{(2)}$ becomes vanished by the boundary condition (4.46), and the P.I. of (5.29) is determined as

$$\begin{aligned}\psi_p^{(2)} = q_1(Z)\psi_{1c}^{(2)} + q_2(Z)\psi_{2c}^{(2)} = \Big[&T_1 Z + T_2 \sinh^2 Z + T_3 \sinh Z \cosh^3 Z + \\ &\tfrac{3}{2}T_3 Z \sinh Z \operatorname{sech} Z + T_4 \sinh^2 Z \cosh^2 Z + T_5 \sinh^3 Z \operatorname{sech} Z + \\ &T_6 \sinh^3 Z \cosh Z + \tfrac{3}{2}T_6\, Z \sinh^2 Z \operatorname{sech}^2 Z + T_7(3\sinh^2 Z \operatorname{sech}^2 Z + \\ &2\cosh Z \sinh Z) + \frac{T_8 + 3T_3 Z}{(e^{2Z}+1)^4}\Big]\, e^{-Z} \operatorname{sech}^3 Z = T(Z), \text{say}\end{aligned} \tag{5.30}$$

Here, $q_1 = -\int \frac{\psi_{2c}^{(2)}\, F(Z)}{W(\psi_{1c}^{(2)}, \psi_{2c}^{(2)})} dZ$, $q_2 = \int \frac{\psi_{1c}^{(2)}\, F(Z)}{W(\psi_{1c}^{(2)}, \psi_{2c}^{(2)})} dZ$, $W(\psi_{1c}^{(2)}, \psi_{2c}^{(2)}) = \frac{8e^{-2Z}(\cosh Z + \sinh Z)}{\cosh^3 Z}$,

$T_1 = \frac{1}{4}(N_1 - 2N_2)$, $T_2 = -\frac{3N_1}{8} + \frac{N_2}{3} + \frac{N_3}{16}$, $T_3 = -\frac{1}{12}(3N_1 - 2N_2)$, $T_4 = -\frac{N_1}{8} + \frac{N_2}{6} + \frac{N_3}{16}$,

$T_5 = \frac{3N_1}{16} + \frac{5N_3}{32}$, $T_6 = \frac{N_1}{8} + \frac{N_3}{16}$, $T_7 = \frac{N_2}{24}$, $T_8 = -\frac{1}{8}(3N_1 + N_3)$.

The stationary solution that incorporates the higher-order nonlinear effect is

$$\psi = \psi^{(1)} + \psi^{(2)} = \psi_m (1 - \tanh Z)^2 + T(Z), \tag{5.31}$$

where $\psi_m = \left(\frac{3U_0}{4A}\right)^2$, $Z = \frac{U_0}{4B}(\xi - U_0\tau)$. Here, $T(Z)$ indicates the impact of higher-order terms.

5.5 Results and discussion

This section aims to investigate numerically the influence of the higher-order nonlinear effect on the waves while the effect of lower-order terms has been analyzed first. The parametric values (viz. $n_{i0} = 5 \times 10^8\ cm^{-3}$, $n_{e0} = 3.3 \times 10^8\ cm^{-3}$, $T_i = 0.05\ eV$, $T_e = 2.5\ eV$, $n_{d0} = 10^4 - 10^5\ cm^{-3}$, $Z_d = 10^3 - 3 \times 10^3$) are taken from the study of Rosenberg et al. (2008) and the fundamental assumptions $\beta_e < 0$, $\mu_e + \mu_d = 1$ (Ergun et al., 1998; Goldman et al., 2003; Cattell et al., 2003; Schippers et al., 2008; Zaghbeer, 2022; Khater, 2022; Abdikian and Eghbali, 2022). The impacts of the trapping parameter, dust concentration, obliquity, etc., have also been thoroughly addressed here because the characteristics of the waves change significantly by these parameters. Specifically, subsection 5.5.1 exemplifies the nature of shock structure when the solution is associated with only first-order potential, and subsection 5.5.2 demonstrates the role of higher-order effect when the solution includes both first- and second-order potentials.

5.5.1 Lower-order effect

The nonlinear term (that governs the wave's steepness) and the dissipation term (that accounts for the loss of energy) balance each other to produce a shock wave. The solution (5.27) gives various types of shock structures depending on several parameters, like β_e, μ_d, γ, θ, etc. The shock wave profiles are depicted in Figure 5.1 for various angles (θ), and it is seen that, in the presence of negatively charged dust particles, θ has an increasing impact on the amplitude. As A and B are found to be positive, the plasma system under consideration can only have a positive potential. From the aforementioned ranges of parametric values, the particular numerical values specified in the figure captions have been chosen.

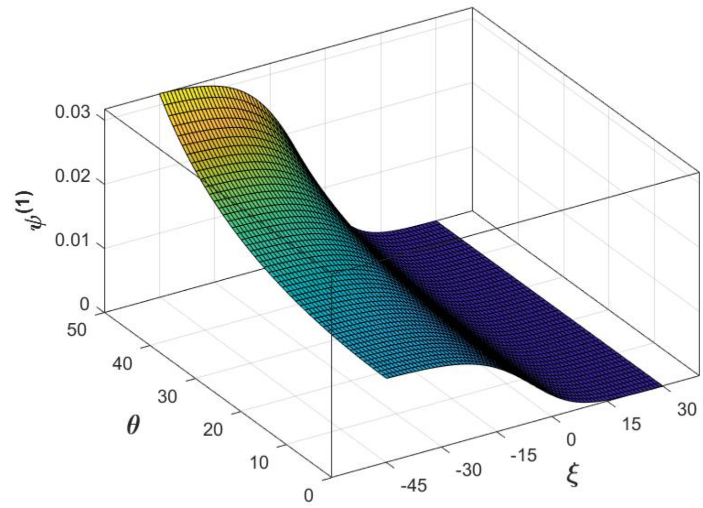

Figure 5.1: Wave profile variations for different angles (θ), when $\mu_d = 0.34$, $\beta_e = -0.9$, $\gamma = 5/3$, $\sigma_i = 0.02$, $U_0 = 0.1$, $\eta = 0.8$, $\tau = 1$.

Figure 5.2 depicts the variation in wave amplitude with μ_d and β_e when $\gamma = 5/3$, $\sigma_i = 0.02$, $U_0 = 0.1$, $\eta = 0.8$, $\theta = 15^0$. The figure demonstrates how the wave amplitudes decrease as μ_d and $|\beta_n|$ increase. Aside from that, the solution (5.27) provides that the amplitudes are unaffected by the magnetic field.

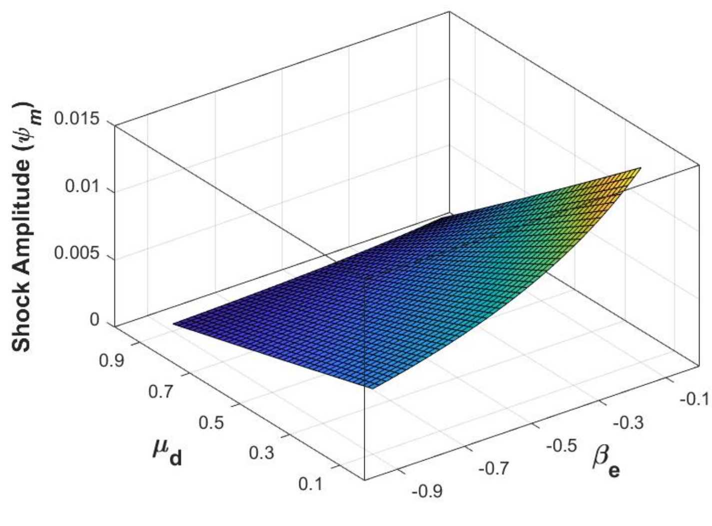

Figure 5.2: Wave-amplitude vs. β_e and μ_d, when $\gamma = 5/3$, $\sigma_i = 0.02$, $U_0 = 0.1$, $\eta = 0.8$, $\theta = 15^0$.

Figure 5.3 illustrates how the shock width changes with kinematic viscosity (η) and wave propagation speed (U_0), while it is seen that increasing values of η and U_0 cause the width to increase and decrease, respectively. Another finding is that the width is not dependent on the other parameters at all.

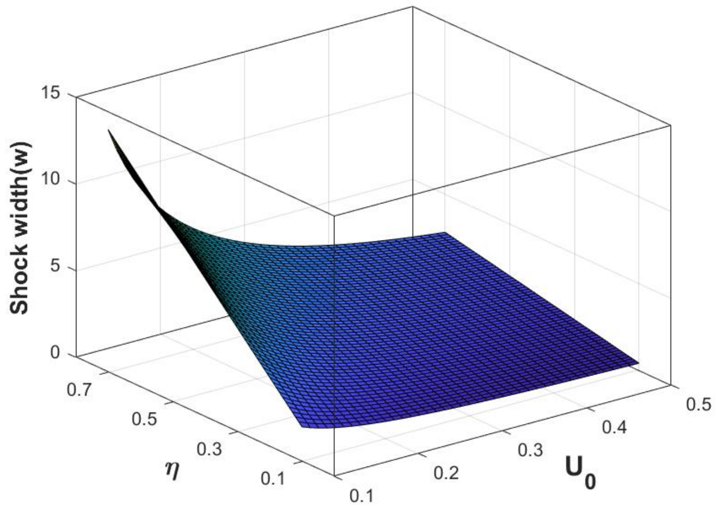

Figure 5.3: Variation in width with η and U_0.

Again, it is clear from (5.14) that l_x, γ, σ_i, μ_d significantly affect the phase speed. Figure 5.4 shows the changes in phase speed (increasing effect) caused by μ_d and σ_i. We observe from the relation (5.14) that the magnetic field and the trapping parameter have no impact on the phase speed. Supersonic waves with a positive potential may be supported by the presence of negatively charged dust particles because they speed up the phase speed of the DIA waves. It occurs as a result of the negative dust species that enlarges the space charge electric field (Mamun and Shukla, 2009-b).

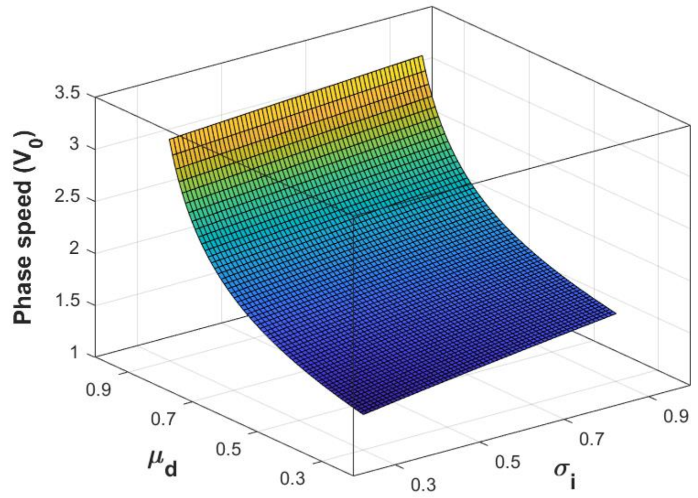

Figure 5.4: Effects of μ_d and σ_i on the phase speed, when $\theta = 15^0, \gamma = 5/3$.

5.5.4 Higher-order effect

This part aims to examine the nature of DIA shock waves under the effect of nonlinear terms of higher-order. From Figure 5.5, it is observed that $\frac{|\psi^{(2)}|}{|\psi^{(1)}|} \leq 1$, and the reductive perturbation technique must meet this requirement in order to include the higher-order effect. Here, the influence of higher-order nonlinear terms is shown by displaying $\psi^{(1)}$, $\psi^{(2)}$, and ψ versus ξ. According to the figure (where $\beta_e = -0.9$, $\sigma_i = 0.02$, $\mu_d = 0.34$, $\gamma = 5/3$, $\omega_{ci} = 0.8$, $U_0 = 0.1$, $\theta = 15^0$, $\eta = 0.8$), the higher nonlinearity leads to a rise in amplitude, and is consistent with earlier studies (El-Labany et al., 2014; El-Monier and Atteya, 2019). Besides, Figure 5.6 illustrates how the trapping parameter affects the shock structure when negatively charged dust particles are present. We can see from the figure that the amplitude drops when $|\beta_e|$ is increased. Besides this, the addition of second-order potential, i.e., $\psi = \psi^{(1)} + \psi^{(2)}$ gives greater amplitude than $\psi^{(1)}$.

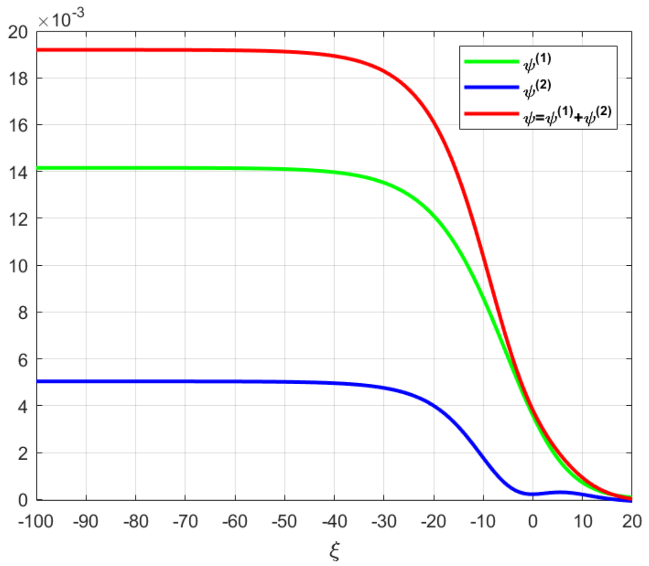

Figure 5.5: Structures of $\psi^{(1)}$, $\psi^{(2)}$ and ψ, when $\beta_e = -0.9$, $\sigma_i = 0.02$, $\mu_d = 0.34$, $\gamma = 5/3$, $\omega_{ci} = 0.8$, $U_0 = 0.1$, $\theta = 15^0$, $\eta = 0.8$, $\tau = 1$.

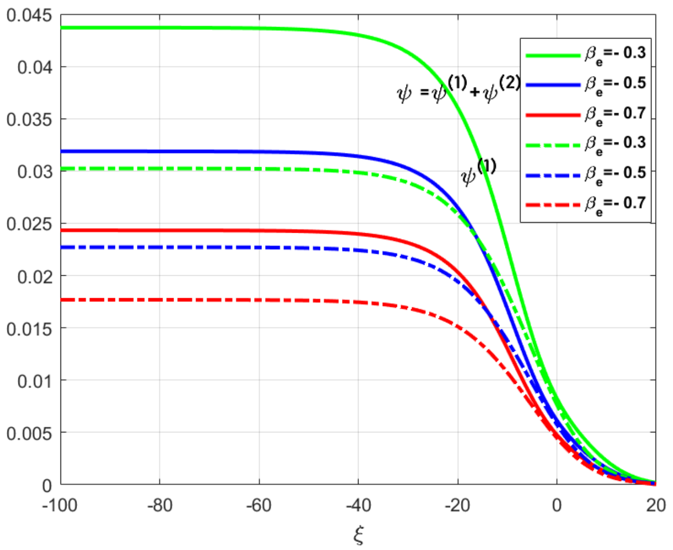

Figure 5.6: Structures of $\psi^{(1)}$ and ψ for $\beta_e = -0.3$ (green), $\beta_e = -0.5$(blue), $\beta_e = -0.7$ (red), when $\sigma_i = 0.02$, $\mu_d = 0.34$, $\gamma = 5/3$, $\omega_{ci} = 0.8$, $U_0 = 0.1$, $\theta = 15^0$, $\eta = 0.8$, $\tau = 1$.

The DIA shock waves' amplitude decreases with negative dust concentration μ_d, as shown in Figure 5.7. But, the impact of the second-order perturbed potential on the amplitude continues to grow under the plasma model under consideration.

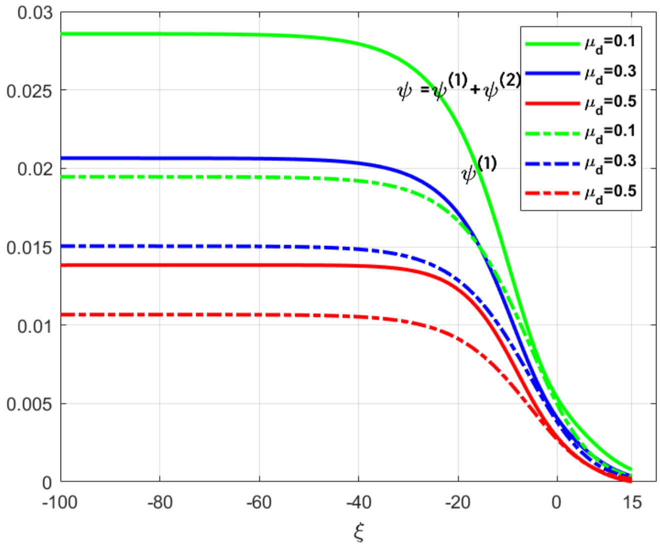

Figure 5.7: Variation in shock structures of ψ and $\psi^{(1)}$ for $\mu_d = 0.1$(green), $\mu_d = 0.3$(blue), $\mu_d = 0.5$(red), when $\beta_e = -0.9$, $\sigma_i = 0.02$, $\gamma = 5/3$, $\omega_{ci} = 0.8$, $U_0 = 0.1$, $\theta = 15^0$, $\eta = 0.8$, $\tau = 1$.

The variation in shock profiles for various ion gyro-frequencies (ω_{ci}) is shown in Figure 5.8, while the shock structures are plotted for $\omega_{ci} = 0.2,\ \omega_{ci} = 0.4,$ and $\omega_{ci} = 0.6$ (when $\beta_e = -0.9,\ \sigma_i = 0.02,\ \mu_d = 0.34,\ \gamma = 5/3,\ U_0 = 0.1,\ \theta = 15^0,\ \eta = 0.8$). The figure illustrates that, under the higher-order nonlinearity effect, amplitude (width) increases (decreases) due to the magnetic field, and Sultana (2021) found a similar result as well. Besides, it is clear that the magnetic field has no impact on the amplitudes for lower-order effects, and this conclusion deviates from the present observation. The consideration of higher-order nonlinearity provides more accurate results. We can infer that this observation has implications for understanding the magnetic field in the plasma system.

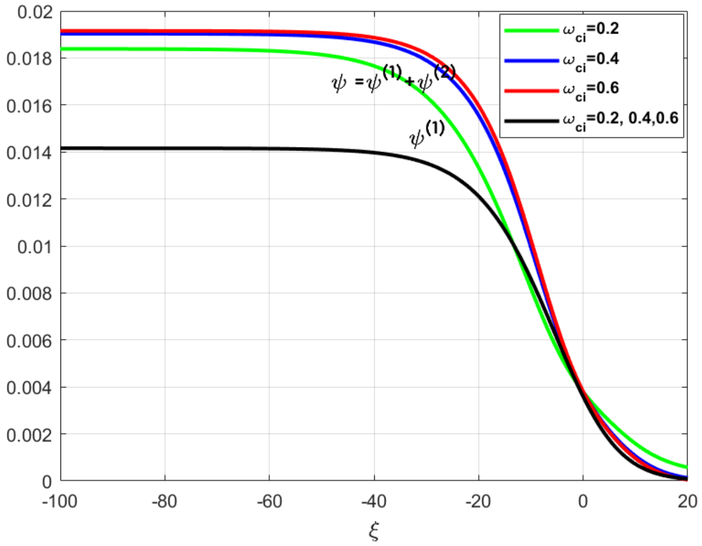

Figure 5.8: Variation in shock profiles of $\psi = \psi^{(1)} + \psi^{(2)}$(solid lines) and $\psi^{(1)}$ (black solid line) for $\omega_{ci} = 0.2$ (green), $\omega_{ci} = 0.4$ (blue), and $\omega_{ci} = 0.6$ (red), when $\beta_e = -0.9$, $\sigma_i = 0.02$, $\mu_d = 0.34$, $\gamma = 5/3$, $U_0 = 0.1$, $\theta = 15^0$, $\eta = 0.8$.

5.6 Summary

The theoretical study focuses on investigating the nonlinear properties of DIA shock waves in a plasma system, and the study shows that the system can only support positive potential. Besides, the combined impact of higher-order nonlinear terms, dust particle concentration, magnetic field, trapping parameter, etc., has been studied. The following is a summary of this chapter.

i. *Higher-order effect*: With the higher-order effect, the amplitude is generally increased, i.e., $\psi = \psi^{(1)} + \psi^{(2)}$ gives a higher amplitude than $\psi^{(1)}$.

ii. *Effect of the trapping parameter*: The amplitude reduces as the values of trapping parameter $|\beta_e|$ increase.

iii. *Effect of the dust concentration*: The increase in dust particles reduces the wave amplitude but increases the phase speed, that is, the waves develop supersonic.

iv. *Effect of the magnetic field*: The field has decreasing and increasing effect on the shock width and amplitude, respectively, but it does not affect the phase speed.

Chapter Six

Dynamic behaviors of DIA solitary waves in magneto-rotating dusty plasmas

6.1 Introduction

Strong magnetic fields cause pulsars, white dwarfs, neutron stars, etc., to rotate in astrophysical environments. As the stars fall, their moment of inertia is significantly reduced. The stars rotate due to the conservation of angular momentum. Rather than being exactly parallel to one another, the rotating axis and magnetic axis are frequently inclined at an angle to one another. Such dense plasmas revolving in magnetic fields were seen in astronomy, geophysical surroundings, and laboratory tokamak experiments (Sahu et al., 2019; Wang et al., 2022; Saini et al., 2022).

Several forces, such as the Lorentz force, Coriolis force, pondermotive force, etc., act on the plasma waves. Both the Coriolis force (which is caused by the small rotation) and the Lorentz force (which is caused by the electric and magnetic fields) are responsible for changing the DIA wave characteristics. Chandrasekhar (1953) provided an explanation of the Coriolis force, while he stated that the force can play an important role in cosmic phenomena, and the subsequent study of Lehnert (1954) supported the finding. Lehnert, in his study, suggested that the Coriolis force affects the magneto-hydrodynamic waves. Rajib et al. (2015) inspected the propagation of solitary waves in a magneto-rotating plasma, and they concluded that the waves move with narrower widths under the effect of pulsar rotation. Very recently, Salam et al. (2021) have investigated theoretically the collective impact of plasma rotation and magnetic field on solitary wave structures.

In most of the magneto-rotating plasma systems discussed above, the directions of the magnetic field and the rotational axis are assumed along the x-axis, and the wave directions are generally taken in the direction of the coordinate axes. The plasma rotation as well as wave propagation can be considered oblique. Considering an angle between the magnetic field and rotational axis, researchers investigated several types of wave propagation in different plasma systems. Mushtaq (2010) discussed the impacts of oblique rotation and magnetic field on the IA solitary waves in plasmas with isothermal and non-isothermal electrons. Hussain et al. (2014) studied a rotating plasma system that contains two components, such as mobile ions and non-extensive electrons. Saini et al. (2016) investigated a magneto-rotating four-species plasma system containing Kappa distributed electrons and positrons, while Das and Nag (2007) examined the waves in the presence of non-extensive electrons and positrons. Akter and Mamun (2022) investigated nucleus-acoustic solitary waves in warm, degenerate magneto-rotating quantum plasmas.

This chapter aims to investigate the effects of oblique plasma rotation and magnetic field on the DIA solitary waves, while the adiabatic positive ions, negative ions, electrons, and arbitrarily charged dust particles are taken as plasma species. We consider that the rotational axis and the magnetic axis (along the x-axis) are not aligned, i.e., they make a small angle θ, and the waves propagate obliquely. In addition to the magneto-rotating influence, we also discuss the plasma parametric effects on the nonlinear nature of the solitary waves, and the effects are found to be significant.

6.2 Plasma model

To investigate the features of DIA waves, we contemplate a magneto-rotating and collisionless plasma system that consists of four species, such as adiabatic inertial ions (positive and mobile), trapped light ions (negative), stationary dust particles (arbitrarily charged), and isothermal electrons. We assume the magnetic field as $\vec{B} = B_0\hat{x}$, and also suppose that the plasma rotates with the rotational frequency Ω_0 around an axis in the xy-plane while the rotational axis makes an angle θ with the magnetic field, i.e., $\vec{\Omega} = \Omega_0 \cos\theta\, \hat{x} + \Omega_0 \sin\theta\, \hat{y}$. The following normalized equations describe the dynamic behaviors of the DIA solitary waves in a magnetized adiabatic plasma with regard to a rotating reference frame:

$$\frac{\partial n_i}{\partial t} + \nabla \cdot (n_i \vec{u}_i) = 0, \tag{6.1}$$

$$\frac{\partial \vec{u}_i}{\partial t} + (\vec{u}_i \cdot \nabla)\vec{u}_i = -\nabla\psi + \omega_{ci}\,(\vec{u}_i \times \hat{x}) + 2\big(\vec{u}_i \times \vec{\Omega}\big) - \frac{\sigma_i}{n_i}\nabla p_i, \tag{6.2}$$

$$\frac{\partial p_i}{\partial t} + (\vec{u}_i \cdot \nabla)p_i + \gamma p_i(\nabla \cdot \vec{u}_i) = 0, \tag{6.3}$$

$$\nabla^2\psi = n_e\mu_e + n_n\mu_n - n_i - j\mu_d, \tag{6.4}$$

where n_s denotes the number density of plasma species s (here $s = i, n, e$ refer to positive ions, negative ions, and electrons, respectively) normalized by its equilibrium value n_{s0}, Ω is the rotational frequency normalized by $\omega_{pi} = \sqrt{\frac{4\pi e^2 n_{i0}}{m_i}}$, $\omega_{ci} = \frac{eB_0}{m_i c}$ is the positive ion gyro-frequency, temperature ratio $\sigma_i = \frac{T_i}{T_e}$, ψ is the wave potential, p_i is the positive ion fluid pressure normalized by p_{i0} $(= n_{i0}\kappa_B T_i)$, $\gamma = 1 + \frac{2}{N}$ (where N indicates the dimension of the plasma system), and the existence of positively (negatively) charged dust particles is indicated by $j = +1(-1)$. Moreover, $\mu_e = \frac{n_{e0}}{n_{i0}}$, $\mu_n = \frac{n_{n0}}{n_{i0}}$, and $\mu_d = \frac{Z_d n_{d0}}{n_{i0}}$.

The term $2\big(\vec{u}_i \times \vec{\Omega}\big)$ in equation (6.2) represents the Coriolis force. Though we have considered the Coriolis force in our plasma system, the centrifugal force $\vec{\Omega}_0 \times (\vec{\Omega}_0 \times \vec{r})$ is ignored due to its negligible effect. Besides, the source and sink terms arising from ionization, dust-plasma interactions, etc., and the collisional terms arising from collisions are neglected in the plasma system.

The vortex-like distribution of trapped negative ions and the isothermal distribution of electrons are assumed, respectively, to follow (Mahmood et al., 2003)

$$n_n = 1 + \alpha\psi - \frac{4}{3}\frac{(1-\beta_n)}{\sqrt{\pi}}\alpha^{\frac{3}{2}}\psi^{\frac{3}{2}} + \frac{1}{2}\alpha^2\psi^2 , \tag{6.5}$$

and $$n_e = e^{\psi}. \tag{6.6}$$

Here, $\alpha = \frac{T_e}{T_n}$ (where T_n and T_e specify the temperature of negative ions and electrons, respectively) and β_n is the trapping parameter. The condition of charge neutrality is

$$n_{e0} + n_{n0} = n_{i0} + j\, Z_d n_{d0}. \tag{6.7}$$

Thus, we can write $\mu_e = 1 - \mu_n + j\mu_d$.

6.3 Derivation of the mKdV equation and its solution

To describe smoothly the DIA solitary waves, which are affected by the magnetic field and propagated in the xy-plane, we follow the procedure of Schamel (Schamel, 1972; Schamel, 1975). Here, the following stretched coordinates are assumed.

$$\xi = \epsilon^{1/4}\,(l_x x + l_y y - V_0 t) \text{ and } \tau = \epsilon^{3/4}\, t. \tag{6.8}$$

The expanded form of the perturbed quantities n_i, p_i, u_{ix}, u_{iy}, u_{iz}, ψ in terms of ϵ is:

$$n_i = 1 + \epsilon\, n_i^{(1)} + \epsilon^{3/2}\, n_i^{(2)} + \cdots, \tag{6.9}$$

$$p_i = 1 + \epsilon\, p_i^{(1)} + \epsilon^{3/2}\, p_i^{(2)} + \cdots, \tag{6.10}$$

$$u_{ix} = \epsilon\, u_{ix}^{(1)} + \epsilon^{3/2}\, u_{ix}^{(2)} + \cdots, \tag{6.11}$$

$$u_{iy} = \epsilon^{3/2}\, u_{iy}^{(1)} + \epsilon^{5/2}\, u_{iy}^{(2)} + \cdots, \tag{6.12}$$

$$u_{iz} = \epsilon^{5/4}\, u_{iz}^{(1)} + \epsilon^{7/4}\, u_{iz}^{(2)} + \cdots, \tag{6.13}$$

$$\psi = \epsilon\, \psi^{(1)} + \epsilon^{3/2}\psi^{(2)} + \cdots. \tag{6.14}$$

Substituting (6.5), (6.6), and (6.8) - (6.14) into (6.1) - (6.4), and assembling the terms in analogous powers of ϵ, the 1st-order equations are found from the lowest-order terms as

$$l_x \frac{\partial\, u_{ix}^{(1)}}{\partial \xi} - V_0 \frac{\partial\, n_i^{(1)}}{\partial \xi} = 0, \tag{6.15}$$

$$l_x \frac{\partial \psi^{(1)}}{\partial \xi} - V_0 \frac{\partial\, u_{ix}^{(1)}}{\partial \xi} + \sigma_i l_x \frac{\partial p_i^{(1)}}{\partial \xi} + 2\Omega_0 \, sin\theta \, u_{iz}^{(1)} = 0, \tag{6.16}$$

$$-\omega_{ci} u_{iz}^{(1)} + \sigma_i l_y \frac{\partial p_i^{(1)}}{\partial \xi} - 2\Omega_0 \, cos\theta \, u_{iz}^{(1)} + l_y \frac{\partial \psi^{(1)}}{\partial \xi} = 0, \tag{6.17}$$

$$\gamma \, l_x \frac{\partial\, u_{ix}^{(1)}}{\partial \xi} - V_0 \frac{\partial p_i^{(1)}}{\partial \xi} = 0, \tag{6.18}$$

$$-(\mu_n \alpha + \mu_e) + n_i^{(1)} = 0. \tag{6.19}$$

Thus, the first-order expressions are given by

$$u_{ix}^{(1)} = \frac{V_0 G_1}{l_x} \psi^{(1)}, \; u_{iz}^{(1)} = \frac{l_y \, (1+\gamma \sigma_i G_1)}{\Omega_{\text{eff}}} \frac{\partial \psi^{(1)}}{\partial \xi}, \;\; p_i^{(1)} = \gamma G_1 \psi^{(1)}, \; n_i^{(1)} = G_1 \psi^{(1)}. \tag{6.20}$$

And the phase speed is

$$V_0 = l_x \sqrt{\frac{(1+\gamma \sigma_i G_1)}{G_1}} \left(1 + \frac{l_y}{l_x} \frac{2\Omega_0 \, sin\theta}{\Omega_{\text{eff}}}\right)^{\frac{1}{2}}, \tag{6.21}$$

where $G_1 = \mu_n \alpha + \mu_e$ and $\Omega_{\text{eff}} = \omega_{ci} + 2\Omega_0 \, cos\theta$. For an irrotational plasma system (i.e., $\Omega_0 = 0$), the phase speed can be written as $V_0 = l_x \sqrt{\frac{(1+\gamma \sigma_i G_1)}{G_1}}$, and for an electron-ion plasma (i.e., $\mu_d = 0$), the neutrality condition takes the form $\mu_n = 1 - \mu_e$.

Equating the coefficients of $\epsilon^{3/2}$ from the z-component of (6.2), and (6.4), we get

$$-2\Omega_0 \, sin\theta u_{ix}^{(2)} - V_0 \frac{\partial\, u_{iz}^{(1)}}{\partial \xi} + \omega_{ci} u_{iy}^{(1)} + 2\Omega_0 \, cos\theta \, u_{iy}^{(1)} = 0, \tag{6.22}$$

and $$\frac{\partial^2 \psi^{(1)}}{\partial \xi^2} = G_1 \psi^{(2)} - \frac{4}{3\sqrt{\pi}} \mu_n \alpha^{\frac{3}{2}} (1 - \beta_n) \left[\psi^{(1)}\right]^{\frac{3}{2}} - n_i^{(2)}. \tag{6.23}$$

Similarly, equating the coefficients of $\epsilon^{7/4}$ from (6.1), the x and y-components of (6.2), and (6.3), the resulting set of equations is:

$$\frac{\partial n_i^{(1)}}{\partial \tau} - V_0 \frac{\partial\, n_i^{(2)}}{\partial \xi} + l_x \frac{\partial u_{ix}^{(2)}}{\partial \xi} + l_y \frac{\partial u_{iy}^{(1)}}{\partial \xi} = 0, \tag{6.24}$$

$$\frac{\partial u_{ix}^{(1)}}{\partial \tau} + 2\Omega_0 \, sin\theta u_{iz}^{(2)} - V_0 \frac{\partial u_{ix}^{(2)}}{\partial \xi} + l_x \frac{\partial \psi^{(2)}}{\partial \xi} + \sigma_i l_x \frac{\partial p_i^{(2)}}{\partial \xi} = 0, \tag{6.25}$$

$$-\omega_{ci}u_{iz}^{(2)}+l_y\frac{\partial\psi^{(2)}}{\partial\xi}+\sigma_i l_y\frac{\partial p_i^{(2)}}{\partial\xi}-2\Omega_0\,cos\theta\,u_{iz}^{(2)}-\,V_0\frac{\partial u_{iy}^{(1)}}{\partial\xi}=0, \tag{6.26}$$

$$\gamma l_x\frac{\partial u_{ix}^{(2)}}{\partial\xi}+\gamma l_y\frac{\partial u_{iy}^{(1)}}{\partial\xi}+\frac{\partial p_i^{(1)}}{\partial\tau}-\,V_0\frac{\partial p_i^{(2)}}{\partial\xi}=0\,. \tag{6.27}$$

Assuming θ as small and $\Omega_0<\omega_{ci}$ in (6.22), we get $u_{iy}^{(1)}\simeq\frac{V_0}{\Omega_{\text{eff}}}\frac{\partial u_{iz}^{(1)}}{\partial\xi}$. Now, to derive the following mKdV equation, the 2nd-order terms $u_{ix}^{(2)}$, $u_{iz}^{(2)}$, $p_i^{(2)}$, $n_i^{(2)}$, and $\psi^{(2)}$ are removed from (6.22) - (6.27).

$$\frac{\partial\psi^{(1)}}{\partial\tau}+\delta_1\sqrt{\psi^{(1)}}\frac{\partial\psi^{(1)}}{\partial\xi}+\delta_2\frac{\partial^3\psi^{(1)}}{\partial\xi^3}=0, \tag{6.28}$$

where $\delta_1=\frac{V_0\,\mu_n\alpha^{3/2}\,(1-\beta_n)}{\sqrt{\pi}\,G_1(1+\gamma\sigma_i G_1)}$, $\delta_2=\frac{V_0}{2G_1(1+\gamma\sigma_i G_1)}\left[1+\frac{l_y^2\,(1+\gamma\sigma_i G_1)^2}{\Omega_{\text{eff}}^2}\left(1-\frac{l_x}{l_y}\frac{2\Omega_0\,sin\theta}{\Omega_{\text{eff}}}\right)\right]$. (6.29)

The solution to the mKdV equation is determined, by using the single variable transformation $Z=\xi-U_0\tau$, as

$$\psi^{(1)}=\psi_m\ \text{sech}^4\left(\frac{Z}{\Delta}\right), \tag{6.30}$$

where the amplitude (ψ_m) and width (Δ) are respectively, given by

$$\psi_m=\left(\frac{15U_0}{8\,\delta_1}\right)^2\ \text{and}\ \ \Delta=\sqrt{\frac{16\,\delta_2}{U_0}}\,. \tag{6.31}$$

The solution (6.30) represents DIA solitary waves of bell-shaped structures and indicates that the waves propagate with amplitude $\left(\frac{15U_0}{8\,\delta_1}\right)^2$ and width $\sqrt{\frac{16\,\delta_2}{U_0}}$ in the magneto-rotating plasmas, such as neutron stars, white dwarfs, pulsars, etc. Since δ_1 and δ_2 are the functions of Ω_0, ω_{ci}, μ_n, μ_e, σ_i, α, etc., we can describe the influence of plasma rotation, magnetic field, electron temperature, and species-concentrations on the wave nature (amplitude, width, and phase speed). If we ignore the effect of magneto-rotation, our result can refer back to the form that was found for unmagnetized as well as non-rotating plasmas (Anowar and Mamun, 2008; Rahman and Haider, 2016).

6.4 Result and discussion

From the solution (6.30), we observe that the features of the waves, such as the amplitude, width, and phase speed are affected pointedly by the plasma parameters. In this section, the consequences of magneto-rotation, electron and dust concentrations, electron temperature, etc., on the wave structure are discussed. In order to investigate the aforementioned impacts, the parametric values are taken from various experimental and theoretical studies of plasmas, such as $T_i = 60\ eV$, $T_n = 100\ eV$, $T_e = 150 - 200\ eV$ (Bennett et al., 2014), $B = 0.1\,T$ (Gorshunov et al., 2017), $n_{d0} = 10^{10}\ m^{-3}$, $n_{i0} = 7 \times 10^{13}\ m^{-3}$, $n_{e0} = 3.5 \times 10^{13}\ m^{-3}$, $Z_d = 3 \times 10^3$ (Bandyopadhyay et al., 2008), $\Omega_0 =$ 0.03 rad/sec (Akter and Mamu, 2022), $\theta = 30^0$, $\beta_n = -0.3$ (Haider et al., 2014). As the motions of ions are considered adiabatic in three dimensions, $\gamma = 5/3$ (Banerjee and Saha, 2021). Hence, the corresponding parametric values are calculated from the above ranges as: $\sigma_i = 0.3 - 0.4$, $\alpha = 1.5 - 2$, $\omega_{ci} = 0.3$ rad/sec, $l_x = 0.87$, $l_y = 0.50$, $\mu_d = 0.42$, $\mu_e = 0.5$.

As illustrated in Figures 6.1 and 6.2, the solitary waves exist with positive potential only, and the waves of different speeds move with different structures. The wave patterns are shown in both figures against the speeds $U_0 = 0.05$, $U_0 = 0.1$, and $U_0 = 0.15$, and they also provide the changes of the wave structures in the presence as well as the absence of rotational effects. From the figures, it is observed that the nonlinear solitary waves having larger wave speeds propagate with higher amplitudes and lower widths. And, the presence of plasma rotation decreases the amplitude and width. Moreover, if we compare the impacts of positively and negatively charged dust particles, we observe that the waves of the same speed move with somewhat taller amplitude and a longer width in the presence of negatively charged dust particles.

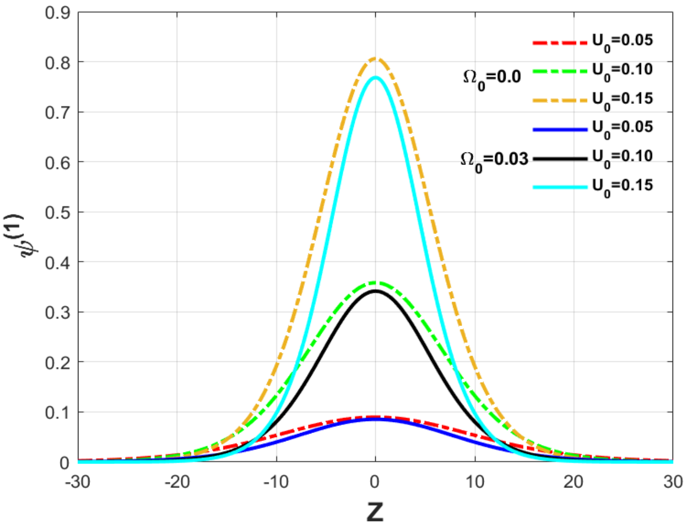

Figure 6.1: Solitary wave structures at different wave speeds for positively charged dust particles (i.e. $j = 1$), while the dashed curves are plotted in the absence of Coriolis force ($\Omega_0 = 0$) at $U_0 = 0.05$ (red), $U_0 = 0.10$ (green), $U_0 = 0.15$ (gold) and the solid curves are plotted in presence of Coriolis force ($\Omega_0 = 0.03$) at $U_0 = 0.05$ (blue), $U_0 = 0.1$ (black), $U_0 = 0.15$ (cyan). The other parameters as $\alpha = 2$, $\mu_d = 0.42$, $\mu_e = 0.5$, $\beta_n = -0.3$, $\gamma = 5/3$, $\sigma_i = 0.3$, $l_x = 0.87$, $l_y = 0.5$, $\theta = 30^0$.

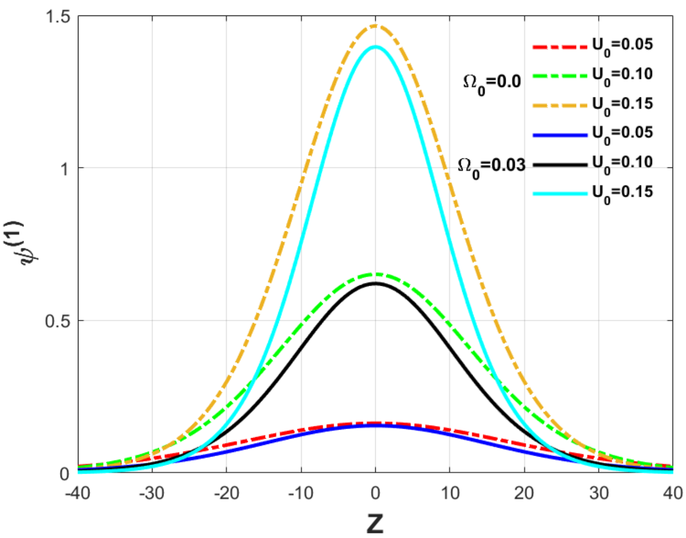

Figure 6.2: Solitary wave structures at different wave speeds for negatively charged dust particles (i.e. $j = -1$), while the dashed curves are plotted in the absence of Coriolis force ($\Omega_0 = 0$) at $U_0 = 0.05$ (red), $U_0 = 0.10$ (green), $U_0 = 0.15$ (gold) and the solid curves are plotted in presence of Coriolis force ($\Omega_0 = 0.03$) at $U_0 = 0.05$ (blue), $U_0 = 0.1$ (black), $U_0 = 0.15$ (cyan). The other parameters as $\alpha = 2$, $\mu_d = 0.42$, $\mu_e = 0.5$, $\beta_n = -0.3$, $\gamma = 5/3$, $\sigma_i = 0.3$, $l_x = 0.87$, $l_y = 0.5$, $\theta = 30^0$.

We now will examine in detail in the following sub-sections how the wave amplitude, width, and phase speed are affected by the plasma parameters.

6.4.1 Effects on the amplitude

The effects of the positive ion gyro-frequency ω_{ci} and rotation frequency Ω_0 on the amplitude, where $\alpha = 2$, $\mu_d = 0.42$, $\mu_e = 0.5$, $\beta_n = -0.3$, $U_0 = 0.1$, $\gamma = 5/3$, $\sigma_i = 0.3$, $l_x = 0.87$, $l_y = 0.5$, $\theta = 30^0$, are depicted in Figures 6.3 and 6.4 for positively and negatively charged dust particles, respectively. The investigation is carried out by changing the values of ion gyro-frequency ω_{ci} and rotational frequency Ω_0. From the figures, it is observed that the plasma rotation (i.e., Ω_0) has a declining consequence on the amplitude, whereas the magnetic field (i.e., ω_{ci}) has an increasing effect (similar observation was found by Saini et al., 2016). Besides, an observation pointed out in (6.21) and (6.31) is that the existence of the magnetic effect on the amplitude depends on the occurrence of plasma rotation, i.e., the effect of the magnetic field on the amplitude disappears if we ignore the rotational effect ($\Omega_0 = 0$) or consider an irrotational plasma system.

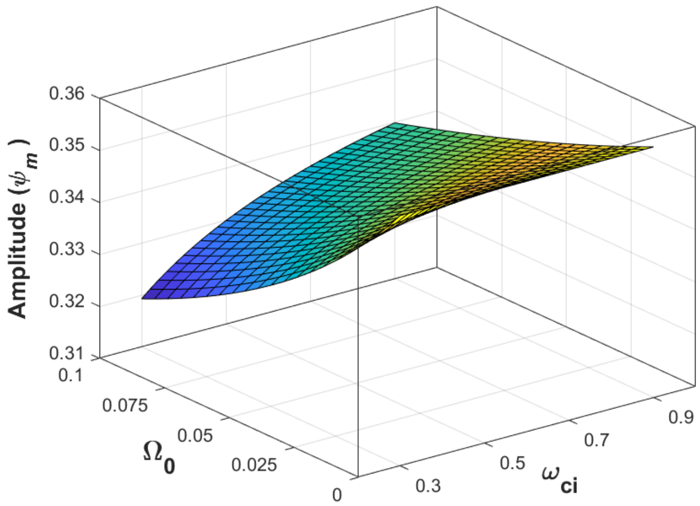

Figure 6.3: Wave-amplitude against ω_{ci} and Ω_0, when $j = 1$ and $\alpha = 2$, $\mu_d = 0.42$, $\mu_e = 0.5$, $\beta_n = -0.3$, $U_0 = 0.1$, $\gamma = 5/3$, $\sigma_i = 0.3$, $l_x = 0.87$, $l_y = 0.5$, $\theta = 30^0$.

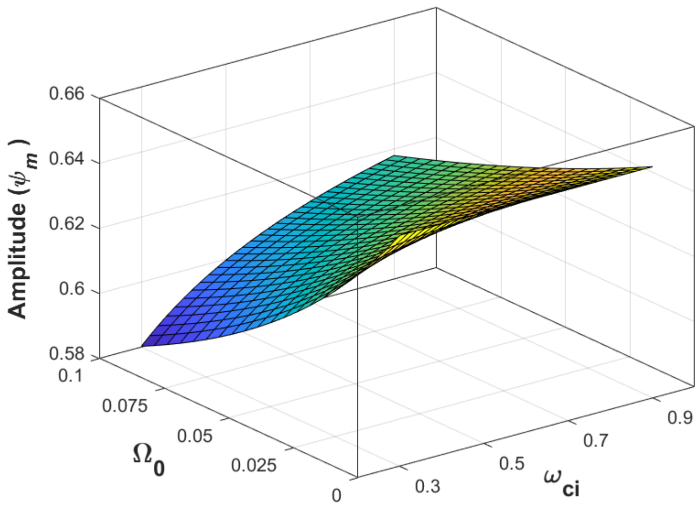

Figure 6.4: Wave-amplitude against ω_{ci} and Ω_0, when $j = -1$ and $\alpha = 2$, $\mu_d = 0.42$, $\mu_e = 0.5$, $\beta_n = -0.3$, $U_0 = 0.1$, $\gamma = 5/3$, $\sigma_i = 0.3$, $l_x = 0.87$, $l_y = 0.5$, $\theta = 30^0$.

Figures 6.5 and 6.6 show the variations of the solitary wave amplitudes with the changes of electron concentration (μ_e) and dust concentration (μ_e), when other parameters are taken as $\alpha = 2$, $\beta_n = -0.3$, $U_0 = 0.1$, $\gamma = 5/3$, $\sigma_i = 0.3$, $l_x = 0.87$, $\omega_{ci} = 0.3$, $\Omega_0 = 0.03$, $l_y = 0.5$, $\theta = 30^0$. It is found from the figures that the wave amplitude is enhanced in the presence of positively or negatively charged dust species if the fraction of electron species increases. However, PCD particle density increases the solitary wave amplitudes, while negatively charged dust particle density shows the opposite behavior. Figure 6.7 depicts the changes in amplitudes by the temperature ratio $\sigma_i = T_i/T_e$ and inclination angle θ, when other parameters are considered as $\alpha = 2$, $\mu_d = 0.42$, $\mu_e = 0.5$, $\beta_n = -0.3$, $U_0 = 0.1$, $\gamma = 5/3$, $l_x = 0.87$, $\omega_{ci} = 0.3$, $\Omega_0 = 0.03$, $l_y = 0.5$. This figure indicates that DIA wave amplitudes decrease with the increasing temperature of electron species (when σ_i decreases), and the amplitudes also decrease with θ but very slowly. Furthermore, if $\theta \sim 0^0$, then $V_0 \simeq l_x\sqrt{\frac{(1+\gamma\sigma_i G_1)}{G_1}}$ that means the magnetic field and plasma rotation do not affect the amplitude. A similar observation was found by Mushtaq (2010).

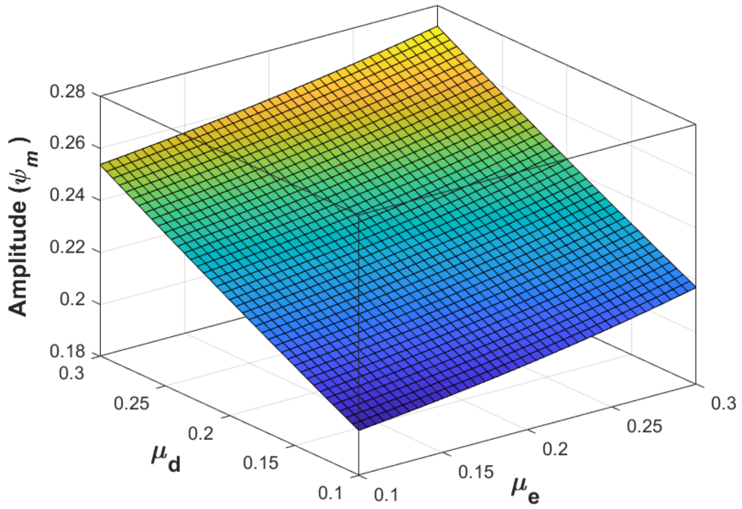

Figure 6.5: Variation of amplitude with μ_e and μ_d for positively charged dust particles, when $\alpha = 2$, $\beta_n = -0.3$, $U_0 = 0.1$, $\gamma = 5/3$, $\sigma_i = 0.3$, $l_x = 0.87$, $\omega_{ci} = 0.3$, $\Omega_0 = 0.03$, $l_y = 0.5$, $\theta = 30^0$.

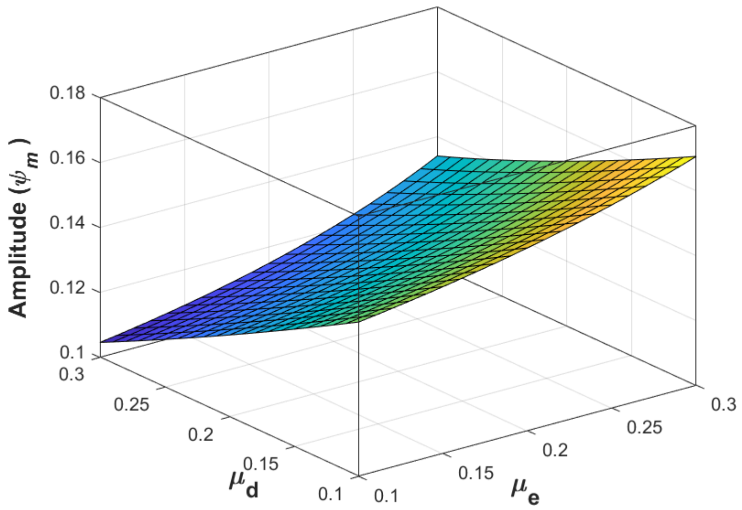

Figure 6.6: Variation of amplitude with μ_e and μ_d for negatively charged dust particles, when $\alpha = 2$, $\beta_n = -0.3$, $U_0 = 0.1$, $\gamma = 5/3$, $\sigma_i = 0.3$, $l_x = 0.87$, $\omega_{ci} = 0.3$, $\Omega_0 = 0.03$, $l_y = 0.5$, $\theta = 30^0$.

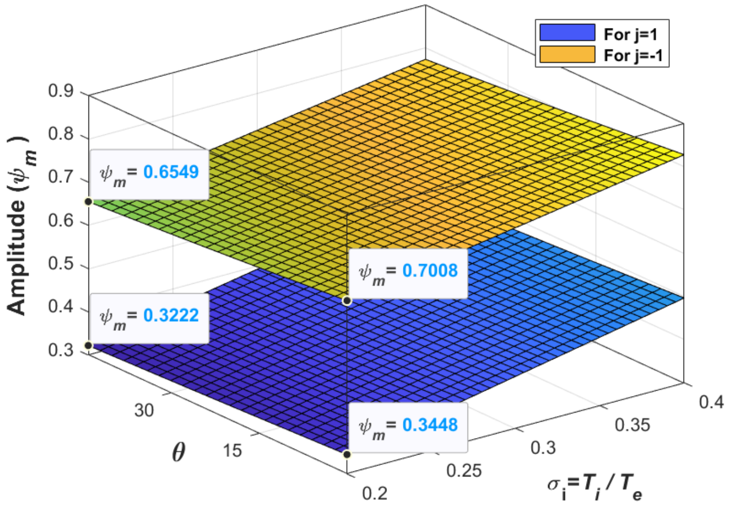

Figure 6.7: Change of amplitude with θ and σ_i for $j = 1$ and $j = -1$ (lower and upper surfaces, respectively) when other parameters are $\alpha = 2$, $\mu_d = 0.42$, $\mu_e = 0.5$, $\beta_n = -0.3$, $U_0 = 0.1$, $\gamma = 5/3$, $l_x = 0.87$, $\omega_{ci} = 0.3$, $\Omega_0 = 0.03$, $l_y = 0.5$.

6.4.2 Effects on the width

Figures 6.8 -6.12 show the variations of the widths with respect to ω_{ci}, Ω_0, μ_d, μ_e, θ, σ_i, etc., for dust particles, and a set of parametric values $\alpha = 2$, $\mu_d = 0.42$, $\mu_e = 0.5$, $\beta_n = -0.3$, $U_0 = 0.1$, $\gamma = 5/3$, $\sigma_i = 0.3$, $l_x = 0.87$, $\omega_{ci} = 0.3$, $\Omega_0 = 0.03$, $l_y = 0.5$, $\theta = 30^0$ is chosen to signify the effects graphically. Each figure is drawn by varying the parameters within their suitable range of values, and the remaining parametric values are chosen from the above list. The variations of the width with respect to positive ion gyro-frequency and rotational frequency of rotating plasmas are plotted in Figure 6.8 for $j = 1$, and in Figure 6.9 for $j = -1$. As shown in Figures 6.8 and 6.9, the widths decrease in the presence of a strong magnetic field and plasma rotation. Again, according to Figures 6.10 and 6.11, the increase in electron and dust concentrations significantly affects the wave width. The investigation shows that the width increases as the fraction of electron species (i.e., μ_e) increases in the presence of positively or negatively charged dust particles. Moreover, the positively charged dust concentration has a decreasing effect, but negatively charged dust concentration has an increasing effect on the width. Figure 6.12 shows the variation of width with the angle of obliqueness θ and temperature ratio σ_i. It is observed that θ has a slightly decreasing effect, whereas σ_i has an increasing effect on the width in the presence of dust particles.

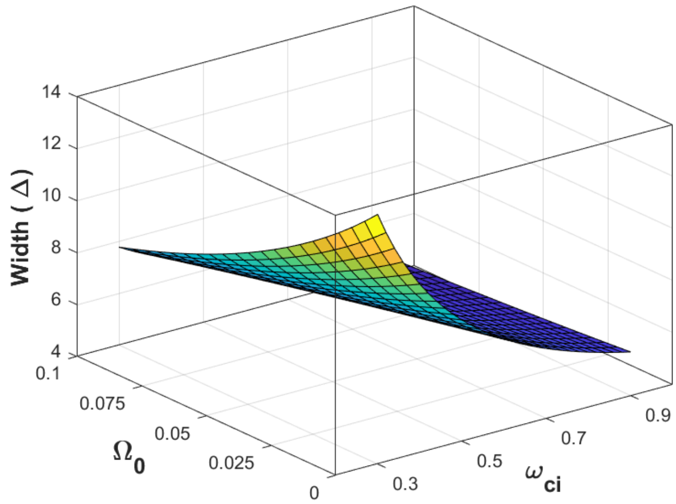

Figure 6.8: Width against ω_{ci} and Ω_0, when $j = 1$ and $\alpha = 2$, $\mu_d = 0.42$, $\mu_e = 0.5$, $\beta_n = -0.3$, $U_0 = 0.1$, $\gamma = 5/3$, $\sigma_i = 0.3$, $l_x = 0.87$, $l_y = 0.5$, $\theta = 30^0$.

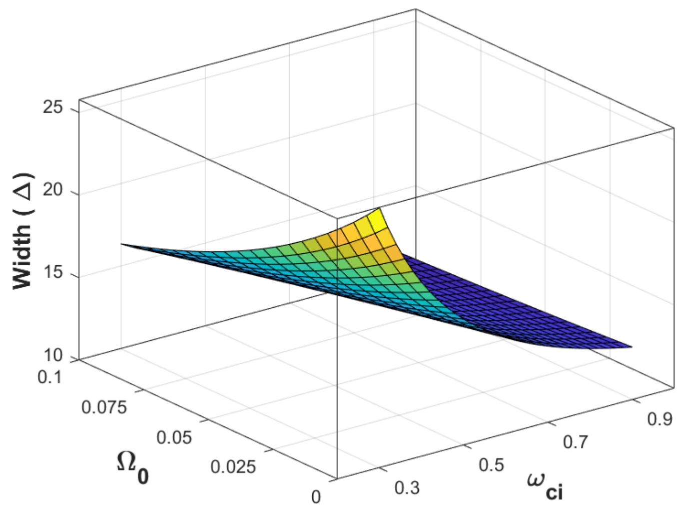

Figure 6.9: Width against ω_{ci} and Ω_0, when $j = -1$ and $\alpha = 2$, $\mu_d = 0.42$, $\mu_e = 0.5$, $\beta_n = -0.3$, $U_0 = 0.1$, $\gamma = 5/3$, $\sigma_i = 0.3$, $l_x = 0.87$, $l_y = 0.5$, $\theta = 30^0$.

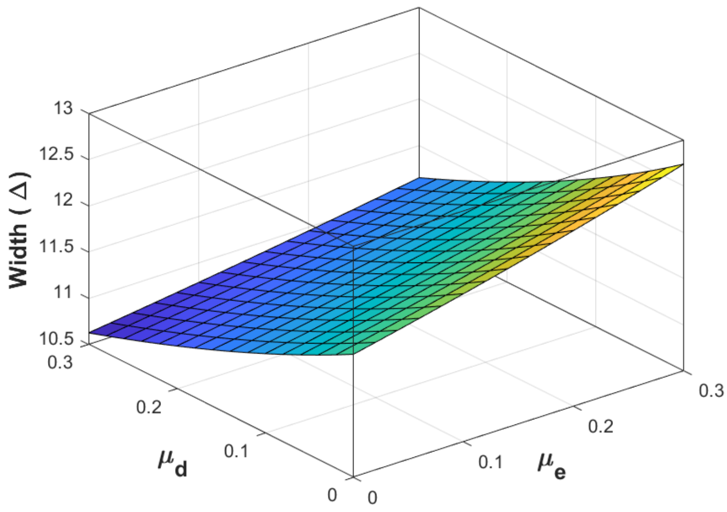

Figure 6.10: Solitary wave-width against μ_e and μ_d, when $j = 1$ and $\alpha = 2$, $\beta_n = -0.3$, $U_0 = 0.1$, $\gamma = 5/3$, $\sigma_i = 0.3$, $l_x = 0.87$, $\omega_{ci} = 0.3$, $\Omega_0 = 0.03$, $l_y = 0.5$, $\theta = 30^0$.

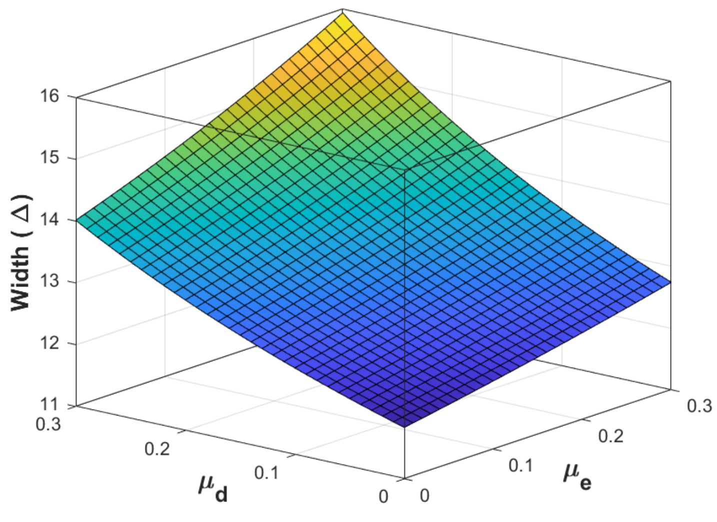

Figure 6.11: Solitary wave-width against μ_e and μ_d, when $j = -1$ and $\alpha = 2$, $\beta_n = -0.3$, $U_0 = 0.1$, $\gamma = 5/3$, $\sigma_i = 0.3$, $l_x = 0.87$, $\omega_{ci} = 0.3$, $\Omega_0 = 0.03$, $l_y = 0.5$, $\theta = 30^0$.

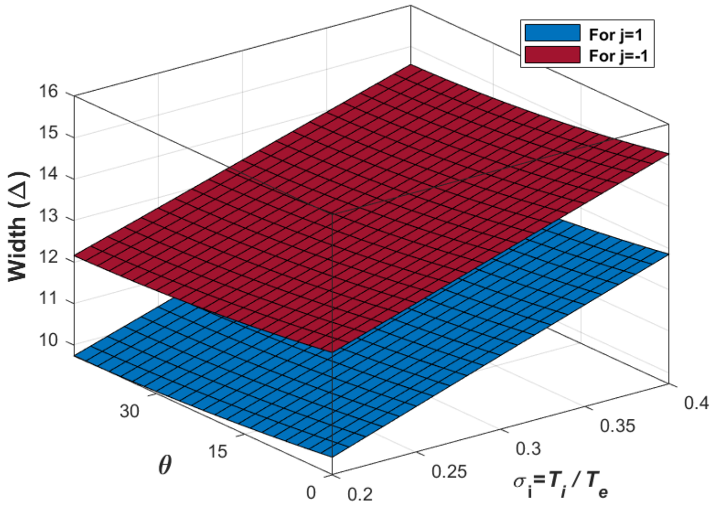

Figure 6.12: Variation of the width with θ and σ_i for $j = 1$ and $j = -1$ (lower and upper surfaces respectively) when $\alpha = 2$, $\mu_d = 0.42$, $\mu_e = 0.5$, $\beta_n = -0.3$, $U_0 = 0.1$, $\gamma = 5/3$, $l_x = 0.87$, $l_y = 0.5$, $\omega_{ci} = 0.5$, $\Omega_0 = 0.03$.

6.4.3 Effects on the phase speed

According to equation (6.21), the magnetic field and Coriolis force noticeably affect the phase speed. But if the rotation axis is parallel to the magnetic field direction (i.e., $\theta = 0^0$), the magnetic field and the plasma rotation do not influence the phase speed. As shown in Figures 6.13 and 6.14, the magnetic field has a slightly decreasing effect on the phase speed, whereas the rotation has a slightly increasing effect.

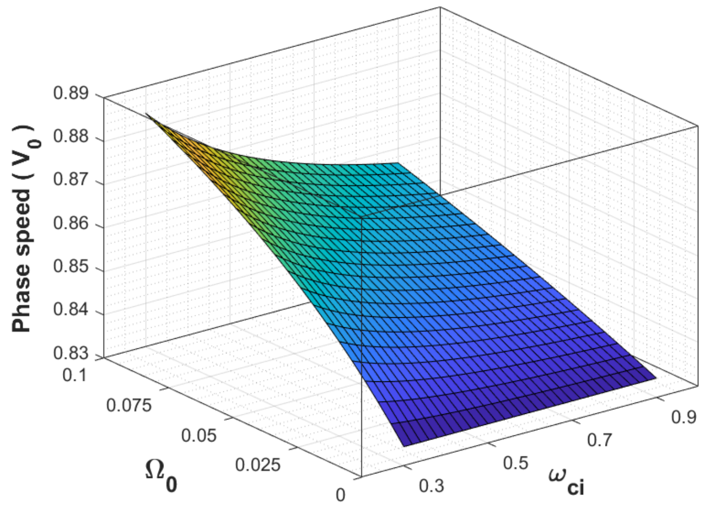

Figure 6.13: Effects of ω_{ci} and Ω_0 on the phase speed for $j = 1$, when $\alpha = 2$, $\mu_d = 0.42$, $\mu_e = 0.5$, $\beta_n = -0.3$, $U_0 = 0.1$, $\gamma = 5/3$, $\sigma_i = 0.3$, $l_x = 0.87$, $l_y = 0.5$, $\theta = 30^0$.

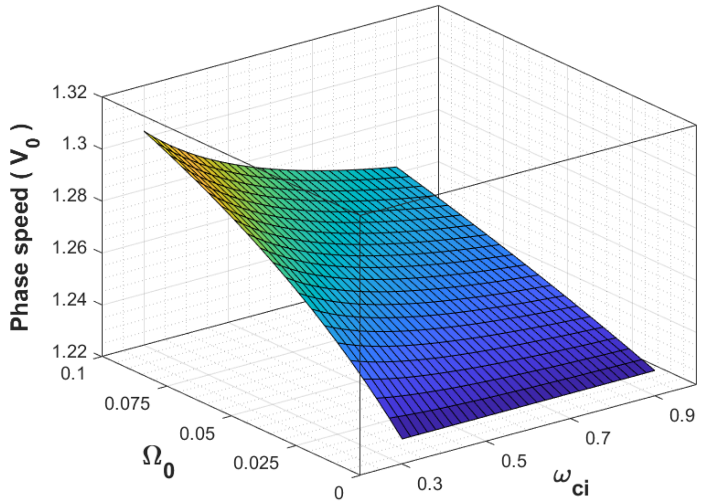

Figure 6.14: Effects of ω_{ci} and Ω_0 on the phase speed for $j = -1$, when $\alpha = 2$, $\mu_d = 0.42$, $\mu_e = 0.5$, $\beta_n = -0.3$, $U_0 = 0.1$, $\gamma = 5/3$, $\sigma_i = 0.3$, $l_x = 0.87$, $l_y = 0.5$, $\theta = 30^0$.

6.5 Summary

We have examined the combined effect of magnetic field and oblique rotation on the DIA solitary waves. From the theoretical study, we observe that the magnetic field, Coriolis force, electron concentration, and different parameters have significant impacts on the wave structures. The following are the main findings (in the presence of positively or negatively charged dust particles):

i. *Magnetic effect*: Under the effect of the magnetic field, the solitary wave structures become spiky, i.e., it increases the wave amplitude but reduces the width.

ii. *Rotational effect*: The rotation has a falling impact on the wave profiles but an increasing impact on the phase speed. Besides, the magnetic impact on the amplitude depends on the existence of rotation, i.e., the effect of the magnetic field vanishes for non-rotating plasma though the effect exists on the width in this case.

iii. *Effect of the propagation angle (θ):* The angle affects the wave amplitudes and widths negatively. If $\theta = 0^0$ (i.e., $\vec{\Omega} \parallel \vec{B}$), the magnetic field and rotation do not influence the amplitude and phase speed at all.

iv. *Adiabatic effect:* The ion fluid temperature has an increasing effect on the amplitude, width, and phase speed.

v. *Effect of the electron concentration:* Under the increasing influence of electron concentration, the solitary waves propagate with larger amplitudes and wider widths.

vi. *Effect of the electron temperature:* The wave amplitude and width decrease with the increasing temperature of electron species.

Chapter Seven

Dynamic behaviors of multi-solitons and multi-shocks in magnetized dusty plasmas

7.1 Introduction

The existence of multi-solitons and multi-shocks was observed experimentally in various plasma phenomena (Chan et al., 1981; Reed et al., 2003; Harvey et al., 2010; Boruah et al., 2016; Medici and Waite, 2016; Tang et al., 2021). Again, the investigations of exact solutions, integrability of NLPDEs, solitons, and shocks were carried out by numerous researchers (Biazar and Ghazvini, 2009; Zhang et al., 2018; Wang and Wang, 2018; Ma et al., 2018; Wang et al., 2019; Ren et al., 2019; Gharib et al., 2021; Alimirzaluo et al., 2021).

As part of an analytical investigation on finding the multi-soliton and multi-shock solutions to the NLPDEs, investigators employed several approaches, such as the Backlund transformation method (Wang and Wang, 2001), the inverse scattering method (Yuan and Shou, 2022; Ma, 2019), the Darboux transformation (Ling et al., 2015), the Lie group theory (Kumar et al., 2020-a; Dhiman and Kumar, 2022), and the Hirota bilinear method (Hirota, 2004; Griffiths, 2012; Kumar and Mohan, 2021; Kumar and Mohan, 2022; Alsayyed et al., 2016; Chen et al., 2019; Ullah et al., 2020-b; Ismael et al., 2020). In order to find an auxiliary function that is very essential for finding the solutions, the Hirota bilinear method requires a bilinear transformation of the examined equation. It is important to note that achieving such a transformation can be challenging for some equations. Besides, in some cases, introducing some new variables (dependent and independent) may be required. On the other hand, the simplified Hirota method is the simplest method to derive auxiliary functions without using the bilinear forms (Hereman and Zhuang, 1991;

Hereman and Zhuang, 1992), and this method minimizes the cumbersome work of the Hirota method. When it comes to finding multi-soliton or multi-shock solutions, the simplified Hirota method is considered to be the best tool. A completely integrable equation can be easily integrated, and its integration yields the desired solutions. The simplified Hirota method has been employed recently (Wazwaz, 2016; Wazwaz, 2021-a; Wazwaz, 2021-b) to examine several higher-order nonlinear equations. The equations derived from plasma problems are generally of the KdV, mKdV, ZK, and Burgers types. As these well-known equations are completely integrable, we can use the simplified Hirota method to examine single as well as multi-soliton (or multi-shock) solutions.

This chapter's key objective is to investigate multiple regular soliton solutions and multiple regular shock solutions for inspecting the fundamental properties of multi-solitons and multi-shocks in a dusty plasma. The system contains four elements, such as inertial positive ions, Maxwellian electrons and positrons, and stationary negatively charged dust particles. To reach the goal, we derive the KdV and Burgers equations using the reductive perturbation technique. Furthermore, we elaborately describe how the magnetic field and various parameters affect the soliton and shock characteristics (such as amplitude, width, etc.). Here, the Cole-Holf transformation (CHT) and the simplified Hirota method are used as helping tools to acquire the expected solutions. To the best of our knowledge, we make use of the simplified Hirota method for the first time for the following contemplated plasma model.

7.2 Plasma model

Let us assume an oblique propagation of waves through a magnetized plasma where inertial positive ions, Maxwellian electrons and positrons, and negatively charged dust particles are the plasma species. Besides, we assume the external magnetic field $\vec{B} = B_0\,\hat{z}$.

Hence, the equations presented underneath govern the nonlinear evolution of DIA waves (Ghosh and Bharuthram, 2008; Sultana, 2021):

$$\frac{\partial n_i}{\partial t} + \nabla \cdot (n_i \vec{u}_i) = 0, \tag{7.1}$$

$$\frac{\partial \vec{u}_i}{\partial t} + (\vec{u}_i \cdot \nabla)\vec{u}_i = -\nabla\psi + \omega_{ci}\left(\vec{u}_i \times \vec{k}\right) + \eta\, \nabla^2 \vec{u}_i, \tag{7.2}$$

$$\nabla^2\psi = \mu_e n_e - \mu_p n_p - n_i + \mu_d, \tag{7.3}$$

where n_i, n_p, n_e denote the inertial ion, positron, and electron number densities respectively, and they are normalized by their respective equilibrium values n_{i0}, n_{p0}, n_{e0}. The normalization of other variables is defined by the equation (5.6). Here, the equations (7.1) - (7.3) are in dimensionless form. For the description of solitons, the coefficient of viscosity (η) is considered zero.

The Maxwellian distributions of electrons and positrons are specified by $n_e = e^{\psi}$ and $n_p = e^{-\alpha\psi}$, respectively (Mushtaq and Shah, 2005), where $\alpha = \frac{T_e}{T_p}$ denotes the ratio of electron temperature (T_e) to positron temperature (T_p). The equilibrium condition $n_{e0} = n_{i0} + n_{p0} - Z_d n_{d0}$ implies $\mu_e = 1 + \mu_p - \mu_d$, where $\mu_e = \frac{n_{e0}}{n_{i0}}$, $\mu_p = \frac{n_{p0}}{n_{i0}}$, and $\mu_d = \frac{Z_d n_{d0}}{n_{i0}}$.

7.3 Derivation of the wave equations

In this section, we are intended to the derivation of the KdV and Burgers equations for investigating different effects on the features of multi-solitons and multi-shocks (multi-fronts), respectively, while two different stretched coordinates will be used for constructing the equations.

7.3.1 The KdV equation

In the derivation of the KdV equation, the stretched coordinates and expanded form of the quantities n_i, u_{ix}, u_{iy}, u_{iz}, and ψ that have been defined in (3.10) – (3.15) will be used.

Now, we put (3.10) - (3.15) into (7.1) - (7.3), and collect the terms in analogous powers of ϵ. Equating the coefficients of the lowest-order of ϵ, the first-order equations are obtained as

$$-V_0\frac{\partial\, n_i^{(1)}}{\partial\xi}+l_z\frac{\partial u_{iz}^{(1)}}{\partial\xi}=0, \tag{7.4}$$

$$l_x\frac{\partial\psi^{(1)}}{\partial\xi}-\ \omega_{ci}\,u_{iy}^{(1)}=0, \tag{7.5}$$

$$l_y\frac{\partial\psi^{(1)}}{\partial\xi}+\ \omega_{ci}\,u_{ix}^{(1)}=0, \tag{7.6}$$

$$l_z\frac{\partial\psi^{(1)}}{\partial\xi}-\ V_0\frac{\partial u_{iz}^{(1)}}{\partial\xi}=0, \tag{7.7}$$

$$n_i^{(1)}-\left(\mu_e+\alpha\,\mu_p\right)\psi^{(1)}=0. \tag{7.8}$$

From (7.4) – (7.8), the following first-order expressions are acquired.

$$u_{ix}^{(1)}=-\frac{l_y}{\omega_{ci}}\frac{\partial\psi^{(1)}}{\partial\xi},\ \ u_{iy}^{(1)}=\frac{l_x}{\omega_{ci}}\frac{\partial\psi^{(1)}}{\partial\xi},\ \ u_{iz}^{(1)}=\frac{l_z}{V_0}\psi^{(1)},\ \ n_i^{(1)}=\left(\mu_e+\alpha\,\mu_p\right)\psi^{(1)}. \tag{7.9}$$

And the phase speed is determined as

$$V_0=\frac{l_z}{\sqrt{\mu_e+\alpha\,\mu_p}}. \tag{7.10}$$

To the next higher power of ϵ, the second-order quantities $u_{ix}^{(2)}$, $u_{iy}^{(2)}$, and $n_i^{(2)}$ are found as

$$u_{ix}^{(2)}=\frac{V_0 l_x}{\omega_{ci}^2}\frac{\partial^2\psi^{(1)}}{\partial\xi^2},\qquad u_{iy}^{(2)}=\frac{V_0 l_y}{\omega_{ci}^2}\frac{\partial^2\psi^{(1)}}{\partial\xi^2}, \tag{7.11}$$

and

$$n_i^{(2)}=(\mu_e+\alpha\,\mu_p)\psi^{(2)}+\frac{1}{2}\left(\mu_e-\mu_p\alpha^2\right)\left[\psi^{(1)}\right]^2-\frac{\partial^2\psi^{(1)}}{\partial\xi^2}. \tag{7.12}$$

Equating the coefficients of $\epsilon^{5/2}$ from (7.1) and the z-component of (7.2), we obtain

$$\frac{\partial n_i^{(1)}}{\partial\tau}-\ V_0\frac{\partial\, n_i^{(2)}}{\partial\xi}+l_x\frac{\partial u_{ix}^{(2)}}{\partial\xi}+l_y\frac{\partial u_{iy}^{(2)}}{\partial\xi}+l_z\frac{\partial u_{iz}^{(2)}}{\partial\xi}+l_z\frac{\partial}{\partial\xi}\left(n_i^{(1)}u_{iz}^{(1)}\right)=0, \tag{7.13}$$

and

$$\frac{\partial u_{iz}^{(1)}}{\partial\tau}-\ V_0\frac{\partial u_{iz}^{(2)}}{\partial\xi}+l_z u_{iz}^{(1)}\ \frac{\partial u_{iz}^{(1)}}{\partial\xi}+l_z\frac{\partial\psi^{(2)}}{\partial\xi}=0. \tag{7.14}$$

Finally, we use (7.9) and (7.10) to remove the second-order quantities from (7.11) - (7.14), and this gives

$$\frac{\partial\psi^{(1)}}{\partial\tau} + A\,\psi^{(1)}\frac{\partial\psi^{(1)}}{\partial\xi} + B\frac{\partial^3\psi^{(1)}}{\partial\xi^3} = 0, \tag{7.15}$$

where $A = \frac{3{l_z}^2}{2\,V_0} - \frac{{V_0}^3}{2{l_z}^2}\left(\mu_e - \mu_p\alpha^2\right)$ and $B = \frac{{V_0}^3}{2{l_z}^2}\left(1 + \frac{1-{l_z}^2}{\omega_{ci}^2}\right)$. (7.16)

Equation (7.15) is known as the KdV equation (Shomen and Pramanik, 2021; Khalid et al., 2021), where the middle term $\psi^{(1)}\frac{\partial\psi^{(1)}}{\partial\xi}$ indicates the nonlinearity and the last term $\frac{\partial^3\psi^{(1)}}{\partial\xi^3}$ indicates the dispersion effect.

7.3.2 The Burgers equation

To derive the Burgers equation, the following stretched coordinates (Hafez et al., 2020)

$$\xi = \epsilon\,(l_x x + l_y y + l_z z - V_0 t),\ \ \tau = \epsilon^2\,t. \tag{7.17}$$

and the extended form of perturbed variables described in (3.11) - (3.15) are used.

In this case, the same relations found in (7.9) and (7.10) are also obtained for the first-order quantities $u_{iz}^{(1)}$, $n_i^{(1)}$, and the phase speed V_0. Similarly, the second-order quantities are determined as (obtained by the coefficients of higher powers of ϵ)

$$u_{ix}^{(2)} = -\frac{l_y}{\omega_{ci}}\frac{\partial\psi^{(1)}}{\partial\xi}\,,\ u_{iy}^{(2)} = \frac{l_x}{\omega_{ci}}\frac{\partial\psi^{(1)}}{\partial\xi},$$

$$n_i^{(2)} = \left(\mu_e + \alpha\,\mu_p\right)\psi^{(2)} + \frac{1}{2}\left(\mu_e - \mu_p\alpha^2\right)\left[\psi^{(1)}\right]^2, \tag{7.18}$$

$$\frac{\partial u_{iz}^{(2)}}{\partial\xi} = \frac{l_z}{V_0}\frac{\partial\psi^{(2)}}{\partial\xi} - \frac{l_z}{V_0^2}\frac{\partial\psi^{(1)}}{\partial\tau} - \left[\frac{2l_z^3}{V_0^3} - \frac{V_0}{l_z}\left(\mu_e - \mu_p\alpha^2\right)\right]\psi^{(1)}\frac{\partial\psi^{(1)}}{\partial\xi}\,.$$

Again, equating the coefficient of ϵ^3 from z-component of (7.2), we get

$$\frac{\partial u_{iz}^{(1)}}{\partial\tau} - V_0\frac{\partial u_{iz}^{(2)}}{\partial\xi} - \eta\frac{\partial^2 u_{iz}^{(1)}}{\partial\xi^2} + l_z u_{iz}^{(1)}\frac{\partial u_{iz}^{(1)}}{\partial\xi} + l_z\frac{\partial\psi^{(2)}}{\partial\xi} = 0. \tag{7.19}$$

The use of first- and second-order quantities in (7.19) yields

$$\frac{\partial u_{iz}^{(2)}}{\partial \xi} - \frac{l_z^3}{V_0^3}\psi^{(1)}\frac{\partial \psi^{(1)}}{\partial \xi} + \frac{\eta l_z}{V_0^2}\frac{\partial^2 \psi^{(1)}}{\partial \xi^2} - \frac{l_z}{V_0^2}\frac{\partial \psi^{(1)}}{\partial \tau} - \frac{l_z}{V_0}\frac{\partial \psi^{(2)}}{\partial \xi} = 0.$$

$$\Rightarrow \frac{2l_z}{V_0^2}\frac{\partial \psi^{(1)}}{\partial \tau} + \left[\frac{3l_z^3}{V_0^3} - \frac{V_0}{l_z}\left(\mu_e - \mu_p\alpha^2\right)\right]\psi^{(1)}\frac{\partial \psi^{(1)}}{\partial \xi} = \frac{\eta l_z}{V_0^2}\frac{\partial^2 \psi^{(1)}}{\partial \xi^2}.$$

$$\Rightarrow \frac{\partial \psi^{(1)}}{\partial \tau} + \left[\frac{3l_z^2}{2V_0} - \frac{V_0^3}{2\,l_z^2}\left(\mu_e - \mu_p\alpha^2\right)\right]\psi^{(1)}\frac{\partial \psi^{(1)}}{\partial \xi} = \frac{\eta}{2}\frac{\partial^2 \psi^{(1)}}{\partial \xi^2}.$$

$$\Rightarrow \frac{\partial \psi^{(1)}}{\partial \tau} + A\,\psi^{(1)}\frac{\partial \psi^{(1)}}{\partial \xi} = C\frac{\partial^2 \psi^{(1)}}{\partial \xi^2}, \tag{7.20}$$

where $A = \frac{3{l_z}^2}{2\,V_0} - \frac{{V_0}^3}{2{l_z}^2}\left(\mu_e - \mu_p\alpha^2\right)$ and $C = \frac{\eta}{2}$.

Equation (7.20) is the Burgers equation, where the term $C\frac{\partial^2 \psi^{(1)}}{\partial \xi^2}$ represents the dissipative effect. Unlike the KdV equation, which combines the nonlinear and dispersion effects, the Burgers equation combines the nonlinear and dissipation effects.

Here, A, B, and C are the nonlinear, dispersive, and dissipative coefficients, respectively. The coefficients depend on various parameters; hence, we cannot choose their numerical values randomly.

7.4 Outline of the solution technique

Both the KdV and Burgers equations are completely integrable, and they have single as well as multi-solitons (or multi-shocks) solutions. To obtain these solutions, we will now use the simplified Hirota method (Wazwaz, 2016; Wazwaz, 2021-a; Wazwaz, 2021-b) while the solutions are obtained in terms of exponential functions. For solving the KdV and Burgers equations, the CHT and auxiliary functions are quite different. Assume a general integrable NLPDE that may be reduced to the KdV or Burgers equation.

$$P(u, u_t, u_x, u_{tt}, u_{xt}, u_{xx}, \ldots\ldots) = 0. \tag{7.21}$$

We just go over the steps that are necessary here, because the method was discussed elaborately in the last decades by numerous researchers (Hirota, 2004; Griffiths, 2012;

Kumar and Mohan, 202, 2022; Alsayyed et al., 2016; Chen et al., 2019; Ullah et al., 2020-b; Ismael et al., 2020).

7.4.1 Solution technique for the KdV equation

We put $u(x,t) = e^{\eta_i}$, $\eta_i = k_i x - \omega_i t$, $i = 1, 2, 3, \ldots, N$ into the linear terms of (7.21) that gives a dispersion relation between k_i and ω_i.

Then the following CHT (Chen et al., 2019) is used to obtain multi-soliton (N-soliton) solutions to the KdV equation.

$$u(x,t) = R \frac{\partial^2}{\partial x^2} (\ln f). \tag{7.22}$$

Use of (7.22) in (7.21) yields the value of R, where the auxiliary function $f(x,t)$ is defined as

(i) For single-soliton solution: $f(x,t) = 1 + e^{\eta_1}$,

(ii) For two-soliton solution: $f(x,t) = 1 + e^{\eta_1} + e^{\eta_2} + a_{12}\, e^{\eta_1+\eta_2}$,

(iii) For three-soliton solution: $f(x,t) = 1 + e^{\eta_1} + e^{\eta_2} + e^{\eta_3} + a_{12}\, e^{\eta_1+\eta_2} + a_{13}\, e^{\eta_1+\eta_3} + a_{23}\, e^{\eta_2+\eta_3} + A_{123}\, e^{\eta_1+\eta_2+\eta_3}$.

If $A_{123} = a_{12}\, a_{23}\, a_{13}$, the three-soliton solution can be found, and this proves that N-soliton solutions exist.

7.4.2 Solution technique for the Burgers equation

Likewise of the solution technique of the KdV equation, we put $u(x,t) = e^{\eta_i}$ (where $\eta_i = k_i x - \omega_i t$, $i = 1, 2, 3, \ldots, N$) into the linear terms of the equation (7.21), and this gives a dispersion relation.

Then the following CHT is used to obtain multi-shock (N-front) solutions to the Burgers equation.

$$u(x,t) = R \frac{\partial}{\partial x} (\ln f). \tag{7.23}$$

Use of (7.23) in (7.21) yields the value of R, where the auxiliary function $f(x, t)$ is defined as

(i) For single-front solution: $f(x, t) = 1 + e^{\eta_1}$,

(ii) For two-front solution: $f(x, t) = 1 + e^{\eta_1} + e^{\eta_2}$,

(iii) For three-front solution: $f(x, t) = 1 + e^{\eta_1} + e^{\eta_2} + e^{\eta_3}$,

… …

(N) For *N*-front solution: $f(x, t) = 1 + e^{\eta_1} + e^{\eta_2} + e^{\eta_3} + \cdots + e^{\eta_N} = 1 + \sum_{i=1}^{N} e^{\eta_i}$.

Finally, by using the values of R and the above auxiliary functions in (7.23), we can find the *N*-front solution in the following form:

$$u(x, t) = R\,\frac{\sum_{i=1}^{N} k_i\, e^{k_i x - \omega_i t}}{1 + \sum_{i=1}^{N} e^{k_i x - \omega_i t}}. \tag{7.24}$$

Practically, there is no need to derive a four-soliton (or shock) solution if the three-soliton (or three-shock) solution is obtained. It is therefore sufficient to derive the solutions for $N = 1, 2, 3$ to show that multi-soliton (or multi-shock) solutions exist (Wazwaz, 2010).

7.5 Multi-soliton and multi-shock solutions

In this section, it is expected to find the multi-soliton solutions and multi-shock solutions to the KdV and Burgers equations, respectively. Substitution of $u(\xi, \tau) = e^{k_i \xi - \omega_i \tau}$ into the linear terms of (7.15) gives

$$\omega_i = B k_i^3. \tag{7.25}$$

Equation (7.25) is the dispersion relation that transforms the phase variable into $\eta_i = k_i\, \xi - B k_i^3\, \tau$.

We assume the single-soliton solution as

$$\psi^{(1)}(\xi, \tau) = R\,\frac{\partial^2}{\partial \xi^2}(\ln f), \tag{7.26}$$

where $f(\xi, \tau)$ is given by

$$f(\xi, \tau) = 1 + e^{\eta_1}, \quad \eta_1 = k_1\, \xi - B k_1^3\, \tau\,. \tag{7.27}$$

The use of (7.26) and (7.27) in (7.15) yields $R = \frac{12\,B}{A}$. Thus, the single-soliton solution is

$$\psi_1^{(1)}(\xi, \tau) = \frac{12\,B}{A}\, \frac{k_1^2\, e^{k_1\,\xi - B k_1^3\,\tau}}{\left(1 + e^{k_1\,\xi - B k_1^3\,\tau}\right)^2} = \frac{3\,B}{A} k_1^2\, \mathrm{sech}^2\left[\frac{1}{2}(k_1\,\xi - B k_1^3\,\tau)\right]. \tag{7.28}$$

The solution (7.28) provides a bell-shaped soliton whose amplitude is $\frac{3\,B}{A} k_1^2 = \frac{3U_1}{A}$ and width is $2/k_1 = \sqrt{4B/U_1}$ (where $U_1 = B k_1^2$). These relations indicate that amplitude and width are dependent on various parameters and forces.

For the two-soliton solution, $f(\xi, \tau)$ is defined as

$$f(\xi, \tau) = 1 + e^{\eta_1} + e^{\eta_2} + a_{12}\, e^{\eta_1 + \eta_2}\,, \tag{7.29}$$

where $\eta_i = k_i\, \xi - B k_i^3 \tau$ (i =1, 2). Using $R = \frac{12\,B}{A}$ and (7.29) in (7.26), and then substituting $\psi^{(1)}$ in (7.15), a_{12} is obtained as

$$a_{12} = \frac{(k_1 - k_2)^2}{(k_1 + k_2)^2}. \tag{7.30}$$

Thus, the two-soliton solution takes the form

$$\psi_2^{(1)}(\xi, \tau) = \frac{12\,B}{A}\left[\frac{k_1^2\, e^{k_1\,\xi - B k_1^3\,\tau} + k_2^2\, e^{k_2\,\xi - B k_2^3\,\tau} + (k_1 - k_2)^2\; e^{(k_1 + k_2)\,\xi - B\left(k_1^3 + k_2^3\right)\tau}}{1 + e^{k_1\,\xi - B k_1^3\,\tau} + e^{k_2\,\xi - B k_2^3\,\tau} + \frac{(k_1 - k_2)^2}{(k_1 + k_2)^2}\; e^{(k_1 + k_2)\,\xi - B(k_1^3 + k_2^3)\tau}}\right.$$
$$\left. - \frac{\left(k_1 e^{k_1\,\xi - B k_1^3\,\tau} + k_2\, e^{k_2\,\xi - B k_2^3\,\tau} + \frac{(k_1 - k_2)^2}{(k_1 + k_2)}\; e^{(k_1 + k_2)\,\xi - B\left(k_1^3 + k_2^3\right)\tau}\right)^2}{\left(1 + e^{k_1\,\xi - B k_1^3\,\tau} + e^{k_2\,\xi - B k_2^3\,\tau} + \frac{(k_1 - k_2)^2}{(k_1 + k_2)^2}\; e^{(k_1 + k_2)\,\xi - B(k_1^3 + k_2^3)\tau}\right)^2}\right]. \tag{7.31}$$

For the three-soliton solution, $f(\xi, \tau)$ is defined as

$$f(\xi, \tau) = 1 + e^{\eta_1} + e^{\eta_2} + e^{\eta_3} + a_{12}\, e^{\eta_1 + \eta_2} + a_{13}\, e^{\eta_1 + \eta_3} + a_{23}\, e^{\eta_2 + \eta_3} + A_{123}\, e^{\eta_1 + \eta_2 + \eta_3}$$

$$= 1 + e^{k_1\,\xi - B k_1^3\,\tau} + e^{k_2\,\xi - B k_2^3\,\tau} + e^{k_3\,\xi - B k_3^3\,\tau} + a_{12}\, e^{(k_1 + k_2)\xi - B(k_1^3 + k_2^3)\,\tau}$$

$$+ a_{13}\, e^{(k_1 + k_3)\xi - B(k_1^3 + k_3^3)\,\tau} + a_{23}\, e^{(k_2 + k_3)\xi - B(k_2^3 + k_3^3)\,\tau} + A_{123}\, e^{(k_1 + k_2 + k_3)\xi - B(k_1^3 + k_2^3 + k_3^3)\,\tau}, \tag{7.32}$$

where $\eta_i = k_i\, \xi - B k_i^3 \tau$ (i = 1, 2, 3).

If we use (7.32) and (7.26) in (7.15), the phase factor a_{12} is obtained as $a_{12} = \frac{(k_1-k_2)^2}{(k_1+k_2)^2}$ that can be generalized to

$$a_{ij} = \frac{\left(k_i-k_j\right)^2}{\left(k_i+k_j\right)^2}, 1 \le i < j \le 3. \tag{7.33}$$

Thus, $$A_{123} = a_{12}\, a_{23}\, a_{13} = \left[\frac{(k_1-k_2)(k_2-k_3)(k_1-k_3)}{(k_1+k_2)(k_2+k_3)(k_1+k_3)}\right]^2. \tag{7.34}$$

Here, the relation (7.33) shows that the KdV equation (7.15) does not show any resonant phenomenon because a_{ij} cannot be zero or infinity for $k_i \neq k_j$ (Wazwaz, 2016).

Thus, the three-soliton solution is found as

$$\psi_3^{(1)}(\xi,\tau) = \frac{12\,B}{A}\left[\frac{T_1}{T_3} - \left(\frac{T_2}{T_3}\right)^2\right], \tag{7.35}$$

where T_1, T_2, and T_3 are given by the following expansions:

$$T_1 = k_1^2 e^{\eta_1} + k_2^2 e^{\eta_2} + k_3^2 e^{\eta_3} + (k_1 - k_2)^2\, e^{\eta_1+\eta_2} + (k_1 - k_3)^2\, e^{\eta_1+\eta_3} +$$
$$(k_2 - k_3)^2\, e^{\eta_2+\eta_3} + \left[\frac{(k_1-k_2)(k_2-k_3)(k_1-k_3)}{(k_1+k_2)(k_2+k_3)(k_1+k_3)}\right]^2 (k_1 + k_2 + k_3)^2 e^{\eta_1+\eta_2+\eta_3},$$

$$T_2 = k_1 e^{\eta_1} + k_2 e^{\eta_2} + k_3 e^{\eta_3} + \frac{(k_1-k_2)^2}{k_1+k_2}\, e^{\eta_1+\eta_2} + \frac{(k_1-k_3)^2}{k_1+k_3}\, e^{\eta_1+\eta_3} + \frac{(k_2-k_3)^2}{k_2+k_3}\, e^{\eta_2+\eta_3} +$$
$$\left[\frac{(k_1-k_2)(k_2-k_3)(k_1-k_3)}{(k_1+k_2)(k_2+k_3)(k_1+k_3)}\right]^2 (k_1 + k_2 + k_3) e^{\eta_1+\eta_2+\eta_3},$$

$$T_3 = 1 + e^{\eta_1} + e^{\eta_2} + e^{\eta_3} + \frac{(k_1-k_2)^2}{(k_1+k_2)^2} e^{\eta_1+\eta_2} + \frac{(k_1-k_3)^2}{(k_1+k_3)^2} e^{\eta_1+\eta_2} + \frac{(k_2-k_3)^2}{(k_2+k_3)^2} e^{\eta_1+\eta_2} +$$
$$\left[\frac{(k_1-k_2)(k_2-k_3)(k_1-k_3)}{(k_1+k_2)(k_2+k_3)(k_1+k_3)}\right]^2 e^{\eta_1+\eta_2+\eta_3}.$$

The derivation of the three-soliton solution approves that N-soliton solutions exist for any order $N \ge 4$, and we can obtain these solutions using the above procedure. In other words, the KdV equation has N-soliton solutions for finite $N \ge 1$.

In a similar procedure, the following multi-shock solutions to the Burgers equation (7.20) can be obtained by using the relation (7.23) and the corresponding auxiliary functions.

Single-shock solution: $\psi_1^{(1)}(\xi,\tau) = -\frac{2\,C}{A}\frac{k_1\,e^{k_1\,\xi+C\,k_1^2\,\tau}}{1+e^{k_1\,\xi+C\,k_1^2\,\tau}} = \frac{U_1}{A}\left[1-\tanh\left(\frac{U_1}{2C}(\xi-U_1\tau)\right)\right].$

Two-shock solution: $\psi_2^{(1)}(\xi,\tau) = -\frac{2\,C}{A}\frac{\sum_{i=1}^{2}k_i\,e^{k_i\,\xi+C\,k_i^2\,\tau}}{1+\sum_{i=1}^{2}e^{k_i\,\xi+C\,k_i^2\,\tau}} = \frac{2}{A}\frac{\sum_{i=1}^{2}U_i\,e^{-\frac{U_i}{C}(\xi-U_i\,\tau)}}{1+\sum_{i=1}^{2}e^{-\frac{U_i}{C}(\xi-U_i\,\tau)}}.$

Three-shock solution: $\psi_3^{(1)}(\xi,\tau) = -\frac{2\,C}{A}\frac{\sum_{i=1}^{3}k_i\,e^{k_i\,\xi+C\,k_i^2\,\tau}}{1+\sum_{i=1}^{3}e^{k_i\,\xi+C\,k_i^2\,\tau}} = \frac{2}{A}\frac{\sum_{i=1}^{3}U_i\,e^{-\frac{U_i}{C}(\xi-U_i\,\tau)}}{1+\sum_{i=1}^{3}e^{-\frac{U_i}{C}(\xi-U_i\,\tau)}}.$

… …

In general, N-shock solution: $\psi_N^{(1)}(\xi,\tau) = -\frac{2\,C}{A}\frac{\sum_{i=1}^{N}k_i\,e^{k_i\,\xi+C\,k_i^2\,\tau}}{1+\sum_{i=1}^{N}e^{k_i\,\xi+C\,k_i^2\,\tau}} = \frac{2}{A}\frac{\sum_{i=1}^{N}U_i\,e^{-\frac{U_i}{C}(\xi-U_i\,\tau)}}{1+\sum_{i=1}^{N}e^{-\frac{U_i}{C}(\xi-U_i\,\tau)}}.$

7.6 Result and discussion

In this section, we investigate the traveling natures of solitons and shocks. Further, we analyze the contribution of different parameters on both types of waves numerically. Based on different assumptions and earlier works (Das et al., 2000; Rahman and Haider, 2016; Wazwaz, 2016), the plasma parametric values have been selected.

7.6.1 Parametric effects on the multi-solitons

We plot the soliton solution (7.28) to observe the wave profiles of single-soliton (shown in Figures 7.1 and 7.2) for different parametric values $\alpha = 1.1$, $\omega_{ci} = 0.6$, $\theta = 15^0$, $\mu_d = 0.5$, $\mu_p = 0.4$, $U_1 = 0.4$, while Figure 7.1 represents the 3D profile of single-soliton and Figure 7.2 is the corresponding 2D view of the soliton at τ =0, 5, 10. The graphs demonstrate that the single-soliton's bell-shaped wave profile has a single global peak, and vanishes at $\xi \to \pm\infty$. As illustrated in Figure 7.2, it is seen that the single-soliton propagates with the same speed and shape at different times.

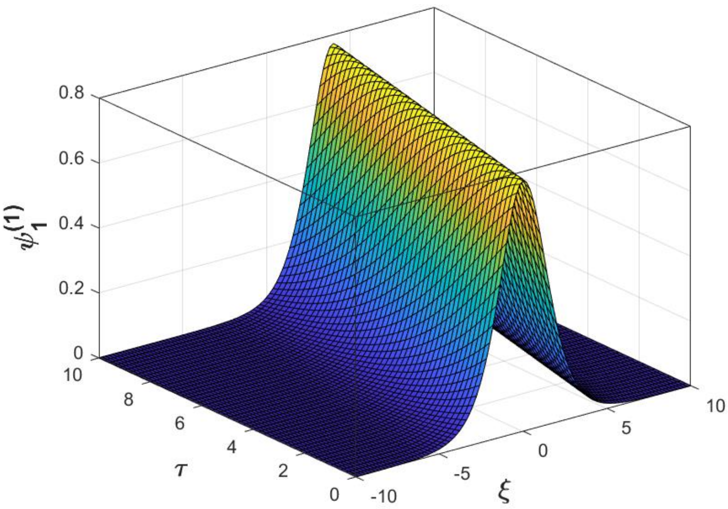

Figure 7.1: Single-soliton of (7.28), when $\alpha = 1.1$, $\omega_{ci} = 0.6$, $\theta = 15^0$, $\mu_d = 0.5$, $\mu_p = 0.4$, $U_1 = 0.4$ in the interval $\xi \in [-10, 10]$ and $\tau \in [0, 10]$.

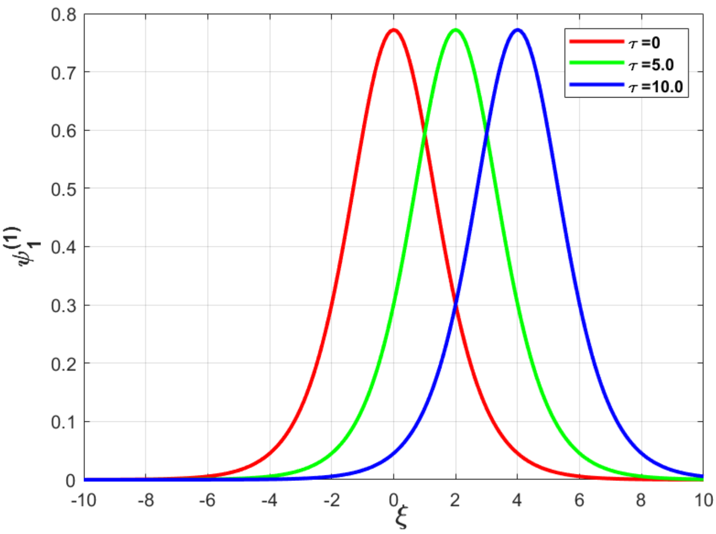

Figure 7.2: Single-soliton at $\tau = 0$, 5, 10 in the interval $\xi \in [-8, 8]$, when $\alpha = 1.1$, $\omega_{ci} = 0.6$, $\theta = 15^0$, $\mu_d = 0.5$, $\mu_p = 0.4$, $U_1 = 0.4$.

Figure 7.3 depicts the traveling paths of the two-solitons, and Figure 7.4 is the 2D depiction of solitons' wave profiles at $\tau = 0$, 5, 10 while $\alpha = 1.1$, $\omega_{ci} = 0.6$, $\theta = 15^0$, $\mu_d = 0.5$, $\mu_p = 0.4$, $U_1 = 0.4$, $U_2 = 0.6$. The figures depict the progressive history of two solitons traveling from left to right at different points of time τ, while they propagate with different amplitudes and widths. At time $\tau = 0$, the greater soliton lies behind the smaller soliton.

Because a soliton of higher amplitude travels more quickly than a soliton of lower amplitude, a larger soliton eventually approaches a smaller one. Two solitons merge, and then they separate from each other again. Each soliton gets back to its previous shape, but the soliton of higher amplitude comes in front.

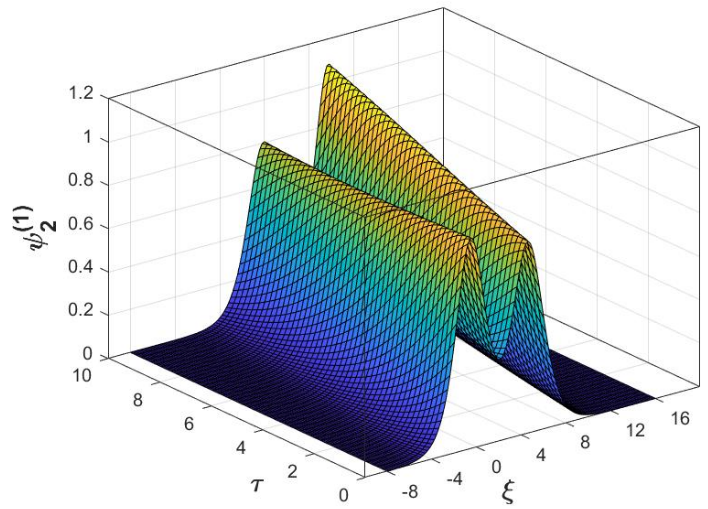

Figure 7.3: Two-soliton profile of (7.31), when $\alpha = 1.1$, $\omega_{ci} = 0.6$, $\theta = 15^0$, $\mu_d = 0.5$, $\mu_p = 0.4$, $U_1 = 0.4$, $U_2 = 0.6$ in $\xi \in [-8, 12]$, $\tau \in [0, 2]$.

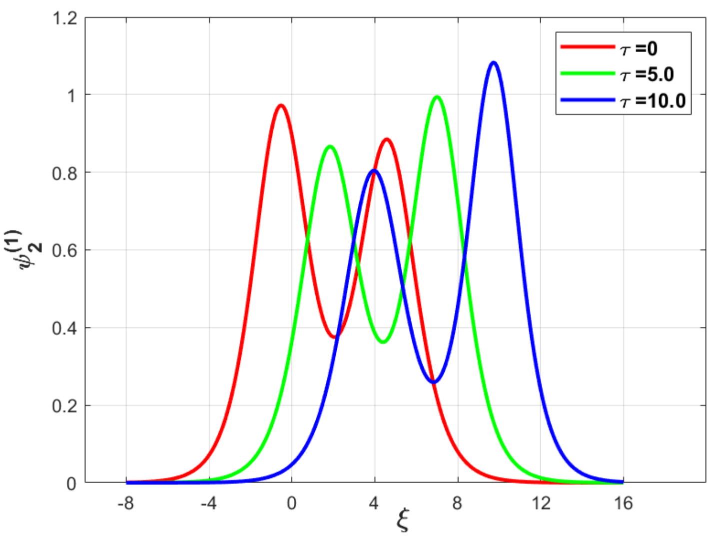

Figure 7.4: Two-solitons at $\tau = 0, 5, 10$ in the interval $\xi \in [-8, 12]$, when $\alpha = 1.1$, $\omega_{ci} = 0.6$, $\theta = 15^0$, $\mu_d = 0.5$, $\mu_p = 0.4$, $U_1 = 0.4$, $U_2 = 0.6$.

Figures 7.5 and 7.6 show the 3D and 2D representations of the three-soliton profiles, respectively, and both are depicted from the solution (7.35) by taking $\alpha = 1.1$, $\omega_{ci} = 0.6$,

$\theta = 45^0$, $\mu_d = 0.5$, $\mu_p = 0.4$, $U_1 = 0.4$, $U_2 = 0.6$, $U_3 = 0.8$. The figures show how the wave moves with three humps. Like the propagation of two-solitons, the three-solitons propagate from left to right, and ultimately the soliton of higher amplitude takes its position in front at time $\tau = 10$.

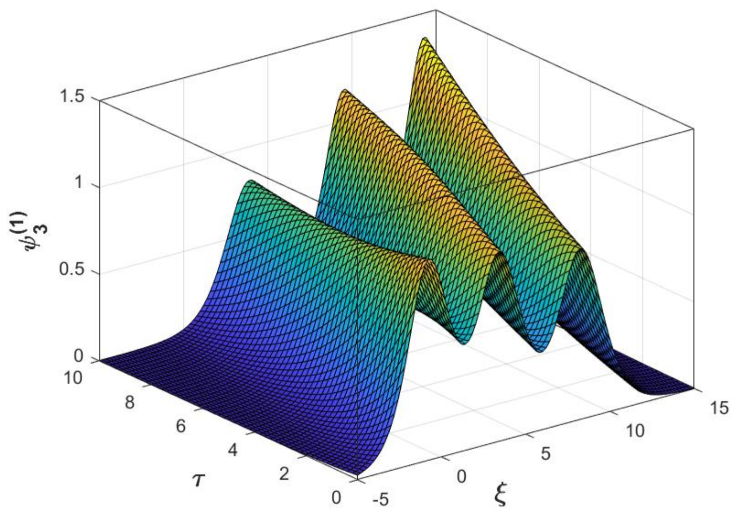

Figure 7.5: Three-soliton profile of (7.35), when $\alpha = 1.1$, $\omega_{ci} = 0.6$, $\theta = 15^0$, $\mu_d = 0.5$, $\mu_p = 0.4$, $U_1 = 0.4$, $U_2 = 0.6$, $U_3 = 0.8$ and $\xi \in [-5, 15]$, $\tau \in [0, 2]$.

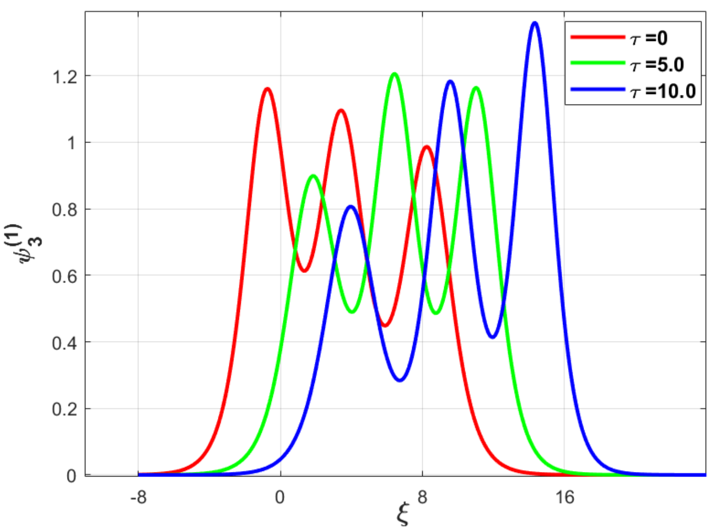

Figure 7.6: Three-solitons at $\tau = 0, 5, 10$ in the interval $\xi \in [-5, 20]$, when $\alpha = 1.1$, $\omega_{ci} = 0.6$, $\theta = 45^0$, $\mu_d = 0.5$, $\mu_p = 0.4$, $U_1 = 0.4$, $U_2 = 0.6$, $U_3 = 0.8$.

Figures 7.7, 7.8, and 7.9 show how the magnetic field affects the fundamental characteristics (amplitudes and widths) of the single-, two-, and three-soliton profiles, respectively. For various cyclotron frequencies $\omega_{ci} = 0.4,\ 0.6,\ 0.8$, we have drawn the figures when $\alpha = 1.1$, $\theta = 45^0$, $\mu_d = 0.5$, $\mu_p = 0.4$, $U_1 = 0.4$, $U_2 = 0.6$, $U_3 = 0.8$. As can be seen in the figures, the magnetic field has a reducing effect on the amplitudes and widths of all forms of solitons (Abdus, et al., 2022). The amplitudes and widths, however, are independent of the magnetic field if $\theta = 0^0$ (i.e., when the wave is directed in the direction of the magnetic field). Moreover, the relation (7.10) suggests that the magnetic field does not affect the phase velocity.

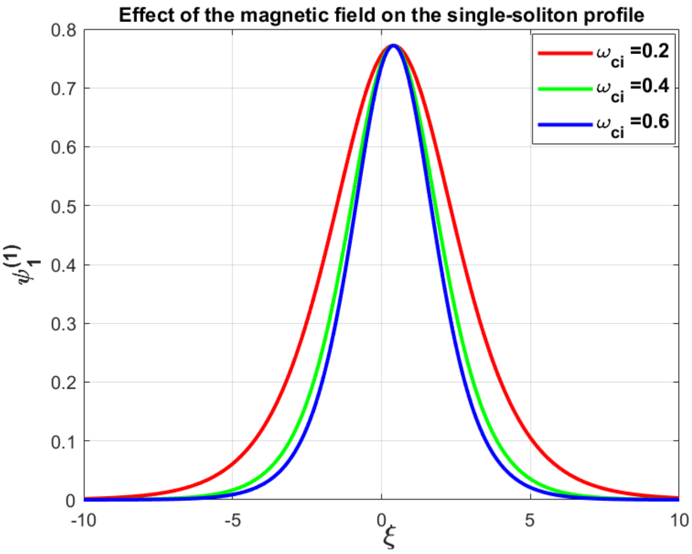

Figure 7.7: Single-soliton profiles for $\omega_{ci} = 0.2, 0.4, 0.6$, when $\alpha = 1.1$, $\theta = 15^0$, $\mu_d = 0.5$, $\mu_p = 0.4$, $U_1 = 0.4$, $\tau = 1$.

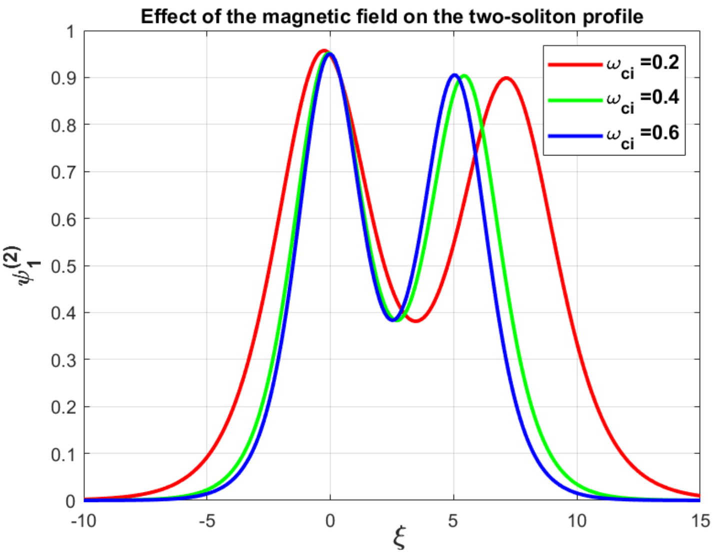

Figure 7.8: Two-soliton profiles for $\omega_{ci} = 0.2, 0.4, 0.6$, when $\alpha = 1.1$, $\theta = 1$, $\mu_d = 0.5$, $\mu_p = 0.4$, $U_1 = 0.4$, $U_2 = 0.6, 0.8$, $\tau = 1$.

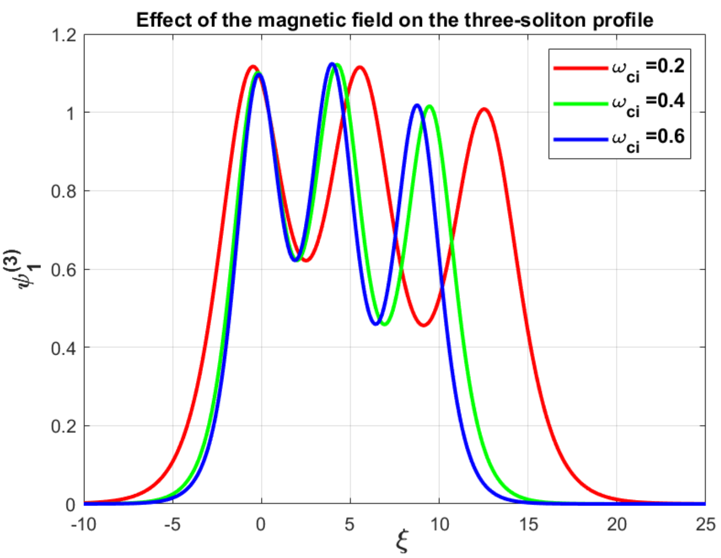

Figure 7.9: Three-soliton profiles for $\omega_{ci} = 0.2, 0.4, 0.6$, when $\alpha = 1.1$, $\theta = 15^0$, $\mu_d = 0.5$, $\mu_p = 0.4$, $U_1 = 0.4$, $U_2 = 0.6$, $U_3 = 0.8$, $\tau = 1$.

Figure 7.10 illustrates the change of the single-soliton structure with respect to the concentration of dust particles while $\alpha = 1.1$, $\mu_p = 0.4$, $\theta = 15^0$, $\omega_{ci} = 0.6$, $U_1 = 0.4$, $\tau = 1$. The figure shows that the waves propagate with greater amplitudes and widths with rising values of μ_d. Figures 7.11 and 7.12 show analogous phenomena for two-solitons and three-solitons, respectively. In addition, we observe from (7.10) that the phase speed decreases with increasing values of dust particle concentration.

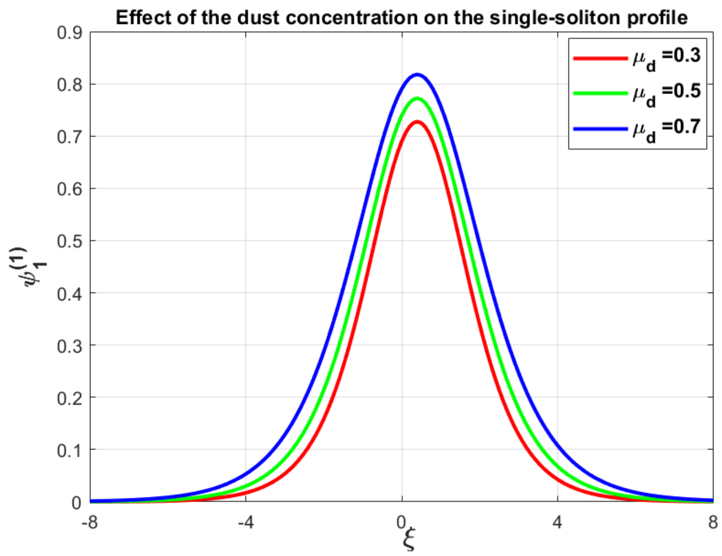

Figure 7.10: Single-soliton profiles for $\mu_d = 0.3, 0.5, 0.7$, when $\alpha = 1.1$, $\mu_p = 0.4$, $\omega_{ci} = 0.6$, $\theta = 15^0$, $U_1 = 0.4$, $\tau = 1$.

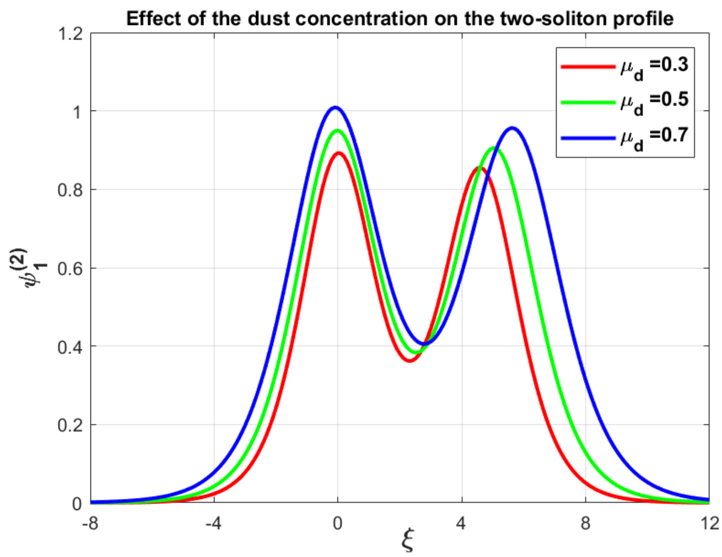

Figure 7.11: Two-soliton profiles for $\mu_d = 0.3, 0.5, 0.7$, when $\alpha = 1.1$, $\mu_p = 0.4$, $\theta = 15^0$, $\omega_{ci} = 0.6$, $U_1 = 0.4$, $U_2 = 0.6$, $\tau = 1$.

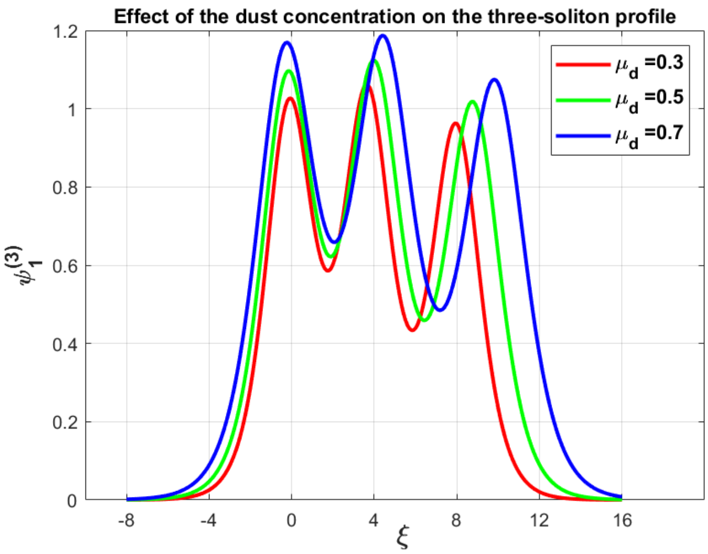

Figure 7.12: Three-soliton profiles for $\mu_d = 0.3, 0.5, 0.7$, when $\alpha = 1.1$, $\mu_p = 0.4$, $\theta = 15^0$, $\omega_{ci} = 0.6$, $U_1 = 0.4$, $U_2 = 0.6$, $U_3 = 0.8$, $\tau = 1$.

The effects of the propagation angle on the characteristics of the single-, two-, and three-solitons are shown in Figures 7.13, 7.14, and 7.15, respectively. The figures are drawn by choosing the parameters as $\alpha = 1.1$, $\mu_p = 0.4$, $U_1 = 0.4$, $\omega_{ci} = 0.5$, $\tau = 1$. We observe from the figures that the propagation angle increases the soliton amplitudes and widths. If $\theta = 90^0$, the wave amplitudes become infinite. To obtain solitons with finite amplitude, the angle should therefore be small.

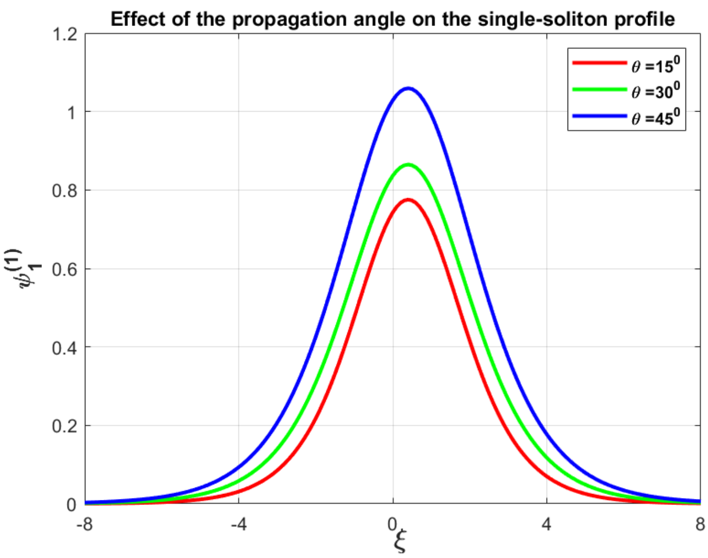

Figure 7.13: Single-soliton profiles for different angles (θ), when $\alpha = 1.1$, $\mu_p = 0.4$, $\mu_d = 0.5$, $U_1 = 0.4$, $\omega_{ci} = 0.6$, $\tau = 1$.

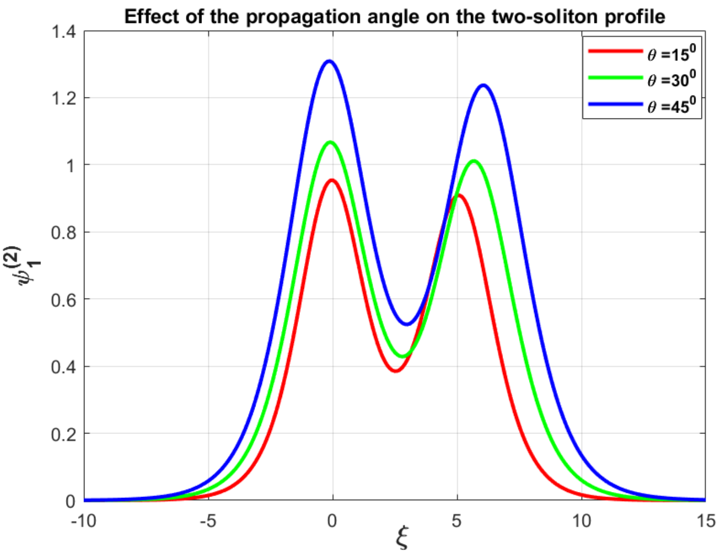

Figure 7.14: Two-soliton profiles for different angles (θ), when $\alpha = 1.1$, $\omega_{ci} = 0.6$, $\mu_d = 0.5$, $\mu_p = 0.4$, $U_1 = 0.4$, $U_2 = 0.6$, $\tau = 1$.

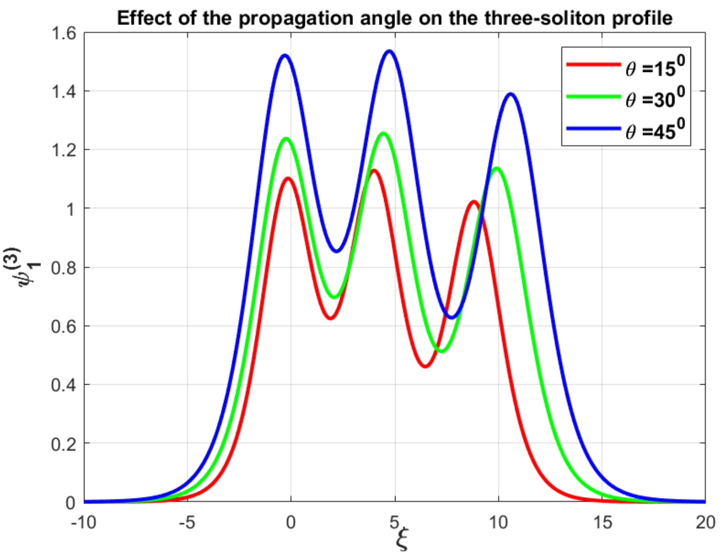

Figure 7.15: Three-soliton profiles for different angles (θ), when $\alpha = 1.1$, $\omega_{ci} = 0.6$, $\mu_d = 0.5$, $\mu_p = 0.4$, $U_1 = 0.4$, $U_2 = 0.6$, $U_3 = 0.8$, $\tau = 1$.

Figures 7.16 - 7.18 depict the influence of positron concentration on the nature of single-, two-, and three-solitons, respectively. We observe from the figures that the positron concentration decreases the soliton's amplitudes and widths.

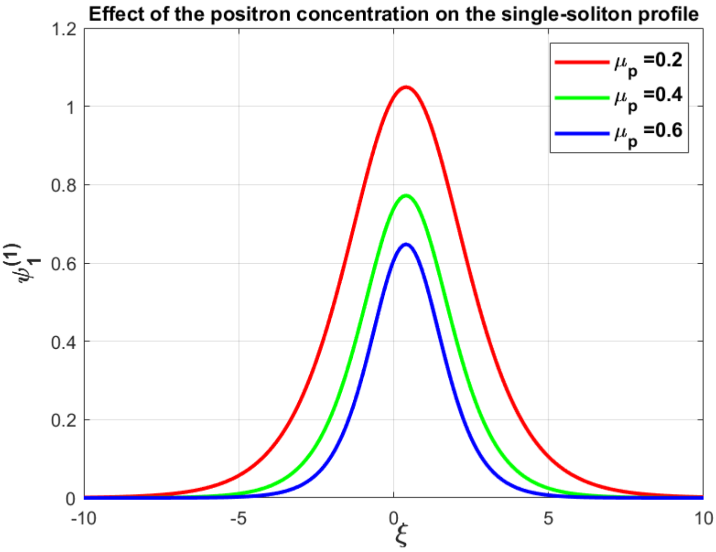

Figure7.16: Single-soliton profiles for $\mu_p = 0.2, 0.4, 0.6$, when $\alpha = 1.1$, $\mu_d = 0.5$, $\theta = 15^0$, $\omega_{ci} = 0.6$, $U_1 = 0.4$, $\tau = 1$.

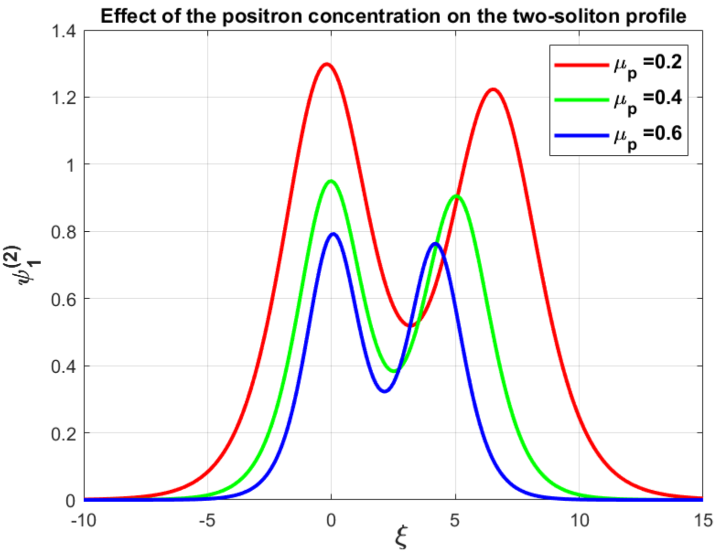

Figure 7.17: Two-soliton profiles for $\mu_p = 0.2, 0.4, 0.6$, when $\alpha = 1.1$, $\mu_d = 0.5$, $\theta = 15^0$, $\omega_{ci} = 0.6$, $U_1 = 0.4$, $U_2 = 0.6$, $\tau = 1$.

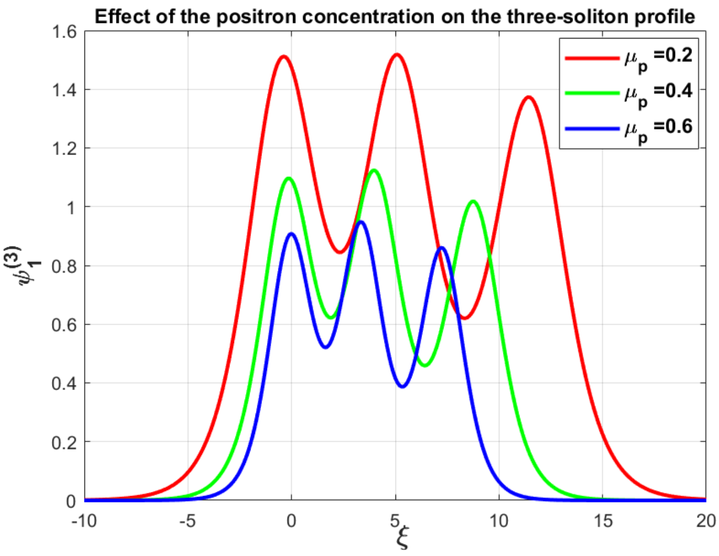

Figure 7.18: Three-soliton profiles for $\mu_p = 0.2, 0.4, 0.6$, when $\alpha = 1.1$, $\mu_d = 0.5,\ \theta = 15^0, \omega_{ci} = 0.6,\ U_1 = 0.4, U_2 = 0.6, U_3 = 0.8, \tau = 1$.

7.6.2 Parametric effects on the multi-shocks

Figures 7.19 -7.21 depict the multi-shock profiles for different plasma parameters. The single-front solution represents a kink-type wave that rises or descends from one asymptotic state to another and approaches a constant at infinity. Similarly, two-fronts and three-fronts are drawn in Figures 7.20 and 7.21, respectively.

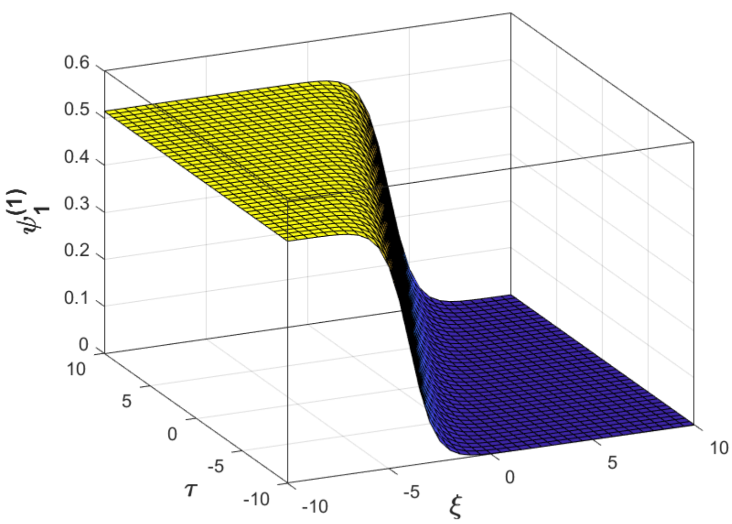

Figure 7.19: Single-front profile when the parameters are: $\alpha = 1.1, \mu_d = 0.5,\ \theta = 15^0, \eta = 0.5,\ U_1 = 0.4$.

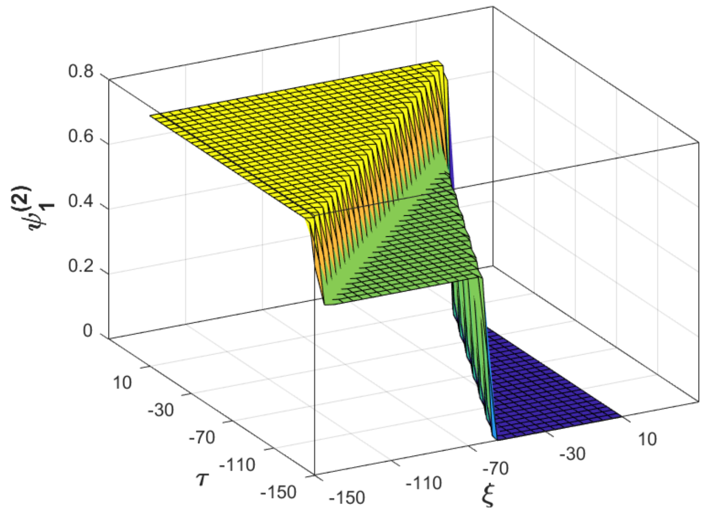

Figure 7.20: Two-front profile when the parameters are:
$\alpha = 1.1$, $\mu_d = 0.5$, $\theta = 15^0$, $\eta = 0.5$, $U_1 = 0.4$, $U_2 = 0.6$.

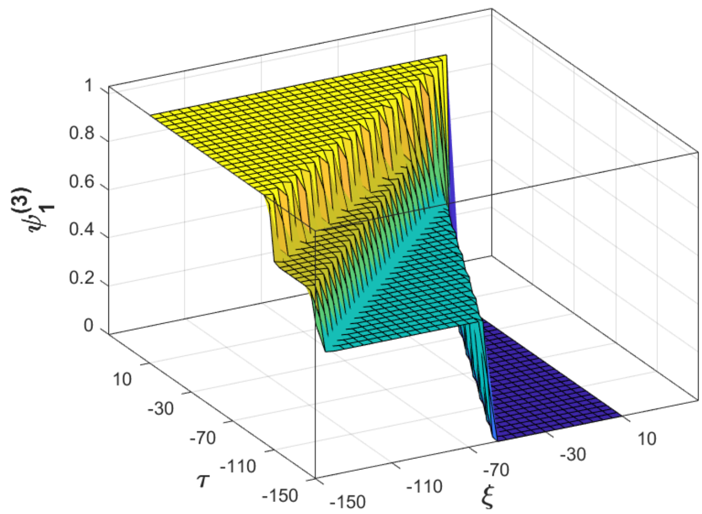

Figure 7.21: Three-front profile when the parameters are: $\alpha = 1.1$, $\mu_d = 0.5$, $\theta = 15^0$, $\eta = 0.5$, $U_1 = 0.4$, $U_2 = 0.4$, $U_3 = 0.6$.

Figures 7.22 -7.24 show how the single-, two-, and three-shock natures are affected by the dust concentration μ_d when $\alpha = 1.1$, $\mu_p = 0.4$, $\theta = 15^0$, $\eta = 0.5$, $U_1 = 0.4$, $U_2 = 0.6$, $U_3 = 0.8$, $\tau = 1$. Figure 7.22 demonstrates that the single-shock propagates with larger amplitudes when the value of μ_d increases. Similar findings for two-fronts and three-fronts are seen in Figures 7.23 and 7.24, respectively.

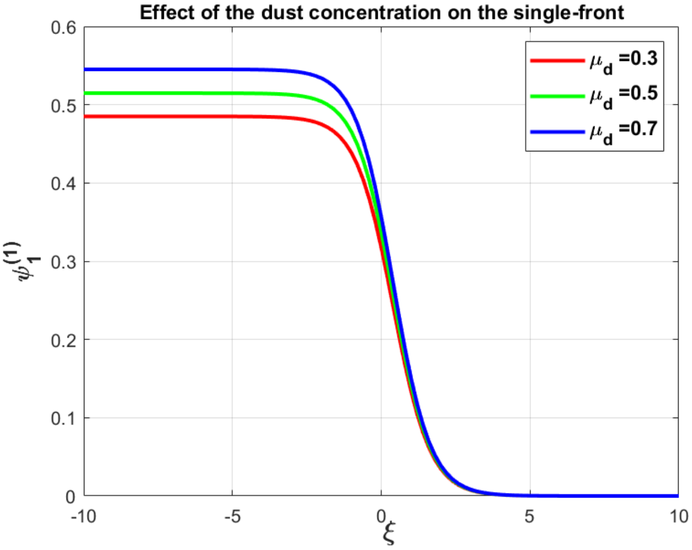

Figure 7.22: Single-front profiles for $\mu_d = 0.3, 0.5, 0.7$, when $\alpha = 1.1$, $\mu_p = 0.4$, $\theta = 15^0$, $\eta = 0.5$, $U_1 = 0.4$, $\tau = 1$.

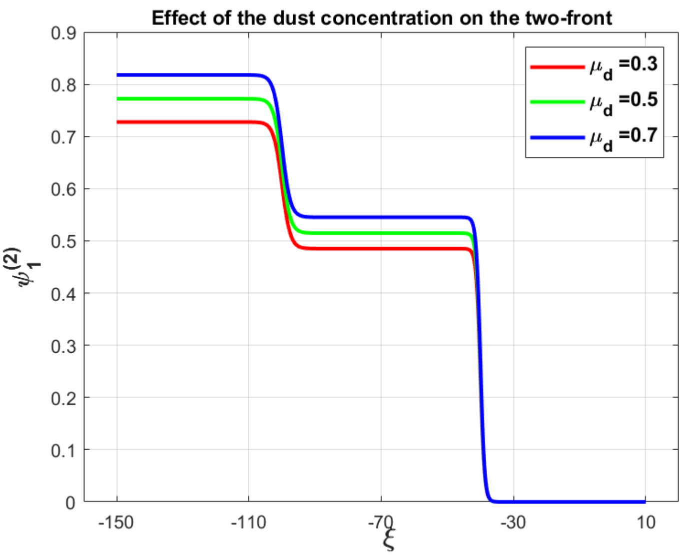

Figure 7.23: Two-front profiles for $\mu_d = 0.3, 0.5, 0.7$, when $\alpha = 1.1$, $\mu_p = 0.4$, $\theta = 15^0$, $\eta = 0.5$, $U_1 = 0.4$, $U_2 = 0.6$, $\tau = 1$.

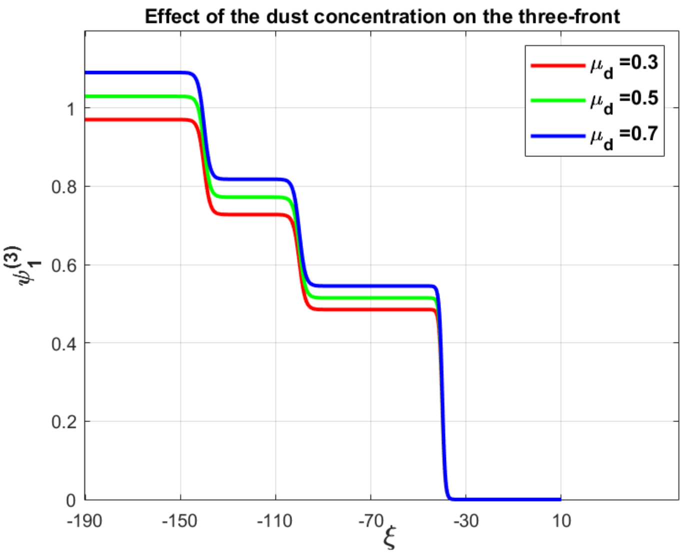

Figure 7.24: Three-front profile for $\mu_d = 0.3,\ 0.5,\ 0.7,$ when $\alpha = 1.1$, $\mu_p = 0.4,\ \theta = 15^0, \eta = 0.5, U_1 = 0.4, U_2 = 0.6,\ U_3 = 0.8, \tau = 1.$

7.6.3 Parametric effects on the phase speed

The relation (7.10) shows that the phase speed is the same for both types of waves, and it depends on temperature ratio α, propagation angle θ, positron concentration μ_p, etc. Both the decreasing impact of dust particles and the increasing impact of the temperature ratio on the phase speed are depicted in Figure 7.25.

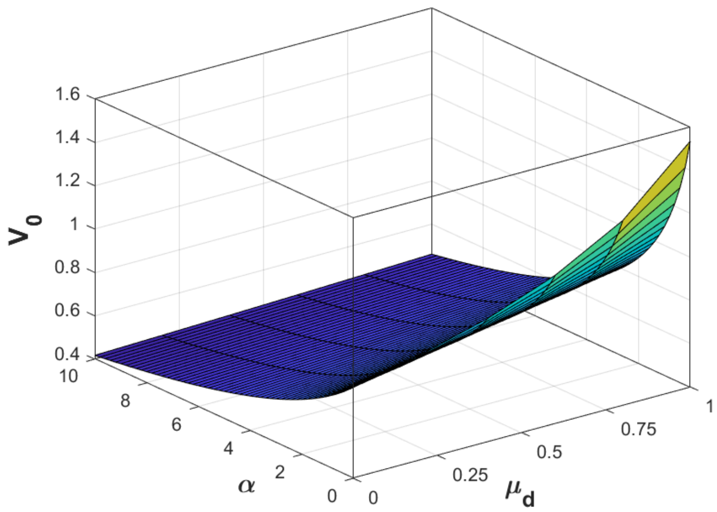

Figure 7.25: Phase speed vs. μ_d and α, when $\mu_p = 0.4, \theta = 15^0$.

7.7 Summary

Based on the results described in section 7.6 of this chapter, we see that the fundamental characteristics of multi-solitons and multi-shocks are significantly influenced by the plasma parameters, while the findings fully support the concept and results of the previous contributions on dusty plasma (Sultana et al., 2019-a; Hafez et al., 2020). The important findings are stated below:

i. *Effect of the magnetic field:* The field has a declining effect on the amplitudes and widths of the solitons, whereas the shock nature and phase speed are not influenced by it.

ii. *Effect of the dust particle density:* It has an increasing effect on the amplitudes and widths of both solitons and shocks.

iii. *Effect of the propagation angle:* It increases the amplitudes and widths of both types of waves.

iv. *Effect of the positron concentration:* The positron concentration decreases the soliton's amplitudes and widths.

Chapter Eight

Conclusion and future studies

8.1 Conclusion

In this thesis, we have described the characteristics of nonlinear waves propagated in dusty plasmas. Several theoretical investigations on the DIA solitary and shock waves, such as the effects of the magnetic field, higher-order nonlinear and dispersive (or dissipative) terms, plasma rotation, numerous plasma parameters, etc., have been discussed. In each investigation, the plasma systems are considered collisionless, three-dimensional, and magnetized. Besides, the reductive perturbation technique is used to illustrate the solitary and shock waves of small but finite amplitudes.

We have incorporated the higher-order nonlinear and dispersive effects on the DIA subsonic solitary waves in an electron-ion-PCD plasma. The KdV-type inhomogeneous equation is obtained by the extended use of the perturbation technique, and the dressed solution is determined by the re-normalization technique, while we observe the growing impacts of higher-order nonlinear and dispersive terms on the amplitude. Moreover, the PCD particles reduce the phase speed, and the solitary waves become subsonic.

We have also derived the inhomogeneous mKdV-type and modified Burgers-type equations to investigate the higher-order effects on the DIA solitary and shock waves, respectively, while the higher-order terms have been included to get a better result. The magnetic, adiabaticity, and other parametric effects on the wave nature are examined.

Then we have examined theoretically the combined effect of the magnetic field and oblique rotation, in which the investigation shows that the magnetic field, the Coriolis force due to small-rotation, and plasma parameters have substantial effects on the solitary waves propagated in rotating stars, the pulsar magnetosphere, and other rotating astronomical objects. It is observed that the wave structures become spiky in the presence of the magnetic field. Besides, the rotation decreases the amplitude and width but increases the phase speed.

In the end, the multi-soliton solutions to the KdV equation and the multi-shock solutions to the Burgers equation are obtained by the Cole-Holf transformation and the simplified Hirota method. Based on the results, it is seen that the magnetic field decreases the amplitudes and widths of multi-solitons, but the multi-shock nature is independent of it.

We expect that the findings of this thesis will be helpful to describe nonlinear waves (specifically, solitary and shock waves) of small amplitudes propagated in dusty plasmas.

8.2 Future studies

All of the theoretical investigations conducted in this thesis have been accomplished by the reductive perturbation method, and this method is valid for the waves of small amplitudes. To overcome this limitation, one should use the pseudopotential approach which is effective for the waves of arbitrary amplitudes.

We have inspected the higher-order nonlinear effect on DIA solitary and shock waves but haven't conducted any investigation on the double layer (a structure consisting of two parallel layers with opposite charges). As the study of double layers is also of recent interest for space and laboratory dusty plasmas, it may be another scope of upcoming research.

Besides, we have conducted our research only on the planar plasma systems. As the part of extensive investigation of the nonlinear DIA waves, the researcher can consider nonplanar (cylindrical and spherical) plasma systems instead of planar systems.

We have examined overtaking collisions of multi-solitons and multi-shocks. So, one can study the same plasma model assuming head-on collisions.

References

Abdelsalam, U. M. (2021). Dust ion acoustic waves for magnetized multi-component plasma. Ain Shams Engineering Journal, 12(4), 4111-4118.

Abdelwahed, H. G. (2015). Higher-order corrections to broadband electrostatic shock noise in auroral zone. Physics of Plasmas, 22(9), 092102.

Abdikian, A. and Eghbali, M. (2022). The role of trapped electrons and charge dust fluctuation on dust-ion-acoustic solitary waves. Indian Journal of Physics, 97(1), 1-9.

Abdus, S. M., Ali, A. M., and Zulfikar, A. M. (2022). Higher-order nonlinear and dispersive effects on dust-ion-acoustic solitary waves in magnetized dusty plasmas. Results in Physics, 32, 105114.

Ahmed, S. M., Hassib, E. R., Abdelsalam, U. M., Tolba, R. E., and Moslem, W. M. (2020). Ion-acoustic waves at the night side of Titan's ionosphere: Higher-order approximation. Communications in Theoretical Physics, 72(5), 055501.

Akter, J., and Mamun, A. A. (2022). Nucleus-Acoustic Solitary Waves in Warm Degenerate Magneto-Rotating Quantum Plasmas. Fluids, 7(9), 305.

Alimirzaluo, E., Nadjafikhah, M., and Manafian, J. (2021). Some new exact solutions of (3+1)-dimensional Burgers system via Lie symmetry analysis. Advances in Difference Equations, 2021(1), 1-17.

Alinejad, H. (2010). Dust ion-acoustic solitary and shock waves in a dusty plasma with non-thermal electrons. Astrophysics and Space Science, 327(1), 131-137.

Alsayyed, O., Jaradat, H. M., Jaradat, M. M. M., Mustafa, Z., Shatat, F. (2016). Multi-soliton solutions of the BBM equation arisen in shallow water. Journal of Nonlinear Science and Applications, 9, 1807-1814.

Anowar, M. G. M. and Mamun, A. A. (2008). Dust ion-acoustic solitary waves in a hot adiabatic magnetized dusty plasma. Physics Letters A, 372(37), 5896-5900.

Atteya, A., Sultana, S., and Schlickeiser, R. (2018). Dust-ion-acoustic solitary waves in magnetized plasmas with positive and negative ions: The role of electrons superthermality. Chinese Journal of Physics, 56(5), 1931-1939.

Bandyopadhyay, P., Prasad, G., Sen, A., and Kaw, P. K. (2008). Experimental study of nonlinear dust acoustic solitary waves in a dusty plasma. Physical review letters, 101(6), 065006.

Banerjee, S., and Saha, A. (2021). Dynamical systems and nonlinear waves in plasmas. CRC Press.

Bansal, S., Gill, T. S., and Aggarwal, M. (2021). Parametric study of cylindrical and spherical dust ion acoustic shock waves with two temperature electrons in dusty plasma relevant to Saturn's E ring. Contributions to Plasma Physics, 61(4), e202000154.

Banu, M. S., Sasikala, P., Dhanapal, A., Kavitha, V., Yazhini, G., and Rajamani, L. (2012). Cold plasma as a novel food processing technology. IJETED, 4(2), 803-818.

Barkan, A., D'angelo, N., and Merlino, R. L. (1996). Experiments on ion-acoustic waves in dusty plasmas. Planetary and Space Science, 44(3), 239-242.

Barkan, A., Merlino, R. L., and D'angelo, N. (1995). Laboratory observation of the dust-acoustic wave mode. Physics of Plasmas, 2(10), 3563-3565.

Bennett, M. J., Lebedev, S. V., Hall, G. N., Suttle, L., Burdiak, G., Suzuki-Vidal, F., ... and Ciardi, A. (2014). Rotating plasma disks in dense Z-pinch experiments. In AIP Conference Proceedings, American Institute of Physics, 1639(1), 71-75.

Biazar, J. and Ghazvini, H. (2009). Exact solutions for nonlinear Burgers' equation by homotopy perturbation method. Numerical Methods for Partial Differential Equations, 25(4), 833-842.

Bittencourt, J. A. (2004). Fundamentals of plasma physics. Springer Science and Business Media.

Bogdanov, E. A. and Kudryavtsev, A. A. (2001). The conditions for realization of the Boltzmann distribution of negative ions in a plasma. Technical Physics Letters, 27(11), 905-907.

Boro, B., Dev, A. N., Saikia, B. K., and Adhikary, N. C. (2020). Nonlinear dust ion acoustic shock wave structures in solar F corona region. Physics of Plasmas, 27(12), 122901.

Boro, B., Dev, A. N., Sarma, R., Saikia, B. K., and Adhikary, N. C. (2021). Dust–Ion–Acoustic Solitary Wave Structure in Magnetized Plasma with Nonthermally Distributed Electrons and Positrons. Plasma Physics Reports, 47(6), 557-567.

Boruah, A., Sharma, S. K., Nakamura, Y., and Bailung, H. (2016). Observation of dust acoustic multi-solitons in a strongly coupled dusty plasma. Physics of Plasmas, 23(9).

Cattell, C., Neiman, C., Dombeck, J., Crumley, J., Wygant, J., Kletzing, C. A., ... and André, M. (2003). Large amplitude solitary waves in and near the Earth’s magnetosphere, magnetopause and bow shock: Polar and Cluster observations. Nonlinear Processes in Geophysics, 10(1/2), 13-26.

Chamel, N. and Haensel, P. (2008). Physics of neutron star crusts. Living Reviews in Relativity, 11(1), 1-182.

Chan, C., Khazei, M., Lonngren, K. E., and Hershkowitz, N. (1981). Excitation of multiple ion-acoustic shocks. The Physics of Fluids, 24(8), 1452-1455.

Chandrasekhar, S. (1931). The maximum mass of ideal white dwarfs. The Astrophysical Journal, 74, 81.

Chandrasekhar, S. (1953). Problems of stability in hydrodynamics and hydromagnetics (George Darwin lecture). Monthly Notices of the Royal Astronomical Society, 113, 667.

Chen, J., Yu, J. P., Ma, W. X., Sun, Y. L., Khalique, and Chaudry, M. (2019). Interaction solutions of the first BKP equation. Modern Physics Letters B, 1950191.

Chen. F. F. (2015). Introduction to Plasma Physics and Controlled Fusion. Springer International Publishing. Third edition, Los Angeles, CA, USA.

Chow, V. W., Mendis, D. A., and Rosenberg, M. (1993). Role of grain size and particle velocity distribution in secondary electron emission in space plasmas. Journal of Geophysical Research: Space Physics, 98(A11), 19065-19076.

Das, G. C. and Nag, A. (2007). Salient features of solitary waves in dusty plasma under the influence of Coriolis force. Physics of Plasmas, 14(8), 083705.

Das, G. C., Sarma, J., Gao, Yi-Tian, Uberoi, C. (2000). Dynamical behavior of the soliton formation and propagation in magnetized plasma. Physics of Plasmas, 7(6), 2374

Dhiman, S. K., and Kumar, S. (2022). Different dynamics of invariant solutions to a generalized (3+ 1)-dimensional Camassa-Holm-Kadomtsev-Petviashvili equation arising in shallow water-waves. Journal of Ocean Engineering and Science. In press.

Drazin, P. G. and Johnson, R. S. (1989). Solitons: an introduction. Cambridge University Press, 2.

El-Helbawy, A. S. (2022). Bifurcation analysis for dust ion acoustic waves in magnetized four-component plasmas with superthermal electrons. Waves in Random and Complex Media, 1-17.

El-Labany, S. K., El-Taibany, W. F., El-Samahy, A. E., Hafez, A. M., and Atteya, A. (2014). Higher-order corrections to nonlinear dust-ion-acoustic shock waves in a degenerate dense space plasma. Astrophysics and Space Science, 354(2), 385-393.

El-Monier, S. Y. and Atteya, A. (2019). Higher order corrections and temperature effects to ion acoustic shock waves in quantum degenerate electron-ion plasma. Chinese Journal of Physics, 60, 695-708.

El-Monier, S. Y. and Atteya, A. (2022). Dynamics of ion-acoustic waves in nonrelativistic magnetized multi-ion quantum plasma: the role of trapped electrons. Waves in Random and Complex Media, 32(1), 299-317.

El-Taibany, W. F. and Moslem, W. M. (2005). Higher-order nonlinearity of electron-acoustic solitary waves with vortex-like electron distribution and electron beam. Physics of Plasmas, 12(3), 032307.

Ergun, R. E., Carlson, C. W., McFadden, J. P., Mozer, F. S., Delory, G. T., Peria, W., ... and Kistler, L. (1998). FAST satellite observations of large-amplitude solitary structures. Geophysical Research Letters, 25(12), 2041-2044.

Esfandyari-Kalejahi, A., Kourakis, I., and Shukla, P. K. (2008). Ion-acoustic waves in a plasma consisting of adiabatic warm ions, nonisothermal electrons, and a weakly relativistic electron beam: Linear and higher-order nonlinear effects. Physics of Plasmas, 15(2), 022303.

Farooq, M. and Ahmad, M. (2017). Dust ion acoustic waves in four component magnetized dusty plasma with effect of slow rotation and superthermal electrons. Physics of Plasmas, 24(12), 123707.

Fayad, A. A., Moslem, W. M., and El-Labany, S. K. (2021). Effect of streaming velocity, magnetic field, and higher-order correction on the nature of ion acoustic solitons in the Venusian ionosphere. Physica Scripta, 96(4), 045602.

Ferdousi, M., Sultana, S., and Mamun, A. A. (2015). Oblique propagation of ion-acoustic solitary waves in a magnetized electron-positron-ion plasma. Physics of Plasmas, 22(3), 032117.

Fortov, V. E., Petrov, O. F., Molotkov, V. I., Poustylnik, M. Y., Torchinsky, V. M., Naumkin, V. N., and Khrapak, A. G. (2005). Shock wave formation in a dc glow discharge dusty plasma. Physical Review E, 71(3), 036413.

Franklin, R. N. and Snell, J. (2000). The Boltzmann relation in electronegative plasmas: When is it permissible to use it? Journal of Plasma Physics, 64(2), 131-153.

Gardner, C. S. and Morikawa, G. K. (1965). The effect of temperature on the width of a small-amplitude, solitary wave in a collision-free plasma. Communications on Pure and Applied Mathematics, 18(1-2), 35-49.

Gharib, G. M. and Özer Ö. (2021). Exact solution for sawada–kotera equation using backland transformations and traveling wave solutions. Advances in Mathematics: Scientific Journal, 10 (2), 923–931.

Ghasemloo, M. (2022). Dust-ion acoustic shock wave in four-component magnetized dusty plasma. Journal of Nuclear Science and Technology, 99(2).

Gill, T. S., Bala, P., and Kaur, H. (2010). Higher-order nonlinear effects on wave structures in a multispecies plasma with nonisothermal electrons. Zeitschrift für Naturforschung A, 65(4), 315-328.

Goldman, M. V., Newman, D. L., and Ergun, R. E. (2003). Phase-space holes due to electron and ion beams accelerated by a current-driven potential ramp. Nonlinear Processes in Geophysics, 10(1/2), 37-44.

Gorshunov, N. M., Dubovitskii, V. V., Pashkovskii, V. G., and Potanin, E. P. (2017). Experimental study of magnetized plasma rotation in crossed fields. Plasma Physics Reports, 43, 533-541.

Griffiths, G. W. (2012). Hirota Direct Method. City University, London.

Hafez, M. G., Akter, P., and Karim, S. A. A. (2020). Overtaking collisions of ion acoustic N-shocks in a collisionless plasma with pair-ion and (α, q) distribution function for electrons. Applied Sciences, 10(17), 6115.

Haggard, P. W. (1988). On Legendre numbers of the second kind. International Journal of Mathematics and Mathematical Sciences, 11(4), 815-822.

Haider, M. M. and Nahar, A. (2017). Dust-Ion-Acoustic Solitary and Shock Structures in Multi-Ion Plasmas with Super-Thermal Electrons. Z. für Naturforschung A, 72(7),627-635.

Haider, M. M., Swarna, S. Y., Khan, N., and Rahman, O. (2020). A study of Chandrasekhar limits in adiabatic degenerate plasmas with superthermal ions. Plasma Research Express, 2(2), 025001.

Haider, M., Ferdous, T., and Duha, S. (2014). The effects of vortex like distributed electron in magnetized multi-ion dusty plasmas. Open Physics, 12(9), 701-706.

Halder, P., Bandyopadhyay, A., Dalui, S., and Sardar, S. (2022). Dust–ion acoustic solitary waves in a collisionless magnetized five components plasma. Zeitschrift für Naturforschung A, 77, 659-673.

Harvey, P., Durniak, C., Samsonov, D., and Morfill, G. (2010). Soliton interaction in a complex plasma. Physical Review E, 81(5), 057401.

Hereman, W. A. and Zhuang, W. (1992). Symbolic computation of solitons with Macsyma. Department of Mathematical and Computer Sciences, Colorado School of Mines, 287-296.

Hereman, W. and Zhuang, W. (1991). A MACSYMA program for the Hirota method. 13th World Congress on Computation and Applied Mathematics, 842–863. 1, 2.

Hirota, R. (2004). The direct method in soliton theory. 155, Cambridge University Press.

Horányi, M. (1996). Charged dust dynamics in the solar system. Annual review of astronomy and astrophysics, 34(1), 383-418.

Horányi, M., Morfill, G., and Grün, E. (1993). Mechanism for the acceleration and ejection of dust grains from Jupiter's magnetosphere. Nature, 363(6425), 144-146.

Hossen, M. A., Hossen, M. R., and Mamun, A. A. (2014). Study of the higher-order shock excitations in a degenerate quantum plasma. Journal of the Korean Physical Society, 65(11), 1883-1889.

Hussain, S., Ur-Rehman, H., and Mahmood, S. (2014). Obliquely propagating solitary wave structures in nonextensive magneto-rotating plasmas. Astrophysics and Space Science, 350(1), 185-190.

Ikezi, H. (1973). Experiments on ion-acoustic solitary waves. The Physics of Fluids, 16(10), 1668-1675.

Islam, K. A., Deeba, F., and Hassan, M. K. A. (2019). Dust ion acoustic solitary waves in multi-ion dusty plasma system with adiabatic thermal change. Australian Journal of Engineering and Innovative Technology, 1(5), 1-5.

Ismael, H. F. Seadawy, A. and Bulut, H. (2020). Multiple solitons, fusion, breather, lump, mixed kink-lump and periodic solutions to the extended shallow water wave model in (2+1)-dimensions. Modern Physics Letters B, 2150138.

Kamran, M., Sattar, F., Khan, M., Khan, R., and Ikram, M. (2021). Dust-ion-acoustic shock waves in the presence of dust charge fluctuation in non-Maxwellian plasmas with Kappa-distributed electrons. Results in Physics, 21, 103808.

Kanti Das, T., Saha, A., Pal, N., and Chatterjee, P. (2017). Effect of dust ion collisional frequency on transition of dust ion acoustic waves from quasiperiodic motion to limit cycle oscillation in a magnetized dusty plasma. Physics of Plasmas, 24(7), 073707.

Kaur, B. and Saini, N. S. (2018). Dust ion-acoustic shock waves in a multicomponent magnetorotating plasma. Zeitschrift für Naturforschung A, 73(3), 215-223.

Kaur, R., Singh, K., and Saini, N. S. (2021). Heavy-and light-nuclei acoustic dressed shock waves in white dwarfs. Chinese Journal of Physics, 72, 286-298.

Khalid, M., Khan, A., Khan, M., and Hadi, F. (2021). Dust ion acoustic solitary waves in unmagnetized plasma with Kaniadakis distributed electrons. Brazilian Journal of Physics, 51(1), 60-65.

Khan, M., Abbas, R., Huzaif, S. M., and Kamran, M. (2022). Effects of non-thermality and plasma parameters on dust-ion-acoustic shock waves. Contributions to Plasma Physics, e202200028.

Khater, M. M. (2022). Two-component plasma and electron trapping's influence on the potential of a solitary electrostatic wave with the dust-ion-acoustic speed. Journal of Ocean Engineering and Science, 2468-0133.

Kodama, Y. and Taniuti, T. (1978). Higher order approximation in the reductive perturbation method. I. The weakly dispersive system. Journal of the Physical Society of Japan, 45(1), 298-310.

Koester, D. and Chanmugam, G. (1990). Physics of white dwarf stars. Reports on Progress in Physics, 53(7), 837.

Kourakis, I. and Shukla, P. K. (2003). Modulational instability and localized excitations of dust-ion acoustic waves. Physics of Plasmas, 10(9), 3459-3470.

Kumar, S. and Mohan, B. (2021). A study of multi-soliton solutions, breather, lumps, and their interactions for kadomtsev-petviashvili equation with variable time coeffcient using hirota method. Physica Scripta, 96(12), 125255.

Kumar, S. and Mohan, B. (2022). A novel and efficient method for obtaining Hirota's bilinear form for the nonlinear evolution equation in (n+ 1) dimensions. Partial Differential Equations in Applied Mathematics, 5, 100274.

Kumar, S., Kumar, A., and Kharbanda, H. (2020). Lie symmetry analysis and generalized invariant solutions of (2+ 1)-dimensional dispersive long wave (DLW) equations. Physica Scripta, 95(6), 065207.

Lai, C. S. (1979). Effects of higher order contribution and of ion temperature on ion-acoustic solitary waves. Canadian Journal of Physics, 57(3), 490-495.

Lehnert, B. (1954). Magnetohydrodynamic Waves Under the Action of the Coriolis Force. The Astrophysical Journal, 119, 647.

Ling, L., Zhao, L. and Guo, B. (2015). Darboux transformation and multi-dark soliton for N-component nonlinear Schrödinger equations, Nonlinearity, 28(9).

Ma, W. X., Yong, X., and Zhang, H. Q. (2018). Diversity of interaction solutions to the (2+ 1)-dimensional Ito equation. Computers and Mathematics with App., 75(1), 289-295.

Ma, Y. R., Qi, X., Sun, J. A., Duan, W. S., and Yang, L. (2013). Effects of dust size distribution on dust negative ion acoustic solitary waves in a magnetized dusty plasma. Physics of Plasmas, 20(8), 083706.

Ma. W. X. (2019). The inverse scattering transform and soliton solutions of a combined modified Korteweg–de Vries equation. Journal of Mathematical Analysis and Applications, 471(1-2), p.796-811.

Mahmood, S., Mushtaq, A., and Saleem, H. (2003). Ion acoustic solitary wave in homogeneous magnetized electron-positron-ion plasmas. New Journal of Physics, 5(1), 28.

Mahmood, S., Ur-Rehman, H., Ali, M. Z., and Basit, A. (2021). Higher-order inertial Alfvén wave dressed solitons, quasiperiodic structures, and chaos in plasmas. Contributions to Plasma Physics, 61(6), e202000211.

Mamun, A. A. (1998). Solitary waves in a three-component dusty plasma with trapped ions. Physica Scripta, 57(2), 258.

Mamun, A. A. (2021). Roles of positively charged dust in the formation of ion-acoustic subsonic solitary waves in electron-ion-positively charged dust plasmas. Contributions to Plasma Physics, 61(7), e202000192.

Mamun, A. A. and Mannan, A. (2021). Solitary waves and double layers in complex plasma media. Waves in Random and Complex Media, 1-12.

Mamun, A. A. and Shukla, P. K. (2009-a). Cylindrical and spherical dust ion-acoustic shock waves in dusty plasmas. EPL (Euro physics Letters), 87(2), 25001.

Mamun, A. A. and Shukla, P. K. (2009-b). Effects of nonthermal distribution of electrons and polarity of net dust-charge number density on nonplanar dust-ion-acoustic solitary waves. Physical Review E, 80(3), 037401.

Mamun, A. A., Jahan, N., and Shukla, P. K. (2009). DIA and DA solitary waves in adiabatic dusty plasmas. Journal of plasma physics, 75(3), 413-431.

Medici, E. F. and Waite, G. P. (2016). Experimental laboratory study on the formation of multiple shock waves observed during volcanic eruptions. Geophysical Research Letters, 43(1), 85-92.

Mehdipoor, M. and Asri, M. (2021). Solitary and periodic waves in magneto–rotating plasmas: effect of the Kappa–Cairns distributed electrons. Advances in Space Research, 67(8), 2470-2482.

Mehdipoor, M. and Esfandyari-Kalejahi, A. (2012). Higher-order corrections to ion acoustic waves in degenerate electron-positron-ion plasmas. Astrophysics and Space Science, 342(1), 93-104.

Mendis, D. A., Wong, W. H., and Rosenberg, M. (2004). On the observation of charged dust in the tropical mesosphere. Physica Scripta, 2004(T113), 141.

Mushtaq, A. (2010). Ion acoustic solitary waves in magneto-rotating plasmas. Journal of Physics A: Mathematical and Theoretical, 43(31), 315501.

Mushtaq, A. and Shah H. A. (2005). Nonlinear Zakharov-Kuznetsov equation for obliquely propagating two-dimensional ion-acoustic solitary waves in a relativistic, rotating magnetized electron-positron-ion plasma. Physics of Plasmas, 12(7), 072306.

Nakamura, Y. (2002). Experiments on ion-acoustic shock waves in a dusty plasma. Physics of Plasmas, 9(2), 440-445.

Nakamura, Y., Bailung, H., and Shukla, P. K. (1999). Observation of ion-acoustic shocks in a dusty plasma. Physical review letters, 83(8), 1602.

Nobahar, D. and Pakzad, H. R. (2019). Obliquely propagating dust-ion acoustic solitary waves in magnetized plasmas with superthermal electrons. Iranian Journal of Astronomy and Astrophysics, 6(2), 95-106.

Pakzad, H. R. and Javidan, K. (2022). Dust-ion acoustic waves in magnetized plasmas with a varying external magnetic field. Waves in Random and Complex Media, 1-9.

Paul, I., Chatterjee, A., and Paul, S. N. (2021). Dressed solitons and double layers of ion-acoustic waves in a dusty plasma having ultra-relativistic degenerate two-temperature electrons. Indian Journal of Physics, 1-15.

Pieper, J. B. and Goree, J. (1996). Dispersion of plasma dust acoustic waves in the strong-coupling regime. Physical review letters, 77(15), 3137.

Rahman O. and Haider M. (2016). Modified Korteweg-de Vries (mK-dV) Equation Describing Dust-ion-acoustic Solitary Waves in an Unmagnetized Dusty Plasma with Trapped Negative Ions. Advances in Astrophysics, 3(1): p.161-172.

Rahman, O. and Haider, M. M. (2019). Dust-ion-acoustic solitary waves and their instability in a magnetized adiabatic dusty electronegative plasma. Theoretical Physics, 4(2), 47-115.

Rajib, T. I., Sultana, S., and Mamun, A. A. (2015). Solitary waves in rotational pulsar magnetosphere. Astrophysics and Space Science, 357(1), 1-6.

Rao, N. N., Shukla, P. K., and Yu, M. Y. (1990). Dust-acoustic waves in dusty plasmas. Planetary and Space Science, 38(4), 543-546.

Reed, E. J., Fried, L. E., and Joannopoulos, J. D. (2003). A method for tractable dynamical studies of single and double shock compression. Physical review letters, 90(23), 235503.

Ren, B., Ma W. X., and Yu, J. (2019). Rational solutions and their interaction solutions of the (2+1)-dimensional modified dispersive water wave equation. Computers and Mathematics with Applications, 77, 2086–2095. 2087

Revans, R. W. (1933). The transmission of waves through an ionized gas. Physical Review, 44(10), 798.

Richard, F. (2008). Introduction to plasma physics: A graduate level course. University of Texas at Austin.

Rosenberg, M. and Mendis, D. A. (1995). UV-induced Coulomb crystallization in a dusty gas. IEEE Transactions on Plasma Science, 23(2), 177-179.

Rosenberg, M., Mendis, D. A., and Sheehan, D. P. (1996). UV-induced Coulomb crystallization of dust grains in high-pressure gas. IEEE transactions on plasma science, 24(6), 1422-1430.

Rosenberg, M., Thomas, E., and Merlino, R. L. (2008). A note on dust wave excitation in a plasma with warm dust: Comparison with experiment. Physics of Plasmas, 15(7), 073701.

Sahu, B., Sinha, A., and Roychoudhury, R. (2019). Ion-acoustic waves in dense magneto-rotating quantum plasma. Physics of Plasmas, 26(7), 072119.

Saini, N. S., Kaur, B., and Gill, T. S. (2016). Obliquely propagating dust ion-acoustic solitary waves and double layers in multicomponent plasmas. Physics of Plasmas, 23(12), 123705.

Saini, N. S., Kaur, M., and Singh, K. (2022). Heavy nucleus acoustic periodic waves in a degenerate relativistic magneto-rotating quantum plasma. Waves in Random and Complex Media, 32(2), 743-754.

Salam, M. A., Akbar, M. A., Ali, M. Z., and Haider, M. M. (2021). The magnetorotating and parametric effects on the dust-ion-acoustic solitary waves in a dusty plasma with trapped negative ions. Results in Physics, 26, 104376.

Samanta, U. K., Saha, A., and Chatterjee, P. (2013). Bifurcations of nonlinear ion acoustic traveling waves in the frame of a Zakharov-Kuznetsov equation in magnetized plasma with a kappa distributed electron. Physics of Plasmas, 20(5), 052111.

Sarma, A. and Nakamura, Y. (2009). Ion-acoustic shock waves with negative ions in presence of dust particulates. Physics Letters A, 373(45), 4174-4177.

Schamel, H. (1972). Stationary solitary, snoidal and sinusoidal ion acoustic waves. Plasma Physics, 14(10), 905.

Schamel, H. (1975). Analytic BGK modes and their modulational instability. Journal of Plasma Physics, 13(1), 139-145.

Schippers, P., Blanc, M., André, N., Dandouras, I., Lewis, G. R., Gilbert, L. K., ... and Dougherty, M. K. (2008). Multi-instrument analysis of electron populations in Saturn's magnetosphere. Journal of Geophysical Research: Space Physics, 113(A7).

Selim, M. M., Abdelaleem, H., El-Bedwehy, N. A., and El-Shamy, E. F. (2022-a). Dust-acoustic solitary and periodic waves in a plasma with ion distribution with trapped particles. Radiation Effects and Defects in Solids, 1-16.

Selim, M. M., Abdelaleem, H., El-Bedwehy, N. A., and El-Shamy, E. F. (2022-b). Effects of trapped ions concentration on the dynamics of dust-acoustic periodic traveling waves in dusty plasmas. Contributions to Plasma Physics, 62(3), e202100153.

Shomen A. and Pramanik, S. (2021). Non-linear coherent structures in multi-species dusty plasma. Contributions to Plasma Physics. e202100025

Shuai, S. and Kasbaoui, M. (2022). Accelerated decay of a Lamb-Oseen vortex tube laden with inertial particles in Eulerian-Lagrangian simulations. Journal of Fluid Mechanics, 936.

Shukla, P. K. and Mamun, A. A. (2002). Introduction to dusty plasma physics. Institute of Physics Publishing, Bristol.

Shukla, P. K. and Silin, V. P. (1992). Dust ion-acoustic wave. Physica Scripta, 45(5), 508.

Singh, K., Kakad, A., Kakad, B., and Saini, N. S. (2021). Evolution of ion acoustic solitary waves in pulsar wind. Monthly Notices of the Royal Ast. Society, 500(2), 1612-1620.

Singh, K., Sethi, P., and Saini, N. S. (2019). Nonlinear excitations in a degenerate relativistic magneto-rotating quantum plasma. Physics of Plasmas, 26(9), 092104.

Sultana S., Mannan A., Schlickeiser, R. (2019-a). Obliquely propagating electron-acoustic solitary waves in magnetized plasmas: the role of trapped superthermal electrons. European Physical Journal D, 73 (10) 220.

Sultana, S. (2021). Shock waves in magnetized plasmas with superthermal trapped electrons. Chinese Journal of Physics, 69, 206-218.

Sultana, S., Islam, S., Mamun, A. A., and Schlickeiser, R. (2019-b). Oblique propagation of ion-acoustic solitary waves in a magnetized plasma with electrons following a generalized distribution function. Physics of Plasmas, 26(1): p.012107.

Sumi, R. A., Tasnim, I., Anowar, M. G. M., and Mamun, A. A. (2019). Dust-acoustic shock waves in a plasma system with opposite polarity dust fluids and trapped ions. Journal of Plasma Physics, 85(6).

Tang, P., Luo, M., Zhao, T., and Mao, Y. (2021). Generation of noise-like pulses and soliton rains in a graphene mode-locked erbium-doped fiber ring laser. Frontiers of Information Technology and Electronic Engineering, 22(3), 303-311.

Taniuti, T. and Wei, C. C. (1968). Reductive perturbation method in nonlinear wave propagation. I. Journal of the Physical Society of Japan, 24(4), 941-946.

Tonks, L. and Langmuir, I. (1929). Oscillations in ionized gases. Physical Review, 33, 195-210.

Tsintikidis, D., Gurnett, D. A., Kurth, W. S., and Granroth, L. J. (1996). Micron-sized particles detected in the vicinity of Jupiter by the Voyager plasma wave instruments. Geophysical research letters, 23(9), 997-1000.

Ullah, G., Saleem, M., Khan, M., Khalid, M., Rahman, A. U., and Nabi, S. (2020-a). Ion acoustic solitary waves in magnetized electron–positron–ion plasmas with Tsallis distributed electrons. Contributions to Plasma Physics, 60(10), e202000068.

Ullah, M.S., Roshid, H. O., and Ali, M. Z. (2020-b). Dynamical structures of multi-soliton solutions to the Bogoyavlenskii's breaking soliton equations. The European Physical Journal Plus, 135, 3, 1-10.

Wang, D. S., and Wang, X. (2018). Long-time asymptotics and the bright N-soliton solutions of the Kundu–Eckhaus equation via the Riemann–Hilbert approach. Nonlinear Analysis: Real World Applications, 41, 334-361.

Wang, D. S., Guo, B., and Wang, X. (2019). Long-time asymptotics of the focusing Kundu–Eckhaus equation with nonzero boundary conditions. Journal of Differential Equations, 266(9), 5209-5253.

Wang, H., Du, J., and Guo, R. (2022). Small amplitude ion-acoustic solitary waves in a four-component magneto-rotating plasma with a modified Cairns-Tsallis distribution. Physica Scripta, 98(1), 015204.

Wang, M. L. and Wang, Y. M. (2001). A new Bucklund transformation and multi-soliton solutions to the KdV eq. with general variable coefficients, Physics Letter A, 287,211–216.

Watanabe, S. (1978). Interpretation of experiments on ion acoustic soliton. Journal of the Physical Society of Japan, 44(2), 611-617.

Wazwaz, A. M. (2010). Partial differential equations and solitary waves theory. Springer Science and Business Media.

Wazwaz, A. M. (2016). The simplified Hirota's method for studying three extended higher-order KdV-type equations, Journal of Ocean Engineering and Science, 1(7), 181-185.

Wazwaz, A. M. (2021-a). New (7+ 1)-dimensional Painlevé integrable fifth-order equation with third-order temporal dispersion. Nonlinear Dynamics, 106(1), 891-897.

Wazwaz, A. M. (2021-b). New integrable (2+ 1)-and (7+ 1)-dimensional shallow water wave equations: multiple soliton solutions and lump solutions. International Journal of Numerical Methods for Heat and Fluid Flow, 32(1), 138-149.

Wiesemann, K. (2014). A short introduction to plasma physics. https://doi.org/10.48550/ arXive.1404.0509.

www.khanacademy.org/science/physics/thermodynamics/temp-kinetic-theory-ideal-gas-law/a/ what-is-the-maxwell-boltzmann-distribution.

Yasmin, S., Asaduzzaman, M., and Mamun, A. A. (2013). Dust ion-acoustic shock waves in nonextensive dusty plasma. Astrophysics and Space Science, 343(1), 245-250.

Younsi, S., Kerrouchi, S., Amour, R., and Zerguini, T. H. (2022). Oblique Propagation of Low-Frequency Solitary Waves in a Magnetized Polarized Complex Plasma with Adiabatically Trapped Nonthermal Ions. IEEE Transactions on Plasma Science, 50(8), 2439-2447.

Yuan L. and Shou F. T. (2022). Inverse scattering transform and soliton solutions of an intgrable nonlocal Hirota equation. Communications on Pure and Applied Analysis, 21(1), 293- 313.

Zaghbeer, S. K. (2022). Instability of opposite polarity charged dusty plasma with vortex-like distributed electrons. Journal of Taibah University for Science, 16(1), 351-361.

Zhang, Y., Liu, Y. P., and Tang, X. Y. (2018). M-lump solutions to a (7+1)-dimensional nonlinear evolution equation. Computers and Mathematics with App., 76(3), 592-601.

Appendix

A.1 The coefficients $\delta_i (i = 3, 4, 5, 6)$ in equation (3.50)

$$\delta_3 = \frac{V_0}{2}\left(\frac{1}{2} - \frac{3\mu_e}{2} - \frac{\delta_1^2}{V_0^2} - \frac{\delta_1}{V_0} - 3\mu_e^2 + \frac{4\,\mu_e\delta_1}{V_0}\right),$$

$$\delta_4 = \frac{V_0}{2}\left[1 - \frac{3V_0\delta_1}{l_z^2} + \frac{2\,\mu_e\delta_2}{V_0} - \frac{3\delta_1\delta_2}{V_0^2} - \frac{3V_0\delta_1(1-l_z^2)}{l_z^2\omega_{ci}^2} + \frac{V_0^2\mu_e(1-l_z^2)}{l_z^2\omega_{ci}^2}\right],$$

$$\delta_5 = \frac{V_0}{2}\left[1 - \frac{V_0\delta_1}{l_z^2} + \frac{3\,\mu_e\delta_2}{V_0} - \frac{2\delta_1\delta_2}{V_0^2} + \frac{V_0\mu_e\delta_2}{l_z^2} - \frac{\delta_1(1-l_z^2)}{l_z^2\omega_{ci}^2}\right],$$

$$\delta_6 = -\frac{V_0}{2}\left[\frac{V_0\delta_2}{l_z^2} + \frac{\mu_e\delta_2^2}{l_z^2} + \frac{\delta_2 V_0(1-l_z^2)}{l_z^2\omega_{ci}^2} - \frac{V_0^4(1-l_z^2)}{l_z^2\omega_{ci}^4}\right].$$

A.2 The solution of equation (3.56)

The equation (3.56) can be written as

$$\frac{d^2\psi^{(1)}}{d\eta^2} = \frac{\lambda}{\delta_2}\psi^{(1)} - \frac{\delta_1}{2\delta_2}\left[\psi^{(1)}\right]^2. \tag{A.1}$$

Multiplying (A.1) by $\frac{d\psi^{(1)}}{d\eta}$ and integrating the result under the boundary condition $\psi^{(1)} \to 0, \frac{d\psi^{(1)}}{d\eta} \to 0$ at $|\eta| \to \infty$, we obtain

$$\left(\frac{d\psi^{(1)}}{d\eta}\right)^2 = \frac{\lambda}{\delta_2}\left[\psi^{(1)}\right]^2 - \frac{\delta_1}{3\delta_2}\left[\psi^{(1)}\right]^3.$$

$$\Rightarrow \frac{d\psi^{(1)}}{d\eta} = \sqrt{\frac{\lambda}{\delta_2}}\;\psi^{(1)}\sqrt{1 - \frac{\delta_1}{3\lambda}\psi^{(1)}}. \tag{A.2}$$

The transformation $Y = \sqrt{1 - \frac{\delta_1}{3\lambda}\psi^{(1)}}$ reduces (A.2) to

$$\frac{dY}{1-Y^2} = -\frac{1}{2}\sqrt{\frac{\lambda}{\delta_2}}\;d\eta. \tag{A.3}$$

The integration of (A.3) yields

$$\frac{1-Y}{1+Y} = e^{\sqrt{\frac{\lambda}{\delta_2}}\eta}$$

$$\Rightarrow Y = \frac{1-e^{\sqrt{(\lambda/\delta_2)}\,\eta}}{1+e^{\sqrt{(\lambda/\delta_2)}\,\eta}},$$

$$\Rightarrow 1 - \frac{\delta_1}{3\lambda}\psi^{(1)} = \frac{\left(1-e^{\sqrt{(\lambda/\delta_2)}\,\eta}\right)^2}{\left(1+e^{\sqrt{(\lambda/\delta_2)}\,\eta}\right)^2}.$$

$$\Rightarrow \psi^{(1)} = \frac{3\lambda}{\delta_1}\left[1 - \frac{\left(1-e^{\sqrt{(\lambda/\delta_2)}\,\eta}\right)^2}{\left(1+e^{\sqrt{(\lambda/\delta_2)}\,\eta}\right)^2}\right].$$

$$\Rightarrow \psi^{(1)} = \frac{3\lambda}{\delta_1}\left[\frac{4\,e^{\sqrt{(\lambda/\delta_2)}\,\eta}}{\left(1+e^{\sqrt{(\lambda/\delta_2)}\,\eta}\right)^2}\right].$$

$$\Rightarrow \psi^{(1)} = \frac{3\lambda}{\delta_1}\left[\frac{2}{e^{-\sqrt{(\lambda/4\delta_2)}\,\eta}+e^{\sqrt{(\lambda/4\delta_2)}\,\eta}}\right]^2.$$

$$\Rightarrow \psi^{(1)} = \frac{3\lambda}{\delta_1}\mathrm{sech}^2\left[\sqrt{(\lambda/4\delta_2)}\,\eta\right]. \tag{A.4}$$

A.3 The coefficients M_i(i =1, 2, 3, 4, 5) in equation (4.41)

$$M_1 = \frac{1}{2G_1}\Big[V_0(\mu_n\alpha^2+\mu_e) - \frac{V_0G_1^2}{l_x}\left(\frac{2+\gamma\sigma_iG_1}{1+\gamma\sigma_iG_1}\right) + \frac{\sigma_i l_x^2}{V_0}[\gamma G_1^2(1-\gamma) - \gamma(\mu_n\alpha^2+$$

$$\mu_e)] - \frac{G_1\delta_1^2}{V_0}(3+4\gamma\sigma_iG_1)\Big],$$

$$M_2 = -\frac{\delta_1}{8G_1}\left[\frac{(1+\gamma\sigma_iG_1)(1-2\gamma\sigma_iG_1)(1-l_x^2)}{4\omega_{ci}^2} - \frac{G_1\delta_2}{V_0} - \frac{1+2\gamma\sigma_iG_1}{1+\gamma\sigma_iG_1}\right],$$

$$M_3 = \frac{\delta_1}{2G_1}\left[\frac{(1+\gamma\sigma_iG_1)(1-2\gamma\sigma_iG_1)(1-l_x^2)}{\omega_{ci}^2} - \frac{2\gamma\sigma_iG_1\delta_2(2+\gamma\sigma_iG_1)}{V_0} - \frac{1+2\gamma\sigma_iG_1}{1+\gamma\sigma_iG_1}\right],$$

$$M_4 = \frac{3\delta_1}{4G_1}\left[\frac{(1+\gamma\sigma_iG_1)(1-2\gamma\sigma_iG_1)(1-l_x^2)}{\omega_{ci}^2} - \frac{G_1\delta_2}{V_0} - \frac{1+2\gamma\sigma_iG_1}{1+\gamma\sigma_iG_1}\right],$$

$$M_5 = \frac{1}{2G_1}\left[\frac{[\gamma\sigma_iV_0-\delta_2(1+\gamma\sigma_iG_1)](1-l_x^2)}{\omega_{ci}^2} + \frac{V_0^3(1+\gamma\sigma_iG_1)(1-l_x^2)}{\omega_{ci}^4} - \frac{G_1\delta_2^2}{V_0} - \delta_2\left(\frac{1+2\gamma\sigma_iG_1}{1+\gamma\sigma_iG_1}\right)\right].$$

A.4 Derivation of the modified Burgers-type equation (5.25)

From equations (5.15), (5.16), and (5.17), we have (putting the values of $p_i^{(1)}$)

$$u_{iz}^{(2)} = \frac{l_y(1+\gamma\sigma_i\mu_e)}{\omega_{ci}}\frac{\partial\psi^{(1)}}{\partial\xi}, \tag{A.5}$$

$$u_{iy}^{(2)} = -\frac{l_z(1+\gamma\sigma_i\mu_e)}{\omega_{ci}}\frac{\partial\psi^{(1)}}{\partial\xi}, \tag{A.6}$$

$$n_i^{(2)} = \mu_e\psi^{(2)} - \frac{4}{3}\frac{\mu_e\,(1-\beta_e)}{\sqrt{\pi}}\left[\psi^{(1)}\right]^{\frac{3}{2}}. \tag{A.7}$$

Differentiating (A.3) w.r.to ξ and τ, and using (5.31), we get

$$\frac{\partial n_i^{(2)}}{\partial\xi} = \mu_e\frac{\partial\psi^{(2)}}{\partial\xi} - \frac{2\,\mu_e\,(1-\beta_e)}{\sqrt{\pi}}\left[\psi^{(1)}\right]^{\frac{1}{2}}\frac{\partial\psi^{(1)}}{\partial\xi}, \tag{A.8}$$

$$\frac{\partial n_i^{(2)}}{\partial\tau} = \mu_e\frac{\partial\psi^{(2)}}{\partial\tau} - \frac{2B\,\mu_e\,(1-\beta_e)}{\sqrt{\pi}}\left[\psi^{(1)}\right]^{\frac{1}{2}}\frac{\partial^2\psi^{(1)}}{\partial\xi^2} + \frac{2A\,\mu_e\,(1-\beta_e)}{\sqrt{\pi}}\psi^{(1)}\frac{\partial\psi^{(1)}}{\partial\xi}. \tag{A.9}$$

Using $n_i^{(1)}$, $u_{iy}^{(2)}$, $u_{iz}^{(2)}$, $\frac{\partial n_i^{(2)}}{\partial\xi}$, and (5.21) in (5.18), we get

$$u_{ix}^{(2)} = \frac{(1+\gamma\sigma_i\mu_e)l_x}{V_0}\psi^{(2)} - \frac{2}{3}\frac{A\mu_e}{l_x}(1+2\gamma\sigma_i\mu_e)\left[\psi^{(1)}\right]^{\frac{3}{2}} - \frac{\eta\mu_e}{2l_x}\frac{\partial\psi^{(1)}}{\partial\xi}, \tag{A.10}$$

$$\frac{\partial^2 u_{ix}^{(2)}}{\partial\xi^2} = \frac{(1+\gamma\sigma_i\mu_e)l_x}{V_0}\frac{\partial^2\psi^{(2)}}{\partial\xi^2} - \frac{1}{2}\frac{A\mu_e}{l_x}(1+2\gamma\sigma_i\mu_e)\frac{\left(\frac{\partial\psi^{(1)}}{\partial\xi}\right)^2}{\sqrt{\psi^{(1)}}} - \frac{A\mu_e}{l_x}(1+$$

$$2\gamma\sigma_i\mu_e)\sqrt{\psi^{(1)}}\frac{\partial^2\psi^{(1)}}{\partial\xi^2} - \frac{1}{2}\frac{\eta\mu_e}{l_x}\frac{\partial^3\psi^{(1)}}{\partial\xi^3}, \tag{A.11}$$

$$\frac{\partial u_{ix}^{(2)}}{\partial\tau} = \frac{(1+\gamma\sigma_i\mu_e)l_x}{V_0}\frac{\partial\psi^{(2)}}{\partial\tau} + \left[\frac{A\eta\mu_e}{2l_x} - \frac{AB\mu_e(1+2\gamma\sigma_i\mu_e)}{l_x}\right]\left[\psi^{(1)}\right]^{\frac{1}{2}}\frac{\partial^2\psi^{(1)}}{\partial\xi^2} +$$

$$\frac{A^2\mu_e(1+2\gamma\sigma_i\mu_e)}{l_x}\psi^{(1)}\frac{\partial\psi^{(1)}}{\partial\xi} + \frac{1}{4}\frac{A\eta\mu_e}{l_x}\frac{\left(\frac{\partial\psi^{(1)}}{\partial\xi}\right)^2}{\left[\psi^{(1)}\right]^{\frac{1}{2}}} - \frac{1}{2}\frac{B\eta\mu_e}{l_x}\frac{\partial^3\psi^{(1)}}{\partial\xi^3}. \tag{A.12}$$

Using the values of $p_i^{(1)}$, $u_{iy}^{(2)}$, $u_{iz}^{(2)}$, and $\frac{\partial u_{ix}^{(2)}}{\partial\xi}$ in (5.20), and integrating, we get

$$p_i^{(2)} = \gamma\mu_e\psi^{(2)} - \frac{4}{3}\frac{\gamma\mu_e\,(1-\beta_e)}{\sqrt{\pi}}\left[\psi^{(1)}\right]^{\frac{3}{2}} = \gamma\, n_i^{(2)},\ \ \frac{\partial p_i^{(2)}}{\partial\tau} = \gamma\frac{\partial n_i^{(2)}}{\partial\tau}. \tag{A.13}$$

Equating the coefficients of $\epsilon^{5/2}$ from (5.7), the x-component of (5.8), and (5.9), we get

$$l_x n_i^{(1)}\frac{\partial u_{ix}^{(1)}}{\partial\xi} + l_z\frac{\partial u_{iz}^{(4)}}{\partial\xi} + l_y\frac{\partial u_{iy}^{(4)}}{\partial\xi} + l_x\frac{\partial u_{ix}^{(3)}}{\partial\xi} - V_0\frac{\partial n_i^{(3)}}{\partial\xi} + \frac{\partial n_i^{(2)}}{\partial\tau} + l_x u_{ix}^{(1)}\frac{\partial n_i^{(1)}}{\partial\xi} = 0, \tag{A.14}$$

$$-V_0 n_i^{(1)}\frac{\partial u_{ix}^{(1)}}{\partial\xi} - \eta\frac{\partial^2 u_{ix}^{(2)}}{\partial\xi^2} + n_i^{(1)} l_x\frac{\partial\psi^{(1)}}{\partial\xi} - V_0\frac{\partial u_{ix}^{(3)}}{\partial\xi} + l_x\frac{\partial\psi^{(3)}}{\partial\xi} + \frac{\partial u_{ix}^{(2)}}{\partial\tau} + l_x u_{ix}^{(1)}\frac{\partial u_{ix}^{(1)}}{\partial\xi} +$$
$$l_x\sigma_i\frac{\partial p_i^{(3)}}{\partial\xi} = 0, \tag{A.15}$$

$$\gamma l_x\frac{\partial u_{ix}^{(3)}}{\partial\xi} + \gamma l_x p_i^{(1)}\frac{\partial u_{ix}^{(1)}}{\partial\xi} + \gamma l_z\frac{\partial u_{iz}^{(4)}}{\partial\xi} + \gamma l_y\frac{\partial u_{iy}^{(4)}}{\partial\xi} - V_0\frac{\partial p_i^{(3)}}{\partial\xi} + \frac{\partial p_i^{(2)}}{\partial\tau} + l_x u_{ix}^{(1)}\frac{\partial p_i^{(1)}}{\partial\xi} = 0. \tag{A.16}$$

Equating the coefficients of ϵ^2 from the y and z-components of (5.8), and (5.10), we get

$$-\omega_{ci}u_{iz}^{(4)} + l_y\frac{\partial\psi^{(2)}}{\partial\xi} - V_0\frac{\partial u_{iy}^{(2)}}{\partial\xi} + l_y\sigma_i\frac{\partial p_i^{(2)}}{\partial\xi} = 0, \tag{A.17}$$

$$\omega_{ci}u_{iy}^{(4)} + l_z\frac{\partial\psi^{(2)}}{\partial\xi} - V_0\frac{\partial u_{iz}^{(2)}}{\partial\xi} + l_z\sigma_i\frac{\partial p_i^{(2)}}{\partial\xi} = 0, \tag{A.18}$$

$$\frac{\partial^2\psi^{(1)}}{\partial\xi^2} - \mu_e\psi^{(3)} + n_i^{(3)} - \frac{1}{2}\mu_e\left[\psi^{(1)}\right]^2 + \frac{2\mu_e(1-\beta_e)}{\sqrt{\pi}}\left[\psi^{(1)}\right]^{\frac{1}{2}}\psi^{(2)} = 0. \tag{A.19}$$

From (A.19), we get

$$n_i^{(3)} = \mu_e\psi^{(3)} - \frac{2\mu_e(1-\beta_e)}{\sqrt{\pi}}\sqrt{\psi^{(1)}}\,\psi^{(2)} + \frac{1}{2}\mu_e\left[\psi^{(1)}\right]^2 - \frac{\partial^2\psi^{(1)}}{\partial\xi^2}, \tag{A.20}$$

$$\frac{\partial n_i^{(3)}}{\partial\xi} = \mu_e\frac{\partial\psi^{(3)}}{\partial\xi} - \frac{\mu_e(1-\beta_e)}{\sqrt{\pi}\,\sqrt{\psi^{(1)}}}\psi^{(2)}\frac{\partial\psi^{(1)}}{\partial\xi} - \frac{2\mu_e(1-\beta_e)}{\sqrt{\pi}}\sqrt{\psi^{(1)}}\frac{\partial\psi^{(2)}}{\partial\xi} + \mu_e\psi^{(1)}\frac{\partial\psi^{(1)}}{\partial\xi} - \frac{\partial^3\psi^{(1)}}{\partial\xi^3}. \tag{A.21}$$

Equations (A.17) and (A.18) yield

$$\frac{\partial u_{iz}^{(4)}}{\partial\xi} = \frac{l_y(1+\gamma\sigma_i\mu_e)}{\omega_{ci}}\frac{\partial^2\psi^{(2)}}{\partial\xi^2} - \frac{\gamma\sigma_i\, l_y\mu_e(1-\beta_e)}{\omega_{ci}\sqrt{\pi}}\frac{\left(\frac{\partial\psi^{(1)}}{\partial\xi}\right)^2}{\sqrt{\psi^{(1)}}} - \frac{2\gamma\sigma_i\, l_y\mu_e(1-\beta_e)}{\omega_{ci}\sqrt{\pi}}\sqrt{\psi^{(1)}}\frac{\partial^2\psi^{(2)}}{\partial\xi^2} +$$
$$\frac{l_z V_0(1+\gamma\sigma_i\mu_e)}{\omega_{ci}^2}\frac{\partial^3\psi^{(1)}}{\partial\xi^3}, \tag{A.22}$$

$$\frac{\partial u_{iy}^{(4)}}{\partial \xi} = -\frac{l_z(1+\gamma\sigma_i\mu_e)}{\omega_{ci}}\frac{\partial^2\psi^{(2)}}{\partial \xi^2} + \frac{\gamma\sigma_i\, l_z\mu_e(1-\beta_e)}{\omega_{ci}\sqrt{\pi}}\frac{\left(\frac{\partial\psi^{(1)}}{\partial\xi}\right)^2}{\sqrt{\psi^{(1)}}} + \frac{2\gamma\sigma_i\, l_z\mu_e(1-\beta_e)}{\omega_{ci}\sqrt{\pi}}\sqrt{\psi^{(1)}}\frac{\partial^2\psi^{(2)}}{\partial\xi^2} +$$

$$\frac{l_y V_0(1+\gamma\sigma_i\mu_e)}{\omega_{ci}^2}\,\frac{\partial^3\psi^{(1)}}{\partial\xi^3}\,. \tag{A.23}$$

Multiplying (A.10) by γ and adding to (A.16), we get

$$\frac{\partial p_i^{(3)}}{\partial\xi} = \gamma\mu_e\frac{\partial\psi^{(3)}}{\partial\xi} - \frac{\gamma\mu_e(1-\beta_e)}{\sqrt{\pi}\,\sqrt{\psi^{(1)}}}\psi^{(2)}\,\frac{\partial\psi^{(1)}}{\partial\xi} - \frac{2\gamma\mu_e(1-\beta_e)}{\sqrt{\pi}}\sqrt{\psi^{(1)}}\,\frac{\partial\psi^{(2)}}{\partial\xi} + \gamma\mu_e\psi^{(1)}\frac{\partial\psi^{(1)}}{\partial\xi} -$$

$$\gamma\frac{\partial^3\psi^{(1)}}{\partial\xi^3} - \gamma(1-\gamma)\mu_e^2\psi^{(1)}\frac{\partial\psi^{(1)}}{\partial\xi}. \tag{A.24}$$

Multiplying (A.14) by $\frac{1}{l_x}$ and (A.15) by $\frac{1}{V_0}$, adding the results, we obtain [using (A.9), (A.11), (A.12), (A.21) - (A.24)] the required form of (5.25)

$$\frac{\partial\psi^{(2)}}{\partial\tau} + A\,\frac{\partial}{\partial\xi}\left(\sqrt{\psi^{(1)}}\psi^{(2)}\right) - B\frac{\partial^2\psi^{(2)}}{\partial\xi^2} = S\left(\psi^{(1)}\right).$$

A.5 The coefficients $M_i(i = 1, 2, 3, 4)$ in equation (5.26)

$$M_1 = -\frac{1}{2}\left[\frac{A^2}{V_0}(3+4\gamma\sigma_i\mu_e) + \frac{l_x^2}{V_0}(3+2\gamma\sigma_i\mu_e) - \frac{l_x^2}{V_0\mu_e} - \frac{\sigma_i\mu_e l_x^2}{V_0}\gamma(1-\gamma)\right],$$

$$M_2 = -\frac{1}{2}\left[\frac{\eta A}{4V_0} + \frac{\eta A}{2V_0}(1+2\gamma\sigma_i\mu_e)\right],$$

$$M_3 = -\frac{1}{2}\left[\frac{\eta A}{2V_0} - \frac{AB}{V_0}(1+2\gamma\sigma_i\mu_e) + \frac{\eta A}{V_0}(1+2\gamma\sigma_i\mu_e) - \frac{2B(1-\beta_e)}{\sqrt{\pi}}\right],$$

$$M_4 = -\frac{1}{2}\left[\frac{(1-l_x^2)(1+\gamma\sigma_i\mu_e)V_0}{\omega_{ci}^2\mu_e} - \frac{l_x^2}{V_0\mu_e^2} + \frac{1}{4}\frac{\eta^2}{V_0}\right].$$